Computer Modelling of Crystalline and Vitreous Boric Oxide

Department of Geological Sciences
University College London

The Royal Institution of Great Britain
Davy Faraday Laboratory

Akira Takada

Thesis submitted for the degree of PhD
University of London
October 1993

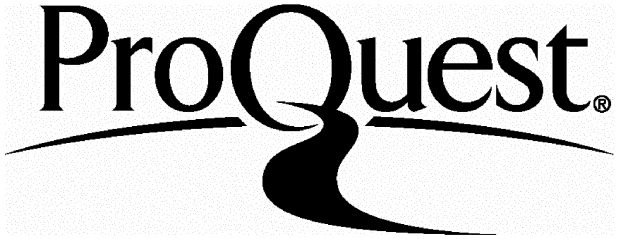

ABSTRACT

There is a long standing controversy concerning the structure of vitreous B_2O_3. Some experiments have suggested that the boroxol ring (6-membered ring) is a dominant structure feature. However, molecular dynamics simulations using the empirically-derived pair-potentials have failed to demonstrate the presence of boroxol ring. This difficulty seems to be due to the complexity of boron-oxygen bonding, which includes not only the partial covalency, but also allows the boron coordination number to change depending on its environment.

In the first half of this thesis, it is shown how quantum-mechanical calculations using a range of techniques (including periodic ab-initio Hartree-Fock and LDF) explain the nature of the structure and bonding in boric oxide. Although these calculations each have their limitations, their results are in accordance with accumulated concepts regarding the nature of the structure and bonding in boric oxide.

In the latter half of this thesis, we develop a new many-body potential model which can reproduce the structures of crystalline and vitreous boric oxide. As a transferable many-body potential could not reproduce the vitreous structure of B_2O_3, we developed a potential in which the pair terms were changed depending on the environment, in order to reproduce not only internal coordinates but also the relative stability (i.e. the difference in total energies) of the two phases of the crystalline material. The inclusion of a dependence of the pair-potential terms on the coordination number agrees with classical concepts of chemical bond strength. Parameters for this potential model are derived for crystalline boric oxide and adapted to the vitreous phase. The simulated structural model is checked by comparison with X-ray and

neutron scattering data. We find that this final theoretical study not only confirms the existence of the boroxol ring, but also leads to proposals for structural aspects of the intermediate-range order in boric oxide.

To

my family

and

my parents

'Nature

never did betray

the heart that loved her'

William Wordsworth (1798)

ACKNOWLEDGEMENTS

First and foremost I am indebted to my project supervisors, Professor C.R.A. Catlow and Professor G.D. Price for the fruitful discussions and advices concerning the study in this thesis.

I am also indebted to the Asahi Glass Company, for financial support and my superiors in Japan, Drs. T. Uchino, H. Mase and T. Kawaguchi, for providing chance of accomplishing the project in London.

I would like to thank the following for their valuable contributions to the project, Dr. C.L. Hayward for enjoyable discussions on vibrational spectroscopy, Drs. R. Nada and S. Hill for their help with 'CRYSTAL' simulations, Dr. J.S. Lin, Mr. M.H. Lee and Dr. V. Milman for their help with 'CASTEP' simulations, Dr. J.D. Gale for his help with 'THBREL' and "GULP' simulations, Dr. B. Vessal and Mr. E. Hernandez for their help with 'FUNGUS' simulations, Dr. R.G. Bell, Mr. A.R. George and Mr. A. Dornford-Smith for their help with the use of the Convex system.

Finally I am indebted for much assistance afforded to me by other members of the Davy Faraday Laboratory.

TABLE OF CONTENTS

LIST OF FIGURES

LIST OF TABLES

1. INTRODUCTION

Boric oxide (B_2O_3) and its compounds (borates) form an important class of minerals. They have a great range of structural types (oligomer, ring and chain polymers are all found) and exhibit a number of peculiarities in their structures and properties. Although some analogies with silicate systems are applicable for borate systems, they are limited owing to the existence of boron in both three-fold and four-fold coordination. Therefore, they are of much interest in structural chemistry as well as in geology.

The most important fields of application, however, for borate materials are in the glass and ceramics industries. Boric oxide plays a key role in numerous glasses of high technological importance. It promotes chemical resistance, although being strongly hygroscopic itself. It reduces thermal expansion in glasses, despite having itself a high coefficient of thermal expansion. However, it keeps its high fluidity and glass-forming properties when a component of glasses, thus improving the meltability and glass-forming ability of multi-component systems. The liquidus temperature is moreover strongly reduced by the introduction of B_2O_3 into a glass.

Borosilicate glasses are also of considerable technological importance. They constitute a large proportion of industrial glasses (for example, laboratory glasses, neutral glasses for pharmacy, sealing glasses for electronics, microporous glasses, glasses for fertilizers). Despite their industrial and fundamental interest the structures of vitreous borates are far from clear. Moreover, the existing structural concepts for crystalline and vitreous borates are not fully compatible.

What is the difficulty of understanding the structure and bonding in borate materials? Some of the peculiarities of these systems are as follows:

i. The high field strengths of $^{(3)}B$ and $^{(4)}B$ coming from the NMR chemical shift data indicate that the B-O bond is very strong. However, the viscosity of B_2O_3 is much lower than SiO_2. B_2O_3 acts as a very good efficient flux. (Volf 1984)

ii. The alkali borate glasses have been of considerable interest because of the so-called "boron oxide anomaly", which concerns the existence of maxima and minima in some of the physical properties with increase in the alkali metal oxide content, at temperatures below about 900°C. Such maxima and minima are not observed in most common boron-free glasses. (Griscom 1978)

iii. The vitreous boric oxides are thought to contain high concentrations of boroxol rings B_3O_6 (a hexagonal ring of three boron atoms and three oxygen atoms with three corner oxygen atoms outside the ring), although such a structural unit is not found in B_2O_3 crystals and its existence in the glassy materials is still controversial. (Griscom 1978)

A possible clue to the solution of these problems lies in the complexity of the boron-oxygen bond. It has partial covalency, and the latter is believed to be stronger than the silicon-oxygen bond. Its π-bonding strength varies with its environment, as pointed out by Pauling (1960) and Coulson (1968). Another factor of great significance is that the structural unit is easily changed from BO_3-planar to BO_4-tetrahedral, or vice versa, depending upon its environment.

In view of these complexities, the starting point of this thesis is the investigation of the nature of boron-oxygen bonding in crystals and molecules, using theoretical techniques. At the present time no single comprehensive theoretical method exists. Therefore, different points of view and methods are employed in a complementary manner as discussed in chapters 3 and 4. All these techniques are, however, based on the same basic quantum mechanical theory.

In view of the success of computer modelling of inorganic materials (see e.g. Catlow and Mackrodt 1982; Price and Parker 1988; Vessal et al 1989), and using the knowledge obtained from the first half of this thesis, we proceed to develop new many-body potential models for crystalline and vitreous boric oxide, which are consistent with the classical concept of chemical bonding. We then employ Molecular Dynamics (MD) simulations, with this new potential model, which confirm the existence of the boroxol ring, in contrast to the previous MD studies based on pair potentials.

Indeed, one of the main achievements of this thesis is that this new potential model reproduces for the first time not only the two different crystal structures but also the boroxol ring content of the glassy material.

CHAPTER 2 STRUCTURE AND BONDING IN BORATE MATERIALS

2.1 CRYSTAL STRUCTURES OF BORON TRIOXIDE

Crystals of boron trioxide do not exist naturally. Two different crystal phases have been synthesized and their structures determined (see Figure 2.1).

Crystalline boron trioxide (B_2O_3-I) was first isolated by Kracek et al (1938). Berger (1952,1953) first determined its structure by an X-ray diffraction techniques. He concluded that oxygen atoms in B_2O_3-I form two different distorted tetrahedra around the boron atoms with B-O distances ranging from 1.31 to 2.14 Å.

Later Strong and Kaplow (1968) showed from an X-ray diffraction study that all borons in B_2O_3-I are in planar trigonal configurations and that they consist of ribbons of interconnected BO_3 triangles, thereby demonstrating that Berger's structure is incorrect. Gurr et al (1970) subsequently corrected the structure of Strong and Kaplow, by using a single crystal sample, though it was pointed out later by Strong et al (1971) that the two structures are essentially the same, being related by transformation of an axis.

The other crystalline polymorph B_2O_3-II was studied by Prewitt and Shannon (1968). B_2O_3-II was obtained at high pressures (>20 Kbar) and temperatures in excess of 400 °C. It consists of a network of corner-linked BO_4 tetrahedra.

B_2O_3-I has a trigonal structure with a= 4.336 Å, c= 8.340 Å, Z= 3, ρ= 2.56 gcm^{-3}, space group= P3 (Gurr et al 1970; see Figure 2.2). Its average B-O bond length is 1.372 Å and it agrees well with 1.365 Å for a bond of 'strength' 1.0 calculated by Zachariasen (1963). It is known that the crystal

cannot easily be prepared. It has been impossible to grow crystals of B_2O_3 at atomospheric pressure from a dry B_2O_3 melt, even when the melt was seeded with B2O3-I crystals (Kracek 1938). A possible reason for the difficulty in crystallizing B_2O_3-I from the melt, as discussed by Ulmann et al (1967), may stem from the necessity of opening boroxol rings to form the ribbons of B_2O_3-I.

B_2O_3-II has an orthorhombic structure with a= 4.163 Å, b=7.803 Å, c= 4.129Å, Z= 4, ρ= 3.11 gcm^{-3}, space group Ccm2 (Prewitt 1968; see Figure 2.3). The BO_4 tetrahedron is very distorted: one short B-O bond length is 1.373 Å and the other three long B-O bond lengths are 1.507, 1.506 and 1.512 Å, although the average B-O bond length is 1.475 Å, exactly that proposed by Zachariasen (1963). The oxygen associated with the short B-O bond is coordinated by only two boron atoms, whereas the others are coordinated by three boron atoms. Prewitt (1968) concluded that the distortions are necessary to balance the variations in the electrostatic potential in the crystal.

Finally, it is interesting to note no crystalline polymorph comprising boroxol rings is found, although, as noted, these have been suggested to be important in the glassy phases, and are observed in a number of borate crystals as discussed below.

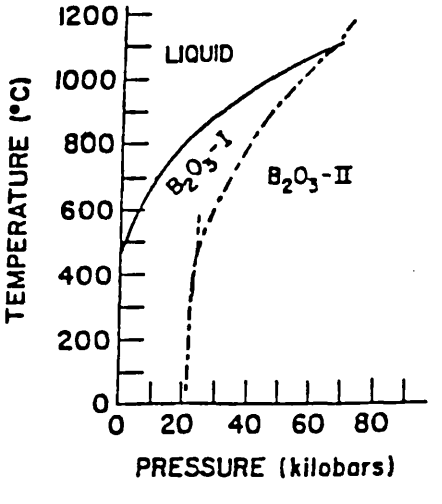

Figure 2.1. The phase diagram of B_2O_3 (MacKenzie and Claussen 1961)

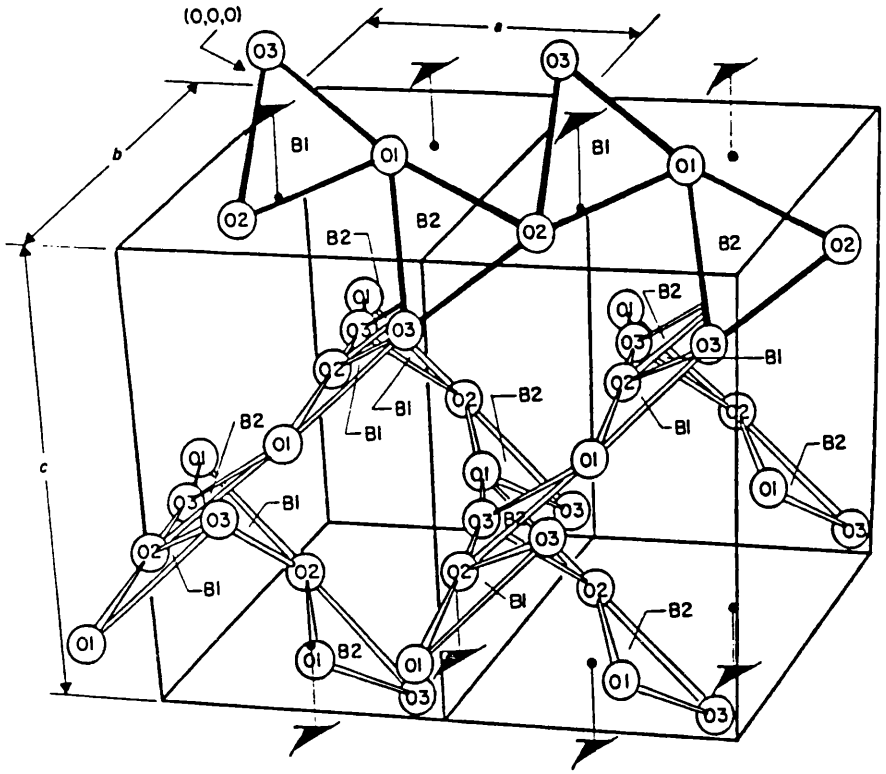

Figure 2.2. The B_2O_3-I structure
(Gurr et al 1970)

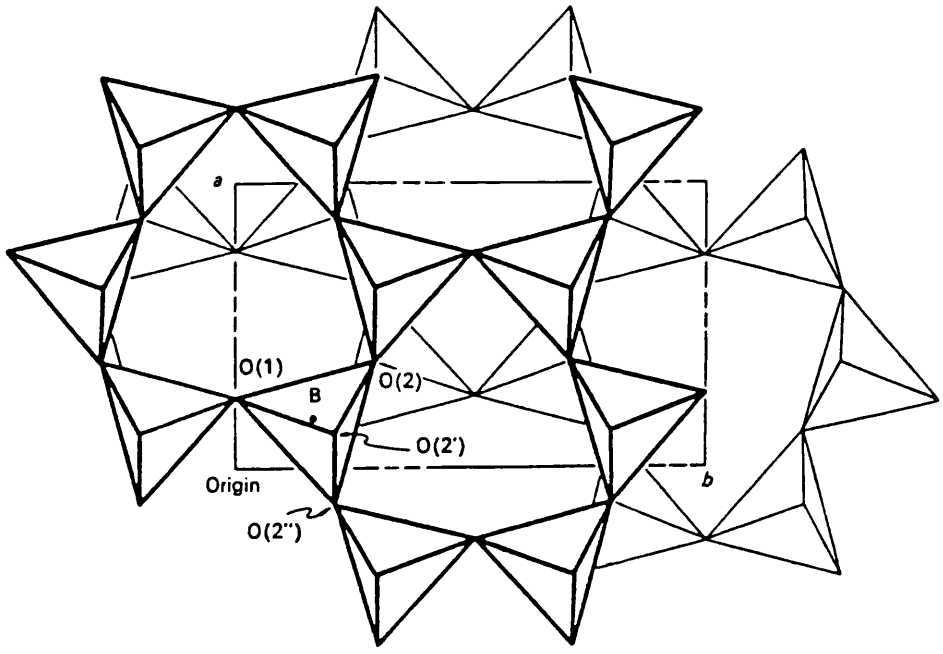

Figure 2.3. The B_2O_3-II structure
(Prewitt et al 1968)

2.2 CRYSTAL STRUCTURES OF BORIC ACID AND BORATES

Many X-ray analyses of crystal structures of boric acids and borates have been reported.

Boric acid and the whole H_2O-B_2O_3 system is important, because B_2O_3 is strongly hygroscopic and nearly all borate minerals are attacked by aqueous solutions. It is also significant in relation to the volatilization of B_2O_3 with water vapour, which takes place during glass melting. Kracek et al (1938) studied the solubility diagram for the system H_2O-B_2O_3 (see Figure 2.4). Metaboric acid has three polymorphs, and it is interesting to note that only the orthorhombic metaboric acid (HBO_2-III) contains boroxol rings and exhibits the same 808 cm^{-1} Raman line as vitreous B_2O_3 (Galeener et al 1980). The least stable metaboric acid (HBO_2-I) is also interesting because it promotes nucleation of the anhydrous B_2O_3 (Kracek 1938).

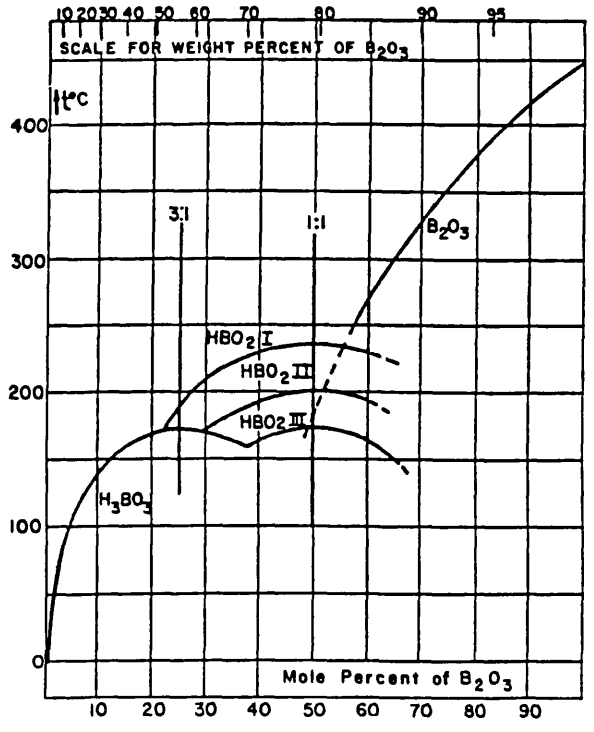

Figure 2.4. The solubility diagram for the system, H_2O-B_2O_3 (Kracek et al 1938)

On the other hand, it is known that crystalline borates are built up of large borate groups (see Figure 2.5) and in vitreous borates these groups are thought to be retained to some extent. The crystal-chemical classification is reviewed by Bokii and Kravchenko (1966), who distinguished borates by two structural criteria. One approach classifies structures in terms of (1) ringless borates, (2) one-ring, two-ring and three-ring borates and (3) borates with mixed polyions and borosilicates. Another classification is in terms of (1) island borates (isolated polyions and dimers), (2) chain borates, (3) sheet borates and (4) network borates. On the other hand, Christ and Clark (1977) propose another classification based on different criteria and which has special reference to hydrated borates (see Appendix A).

It is also interesting to note that sodium metaborate $Na_3B_3O_6$ (Fang 1938, Marezio et al 1963) and potassium metaborate $K_3B_3O_6$ (Zachariasen 1937, Schneider 1970) have boroxol rings and exhibit the same 808 cm^{-1} Raman line as vitreous B_2O_3 (Bril 1976). Cesium enneaborate, $Cs_2O \cdot 9B_2O_3$, the borate with the highest molar fraction of boron oxide, also contains boroxol rings (Krogh-Moe and Ihara 1967).

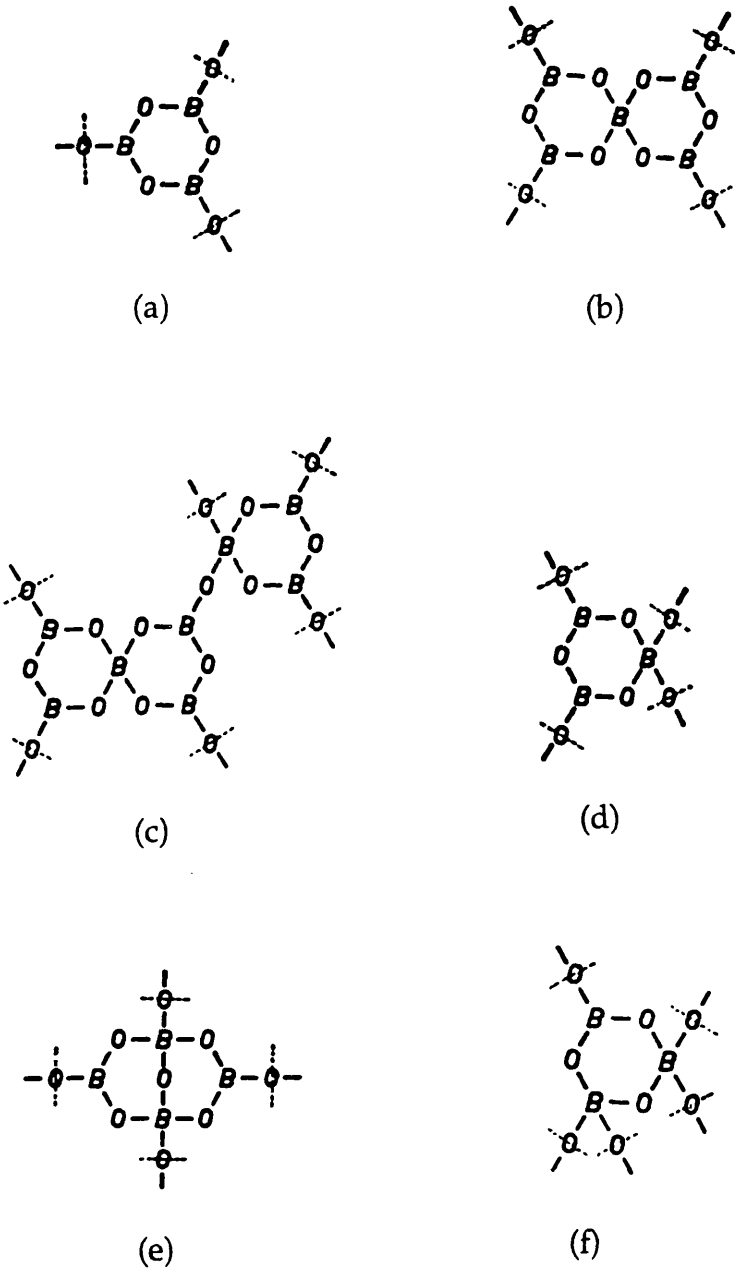

Figure 2.5. Boron-oxygen structure groupings (Konijnendijk 1975)

(a) the boroxol ring in vitreous B_2O_3
(b) the pentaborate group in the compounds α-$K_2O{\cdot}5B_2O_3$ and β-$K_2O{\cdot}5B_2O_3$
(c) the tetraborate group in the compound $Na_2O{\cdot}4B_2O_3$
(d) the triborate group in the compound $Cs_2{\cdot}3B_2O_3$
(e) the diborate group in the compound $Li_2O{\cdot}2B_2O_3$
(f) the diborate group in the compound $K_2O{\cdot}2B_2O_3$

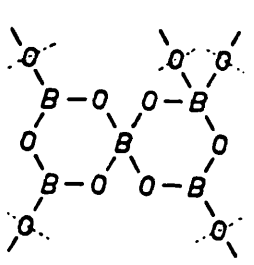

(g)

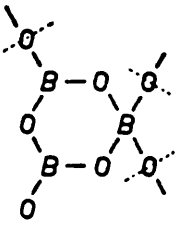

(h)

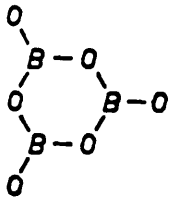

(i)

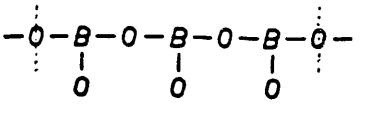

(j)

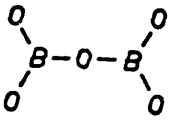

(k)

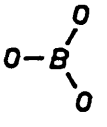

(l)

Figure 2.5.(continued) Boron-oxygen structure groupings

(g) the di-pentaborate group in the compound $Na_2O{\cdot}2B_2O_3$
(h) the triborate group with one non-bridging oxygen in the compound $Na_2O{\cdot}2B_2O_3$
(i) the ring-type metaborate group in the compounds $Na_2O{\cdot}B_2O_3$ and $K_2O{\cdot}B_2O_3$
(j) the chain-type metaborate in the compound $Li_2O{\cdot}B_2O_3$
(k) the pyroborate group in the compounds $2MgO{\cdot}B_2O_3$ and $2CaO{\cdot}B_2O_3$
(l) the orthoborate group in the compounds $3MgO{\cdot}B_2O_3$ and $3CaO{\cdot}B_2O_3$

2.3 STRUCTURE OF VITREOUS BORIC OXIDE AND BORATES

The random network model, proposed by Zachariasen (1932) is amongst the most well-known models for the structures of glassy materials. For example, in vitreous silica, SiO_4 tetrahedra provide the framework (so-called Network-former), in which the silicon atom is tetrahedrally surrounded by four oxygen atoms and each oxygen atom is bonded to two silicon atoms. Although the first coordination shell is the same as that of the crystalline structure, the tetrahedra are rearranged in a non-periodic manner in three dimensions; that is they have no long-range order.

For boric oxide glass, the simpler random network model, consists of planar BO_3 triangles, as also proposed by Zachariasen (1932). However, several serious objections to this model have been raised, as reviewed in the volume of proceeding edited by Pye et al (1978) and also by Johnson (1982).

Since Zachariasen's model (1932) was published, several rules about vitreous structures of borates (Abe 1952, Eversteijn 1960, Huggins 1957) have been formulated, although subsequently disproved, and several structural models have been published.

Historically, the random network model containing no boroxol rings (Zachariasen 1932), the boroxol ring model (Krogh-Moe 1969), the quasicrystalline model (Borelli and Su 1963) and the model based on the B_4O_6 molecule (Fajans and Barber 1952) have been proposed (see Figure 2.6). From the considerable amount of data accumulated and analyzed, the former two models are now favoured.

As for the coordination of boron in B_2O_3, the hypothesis that almost all the borons have three-fold coordination is supported by all the

experimental data and is widely accepted. And the phenomenon of the coordination change of the three-fold coordinated triangle (BO_3) to a four-fold coordinated tetrahedron (BO_4) in binary alkaline borate glasses has been studied in order to explain so-called "boron oxide anomaly".

However, the mode of connecting the BO_3 triangles is still controversial. Goubeau and Keller (1953) first suggested the existence of boroxol groups in B_2O_3 glass in order to explain the extremely sharp line in the Raman spectrum of 808 cm^{-1}. Krogh-Moe (1969) analyzed NMR data, infrared and Raman spectroscopic data, X-ray diffraction data, density data, energy data and viscosity data. He concluded that a random three-dimensional network of BO_3 triangles with a comparatively high fraction of boroxol rings gives the best explanation of the available data.

In contrast, Elliot (1978) claimed that the continuous random network (C.R.N.) model containing no boroxol rings, modified from the structure of three-fold coordinated amorphous arsenic, can reproduce the radial distribution functions of the X-ray study of Mozzi and Warren (1970). However, the problem with this model is that the density is some 30% lower than that observed experimentally.

The boroxol ring model has, however, the same problem. Although it can give a satisfactory account of the Radial Distribution Function (RDF) obtained from the X-ray diffraction data at small interatomic separations, it does not necessarily reproduce the measured density correctly (Bell and Carnevale 1981). The latter authors proposed a locally layered random network model, in which adjacent layers are weakly bonded by the occasional overlapping of boroxol rings rotated relative to each other by 60°.

To summarize these structural models, a wide range of experimental data favours the boroxol ring model. However, there is no

conclusive evidence for rejecting the continuous random network model containing no boroxol rings. However, all the above approaches based purely on topological considerations seems to have serious limitations. More detailed models are required.

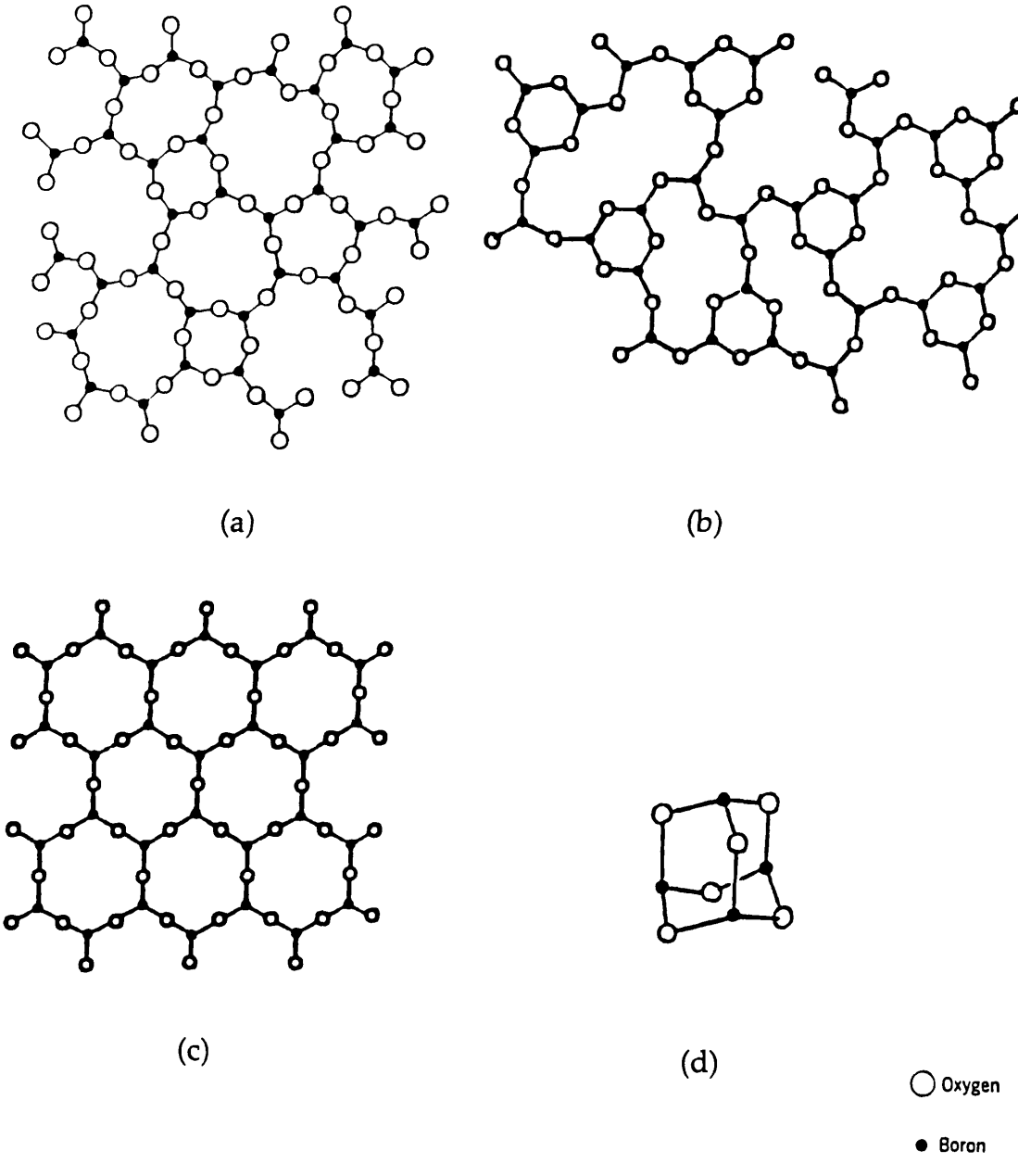

Figure 2.6. Schematic representation for structural models of vitreous boric oxide (Krogh-Moe 1969)
(a) the random network model
(b) the boroxol ring model
(c) the quasicrystalline model
(d) B_4O_6 molecule model

2.4 EXPERIMENTAL APPROACHES

2.4.1 X-RAY DIFFRACTION STUDIES

X-ray diffraction techniques have of course been used to determine structures of crystalline borates, but they also give important RDF data for vitreous borates.

Mozzi and Warren (1970) rigorously interpreted X-ray data for vitreous B_2O_3 in terms of pair functions (see Figure 2.7). They pointed out that there are definite peaks in the experimental curve for distances out to about ~ 6 Å, which requires that there is a structural unit in vitreous B_2O_3 which is larger than the randomly oriented BO_3 groups. They assumed a random network of boroxol groups B_3O_6. They also assumed that all the B-O-B angles outside the rings are 130° and all the B-O-B angles within the rings are 120°. They concluded that there is very good agreement with the experimental curve with regard to peak positions, but the peaks and dips in the calculated curve are a little too pronounced. They suggested that this may indicate that they should have allowed for a little more distance variation; alternatively not all of the structure is in the form of boroxol groups.

Further clues may come from X-ray diffraction studies of molten B_2O_3, which may explain the peculiarities of the glassy state, as the structure of vitreous state is generally said to be very closely related to that of the liquid from which it is quenched. However, Fajans and Barber (1952) observed that at 1260 °C the viscosity of boron oxide is smaller than that of silica by a factor of $10^{-11.6}$. Therefore, the concept of a random network with a strong boron-oxygen bond is said to be difficult to reconcile with the comparatively low viscosity of boron oxide melts.

The change of density with temperature (Macedo et al 1966) and the change of heat capacity with temperature (Shmidt 1966) are also of some

interest. These data exhibit an abrupt change in slope at the glass transition temperature (Tg) and above Tg a structural change may take place progressively with rising temperature (Krogh-Moe 1969). On the other hand, structural models in the molten state, which are different from the vitreous state, were proposed by Mackenzie (1959), Riebling (1966), and Sperry and Mackenzie (1968). From X-ray studies in molten states Zarzycki (1974) observed structural changes at high temperatures of 1200 °C and 1600 °C: a very pronounced decrease of the first coordination number amounting to more than 30% was found at 1600 °C. This may suggest that three-fold coordinated and two-fold coordinated boron atoms coexist in molten states.

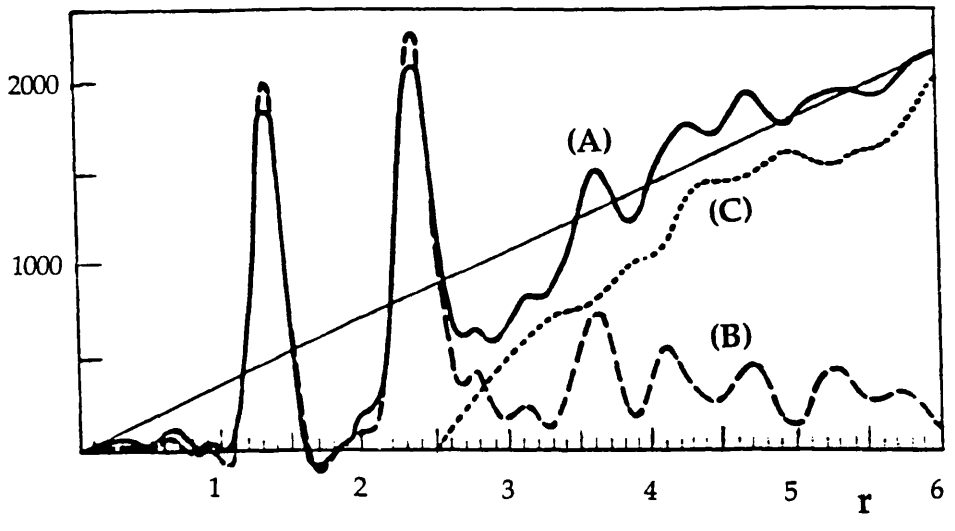

Figure 2.7. Analysis of X-ray diffraction data using boroxol model:
Curve (A): the measured PFD for glassy B2O3;
Curve (B): the sum of computed contribution to the PFD for a model of randomly linked boroxol rings;
Curve (C): the difference (A) - (B)
(Mozzi and Warren 1970)

2.4.2 NMR STUDIES

As Griscom (1978) points out, one of the truly outstanding achievements of solid state NMR is the measurement of the fraction of boron atoms which are in four-fold coordination, N_{BO_4}. The large disparity between the coupling constants for trigonal and tetrahedral boron permits the resonances of each to be separated and quantitatively measured even in materials containing both types of units.

Historically, Bray and O'Keefe (1963) published N_{BO_4} determinations for the entire glass forming ranges of all five alkaline borate systems (see Figure 2.8). Jellison et al (1977) analyzed the environment of ^{10}B, ^{11}B and ^{17}O nuclei within the glass. They concluded that their data are in agreement with the boroxol ring model and from the ^{17}O spectra are able to deduce the fraction of oxygen atoms included in boroxol rings. They estimated the fraction of the boron atoms forming part of boroxol rings (0.82 ± 0.08) and hence the ratio of boroxol rings to independent BO_3 triangles to be ~ 1.5 : 1. The NMR data also give information on the B-O-B angles for the oxygen atoms not included in boroxol rings. These have a narrow distribution (rms deviation ~ 1.7°) centred around either 134.6° or 128.1°, close to the average experimental value of 130° in borate crystals.

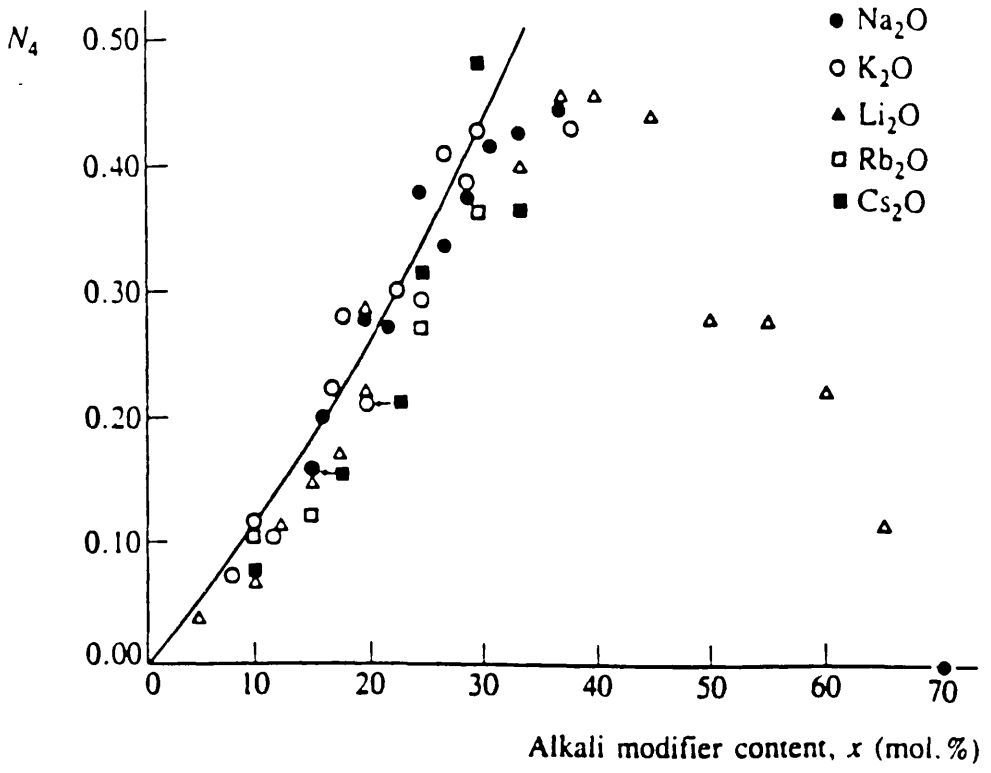

Figure 2.8. Variation of the number of tetrahedral boron sites, N_{BO4}, with alkali-oxide content, as obtained from NMR experiments (Bray and O'Keefe 1963)

2.4.3 RAMAN SCATTERING STUDIES

Historically, Goubeau and Keller (1953) first provided evidence from Raman spectroscopy for the existence of boroxol groups in B_2O_3 glass, explaining the extremely sharp line at 808 cm^{-1}.

Next, Bril (1975) and Konijnendijk (1975) reported several important Raman studies. Bril undertook Raman investigations of a number of metaborate crystals and alkaline borate glasses, carrying out a normal coordinate analysis of the resulting spectra. He concluded that the strong peaks of the Raman spectrum of vitreous alkaline borate at 806 cm^{-1} and 770 cm^{-1} are assigned to the ring breathing (ν_2) of respectively the boroxol group and a group containing a six-membered ring with at least one BO_4 or BO_3^- unit. Figure 2.9 shows three Raman-active symmetric vibrational modes of $B_3O_6^{3-}$. Figure 2.10 shows the change in Raman spectra by adding the sodium oxides. It is interesting to note that his Raman data, obtained as a function of temperature, are unchanged on passing from the glass to the melt (up to 800K).

Konijnedijk reported comprehensive Raman scattering and IR investigations of borate and borosilicates glasses. He concluded for the binary alkali-borate glasses as follows: in the concentration range 0 to about 25 mol% alkali oxide , the boroxol groups, originally present in vitreous B_2O_3, are replaced by six-membered borate rings with one BO_4 tetrahedron which to a certain extent are ordered to tetraborate groups. In the range 20 to 35 mol% alkali oxide, six-membered borate rings with two paired BO_4 tetrahedra are gradually formed which to a certain extent are condensed to diborate groups. Unmixed sodium- and potassium-borate glasses cannot be made in the range above about 40 mol% alkaline oxide. In mixed alkaline-borate glasses with 40 to 50 mol% alkali oxide the

presence of orthoborate , pyroborate and ring-type metaborate groups is indicated, together with diborate groups.

Galeener et al (1980) analyzed their Raman data on vitreous B_2O_3 in terms of a model based on a nearest-neighbour, central-force network dynamics model and concluded that their data are inconsistent with an idealized random network of BO_3 triangles with a random dihedral angle, and favoured a structural model containing a large fraction of boroxol rings.

As for the temperature dependence of Raman intensities, Walrafen et al (1980) studied Raman data for vitreous B_2O_3 and molten B_2O_3 from -196 to 1594 °C. They concluded that vitreous B_2O_3 is composed predominantly of boroxol rings, but the boroxol ring concentration decreases with increasing temperature in the melt, and becomes small at temperature above 1600 °C.

Recently Kamitsos and Chryssikos (1991) studied Raman spectra of several alkali borate glasses and concluded that their results point to the strong dependence of the network modification on the nature of the cation modifier.

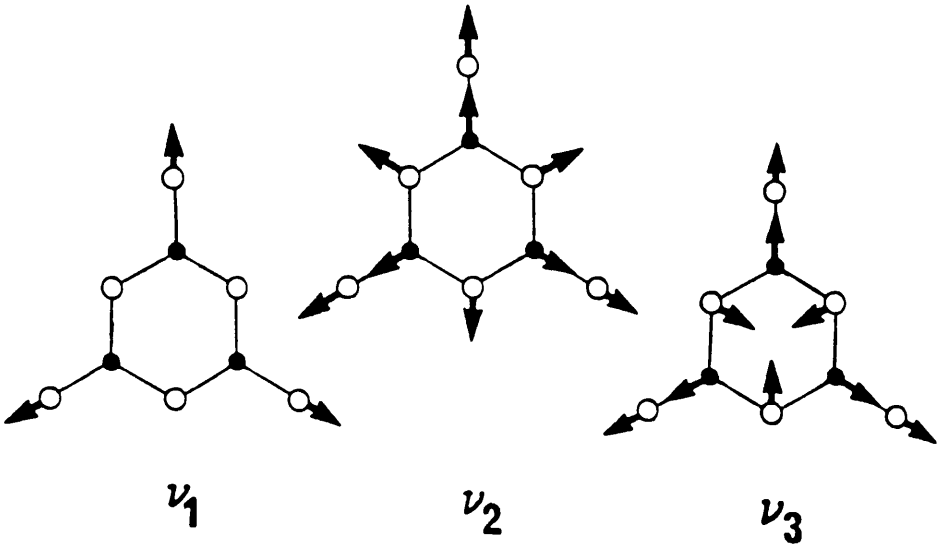

Figure 2.9. Symmetric vibrational modes of the "free" metaboric anion, $B_3O_6^{3-}$. All three are Raman active and polarized. (Griscom 1978)

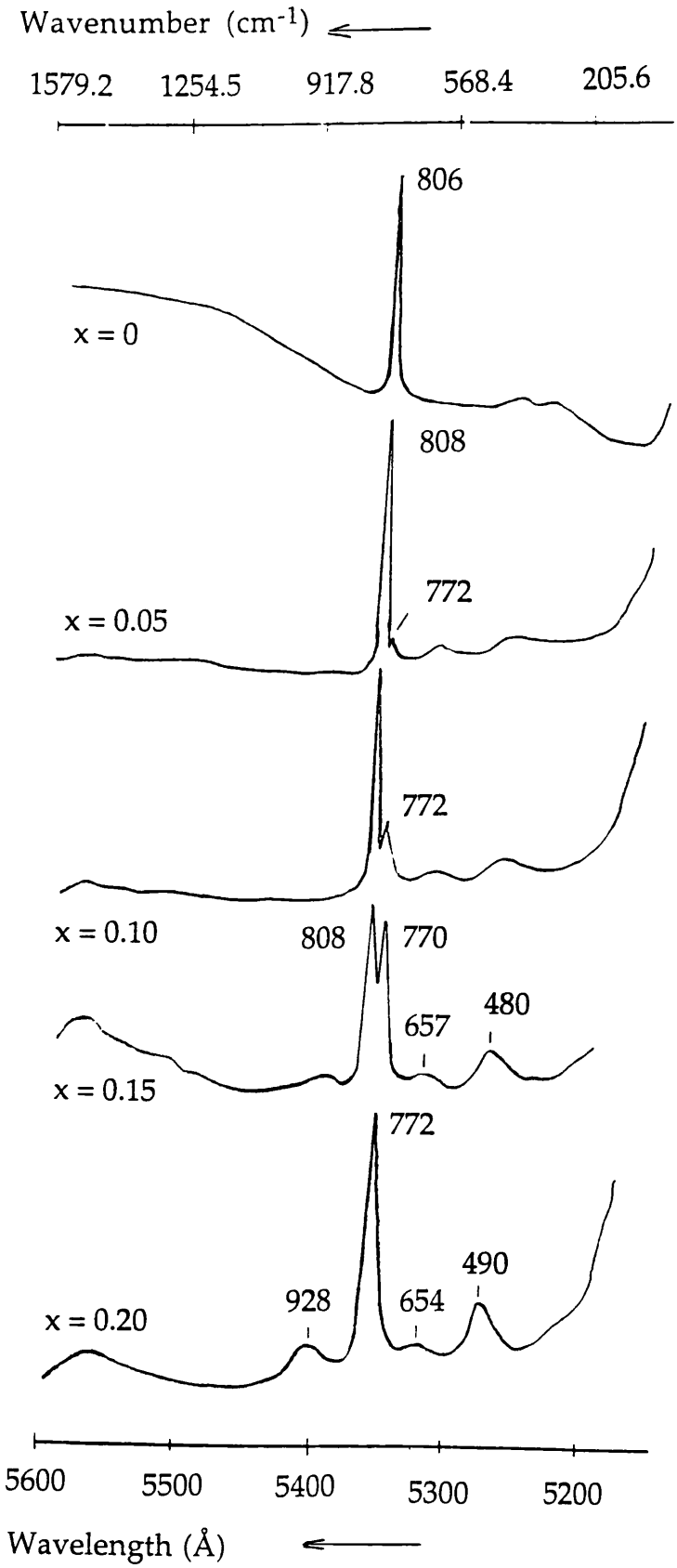

Figure 2.10. Raman spectra of sodium borate glasses: $xNa_2O \cdot (1-x)B_2O_3$ (Konijnendijk 1975)

2.4.4 NEUTRON SCATTERING STUDIES

Johnson et al (1982) performed neutron diffraction investigations of vitreous B_2O_3. The neutron scattering length for ^{11}B is slightly greater than that for oxygen, so that neutrons should be more sensitive than X-rays to the presence of boroxol groups. They fitted Elliot's model and the boroxol ring model to Mozzi and Warren's X-ray data and their neutron data. They concluded that the X-ray data of Mozzi and Warren and the neutron diffraction data of Johnson et al are consistent with a structure for vitreous B_2O_3 containing a proportion of 0.6 ± 0.2 of the boron atoms in boroxol rings (see Figures 2.11 and 2.12).

In another approach, Hannon et al (1988) studied inelastic neutron scattering from vitreous B_2O_3. They showed the boroxol ring breathing mode is a relatively small feature in the VDOS (vibrational density of states) of vitreous B_2O_3 and the matrix element for this mode is enhanced for both the HH and the HV Raman spectra. Despite this, they find that their ball-and-stick model containing a high concentration of boroxol rings is consistent with their inelastic neutron scattering data.

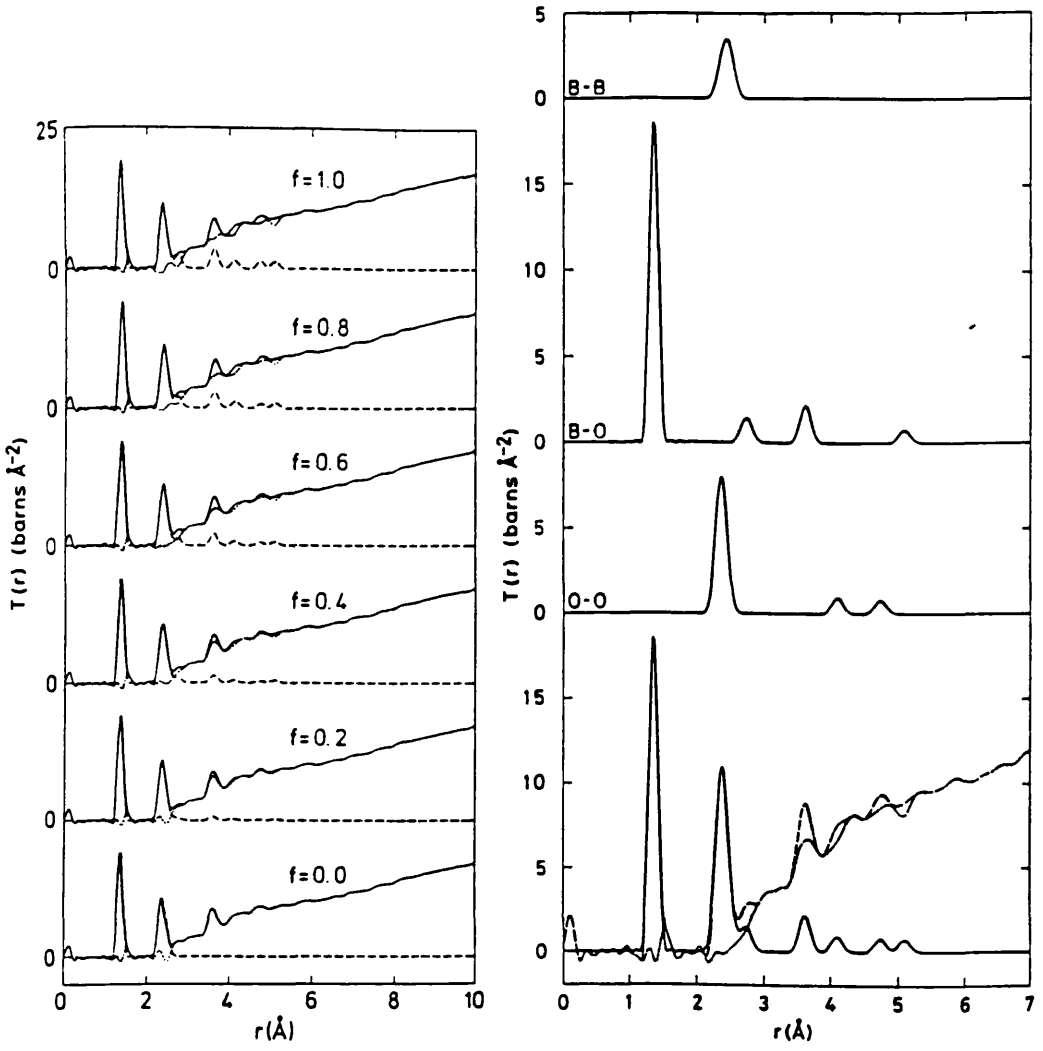

Figure 2.11. (left) The neutron total correlation function as a function of the fraction, f, of the boron atoms in boroxol rings. Full curve, experiment; dashed curve, model and dotted curve, residual. (Johnson et al 1982)

Figure 2.12. (right) Component correlation functions for a boroxol ring model with f=0.6 (Fixed distances only). Full curve, model; dashed curve, experiment; and dotted curve, residual. (Johnson et al 1982)

2.5 COMPUTER SIMULATION

2.5.1 QUANTUM MECHANICAL STUDIES

Quantum mechanical techniques provide the most fundamental approach for explaining the nature of electronic structure, and its relation to structure and bonding.

For silicate systems, molecular orbital (MO) calculations have been reported for various clusters (see O'Keeffe and Navrotsky *eds*. 1981). These calculations on molecular clusters have been used to study potential energy surfaces and obtain interatomic potentials for SiO_2 (Lasaga and Gibbs 1988,1991; Tsuneyuki et al 1988; Beest et al 1990). In addition, periodic Hartree-Fock method (Nada 1990; Silvi 1991) and Local Density Functional method (Allan and Teter 1987) have been applied for SiO_2 polymorphs.

The first MO calculations for borate systems were performed by Coulson (1964) and Coulson and Dingle (1968). Variations in the B-O bond length have been thought to be due to π bonding, since the early suggestion of Pauling (1960) and Zachariasen (1963). To investigate the nature of the bonding, they calculated the π bond order for several metaborate ions using the Hückel method.

Snyder et al (1976) performed the first ab-initio calculation (STO-3G) of small clusters, $B(OH)_3$ and BH_3. They found that there is a strong relationship between the quadrupole coupling parameter and the molecular environment. Later Snyder (1978) discussed the structure, the heat of formation and the resonance energy of the π electron system, using small clusters. He concluded that the resonance energy of the boroxol ring (1Kcal$\pm$4 Kcal/mol) is a negligible driving force for the condensation-dehydration reaction.

Gupta and Tosell (1981,1983) and Zhang et al (1985) performed ab-initio calculations (STO-3G and 6-31G*) of molecular clusters (monomers, dimers and trimers), following a successful simulation of SiO_2. They both concluded that these calculations are adequate for reasonable predictions of bond angles and bond distances for borate minerals, although the crystal field effect is disregarded. Tossell showed that modified electron-gas (MEG) ionic model calculations based on B^{3+} and OH^- ions also give reasonable accurate B-O bond distances. These calculation results were reviewed by Tossel and Vaughan (1992) (see Table 2.1).

On the other hand, Uchida et al (1985,1986) used a semi-empirical SCF-MO method employing the MNDO technique on small clusters. They discussed the structure, the heat of formation, the π electron system and the electronic structures. They concluded that the resonance stabilization effect of the π electron system is not so large as to control the geometry and reactions, as had been previously found by Snyder (1978).

They also discussed the "hardness and softness" of basicity in the binary borate system. The other studies of the basicity in alkali borate glasses were also discussed by Kawazoe et al (1978). They use a new quantity "Sparkle Affinity" as a measure of the hard basicity of borate anion clusters. The sparkle is a virtual chemical species whose behaviour is expected to be similar to the alkali or alkaline earth metal cation. The sparkle affinity is defined as the energetic gain when one sparkle is set near a borate anion cluster. They concluded that the four-fold coordinated boron unit BO^{4-} is a rather hard base and the non-bridging oxygen is a rather soft base. The also concluded that a proton binds to one oxygen atom with high covalency, in contrast to alkali metal ions, the latter coordinating several oxygen atoms via the Coulombic interactions.

The discrete B_2O_3 molecule has been presumed to be the dominant species in molten B_2O_3. Accurate calculations have been performed on gas-phase B_2O_3, establishing clearly that the equilibrium geometry is planar and V shaped with C_{2v} symmetry (Sellers et al 1981; Barone et al 1981) and that the bipyramidal D_{3h} structure is of much higher energy (Snyder and Wasserman 1980).

Finally, it is interesting to note that the lowest energy form of $(OH)_2BOB(OH)_2$ has a nonplanar C_2 geometry with a 60° dihedral angle between the two BO_3 groups (Zhang et al 1985), and that boroxol rings in large clusters are connected by bridging oxygens in a twisted manner (Uchida et al 1985,1986).

2.5.2 MOLECULAR DYNAMICS SIMULATION

Since the pioneering study of Woodcock et al (1976) on the simulation of vitreous silica, Molecular Dynamics (MD) simulations have been recognized as a very useful tool for the study of structural and rheological properties of glasses. However, compared to the many studies of silicates, there are few investigations of borate glasses. Because of the complexity of the boron-oxygen bonding, both the experimental and modelling techniques seem to be insufficient and there is still a considerable discrepancy between experimental data and simulations.

The first modelling studies of borate glasses were initiated by Soules (1979,1980) and Soules and Varshneya (1981). They calculated the structures of vitreous B_2O_3 and sodium borosilicate glass. They showed that in vitreous B_2O_3 boron atoms are trigonally coordinated to oxygen atoms, while in sodium borosilicate glasses the trigonal to tetrahedral conversion of boron atoms accompanies the addition of sodium atoms.

These two aspects of their results agree well with the experimental data. However, no boroxol group formation is observed in their simulation.

A series of more detailed studies were carried out by Soppe et al (1988), Soppe and Hartog (1988), Soppe and Hartog (1989). Their consistent result is that they do not find any boroxol rings. They found that for both non-pressure scaled and pressure scaled systems, and for a variety of different quench rates, oxygen atoms have no tendency to become equiplanar with adjacent BO_3 triangles. They also attempted an interesting simulation in which half of the number of B-O-B and O-B-O angles were constrained at 120°. Even with such artificial constraints, they do not find any boroxol rings. They concluded that their continuous random network structure without any boroxol rings reasonably reproduced the RDF of X-ray data.

Amini et al (1981), Abramo et al (1986), Xu et al (1988) also performed MD simulations on B_2O_3, and on silver borate and sodium borate glasses. In none of these studies were boroxol groups found.

All of these studies have two limitations. The first is that very rapid quenching rates (10^{13} ~ 10^{15} K/sec) have to be used. Even with supercomputers, simulated quench rates are still far from the rates (less than 10^3 K/sec) in the real process. However, in spite of such rapid quench rates, several simulations of silica glass have succeeded in reproducing the structures of the vitreous material.

The second limitation is the use of pair-potential models with formal charges. Pair-potential models succeed in modelling many ionic materials and all the pioneers in this field employed such models. However, such pair-potentials may not be sufficient to express the structure and bonding of materials with partial covalency.

In order to account for covalency, Hirao and Soga (1985) applied a new potential with the extra term $-Aexp[-C(r-0.239)^2]$ (r is the distance between boron atoms) for B-B interactions to sodium borate glasses. They presumed that their structure may include boroxol groups from the calculated population of B-O-B angles at $\approx 120°$.

The MD study of Inoue et al (1987) included three body effects and is the only one that generates boroxol rings in B_2O_3 glass and diborate groups in sodium borate glass. They put ghost atoms (G) on the centre of gravity of both BO_2 and B_2O triangles. A positive point charge with a Born-Mayer type short-range potential is assumed to exist at G when the G-O potential is calculated, and a negative point charge with a different Born-Mayer type short-range potential is assumed to exist at G when the G-B potential is calculated. These ghost atoms thus provide O-B-O and B-O-B three body potentials. Boron and oxygen atoms have formal charges, and all the other potential parameters are derived from the potential energy of H_3BO_3 by the INDO (intermediate neglect of differential overlap) method.

They concluded that their "pseudo-atom" three-body type of model reproduces the RDF of Mozzi and Warren (1970) with the presence of boroxol rings. However, the ratio of boron atoms present in the boroxol rings is less than 22.5% and smaller than that reported ($82\pm8\%$ by Jellison et al 1977 and $60\pm20\%$ by Johnson et al 1982). This result is encouraging in that it shows that structures with boroxol rings can be reproduced by three body potentials, even if a rapid quench rate is used. It is, moreover, interesting to note that calculated B-O-B bond angles are distributed around 120°. In contrast, all pair-potential studies show B-O-B angles of ~ 160°. The NMR data of Jellison et al (1977) give information on the B-O-B angles for oxygen atoms not included in boroxol rings. The NMR result

shows a narrow distribution centred around either 134.6° or 128.1°, close to the value of 130° used by Mozzi and Warren (1970).

On the other hand, recently Verhoef and Hartog (1992) carried out MD simulations of B_2O_3 glass, using different sets of pair-potentials (Born-Mayer-Huggins type) and in some cases three-body, bond-bending terms were applied. For the latter a simple harmonic form was used. The equilibrium angle was set as 120° for O-B-O and 130° for B-O-B. The force constant for O-B-O was fixed so as to obtain the correct energy for the high-frequency mode in the simulated infrared spectrum.

Their first conclusion is that all the models investigated generate continuous random network glass structures without any boroxol rings, even if three body bond-bending terms are added. Their second conclusion is that all the models reproduce the experimental data reasonably well, although there are detailed discrepancies mainly within the distance range of 2 - 4 Å in the RDF. Their third conclusion is that the peak at 805 cm^{-1} in the experimental Raman spectra can be assigned to a breathing mode of the three oxygen atoms within each BO_3 triangle. However, no peak at around 805 cm^{-1} is experimentally observed in borate crystals which consist of BO_3 triangles. Their fourth conclusion is that three body interactions are necessary to reproduce the high-frequency modes in the simulated infrared spectra and density of state.

To summarize the results of all the MD simulations;

(1) Pair-potential models can reproduce the short-range data of X-ray and Neutron scattering well. However, discrepancies remain for medium range distances. B-O-B angles are far from the average of the experimental values of 130° estimated from NMR data. Pair-potential models always generate continuous random networks without any boroxol rings.

(2) Three-body potential models can reproduce boroxol rings, although this is not always the case. They can reproduce some characteristics of the medium-range order which are similar to Mozzi and Warren's model. The inclusion of the three-body potential affects not only the generation of boroxol rings but also the vibrational properties of the simulated vitreous material.

The work reported later in this thesis will advance the description of the interatomic potential models for B_2O_3 and will achieve improved agreement with experiment compared with the results discussed above.

Bond lengths [R(B-O) in Å]	Ab initio calculated values					Experimental values	
cluster	STO-3G basis	4-31G basis	6-31G* basis	MEG method	MNDO method	Average	Range
BO_3^-	1.419	1.435	---			1.37	1.34 - 1.40
$B(OH)_3$	1.364	1.364	1.358	1.37	1.371	1.361	1.353 - 1.365
$B(OH)_4^-$	1.48	---	1.474	1.53	~ 1.47	1.478	

Bond angles [B-Obr-B in degrees]	Ab initio calculated values			Experimental values	
Cluster	STO-3G basis	4-31G basis	6-31G* basis	Average	Range
$[(OH)_2B]O$	130	180	131.3	134	128 - 153
$(OH)_3B\text{-}O\text{-}B(OH)_2^-$					118 - 128
$H(OH)_3B\text{-}O\text{-}B(OH)_3H$	123			119	

$B_3O_6H_3$	Ab initio calculated values				Experimental values	
	STO-3G	6-31G	3-21G*	MNDO	Average	v-B_2O_3
R(B-O)br (Å)	1.374	1.390	1.371	1.389	1.401	1.36
R(B-O)nbr (Å)	1.289	1.351	1.351	1.354	1.322	
B-Obr-B (deg)	121	123.8	119.9	120	122.7	121

Table 2.1. Calculated and experimental geometries in borate polyhedra and protonated boroxol ring $B_3O_6H_3$ (Tossel and Vaughan 1992)

CHAPTER 3 BORATES AS MINERALS

. . . a geologist's view and a solid state chemist's view

3.1 INTRODUCTION

The beauty and variety of the crystal structures of minerals has long fascinated scientists, and many crystal structures have been determined including several borate structures. These accumulated data helped geologists and solid state chemists to establish empirical concepts of structure and bonding in borates and to develop ideas of the underlying behind them.

On the other hand, the quantum-chemical theory (e.g. Szabo and Ostlund 1989) has its origin in physics. It has helped material scientists to understand complex phenomena with a minimum of empiricism. Although there is no direct equivalence between the empirical concept and the quantum-chemical theory, both approaches can supplement one another and can be used to explain the structure and bonding of materials.

As for quantum-chemical approaches in the simulation of borates, there have been several cluster-type or molecule-type simulations, which have been used not only to discuss the π electron system and the basicity of borates, but which have also succeeded in reproducing bond lengths and bond angles in the crystalline state (see Section 2.5.1). However, such simulations have generally neglected crystal field effects, which are generally thought to be necessary in discussing solids more realistically.

Therefore, in this chapter we present the first results of quantum-chemical calculations on borate crystals in the crystalline state. First, we

explain periodic ab-initio Hartree-Fock methods, which are suitable for the quantum-chemical simulation of crystalline systems, is explained. Next, quantum-chemical results are presented, with emphasis on the Mulliken population analyses (Mulliken 1955), for a variety of crystal structures of borates. These results are then discussed and compared with empirical concepts (for example, Pauling 1960). Finally, we show that these calculations accord well with empirical concepts regarding to the structure and bonding of borates.

3.2 THEORETICAL METHOD

In order to perform the quantum chemical calculations, we used the periodic ab-initio Hartree-Fock code CRYSTAL-92. As the program uses basis sets constructed from atomic orbital (AO) as with standard molecular orbital programs (for example, GAUSSIAN, GAMESS, HONDO, MOPAC, AMPAC), it is easy for chemists to use. Furthermore, calculated properties, such as electron charge density maps and Mulliken charges, can be analyzed using chemical concepts. The details of the theory are described in the monograph of Pisani et al (1988). Here, some computational assumptions and restrictions especially when applying the method to borate crystals are mentioned.

3.2.1 SELECTION OF A MODEL

In solid state physics, plane waves (PW) are usually used as a basis function of crystalline orbitals ψ which satisfy Bloch's theorem:

$$\psi(k;r+g) = \psi(k;r) \exp(ik \cdot g) \qquad (3.1)$$

where r is real-space vector, k is wavevector, and g is a direct lattice vector of the crystal.

Instead of PWs, CRYSTAL-92 uses Bloch functions $\phi_\mu(k)$, constructed from a limited number of local functions $\chi_\mu(r)$:

$$\phi_\mu(k;r) = \Sigma_g \chi_\mu(r-g) \exp(ik \cdot g) \qquad (3.2)$$

The "generating" functions χ_μ are centred at the atomic nuclei and are expressed as a linear combination of Gaussian-type atomic orbitals (GTOs), similar to molecular quantum chemistry techniques.

Generally speaking, the larger number of GTOs which are employed, the more accurate becomes the calculated result within the Hartree-Fock (HF) limit. However, in contrast to the calculation on molecular groups, diffuse Gaussian orbitals (exponent of the order of 0.2

a.u. or less) play a crucial role in crystalline-state calculations and cause two problems (Pisani et al 1988).

The first is that the number of integrals to be explicitly calculated increases dramatically with a decreasing exponent. The second is that on decreasing the exponent the risks of pseudo-linear dependence increase rapidly, demanding higher precision in order to avoid "catastrophic" behaviour.

However, such very diffuse AOs are much less important in three-dimensional densely packed crystals than in atoms and molecules, where they serve to describe the tails of the electronic distribution toward vacuum. Therefore, except for the case of the minimal basis set (STO-3G), starting from the standard Pople's basis set (Pople and Binkley 1975), the exponent of the outermost shell is reoptimized.

Furthermore, in the present version of CRYSTAL-92, large systems cannot be simulated, except at the minimal basis set level, because of restrictions related to the size of vectors and matrices. Therefore, several different basis sets are applied for simulation of small B_2O_3 systems, while only a minimal basis set is applied for other larger systems.

In order to overcome the limitation of system size in the all-electron calculations, pseudopotentials techniques have been developed (Hay and Wadt 1985; Durand and Barthelat 1975; Bouteiller et al 1988). This technique has also been tested for the B_2O_3 systems.

The other possible problem associated with our method may come from electron correlation which can only be represented using post Hartree-Fock techniques (Hehre et al 1986). In addition, however, several correlation correction schemes are available for the HF energy. Here, these precise corrections are not required in this chapter, because only the relative orders in energies or charges are mainly discussed.

3.2.2 OPTIMIZATION OF STRUCTURE

The experimental determination of crystal structures has, of course, associated errors. For example, the positions of hydrogen atoms in boric acid crystals determined by X-ray techniques have errors of as much as 0.1 Å. For this, and for other reasons, it is desirable in simulations to relax not only unit cell dimensions but also internal coordinates. To relax the structure means to search for the structure which has the minimum total energy. However, the automatic relaxation of cell dimensions or internal coordinates is not available in the present version of CRYSTAL. Although manual optimization is possible point by point, it is not efficient.

Therefore, in B_2O_3 crystals cell dimensions and internal coordinates are varied in a point by point manner and the variations in energy are tabulated. These potential energy surface data are also used for modelling interatomic potentials in Chapter 5. In contrast, the calculations on the other borate crystals are carried out using fixed (experimentally determined) cell dimensions and atomic positions. We note that a full relaxation treatment using ab-initio, LDA techniques is possible employing the code CASTEP, as discussed in Chapter 4.

3.2.3 MULLIKEN POPULATION ANALYSIS

It may be useful to define the total electronic charge on a particular atom in order that quantitative meaning may be given to such concepts as electron withdrawing or donating ability. The Mulliken population analysis is one of such methods, and it is often used for discussing the relative covalency and ionicity of materials.

Although Mulliken population analysis is employed in this chapter, some caution is required.

One problem concerns the definitions of 'ionicity' and 'covalency', as discussed by Catlow and Stoneham (1983). There is a considerable arbitrariness in their nature and different charge partitioning schemes exist. Another concerns the high sensitivity of the Mulliken charges to the basis-set (Hehre et al 1986) A third difficulty is that the charges are often not comparable with effective charges obtained from experimental studies, and indeed the absolute value may be meaningless.

In this chapter, only the relative order in the Mulliken charges at different sites and among a variety of structures are used in order to discuss relative degrees of 'ionicity' or 'covalency'.

3.3 PERIODIC AB-INITIO HARTREE-FOCK SIMULATION

3.3.1 MODELS FOR BORON-OXYGEN BONDING

The boron atom has the gas-phase electron configuration: $1s^2$, $2s^2$, $2p^1$. The chief oxidation state of boron is +3 and boron normally combines with oxygen (of electron configuration $1s^2$, $2s^2$, $2p^4$) to form three triangular-planar bonds by sp^2 orbital hybridization. The boron-oxygen radius ratio is 0.20 and from spatial considerations alone, boron would be expected to occur in three- or four-fold coordination. The transition to tetrahedral sp^3 orbital hybridization is facilitated by the easy acceptance of an electron pair from a base into the low-energy fourth orbital of the boron valence shell. The measured B-O bond distances in trigonal borates range from 1.28 to 1.44 Å and the mean is 1.37 Å. The mean tetrahedral bond length is 1.48 Å and the individual values vary from 1.42 to 1.54 Å. For refined structures having an experimental error of ≤0.05 Å, the difference between trigonal and tetrahedral bond lengths of 0.1 Å is significant (Ross and Edwards 1967).

The calculated trigonal B-O bond length, which is the theoretical, single covalent B-O bond distance, is slightly less than 1.43 Å (Pauling 1960); its discrepancy with the measured lengths has been attributed to about 20% double bond character. The measured B-O bond distances in some borate crystals are shown in Table 3.1. The structure and bonding in these crystals are discussed later in this chapter.

Compound	B-O (Å) Triangular BO_3	B-O (Å) Tetrahedral BO_4
Boron Trioxide		
B_2O_3-I	1.337, 1.366, 1.404	
	1.336, 1.384, 1.401	
B_2O_3-II		1.373, 1.506, 1.507, 1.512
Potassium metaborate		
KBO_2	1.331 (in-ring)	
	1.398, 1.398 (out-of-ring)	
Sodium metaborate		
$NaBO_2$	1.280 (in-ring)	
	1.433, 1.433 (out-of-ring)	
Kotoito		
$Mg_3(BO_3)_2$	1.376, 1.392, 1.392	
Magnesium Pyroborate		
$Mg_2B_2O_5$-II	1.35, 1.38, 1.38	
	1.33, 1.33, 1.37	
Calcium Metaborate		
CaB_2O_4-I	1.326, 1.385, 1.401	
Sinhalite		
$AlMgBO_4$		1.442, 1.483, 1.483, 1.586
Orthoboric acid		
$B(OH)_3$	1.356, 1.365, 1.365	
	1.353, 1.359, 1.365	
Metaboric acid		
HBO_2-I		
	1.345, 1.371, 1.386	
	1.356, 1.366, 1.378	
		1.433, 1.451, 1.452, 1.553
HBO_2-II		
		1.436, 1.465, 1.482, 1.505
HBO_2-III		
	1.373, 1.377,	
	1.391, 1.353,	
	1.372, 1.372 (in-ring)	
	1.351, 1.367, 1.347 (out-of-ring)	

Table 3.1. B-O bond distances in borate minerals (References are found in the text.)

3.3.2 BORON TRIOXIDE CRYSTALS

The outline of B_2O_3 crystal structures is reviewed in Section 2.1.

3.3.2.1 BASIS SET EFFECTS

The basis set plays a crucial role in the description of crystalline orbitals. Starting from the standard Pople's basis sets, the exponents of outer shell are reoptimized. The reoptimized exponents and the Mulliken charges are compared in Table 3.2 and 3.3.

i. *Minimal basis set*

As generally recognized, the Mulliken charges obtained employing STO-3G tend to be smaller than with other basis sets (Hehre et al 1986). The bigger problem is that the STO-3G result in B_2O_3-II is not consistent with the results of the other basis sets. The Mulliken charge on O(2) seems to be too small and that on O(1) is larger than expected. O(1) is two-fold coordinated by boron which is the same in B_2O_3-I, while O(2) has three-fold coordination (see Figure 2.3). The two charge distributions are expected to be different, which is difficult to express by using minimal basis set. Therefore, caution is needed when a minimal basis set is applied to three-fold coordinated oxygen or four-fold coordinated boron.

ii. *Split-valence and polarization function*

As even B_2O_3 crystals represent a large system, basis set better than 6-21G, such as 8-51G, are not possible in the present version of CRYSTAL. For both polymorphs, the 6-21G basis set may be assumed to be good basis set, as Dovesi et al (1987) and Nada (1990) suggested for SiO_2. The 3-21G basis set gives almost the same result as that for 6-21G.

We investigated the effect of adding a single Gaussian d-type function to boron, because such a polarization function proved to be useful in SiO_2 for describing the distortion of cation orbitals in the different environments (Nada 1990). However, in B_2O_3-I crystal the

Mulliken charges are reduced unexpectedly. The reason for this trend could be the BSSE (Basis Set Superposition Error) (see, for example, Clark 1985). That is, the extra orbitals on boron are used to improve the description of the charge distribution around oxygen.

iii. *Pseudopotentials*

All electron calculations restrict the feasible system size. In order to overcome this problem, several types of pseudopotentials have been developed. In these pseudopotential techniques the role of core electrons are substituted by the effective core potentials and only the orbitals of valence electrons are calculated. Here only one available set, PS-31G (Bouteiller 1988), is tested. The original PS-31G sets were optimized for atoms and tested only on small molecule. Therefore, the exponents of outermost shell were reoptimized. The Mulliken charges turned out to be larger than those calculated with the all electron cases. This may be due to electron rich second shells, which are composed of three gaussians, whereas the second shell in the other all-electron calculations were composed of two gaussians. The order of the charges seems reasonable, but it is difficult to evaluate these pseudopotentials, because they have not been fully tested for the crystalline state. However, these results show that the pseudopotential technique is promising. If refined these pseudopotentials could become a powerful tool for calculations on larger systems.

3.3.2.2 GEOMETRY OPTIMIZATION

In order to check the accuracy of our calculations, unit cell dimensions were optimized using the 3-21G basis set. The experimental lattice parameters and atomic parameters are given in Table 3.4. The interatomic distances and interbond angles are also reported in Table 3.5,

while the calculated energies are summarized in Table 3.6. The errors in the unit cell volume are 1.5% for B2O3-I and 1.5% for B_2O_3-II. The errors in the lattice parameters are 1% for either crystal structure. The atomic parameters are also varied in a point by point manner using the 3-21G basis set. The calculated results are shown Table 3.7. Regarding to the B-O bond lengths, only the error in B-O(1) bond (the shortest B-O bond) of B_2O_3-II is 10% and all the other errors are within 5%. On the other hand, all the errors in O-B-O bond angles are within 5%. When the general accuracy of 3-21G basis set is taken into account, these calculations reproduce both crystal structures well. The optimized geometry is also discussed in Chapter 4.

3.3.2.3 DISCUSSION

The average experimental B-O bond distance of 1.372 Å in B_2O_3-I agrees well with the length assumed by Zachariasen (1963) for a bond of 'strength' 1.0 (1.365 Å), and also with a value of 1.37±0.02 Å which was quoted as the mean B-O distance for three-coordinated boron by Waugh (1968).

When the charges of three different oxygen in B_2O_3-I are compared, the charge of O(3) is larger than those of the other two oxygens. Gurr et al (1970) distinguished O(3) for the other oxygen atoms by using the term ' higher coordination' of O(3) through which adjacent ribbons are linked, although O(3) is two-fold coordinated as well as O(1) or O(3). Here, Madelung potentials (i.e. the total Coulomb contributions from all atoms) are calculated as -66.42, -65.49 and -67.18 for O(1), O(2) and O(3). The Madelung potential of O(3) is larger than those of the other oxygens. In agreement with Gurr's interpretation, it is the obvious explanation for the large Mulliken charge of O(3).

Regarding B_2O_3-I, the near planar shape of the BO_3 triangle and the small Mulliken charges emphasize the partially covalent character, while the distortion of the triangle and the larger Mulliken charge of O(3) indicate the presence of some ionic character.

On the other hand, the average B-O distance for B_2O_3-II is 1.475 Å, exactly that proposed by Zachariasen (1963) as an average tetrahedral B-O distance. However, the tetrahedron is very distorted, with one short B-O(1) distance of 1.373 Å and three long B-O(2) distances of 1.507, 1.506 and 1.512 Å. O(1) is two-fold coordinated, while O(2) is three-fold coordinated.

Prewitt and Shannon (1968) calculated electrostatic bond strengths in B_2O_3-II using Zachariasen's table of bond strength versus B-O bond length (Zachariasen 1963). The calculated net bond strength is 3.01 around B, 1.96 around O(1), and 2.03 around O(2). They concluded that the distortions are necessary to balance the electrostatic charge in the crystal.

When the Mulliken charges of the four different oxygens in B_2O_3-II (except in the case of minimal basis set) are compared, the charge of O(1) is found to be much smaller than the others. It is also interesting to note that the O-O distances of the four oxygens are almost same, although the distance of B and O(1) is shorter than the others. This means that the tetrahedral arrangement of the four oxygens is not very distorted; but rather within the tetrahedron, B approaches to O(1). Therefore, it seems reasonable to assume that the difference in coordination number around oxygen chiefly changes B-O bond strength rather than the O-O repulsion in the interatomic potential model for the system. To check whether the distortion can be explained in terms of charge transfer between boron and oxygen atoms, we performed lattice energy minimizations using a simple rigid ion model. Such a model, which assigns the Mulliken

charge to each atom, cannot, however, explain the short B-O(1) bond length, because the B-O(1) distance becomes longer, if the charge of O(1) is set to be smaller since the attraction between B and O(1) is reduced. However, the other interpretation namely that B-B repulsion shortens the B-O bond length is also possible. But the results of a perfect lattice relaxation simulation, discussed in Chapter 5, show that the change in the B-O bond strength can reproduce the detailed structure better than can be achieved by changing the B-B repulsive term.

Next, the bond lengths in B_2O_3-I and B_2O_3-II are compared. As Johnson et al (1982) pointed out, one short bond B-O(1) distance (1.373 Å) in B_2O_3-II (1.373 Å) is close to the average B-O distance in B_2O_3-I (1.372 Å) and in B_2O_3 glass (1.37Å). The calculated Mulliken charges also show that the charge of O(1) in B_2O_3-II (-0.708 with STO3-21G) is close to the average oxygen charge in B_2O_3-I (-0.698 with STO3-21G). Regarding the two B_2O_3 crystal structures, it is interesting to note that the coordination number of boron around oxygen seems to affect the B-O distance much, more than the coordination around the boron.

To sum up, B_2O_3-II is more ionic than B_2O_3 -I, which is compatible with the idea that a high-pressure form or high-coordination form is generally thought to be more ionic. The difference in the Mulliken charges agrees with Pauling's electrostatic valence sum rule in terms of the explanation of the short B-O bond length in B_2O_3-II. This acquired knowledge will be utilized in the development of interatomic potentials in Chapter 5.

basis set	boron	oxygen
3-21G	0.15	0.40
3-21G*	0.15, 0.60	-----
6-21G	0.12	0.40
PS31G	0.21	0.30

Table 3.2. Reoptimized exponents of outer shell for B_2O_3-I and B_2O_3-II

B_2O_3-I

basis set boron/oxygen	B(1)	B(2)	O(1)	O(2)	O(3)	E (a.u./B_2O_3)
STO-3G/3G	+0.664	+0.661	-0.439	-0.435	-0.451	-270.6795
3-21G/3-21G	+1.048	+1.046	-0.688	-0.685	-0.721	-272.8511
3-21G*/3-21G	+0.792	+0.693	-0.446	-0.473	-0.466	-272.9254
6-21G/6-21G	+1.010	+1.005	-0.661	-0.660	-0.694	-273.9886
PS31G/PS31G	+1.404	+1.405	-0.925	-0.925	-0.959	----

B_2O_3-II

basis set boron/oxygen	B(1)	O(1)	O(2)	E(a.u./B_2O_3)
STO-3G/3G	+0.659	-0.488	-0.415	-270.7587
3-21G/3-21G	+1.164	-0.708	-0.810	-272.8709
6-21G/6-21G	+1.128	-0.677	-0.790	-274.0111
PS31G/PS31G	+1.569	-0.947	-1.095	----------

Table 3.3. Net Mulliken charges and total energies for B_2O_3-I and B_2O_3-II

B_2O_3-I	space group $P3_1$ (trigonal)		
	a = b = 4.339 Å, c = 8.340 Å		
	x	y	z
B(1)	0.2229	0.3926	-0.0198
O(1)	0.5468	0.3972	0.0
O(2)	0.1485	0.6004	0.0775
O(3)	0.0045	0.1608	-0.1291

B_2O_3-II	space group $Ccm2_1$ (orthorhombic)		
	x	y	z
B(1)	0.1646	0.1606	0.4335
O(1)	0.	0.3475	0.5
O(2)	0.2911	0.3698	0.5802

Table 3.4. Experimental lattice parameters and atomic parameters in B_2O_3-I and B_2O_3-II (Gurr et al 1970; Prewitt et al 1968)

B_2O_3-I		B_2O_3-II	
	Distances (Å)		Distances (Å)
B(1)-O(1)	1.404	B(1)-O(1)	1.373
-O(2)	1.366	-O(2)	1.507
-O(3)	1.337	-O(2)'	1.506
B(2)-O(1)	1.336	-O(2'')	1.512
-O(2')	1.400	O(1)-O(2)	2.364
-O(3')	1.384	-O(2')	2.440
O(1)-O(2)	2.387, 2.388	-O(2'')	2.409
O(2)-O(3)	2.409, 2.333	O(2)-O(2')	2.428
O(3)-O(1)	2.309, 2.408	-O(2'')	2.394
B(1)-B(2)	2.489, 2.489,	O(2')-O(2'')	2.388
	2.498	B(1)-B(1')	2.569
		-B(1'')	2.664
		-B(1''')	2.664
		-B(1'''')	2.592
Angles (deg)			
O(1)-B(1)-O(2)	119.0	O(1)-B(1)-O(2)	110.2
-O(3)	114.7	-O(2')	115.8
O(2)-B(1)-O(3)	126.1	-O(2'')	113.1
O(1)-B(2)-O(2)	121.5	O(2)-B(1)-O(2')	107.4
-O(3)	124.6	-O(2'')	104.9
O(2)-B(2)-O(3)	113.8	O(2')-B-O(2'')	104.7
B(1)-O(1)-B(2)	130.5	B(1)-O(1)-B(1')	138.6
-O(2)-B(2)	128.3	-O(2)-B(1'')	123.8
-O(3)-B(2)	133.4	-O(2'')-B(1''')	123.8
		-O(2')-B(1'''')	118.7

Table 3.5. Interatomic distances and interbond angles for B_2O_3-I and B_2O_3-II (Gurr et al 1970; Prewitt et al 1968)

1) $(v/v_0)^{1/3}$	B_2O_3-I ΔE(a.u./B_2O_3)	B_2O_3-II ΔE(a.u./B_2O_3)
1.08	+0.05575	
1.06	+0.03150	
1.04	+0.01348	
1.02	+0.00261	
1.01	+0.00021	-0.00021
1.005	-0.00019 @	-0.00044 @
1.0	0	0
0.995	+0.00077	+0.00100
0.99	+0.00210	+0.00273
0.98	+0.00661	
0.96	+0.02299	

Table 3.6. Potential energies with different lattice parameters for B_2O_3-I and B_2O_3-II (@ indicate the minimum point)

	B_2O_3-I	B_2O_3-II
	ΔE(a.u./B_2O_3)	ΔE(a.u./B_2O_3)
2) a/a_0		
1.02	+0.00136	-0.00066
1.01	+0.00002	-0.00072 @
1.0	0 @	0
0.99	+0.00128	+0.00154
0.98		+0.00395
3) b/b_0		
1.04		+0.01281
1.02		+0.00050
1.01		-0.00002 @
1.0		0
0.99		+0.00052
0.98		+0.00158
4) c/c_0		
1.03	+0.00022	
1.02	+0.00013	+0.00136
1.01	-0.00020 @	+0.00002
1.0	0	0 @
0.99		+0.00128
0.98	+0.00119	

Table 3.6.(continued) Potential energies with different lattice parameters for B_2O_3-I and B_2O_3-II (@ indicate the minimum point)

B_2O_3-I		ΔE (a.u./B_2O_3)			
change of bond length	(Å)				
		-10%	-5%	+5%	+10%
R (B-O(3))	1.337	+0.03754	+0.01590	+0.00166	+0.01341
R (B-O(1))	1.404	+0.02061	+0.00318	+0.00823	+0.02614
R (B-O(2))	1.366	+0.02740	+0.00685	+0.01691	+0.00406
change of bond angle	(deg)				
		-10°	-5°	+5°	+10°
∠ O(1)-B-O(3)	114.8			+0.00711	+0.02535
∠ O(2)-B-O(3)	126.1	+0.02398	+0.00326		
∠ O(1)-B-O(3)	114.8			+0.00702	+0.02985
∠ O(2)-B-O(1)	119.0	+0.05140	+0.01452		
∠ O(2)-B-O(3)	126.1			+0.00669	+0.03270
∠ O(2)-B-O(1)	119.0	+0.01016	+0.03480		

B_2O_3-II		ΔE (a.u./B_2O_3)			
change of bond length	(Å)				
		-10%	-5%	+5%	+10%
R (B-O(1))	1.373	+0.00111			-0.00003
R (B-O(2))	1.507	+0.01001	+0.00814		
change of bond angle	(deg)				
		-10°	-5°	+5°	+10°
∠ O(2)-B-O(2)''	104.9		+0.00769		
∠ O(2)-B-O(1)	110.2		+0.01064		

Table 3.7. Potential energies with different internal coordinates for B_2O_3-I and B_2O_3-II

3.3.3 ALKALI BORATES

Only a minimal basis set was applied in the modelling of sodium metaborate ($NaBO_2$) (Fang 1938; Marezio et al 1963) and potassium metaborate (KBO_2) (Zachariasen 1937; Schneider and Carpenter 1970). It is interesting to note that these isostructural compounds contain the metaborate ion $B_3O_6^{3-}$ (see Figure 2.9). The interatomic distances are shown in Table 3.8. The calculated Mulliken charges are shown in Figure 3.1 and 3.2.

In order to explain the observed deformation within the BO_3 triangles (that is, the distance of B-O(1) outside the ring is longer than that of B-O(2) in the ring), Zachariasen (1937) pointed out that in the covalent interpretation $B_3O_6^{3-}$ has 'resonates' between three electronic structures (one structure is stronger than the other two), while in the ionic interpretation the repulsion between boron ions may be responsible. Schneider and Carpenter (1970) used the interpretation of Pauling (1945) that the fourth orbital of boron is used to form a double bond formation.

From the Mulliken analysis, the charge on the oxygen outside the ring (O1) is larger than that in the ring (O2). It seems reasonable to assume that the charge transfer from the alkali atom to O(1) tightens the B-O(1) bonding outside the ring rather than B-O(2) bonding inside the ring. When the results on $NaBO_2$ are compared with those on KBO_2, we can propose that the B-O(1) π bonding is strengthened while the B-O(2) π bonding is weakened. It is also found that O(1)-O(2) distances are almost the same in the two compounds, although the O(2)-O(2) distances are a little different. The changes in boron-oxygen bonding seems to be able to explain the features of these structures better than changes in the oxygen-oxygen or boron-boron repulsion.

The comparison of the Mulliken charges with those calculated for the B_2O_3 crystals (Table 3.3) shows that the oxygen ions becomes more ionic while the charges on the borons are reduced by the introduction of the alkali metal oxide. The charges on the oxygens increase in the order:

B_2O_3-I < B_2O_3-II < alkali borates

However, some knowledge of the acid-base relationships in alkali borate glasses suggested the following changes in the structure of the borate lattice on increasing the alkali metal oxide content (see, for example, Paul 1982):

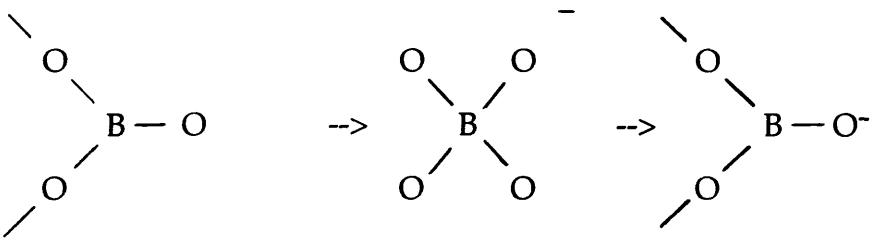

The order of the calculated Mulliken charges agrees with the above models.

M = Na or K		**$NaBO_2$**	**KBO_2**
		Distances (Å)	Distances (Å)
B-O(1)	x1	1.280	1.331
B-O(2)	x2	1.433	1.398
O(1)-O(2)	x2	2.383	2.381
O(2)-O(2)	x1	2.410	2.389
M-O(1)	x1	2.461	2.849
M-O(1)	x2	2.474	2.801
M-O(1)	x2	2.607	2.835
M-O(2)	x2	2.482	2.775

Table 3.8. Interatomic distances in $NaBO_2$ and KBO_2 (Marezio et al 1963; Schneider and Carpenter 1970)

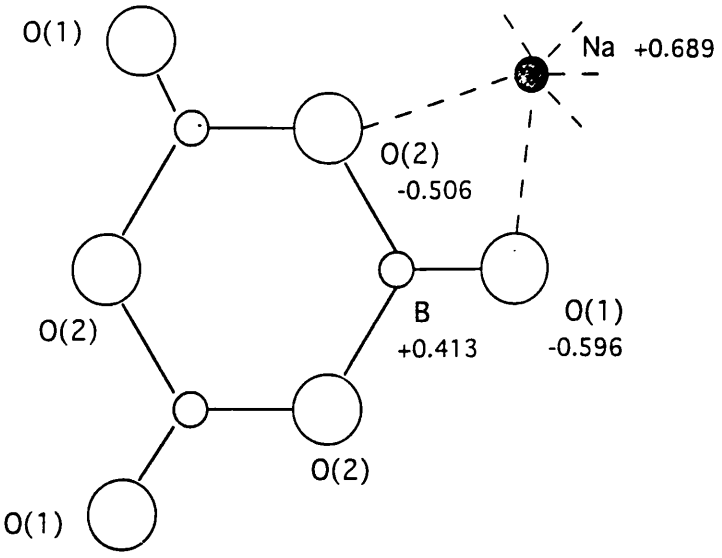

Figure 3.1 The net Mulliken charges in NaBO2

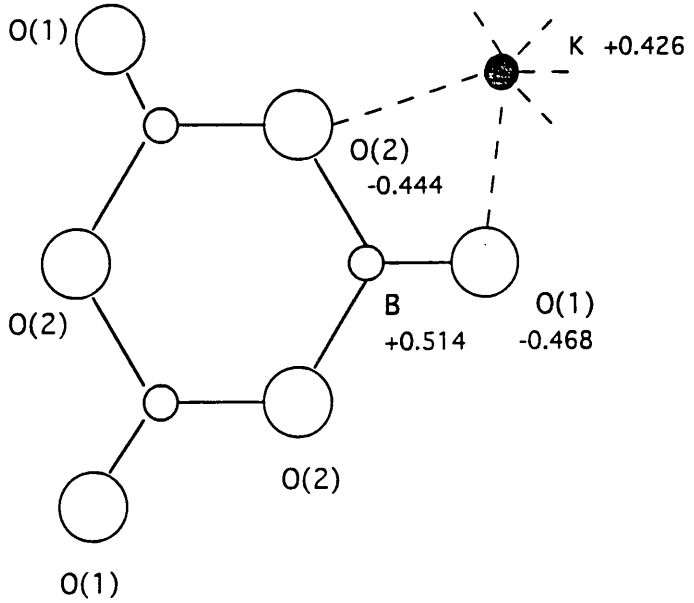

Figure 3.2 The net Mulliken Charges in KBO2

3.3.4 ALKALINE-EARTH BORATES

We have used a minimal basis set to study a number of alkaline-earth borates; $Mg_3(BO_3)_2$ (Kotoito) (Effenberger and Pertlik 1984), $Mg_2B_2O_5$-II (Takeuchi 1952), CaB_2O_4-I (Marezio 1963) and $AlMgBO_4$ (Fang and Newnham 1965; Hayward 1993). These compounds have different structural units. They consist of discrete BO_3, discrete B_2O_5, infinite BO_3 chains and discrete BO_4 units respectively. Their interatomic distances are given in Table 3.9 and 3.10. The calculated Mulliken charges are shown in Figure 3.4 to 3.6.

When the geometry of the BO_3 unit in $Mg_3(BO_3)_2$ is compared with that in $NaBO_2$, the difference in the B-O distances is small, but the difference in the O-O distances is larger, that is, the BO_3 triangle is more distorted. The calculated Mulliken charges of the oxygens in $Mg_3(BO_3)_2$ are larger than in B_2O_3-I and in the two alkali borates. This suggests that this compound is more ionic. This appears to be reasonable when the modifier oxide ratio is taken into account, MgO/B_2O_3 (mole ratio) is 3 in $Mg_3(BO_3)_2$, while Na_2O/B_2O_3 or K_2O/B_2O_3 is 1 in $NaBO_2$ or KBO_2. Generally speaking, the larger the proportion of modifier oxide, the more ionic the compound. The distortion of the BO_3 triangle may be explained using the ionic model from which we would expect that the shared edge between the BO_3 triangle and the MgO_6 octahedron is distorted.

For $Mg_2B_2O_5$-II, the MgO/B_2O_3 mole ratio is 2 and the charges of the oxygen atoms are reduced a little, relative to $Mg_3(BO_3)_2$. The Mulliken charge of the bridging oxygen O(3) is smaller than the others, because O(3) is coordinated by one magnesium atom, while the other oxygens are coordinated with two or three magnesium atoms.

In CaB_2O_4-I crystal, the non-bridging B-O(1) distance (1.325 Å) is much shorter than the bridging B-O(2) distance (1.385 Å) and the B-O(2')

distance (1.401 Å). The Mulliken analysis shows that the O(1) charge is larger than the O(2) charge. Therefore, B-O(1) bonding may have double bond character, as shown in the case of alkali borates. In common with $Mg_3(BO_3)_2$ we find that the BO_3 triangle is distorted.

$AlMgBO_4$ is made up of BO_4 tetrahedra, AlO_6 octahedra and MgO_6 octahedra. It is interesting to note that one B-O(2) distance is much larger than the other B-O distances. Hayward (1993) concluded that the long B-O bond length is due to the repulsion between boron and two neighbouring aluminiums. However, another interpretation is also possible when the analysis posed on the structures of B_2O_3 crystals are taken into account, where the calculated oxygen charges are almost same. The geometry suggests that charge is more easily transferred from Al and Mg to O(2) than to O(1) or O(3). Therefore, in order to balance the oxygen charges, B-O(1) or B-O(3) bonds may become stronger and shorter than B-O(2) bonding.

Compared with B_2O_3 crystals, the alkaline-earth borates show some ionic features, that is, not only is the B-O distance changed, but also the BO_3 triangle or BO_4 tetrahedra are distorted. Furthermore, as the modifier oxide ratios increase, the Mulliken charges show higher charges. This corresponds with the increasing tendency for the 'borate' structural unit to become discrete unit as the number of non-bridging oxygens increases. In the glass field, similar behaviour is observed when the B-O network becomes depolymerized by the introduction of modifier oxide.

$Mg_3(BO_3)_2$		$Mg_2B_2O_5$-II	
	Distances (Å)		Distances (Å)
B-O(1)	1.376	B(1)-O(1)	1.35
B-O(2) x2	1.392	B(1)-O(2)	1.38
Mg(1)-O(1) x2	2.071	B(1)-O(3)	1.38
Mg(1)-O(2) x4	2.090	B(2)-O(3)	1.37
Mg(2)-O(1) x2	2.161	B(2)-O(4)	1.33
Mg(2)-O(2) x2	2.049	B(2)-O(5)	1.33
Mg(2')-O(2') x2	2.120	Mg(1)-O(3)	2.09
O(1)-O(2) x2	2.431	Mg(1)-O(4')	2.19
O(2)-O(2')	2.335	Mg(1)-O(1)	2.29
		Mg(1)-O(1'')	2.29
		Mg(1)-O(5')	2.03
		Mg(1)-O(5'')	2.03
		Mg(2)-O(1)	1.95
		Mg(2)-O(2'')	2.43
		Mg(2)-O(4')	2.19
		Mg(2)-O(4'')	2.19
		Mg(2)-O(2')	1.96
		Mg(2)-O(2'')	2.19
		O(1)-O(2)	2.41
		O(1)-O(3)	2.36
		O(2)-O(3)	2.38
		O(3)-O(4)	2.33
		O(3)-O(5)	2.34
		O(4)-O(5)	2.40

Table 3.9. Interatomic distances in $Mg_3(BO_3)_2$ and $Mg_2B_2O_5$-II (Effenberger and Pertlik 1984; Takeuchi 1952)

CaB_2O_4-I		$AlMgBO_4$	
	Distances (Å)		Distances (Å)
B-O(1)	1.326	B-O(1)	1.442
B-O(2)	1.385	B-O(2)	1.586
B-O(2')	1.401	B-O(3) x2	1.483
Ca-O(1) x2	2.347	Al-O(1) x2	1.978
Ca-O(1) x2	2.399	Al-O(2) x2	1.853
Ca-O(1) x2	2.727	Al-O(3) x2	1.877
Ca-O(2) x2	2.549	Mg-O(1)	2.202
O(1)-O(2)	2.319	Mg-O(2)	2.035
O(1)-O(2')	2.440	Mg-O(3) x2	2.119
O(2)-O(2')	2.356	Mg-O(3) x2	2.038
		O(1)-O(2)	2.543
		O(1)-O(3)	2.480
		O(2)-O(3)	2.354
		O(3)-O(3)	2.403

Table 3.10. Interatomic distances in CaB_2O_4-I and $AlMgBO_4$ (Marezio et al 1963; Hayward 1993)

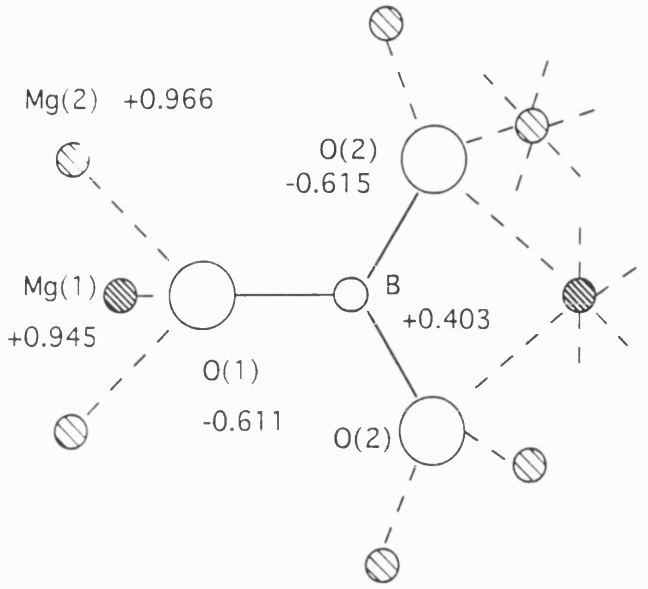

Figure 3.3 The net Mulliken charge in Mg3(BO3)2

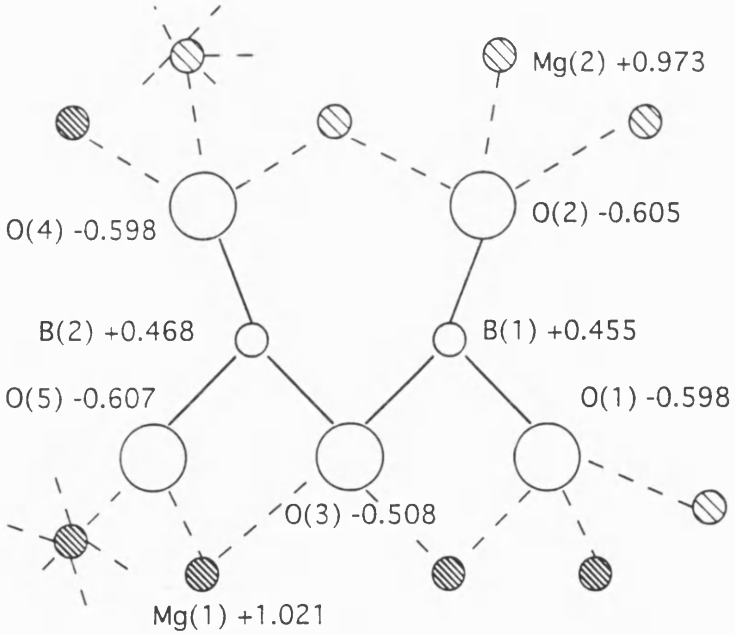

Figure 3.4 The net Mulliken charges in Mg2B2O5-II

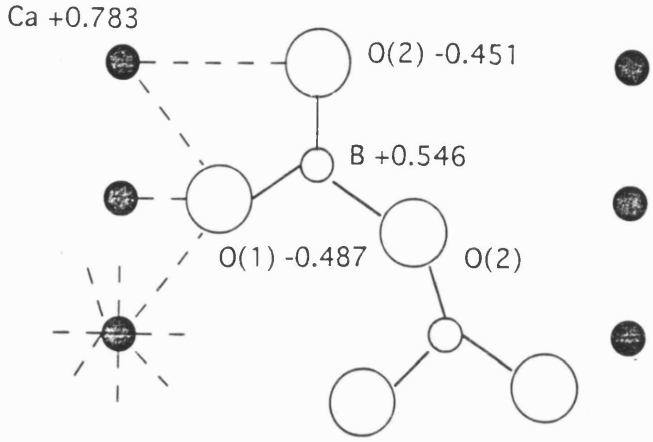

Figure 3.5 The net Mulliken charges in CaB2O4-I

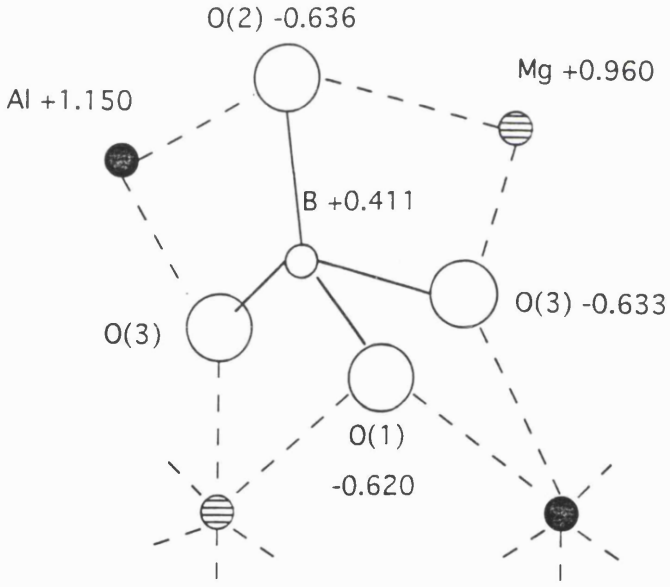

Figure 3.6 The net Mulliken charges in AlMgBO4

3.3.5 BORIC ACID CRYSTALS

Four crystal structures of boric acid have been determined. The first is $B(OH)_3$, orthoboric acid (Zachariasen 1934; Zachariasen 1954). It is built up of $B(OH)_3$ molecules (Figure 3.3). The other three are HBO_2, metaboric acid. HBO_2-I consists of a three-dimensional network of BO_4 tetrahedra (Zachariasen 1963); HBO_2-II consists of infinite zigzag chains $[B_3O_4(OH)(OH_2)]_\infty$ (complex of BO_3 group) (Zachariasen 1963); HBO_2-III consists of planar B_3O_6 groups (Tazaki 1940; Peters and Milberg 1964). It is interesting to note that $B(OH)_3$ and HBO_2-III have layer-type structures, while HBO_2-III is based on boroxol rings. The interatomic distances and the Mulliken charges are shown in Table 3.11 to 3.12 and in Figure 3.7 to 3.10. Only the HBO_2-I could not be simulated because of the restrictions of the code related to the size of vectors and matrices.

$B(OH)_3$ is similar to B_2O_3-I, except that $B(OH)_3$ molecules are linked together by hydrogen bonds. When we compare its Mulliken charges with those of B_2O_3-I, $B(OH)_3$ has larger oxygen charges. Therefore, it may be said that hydrogen has the same role as alkali metals and alkaline-earth metals as a electron donor.

HBO_2-III is similar to $NaBO_2$ or KBO_2, with B-O distances outside the ring shorter than those in the ring. The reason is that B-O bonding outside the ring has a double bonding character, as in the case of alkali borates.

HBO_2-II has a more complex structure. O(5) and O(6) are a little different from the other oxygens. They are connected to only one boron, while the other oxygens are connected to two borons. O(5) is thought to be the oxygen of a hydroxyl group and O(6) is thought to be the oxygen of a water molecule (Zachariasen 1963). These features are compatible with the largest oxygen charge in case of O(5) and a smallest oxygen charge in

case of O(6) in the Mulliken analysis. However, as long as a minimal basis set is employed, it is difficult to obtain more details.

To summarize, boric acid crystals have an ionic character which is intermediate between these of B_2O_3 and alkali borates from the view point of the effective charges given by the Mulliken population analysis.

$B(OH)_3$		**HBO_2-I**	
	Distances (Å)		Distances (Å)
B(1)-O(1)	1.365	B-O(1)	1.436
B(1)-O(2)	1.365	B-O(1')	1.465
B(1)-O(3)	1.365	B-O(2)	1.505
B(2)-O(4)	1.365	B-O(2')	1.482
B(2)-O(5)	1.353	O(1)-O(1')	2.413
B(2)-O(6)	1.359	O(1)-O(2)	2.431
O(1)-O(2)	2.351	O(1)-O(2')	2.360
O(2)-O(3)	2.359	O(1')-O(2)	2.381
O(3)-O(1)	2.366	O(1')-O(2')	2.421
O(4)-O(5)	2.339	O(2)-O(2')	2.412
O(5)-O(6)	2.360	H...O(1)	1.43
O(6)-O(4)	2.362	H-O(2'')	1.06
O(1)-H(1)	0.83	O(1)...H-O(2'')	2.487
O(2)-H(2)	0.96		
O(3)-H(3)	0.90		
O(4)-H(4)	0.83		
O(5)-H(5)	0.80		
O(6)-H(6)	0.96		
O(1)-H(1)...O(5)	2.727		
O(2)-H(2)...O(4)	2.716		
O(3)-H(3)...O(6)	2.715		
O(4)-H(4)...O(3)	2.722		
O(5)-H(5)...O(2)	2.734		
O(6)-H(6)...O(1)	2.707		

Table 3.11. Interatomic distances in $B(OH)_3$ and HBO_2-I (Zachariasen 1954,1963)

HBO_2-II		HBO_2-III		
	Distances (Å)		Distances (Å)	
B(1)-O(1)	1.345	B(1)-O(2)	1.373	(in-ring)
B(1)-O(2)	1.371	B(1)-O(4)	1.377	(in-ring)
B(1)-O(3)	1.386	B(2)-O(2)	1.391	(in-ring)
B(2)-O(3)	1.378	B(2)-O(5)	1.353	(in-ring)
B(2)-O(4)	1.354	B(3)-O(4)	1.372	(in-ring)
B(2)-O(5)	1.366	B(3)-O(5)	1.372	(in-ring)
B(3)-O(1')	1.433	B(1)-O(1)	1.351	
B(3)-O(2)	1.452	B(2)-O(3)	1.367	
B(3)-O(4)	1.451	B(3)-O(6)	1.347	
B(3)-O(6)	1.553	O(1)-O(4)	2.376	
O(1)-O(2)	2.335	O(1)-O(2)	2.340	
O(2)-O(3)	2.392	O(2)-O(4)	2.385	
O(1)-O(3)	2.380	O(3)-O(2)	2.410	
O(3)-O(4)	2.378	O(2)-O(5)	2.384	
O(3)-O(5)	2.350	O(6)-O(4)	2.381	
O(4)-O(5)	2.368	O(6)-O(5)	2.335	
O(1')-O(6)	2.423	O(4)-O(5)	2.367	
O(1')-O(2)	2.449	O(1)-H(1)	0.90	
O(1')-O(4)	2.333	O(3)-H(2)	0.80	
O(2)-O(4)	2.423	O(6)-H(3)	0.92	
O(2)-O(6)	2.386	O(3)-H(2)...O(1)	2.680	(in-layer)
O(4)-O(6)	2.325	O(6)-H(3)...O(3)	2.748	(in-layer)
H(1)-O(6)	0.87	O(1)-H(1)...O(6)	2.827	(in-layer)
H(1)...O(5)	1.84	O(1)...H(2)	1.88	(in-layer)
O(6)-H(1)...O(5)	2.676	O(3)...H(3)	1.88	(in-layer)
H(2)-O(5)	0.89	O(6)...H(1)	1.91	(in-layer)
H(2)...O(4)	1.80			
O(5)-H(2)...O(4)	2.685			
H(3)-O(6)	1.10			
H(3)-O(2)	1.57			
O(6)-H(3)...O(2)	2.683			

Table 3.12. Interatomic distances in HBO_2-II and HBO_2-III (Zachariasen 1963; Peters and Milberg 1964)

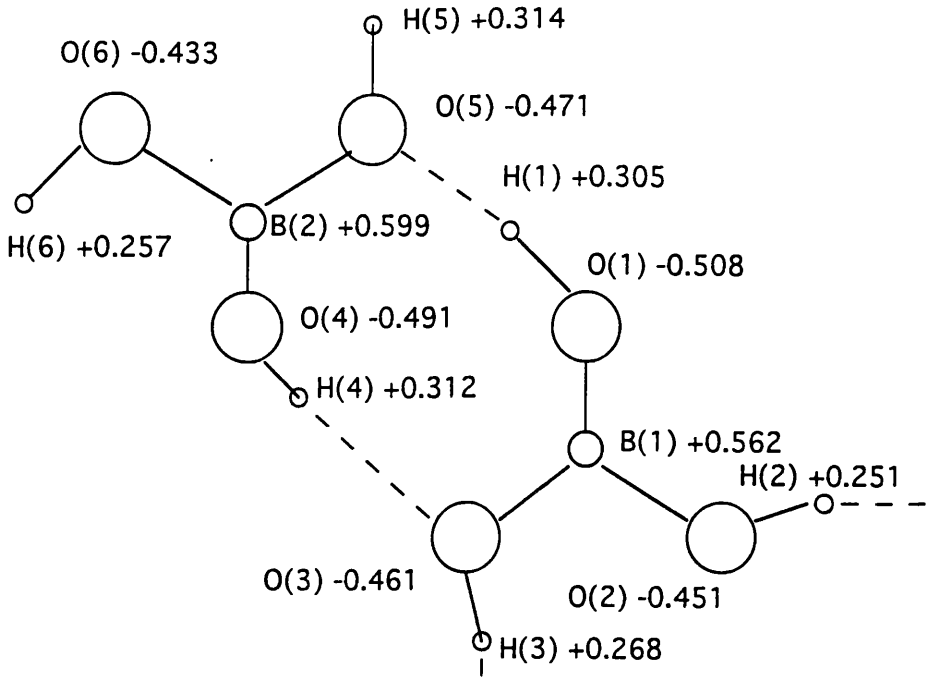

Figure 3.7 The net Mulliken charges in B(OH)3

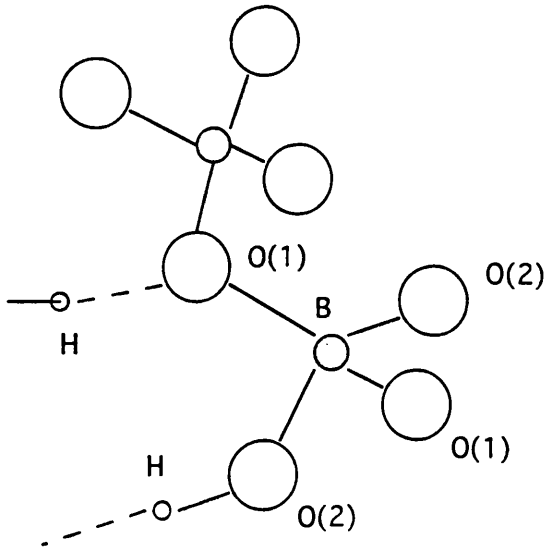

Figure 3.8 The crystal structure of HBO2-I

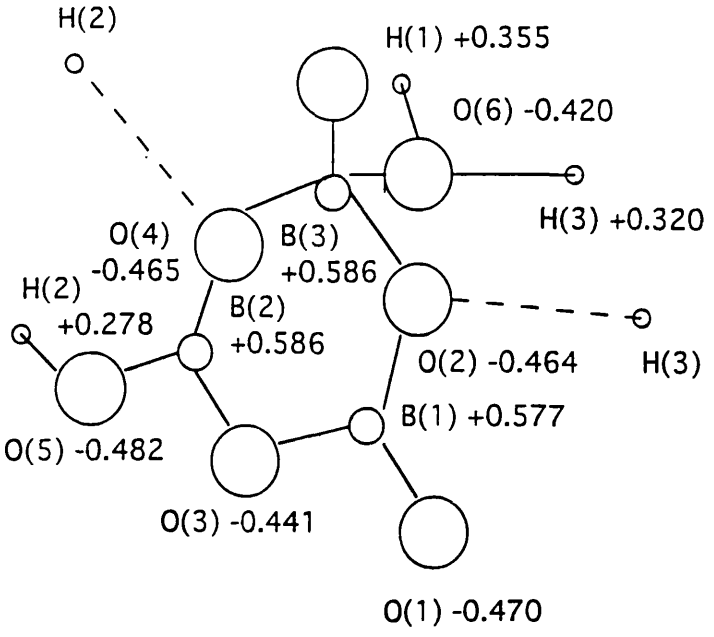

Figure 3.9 The net Mulliken charges in HBO2-II

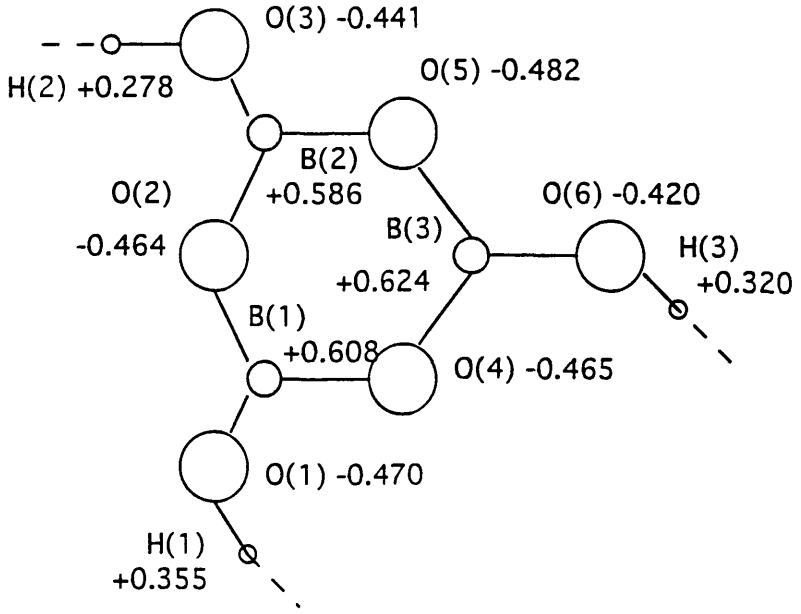

Figure 3.10 The net Mulliken charges in HBO2-III

3.4 CONCLUSION

The following general features concerning the structure and bonding in borate crystals have been suggested by the quantum-chemical calculations reported in this chapter.

i. When borate crystal include modifier oxide (alkali, alkaline-earth or water), they show a variety of structural units Generally speaking, as the content of modifier oxide increases the oxygen charges become more ionic.

ii. When the 'borate' structural unit is a BO_3 triangle, it shows some covalent character, especially when charge is transferred from modifier cations to oxygens; B-O bonding of non-bridging oxygens can be assumed to be strengthened. In other words, it has a double bonding character. It is interesting to find that the 'floppy' boron moves rather than the oxygen frame being distorted. This trend is not noticeable in silicates.

iii. When the ' borate' structural unit is a BO_4 tetrahedron, it shows some ionic character. The tetrahedron is often distorted, because its edges are shared with the other polyhedra. On the other hand, one B-O distance often becomes longer or shorter than the other B-O distances. Pauling's electrostatic valence sum rule or the distortion of the shared edge between different polygons can explain this phenomena.

This variety of structure and bonding in borates may suggest a possibility for other polymorphs of B_2O_3 crystal and also the existence of boroxol ring in B_2O_3 glasses. The knowledge obtained from this analysis will be utilized in developing interatomic potential models discussed in Chapter 5 and 6.

CHAPTER 4 BORON TRIOXIDE AS CRYSTALLINE SOLID

. . . a solid state physicist's view

4.1 INTRODUCTION

Neither form of crystalline boron trioxide occurs naturally. Furthermore, it is not easy even under special conditions to prepare crystals and measure their properties. In such cases computer simulations can play a important role in determining the structural and physical properties. This is because advances in the state of electronic structure calculations make it possible to calculate total energies with high accuracy and computer simulations from first-principles are now possible. These computer simulation techniques are currently used to study not only static but also dynamical structures in both the crystalline and amorphous states, although there are still considerable limitations on the size of system (e.g. the number of independent atoms in unit cell) that can be studied because of the constants imposed by computer resources.

In this chapter we discuss how the structures and bulk moduli of B_2O_3 crystals have been determined employing the LDF electronic structure methods rather than the Hartree-Fock techniques described in Chapter 3. Calculations were performed employing the code CASTEP (Payne et al 1992), which is a powerful program code for total energy pseudopotential calculation. CASTEP has two distinctive features: one is that the internal coordinates can be automatically relaxed so that the structure with the minimum total energy is obtained; the other is that it has the option of ab-initio Molecular Dynamics simulation (Car and Parrinello 1985), although this was not applied to B_2O_3, as it would have required an enormous amount of computer resources.

First, we explain the contrast between the theoretical approaches adopted in this chapter compared with the quantum-chemical method, described in Chapter 3. Next, we apply the LDF techniques to optimizing the lattice parameters and internal coordinates of B_2O_3. After their optimized structures of both phases have been identified, the total energies of several points with different cell volumes are calculated and bulk moduli are estimated for subsequent use in the development of interatomic potentials for B_2O_3 crystals and glasses as discussed in Chapter 5 and 6. Furthermore, the results of these calculations provide the first suggestion of an important mechanism for structural transformation between B_2O_3 polymorphs.

4.2 THEORETICAL METHOD

CASTEP (Payne et al 1992) is a powerful tool for calculating the quantum mechanical total energy and then minimizing it with respect to its electronic and nuclear coordinates. Compared with the quantum-chemical method, CASTEP uses three distinctly different approaches;

i. Density functional theory (Hohenberg and Kohn 1964) and local density approximation (LDA) (Kohn and Sham 1965) are employed to model the electron-electron interactions. The difference in formulation between Hartree-Fock (HF) theory and density functional theory (DFT) is shown as follows (see, for example, Wimmer 1991):

DFT

$$E = E[\rho,R] \tag{4.1}$$

$$E = T[\rho] + U[\rho] + E_{xc}[\rho] \tag{4.2}$$

$$\rho(r) = \Sigma_{occ} \mid \psi_i(r) \mid 2 \tag{4.3}$$

$$\partial E / \partial \rho = 0 \tag{4.4}$$

$$[-1/2\nabla^2 + V_c(r) + \mu_{xc}(r)]\ \psi_i = \varepsilon_i \psi_i \tag{4.5}$$

HF

$$E = E[\psi,R] \tag{4.6}$$

$$E = \int \psi^*[\Sigma_i h_i + \Sigma_{i>j} 1/r_{ij}]\psi\ \delta\tau \tag{4.7}$$

$$\psi = \mid \psi(1),\psi(2),...,\psi(n)] \tag{4.8}$$

$$\partial E / \partial \psi = 0 \tag{4.9}$$

$$[-1/2\nabla^2 + V_c(r) + \mu^i_x(r)]\ \psi_i = \varepsilon_i \psi_i \tag{4.10}$$

where E is total energy, ψ is wave vector, ρ is electron density, R or r is coordinate for nucleus or electron, h is hamiltonian, T is kinetic energy, U is electrostatic or Coulomb energy term, μ_{xc} or μ_x is a many-body term or exchange term and ε is the eigenvalue.

The biggest difference between the two theories is in the term μ_{xc} or μ_x. In HF theory the exchange term μ_x only describes exchange effects and is calculated from all the wavefunctions based on the orbitals.

$$\mu^i_x(r) = -\Sigma_j\ \delta(\sigma_i,\sigma_j)\ x$$
$$[\int \psi_i^*(r)\psi_j^*(r')\ 1/|r-r'|\ \psi_j(r)\psi_i(r')dr'] \ /\ [\psi_i^*(r)\psi_i(r)] \qquad (4.11)$$

where σ is the spin.

On the other hand, in DFT theory μ_{xc} contains all the many-body effects and it is calculated from the total electron density.

$$\mu_{xc}(r) = \delta E_{xc}[\rho] \ /\ d\rho(r) \qquad (4.12)$$

Further, LDA provides a good approximation,

$$E_{xc}[\rho] \approx \int \rho(r)\varepsilon_{xc}[\rho(r)]dr \qquad (4.13)$$

where $\varepsilon_{xc}[\rho]$ is the exchange-correlation energy per electron in an interacting electron system of constant density ρ, and

$$\mu_{xc}(r) = \varepsilon_{xc}[\rho(r)] + \rho(r)\ \{\delta E_{xc}[\rho(r)] \ /\ d\rho(r)\} \qquad (4.14)$$

This approximation is generally known to yield only small percentage error both in the total energy and in the structural parameters. However, cohesive energies can be in error by more than 10%.

ii. Pseudopotential theory (Phillips 1958; Heine and Cohen 1970) is used to model the electron-ion interactions. The strong electron-nuclear potential is replaced by a much weaker pseudopotential, and plane waves are used as basis functions to approximate the potential outside the core region. This pseudopotential technique makes the solution of Schrödinger's equations much simpler. The important point is that the selection of the pseudopotential is as crucial as the selection of the basis set in the quantum-chemical calculation. Lin et al (1993) have developed an efficient and general procedure to generate optimized and transferable

non-local separable ab-initio pseudopotentials. Another point is that the cut-off energy, i.e. the number of plane waves, has to be large enough so that the total energy is converged. For oxides a larger number of plane waves are necessary than in semiconductors, to express the complex charge density distribution.

iii. The counterpart to the SCF (self-consistent field) method in the quantum-chemical terms is the use of the conjugate gradients technique, i.e. one of the new iterative diagonalization approaches (Car and Parrinello 1985; Payne et al 1986; Gilan 1989; Teter et al 1989), is employed to relax electronic coordinates. It provides an efficient method to minimize the Kohn-Sham energy functional for large systems and it is applicable to oxide materials.

4.3 STRUCTURAL SIMULATION FROM FIRST-PRINCIPLES

4.3.1 SELECTION OF MODEL

The pseudopotentials for boron (B00 potential*) and oxygen (O020 potential*) were generated using Lin's scheme (Lin et al 1993) by Lee (Lee 1992) in the Cavendish laboratory. For both crystal structures of B_2O_3, the same cut-off energy of 500 eV for the plane wave basis set was used to achieve a reasonable convergence of the total energy. The number of plane waves used was 3459 for the B_2O_3-I system (15 atoms) and 1890 for B_2O_3-II (10 atoms).

The other important factor is the k-point sampling. The Bloch theorem changes the problem of calculating an infinite number of electronic wavefunctions to calculating a finite number of electronic wavefunctions at an infinite number of k-points. However, it is possible to represent the electronic wavefunctions over a region of k-space by the wavefunctions at a single k-point. Several methods (Chadi and Cohen 1973; Monkhorst and Pack 1976) have been devised for obtaining an accurate approximation for the total energy with a very small number of k-points. Generally speaking, the denser the set of k-points sampled, the more accurate is the result. However, both the unit-cells for B_2O_3 crystals are too large for the calculation with multi k-points. Therefore, several single k-points were investigated, and among them the single k-point, which gives the smallest cell stress and internal force, was selected. The resulting k-point was (1/3, 1/3, 1/4) for B_2O_3-I and (1/4, 1/4, 1/4) for B_2O_3-II. This difference results from the difference in crystal symmetry between the two polymorphs. (see Section 2.1 and Table 3.4).

---

* These pseudo potentials are catalogued in the data base of the Cavendish laboratory.

4.3.2 OPTIMIZATION OF STRUCTURE

At first, the relation between cell volume and total energy was calculated under the condition that the internal coordinates remained fixed (see Table 4.1). When the optimized structure (i.e. the structure with minimum total energy) is compared with experiment, the error in the lattice constant is -2.0% for B_2O_3-I and -2.5% for B_2O_3-II. The error in volume is converted into -5.9% for B_2O_3-I and -7.3% for B_2O_3-II. This result is satisfactory, considering that a common pseudopotential set for boron and oxygen was used for both polymorphs, and only one k-point was sampled.

As the second step, internal coordinates were relaxed, with the constraint that the optimized cell parameters remain fixed. The final total energies, bond lengths and angles are shown in Tables 4.2 and 4.3.

As for crystal stability between two polymorphs, the total energy of B_2O_3-II is lower than that of B_2O_3-I, regardless of the relaxation of internal coordinates. CRYSTAL calculations also show the same result (see Table 3.3). However, the phase diagram of B_2O_3 system shown in Table 2.1 suggests that B_2O_3-I is more stable than B_2O_3-II under ambient conditions. Maybe more sophisticated calculations are required in order to reproduce the small difference in total energy in either method. CRYSTAL calculations need better basis set as Nada et al (1990) showed for quartz and stishovite. On the other hand, CASTEP calculations may need more dense set of k-points sampling and higher cut-off energy. Entropic factors may also be significant.

When the calculated bond lengths and bond angles are compared with the experimental values, the errors in the bond lengths and bond angles are within 0.055Å and 3.5°. Both calculated structures reproduce the corresponding experimental structures well. It is interesting to note

the change of the B(1)-O(1) bond length in B_2O_3-II. In the CRYSTAL calculations the B(1)-O(1) bond is elongated by 10% with the constraint that all the other atomic positions are fixed. On the other hand, the B(1)-O(1) bond is shortened by 4% in the same manner as the other B-O bonds when all the atomic positioned are relaxed. Therefore, the full relaxation of internal coordinates is almost certainly important for discussing the detailed structure.

4.3.3 ESTIMATION OF BULK MODULUS

As discussed in Chapter 5, to construct an interatomic potential model from empirical sources, we need not only structural data but also data on other properties, for example, bulk moduli, elastic constants and phonon dispersion curves. However, there is no such data available for either crystal. Therefore, an estimation of the bulk modulus was obtained using the total energy calculation technique. The procedure used was based on Murnaghan's equation (Murnaghan 1944). Several values for the total energy as a function of cell volume were fitted using least square technique to Murnaghan's equation (Yin and Cohen 1982);

$$E_{tot}(V) = B_0V/B_0' [(V_0/V)^{B0'}/(B_0'-1) +1] + const \qquad (4.15)$$

where B_0 and B_0' are the bulk modulus and its pressure derivative at the equilibrium volume V_0; both B_0 and B_0' were fitted.

As each calculation of ionic relaxation requires a large amount of CPU time, only six points were calculated for either polymorph. The cell volume was isotropically varied and then internal coordinates relaxed in each case. The relation between the cell volumes and the corresponding total energies is shown in Table 4.4. The calculated bulk moduli and the curve fitted to Murnaghan's equation are shown in Table 4.5 and Figure

4.1. The estimated bulk modulus is 26 [GPa] for B_2O_3-I and 126 [GPa] for B_2O_3-II.

An alternative approach to determining the bulk modulus K(=B0) comes by employing the empirical equation between the density and the bulk modulus (see, for example, Poirier 1991).

$$V_\phi = -1.75 + 2.36\rho \qquad (4.16)$$

and

$$V_\phi = \sqrt{(K/\rho)} \qquad (4.17)$$

then

$$\sqrt{(K/\rho)} = -1.75 + 2.36\rho \qquad (4.18)$$

where V_ϕ is velocity propagating the material and ρ is the density of the material. The estimated values are shown in Table 4.5.

There are considerable difference between the results of the two methods. The prediction of the bulk modulus or elastic constant is generally more difficult than that of lattice constants, and it is also very difficult to evaluate the error of these estimations. For the CASTEP calculation, the cell volume is only varied isotropically. Furthermore, a higher cutoff energy, a more dense set of k-points would improve its accuracy. For the empirical equation detailed structural information is not taken into consideration. However, these estimated values, even if they are rough, are very useful for constraining the interatomic potentials in Chapter 5 and 6.

4.3.4 STRUCTURAL TRANSFORMATION

The manner of ionic relaxation under different cell volumes can be used as one of methods of studying the structural transformation.

The optimized cell volume was changed by -40, -20, +10, +20, +30%, +70% and +100% for B_2O_3-I, and changed by -40, -20, +10, +20 and +30%

for B_2O_3-II. Their relaxed bond lengths and angles are summarized in Tables 4.6 and 4.7.

The structural features in B_2O_3-I are discussed for three ranges of the cell volume as follows.

i. *relative cell volume = 0.80 ~ 1.30*

For the initial configuration all the B-O bond lengths are varied in the same proportion as the cell volume change. After optimization the inter-triangle angles (O-B-O) do not change much, but the connecting angles (B-O-B) change considerably. The shape of the BO_3 triangle does not change much. Moreover, the B-O bonds expand by 5%, so that they come loose to the uncompressed values. The change in volume is accommodated largely by the change in the B-O-B connecting angles. Among the contributions to the volume change, the change in the B-O bond lengths contributes 28%, while the change in the connecting angles contributes 72%. Therefore, near the stable structure, the change in the B-O-B connecting angles dominates the deformation of the structure.

ii. *relative cell volume ≈ 0.60*

The most interesting result is that the BO_3 triangle structural unit in the 60% cell volume turns into a BO_4 tetrahedron. This corresponds to a pressure-induced phase transition. Although the original cell is only isotropically compressed and the final structure is not completely the same as B_2O_3-II, it agrees with the phase diagram in that the four-fold BO_4 structural unit is more stable than three-fold BO_3 structural unit at high pressure (see Figure 2.1).

In the case of B_2O_3-II, the structure at 130% volume does not exactly show the reverse structural transformation, but it shows the

fourth B-O bond becoming much larger than the other B-O bonds. Therefore, this suggests that this transformation is probably reversible at zero Kelvin. On the other hand, it is interesting to note that no transformation from B_2O_3-II to B_2O_3-I has been ever observed (Uhlmann et al 1967). This fact suggests that entropic factors may affect such transformation considerably.

We now consider the manner of the transformation. We note first that it was found that the original structure of B_2O_3-I is not far from that of B_2O_3-II. When the B-O bond length is assumed to be within 1.51Å in B_2O_3-II, that is, only the first three shortest B-O distances participate in the B-O bonding, all boron atoms become 3-fold coordinated and all the oxygen atoms become 2-fold coordinated. These coordination numbers are the same as for B_2O_3-I. Conversely, when B-O bonding is assumed to be within 2.7Å in B_2O_3-I, that is, the first four shortest B-O distances participate in B-O bonding, all the boron atoms become 4-fold coordinate, and one-third of the oxygen atoms become 2-fold coordinated and the remaining two-third become 3-fold coordinated. These coordination numbers are the same as for B_2O_3-II. It is interesting that Berger's data (1952,1953) which was shown by Strong and Kaplow (1968), and by Gurr et al (1970) to be incorrect (see Section 2.1), has the same distribution of coordination numbers if the cut-off in the B-O bonding is assumed to be 1.8Å. Therefore, Berger's data is not far from those of the other two authors, although Berger concluded that B_2O_3-I consists of BO_4 tetrahedra.

With this background we can explain the observed manner of the transformation in B_2O_3-I as follows. As its cell volume is reduced, the O(1) or O(2) atom approaches the third new boron atom, B(2') or B(1'), which lies on the other ribbon, and the oxygen and boron atoms start to

bond. However, the O(3) atom, which cross-links the different ribbons of the BO_3 triangle, keeps its coordination. The change in the B-O bond distances are shown in Figure 4.2. The pattern of the structural transformation is shown in Figure 4.3 (see also the crystal structure in Figure 2.2).

The B-O coordination number changes from three to four smoothly without breaking any B-O bonds. It is interesting to note that Tsuneyuki (1990) also observed the smooth structural transformation from SiO_4 tetrahedron into SiO_6 octahedron in his MD study.

What is the driving force for this transformation? It is useful to analyze the individual energy contributions to the total energy, as was shown by Yin and Cohen (1982). These are shown in Table 4.8, and Figures 4.4 and 4.5. The contribution of the Coulombic energy (E_C) is much larger than that of the others. When the cell volume is reduced, the Coulombic energy is also reduced, since as is well known this Coulombic energy favours high coordination. On the other hand, when the cell volume increases, the electronic kinetic energy (E_K), the electron-electron Coulomb energy (E_H) and nonlocal pseudopotential energy (E_{NL}) are reduced. This means that in the lower coordination state the valence electrons prefer to be uniformly distributed and to generate covalent bonding. Finally, on comparing all the contributions the Coulombic contribution is judged to be the driving force for this transformation.

iii. *relative cell volume* $\approx$ *2.0*

The 170% cell volume corresponds to the volume in the 1500K molten state. However, even in the case of 200% cell volume, the structure still keeps the same structural units and the boroxol ring is not observed. It is interesting to note that one of the longest B-O bonds is

elongated, while the other two bonds begin to be shortened. Although the longest bond is still thought not to be broken, its bonding is weakened and the other two bonds are strengthened. This means that the bonding state is changing from three-fold into two-fold coordination. This feature may simulate some features of the molten state.

The well-known thermodynamic theorem is that the phase transformation should occur when the Gibbs free energy,

$$G \equiv E + PV - TS \tag{4.19}$$

becomes equal between the two phases. These total energy calculations at zero-temperature shows that the structural transformation between three-fold and four-fold coordination occurs due to the PV term. On the other hand, the fact that no boroxol-ring is observed during the calculations, although they have some restrictions (e.g. cell shape, number of atoms), may show that entropy effects may be important for the structural transformation into the real vitreous structure.

4.4 CONCLUSION

The application of first-principles total energy calculations to B_2O_3 has given the following important results:

i. A common set of pseudopotentials for boron and oxygen can reproduce two different crystal structures (B_2O_3-I and B_2O_3-II) very well. With this pseudopotential, not only lattice parameters but also internal coordinates are well modelled.

ii. The bulk modulus is estimated as 26 [GPa] for B_2O_3-I and 126 [GPa] for B_2O_3-II.

iii. When the cell volume is reduced, the structural transformation from the BO_3 triangular structural unit into the BO_4 tetrahedral unit is observed. The manner of its transformation has also been elucidated.

The CASTEP program can be used for MD. In the near future, the structure of a large system, that is a super cell of a disordered system, will be performed. At the moment the feasible number of atoms would be 50~60 and it seems that it would be difficult to reproduce realistically the vitreous structure. However, the observed phenomenon that boron trioxide prefers the vitreous to the crystal structures suggests that the first-principles simulation, even if the number of atoms is not big, may reproduce the structural unit of glass, if the TS term in the Gibbs free energy is taken into account.

B_2O_3-I	
$(v/v0)^{**1/3}$	total energy ($eV/0.2B_2O_3$)
1.005	-288.568
1.0	-288.578
0.995	-288.585
0.990	-288.593
0.985	-288.594
0.980	-288.595
0.975	-288.591

B_2O_3-II	
$(v/v0)^{**1/3}$	total energy ($eV/0.2B_2O_3$)
1.0	-288.625
0.99	-288.644
0.98	-288.651
0.975	-288.652
0.97	-288.647

Table 4.1. Relation between cell volume and calculated total energy in B_2O_3-I and B_2O_3-II

	E1 ($eV/0.2B_2O_3$) before relaxation	E2($eV/0.2B_2O_3$) after relaxation	E2-E1($eV/0.2B_2O_3$) difference
B_2O_3-I	-288.595	-288.612	-0.017
B_2O_3-II	-288.652	-288.716	-0.020

Table 4.2. Effect of cell volume on total energy
$(v/v0)^{**1/3}$ = 0.980 or 0.975 for B_2O_3-I or B_2O_3-II

	B_2O_3-I			B_2O_3-II	
Distances (Å)	experiment	calculation		experiment	
	calculation				
B(1)-O(1)	1.404	1.354	B(1)-O(1)	1.373	1.358
-O(2)	1.366	1.329	-O(2)	1.507	1.461
-O(3)	1.336	1.338	-O(2')	1.506	1.451
B(2)-O(1)	1.336	1.329	-O(2'')	1.512	1.507
-O(2')	1.400	1.355	O(1)-O(2)	2.364	2.313
-O(3')	1.384	1.337	-O(2')	2.440	2.365
O(1)-O(2)	2.387	2.327	-O(2'')	2.409	2.408
	2.388	2.329	O(2)-O(2')	2.428	2.366
O(2)-O(3)	2.409	2.331	-O(2'')	2.394	2.351
	2.333	2.284	O(2')-O(2'')	2.389	2.350
O(3)-O(1)	2.309	2.285			
	2.409	2.343			
Angles (deg)					
O-B(1)-O	119.0	120.3	O-B(1)-O	110.2	110.2
	114.7	116.2		115.8	114.6
	126.2	122.8		113.1	113.7
O-B(2)-O	121.5	120.4		107.4	108.7
	124.6	123.0		104.9	104.3
	113.9	116.1		104.7	104.7
B-O(1)-B	130.5	131.2	B-O(1)-B	138.6	135.1
	128.3	131.2	-O(2)-	123.8	121.2
	133.3	133.5	-O(2')-	114.7	115.7
			-O(2'')-	118.9	118.9

Table 4.3. comparison of bond lengths and angles between experimental structures and calculated structures in B_2O_3-I and B_2O_3-II

	B_2O_3-I		B_2O_3-II	
volume ratio	total energy ($eV/0.2B_2O_3$)	difference	total energy ($eV/0.2B_2O_3$)	difference
0.6	-288.13	+0.48	-287.62	+1.05
0.8	-288.49	+0.12	-288.53	+0.14
1.0	-288.61	±0	-288.67	±0
1.1	-288.60	+0.01	-288.62	+0.05
1.2	-288.55	+0.02	-288.50	+0.17
1.3	-288.47	+0.14	-288.37	+0.30

Table 4.4. Relation between cell volume and total energy in B_2O_3-I and B_2O_3 -II (Each relative cell volume is the ratio to the corresponding optimized cell volume.)

	B_2O_3-I (1)	**B_2O_3-II** (2)	**Glass** (3)
density (g/cm3)	2.56	3.11	1.84~1.91
bulk modulus (GPa)			
CASTEP	26	126	---
empirical	47	97	15
experiment	---	---	15

Table 4.5. Experimental density and calculated bulk moduli in B_2O_3-I and B_2O_3 -II (1: Gurr et al 1970; 2: Prewitt et al 1968; 3: Mazurin 1983)

volume ratio		0.60	0.80	1.00	1.10	1.20	1.30	1.70	2.00
lattice ratio		0.84	0.93	1.00	1.03	1.06	1.09	1.19	1.26
	exp.	cal.	cal.	cal.	cal.	cal.	cal.	cal.	cal.
distance (Å)									
B(1)-O(1)	1.404	1.340	1.319	1.354	1.379	1.407	1.439	1.535	1.655
-O(2)	1.366	1.387	1.315	1.329	1.343	1.357	1.370	1.387	1.368
-O(3)	1.336	1.290	1.308	1.338	1.355	1.372	1.389	1.399	1.380
-O(2')	2.616	1.422	2.099	2.524	2.670	2.807	2.931	---	---
B(2)-O(1)	1.336	1.338	1.314	1.329	1.344	1.358	1.371	1.390	1.368
-O(2')	1.400	1.340	1.320	1.355	1.379	1.407	1.440	1.542	1.656
-O(3')	1.384	1.289	1.305	1.337	1.354	1.371	1.388	1.398	1.379
-O(1'')	2.636	1.423	2.119	2.529	2.675	2.812	2.935	---	---
O(1)-O(2)	2.387	2.175	2.252	2.327	2.371	2.414	2.457	2.606	2.727
	2.388	2.176	2.254	2.329	2.372	2.417	2.460	2.618	2.727
O(2)-O(3)	2.409	2.271	2.332	2.331	2.346	2.414	2.457	2.373	2.387
	2.333	2.034	2.184	2.284	2.337	2.388	2.439	2.503	2.503
O(3)-O(1)	2.309	2.030	2.184	2.285	2.339	2.372	2.441	2.504	2.502
	2.409	2.273	2.335	2.343	2.347	2.358	2.370	2.375	2.387
angle (deg)									
O-B(1)-O	119.0	105.8	117.5	120.4	121.1	121.7	122.0	126.1	128.7
	114.7	101.1	112.5	116.2	117.7	118.6	119.4	117.0	110.7
	126.2	116.1	125.6	122.8	120.8	119.5	118.5	116.8	120.6
O-B(2)-O	121.5	105.8	117.7	120.4	121.2	121.8	122.2	126.4	128.6
	124.6	116.3	126.1	123.0	120.9	119.5	118.4	116.9	120.6
	113.9	101.3	112.6	116.3	117.6	118.5	119.2	116.7	110.8
B-O(1)-B	130.5	116.1	122.4	131.2	134.5	137.4	139.7	149.4	152.7
-O(2)-	128.3	116.3	122.4	131.2	134.5	137.2	139.1	149.2	152.8
-O(3)-	133.3	110.4	127.0	133.5	135.8	137.2	139.2	139.1	138.5

Table 4.6. Comparison of bond lengths and angles at different cell volumes in B_2O_3-I (Relative cell volume is the ratio to the optimized cell volume.)

volume ratio		0.60	0.80	1.00	1.10	1.20	1.30
lattice ratio		0.84	0.93	1.00	1.03	1.06	1.09
	exp.	cal.	cal.	cal.	cal.	cal.	cal.
distance (Å)							
B(1)-O(1)	1.373	1.274	1.328	1.358	1.376	1.396	1.416
-O(2)	1.507	1.335	1.406	1.461	1.498	1.535	1.561
-O(2')	1.506	1.314	1.390	1.451	1.484	1.517	1.542
-O(2'')	1.512	1.367	1.447	1.507	1.568	1.636	1.725
O(1)-O(2)	2.364	2.142	2.234	2.313	2.376	2.446	2.507
-O(2')	2.440	2.202	2.305	2.365	2.402	2.450	2.499
-O(2'')	2.409	2.205	2.319	2.408	2.464	2.530	2.604
O(2)-O(2')	2.428	2.125	2.257	2.366	2.428	2.489	2.539
-O(2'')	2.394	2.179	2.281	2.351	2.403	2.466	2.525
O(2')-O(2'')	2.389	2.080	2.230	2.350	2.415	2.489	2.567
angle (deg)							
O-B(1)-O	110.2	110.4	109.6	110.2	111.5	113.0	114.6
	115.8	116.6	115.9	114.6	114.2	114.5	115.3
	113.1	111.7	113.3	113.7	113.5	112.8	111.6
	107.4	106.7	107.6	108.7	109.0	107.7	109.9
	104.9	107.5	106.2	104.3	103.3	102.1	100.4
	104.7	101.8	103.6	104.7	104.6	104.2	103.5
B-O(1)-B	138.6	104.5	117.6	135.1	141.7	145.4	148.9
-O(2)-	123.8	112.1	117.0	121.2	121.5	121.8	119.4
-O(2')-	114.7	111.1	114.3	115.7	115.7	115.8	116.0
-O(2'')-	118.9	107.1	113.2	118.9	120.4	121.6	123.2

Table 4.7. Comparison of bond lengths and angles at different cell volumes in B_2O_3-II (Relative cell volume is the ratio to the optimized cell volume.)

B_2O_3-I	(eV/0.2B_2O_3)						
volume ratio	0.6	0.8	1.0	1.1	1.2	1.3	1.7
total kinetic energy	198.59	191.88	188.16	186.50	184.97	183.55	181.17
local pot. energy	-236.58	-248.47	-256.40	-258.88	-260.76	-262.17	-268.29
nonlocal pot. energy	45.40	45.86	46.13	46.36	46.61	46.86	47.22
Hartree energy	-54.11	-70.22	-85.73	-92.32	-98.17	-103.33	-127.12
exchange-correlation	22.09	21.53	21.22	21.08	20.95	20.83	20.61
Coulombic energy	-267.22	-231.86	-204.20	-193.35	-184.01	-175.91	-143.09
pseudopot. core energy	3.70	2.78	2.22	2.02	1.85	1.71	1.31
total energy	-288.13	-288.49	-288.61	-288.60	-288.55	-288.47	-288.19

B_2O_3-II	(eV/0.2B_2O_3)					
volume ratio	0.6	0.8	1.0	1.1	1.2	1.3
total kinetic energy	203.57	193.86	188.83	186.31	183.73	181.58
local pot. energy	-225.78	-237.79	-246.26	-248.38	-249.56	-250.61
nonlocal pot. energy	45.65	46.28	46.74	47.10	47.52	47.87
Hartree energy	-40.48	-56.04	-72.61	-78.34	-82.09	-85.45
exchange-correlation	22.53	21.79	21.36	21.16	20.94	20.76
Coulombic energy	-297.72	-260.06	-229.47	-218.96	-211.36	-204.63
pseudopot. core energy	4.58	3.434	2.75	2.50	2.29	2.11
total energy	-287.62	-288.53	-288.67	-288.62	-288.50	-288.37

Table 4.8. Comparison of various contributions to the total energy in B_2O_3-I and B_2O_3-II (Relative cell volume is the ratio to the optimized cell volume.)

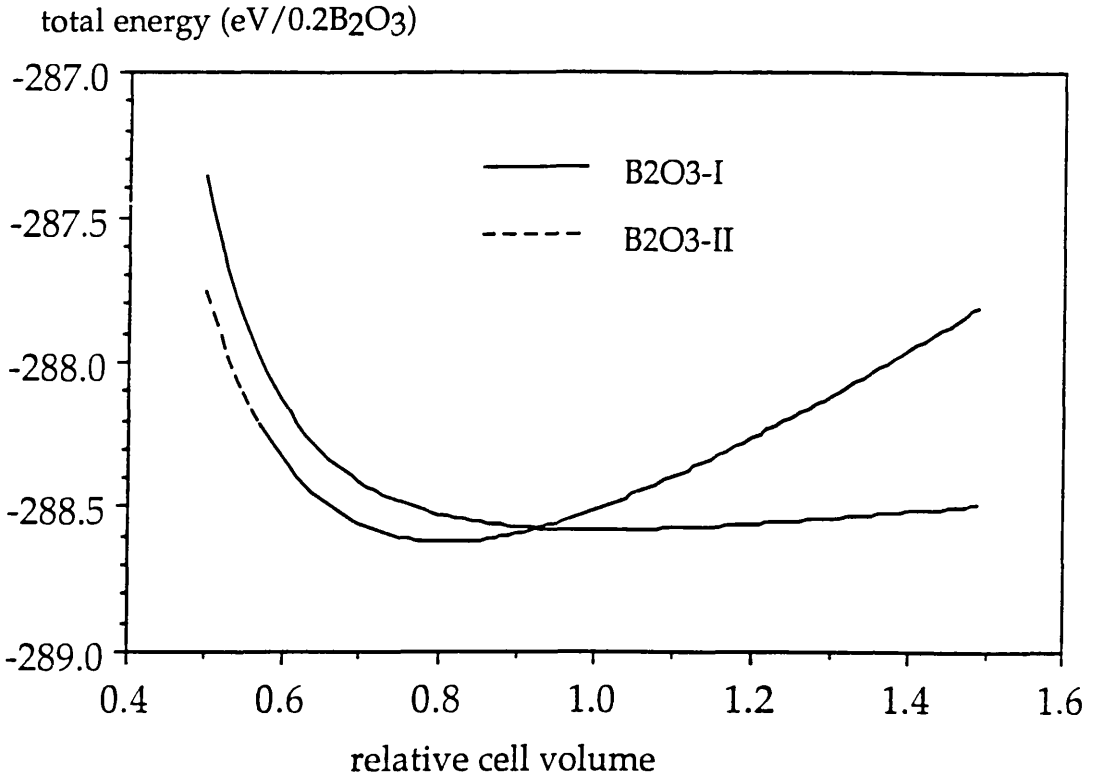

Figure 4.1. Calculated "Murnaghan" curve for B_2O_3-I and B_2O_3-II

(The relative cell volume is the ratio to the optimized B_2O_3-I cell volume.)

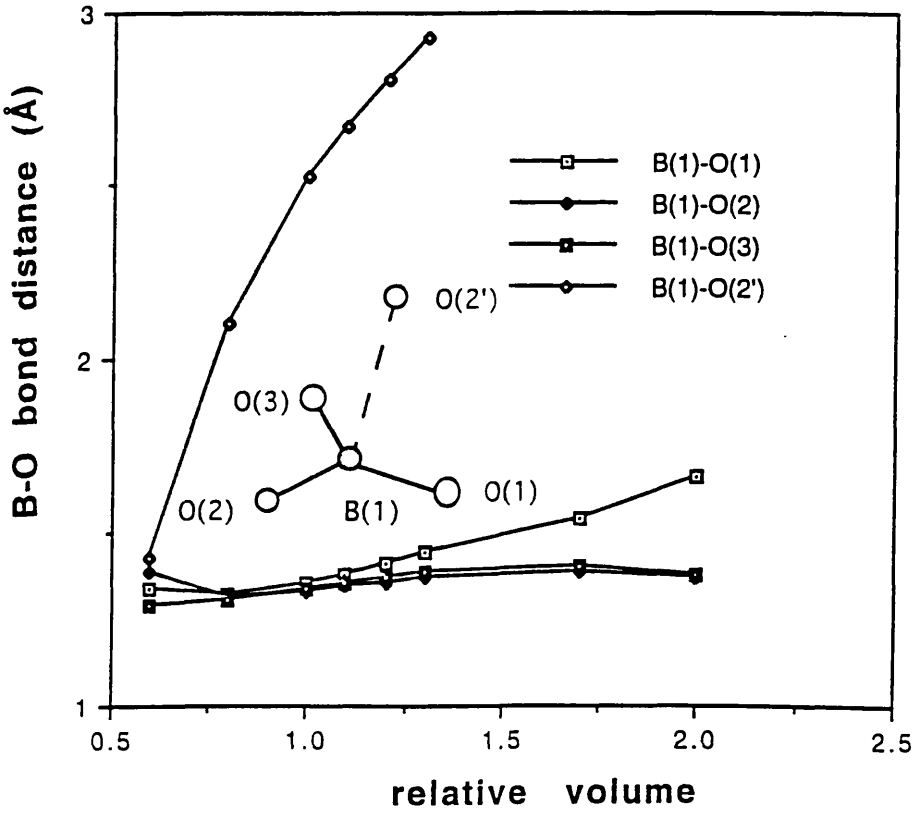

Figure 4.2. Relation between the cell volume and B-O bond length in B_2O_3-I

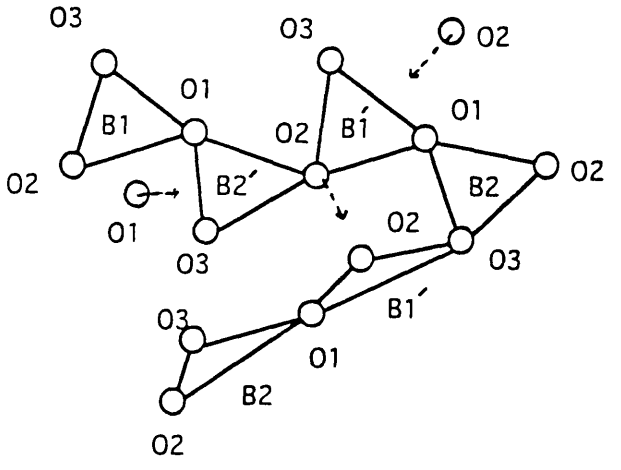

(a) relative cell volume = 1.0 (BO_3 structural unit)

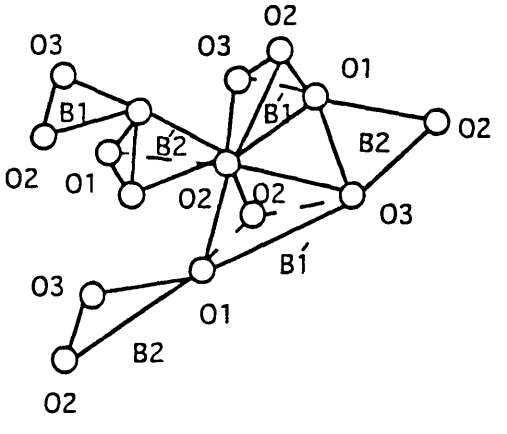

(b) relative cell volume = 0.6 (BO_4 structural unit)

Figure 4.3. Schematic diagram for structural transformation

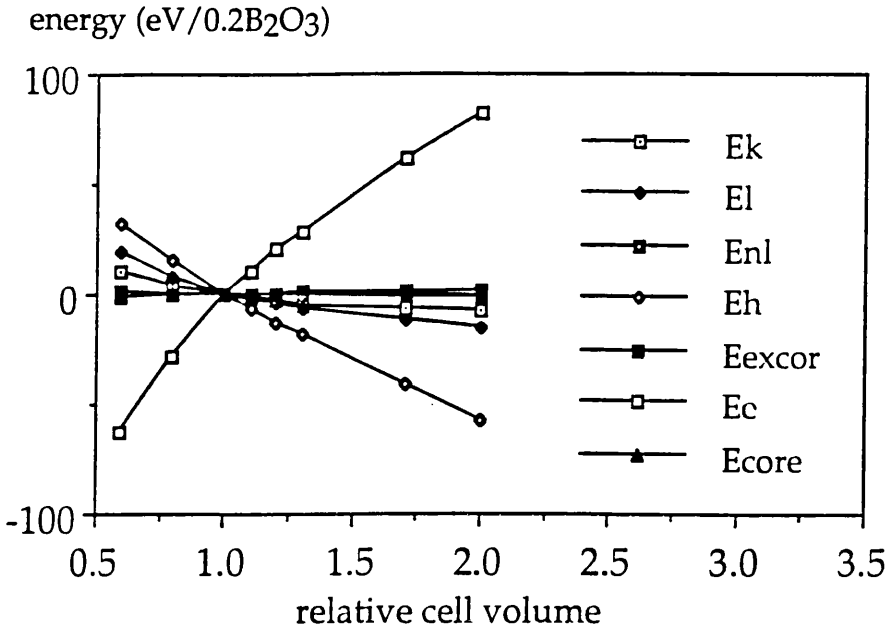

Figure 4.4. Various energy contributions to the total energy in B_2O_3-I

(Ek = total kinetic energy; El = local psedopotential energy; Enl = non-local pseudopotential energy; Eh = Hartree energy; Eexcor = exchange-correlation energy correction; Ec = Coulombic energy; Ecore = core energy)

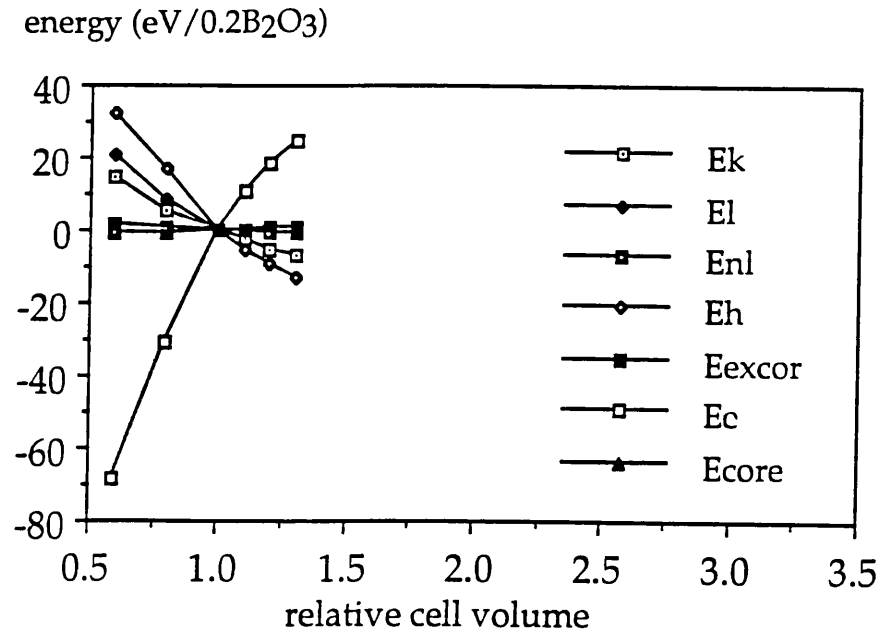

Figure 4.5. Various energy contributions to the total energy in B_2O_3-II

(Ek = total kinetic energy; El = local psedopotential energy; Enl = non-local pseudopotential energy; Eh = Hartree energy; Eexcor = exchange-correlation energy correction; Ec = Coulombic energy; Ecore = core energy)

CHAPTER 5 COMPUTER MODELLING OF CRYSTALLINE B_2O_3

5.1 INTRODUCTION

Several interatomic potentials have been reported for the study of vitreous structures of B_2O_3. However, no attempts have been made to model the crystal structures of B_2O_3. The consistent philosophy in this thesis is that crystal structures have much information on bonding and that it is necessary to derive such interatomic potentials that reproduce several different crystal structures before proceeding to model vitreous materials.

First, we review the field of atomistic simulation techniques and interatomic potential models, with an emphasis on the difference between them and the quantum-mechanical techniques discussed in Chapter 3 and 4. Next, in order to overcome the difficulties in deriving interatomic potentials, a new deriving procedure known as the LP fitting method is developed. The newly derived potentials obtained using the LP fitting method are applied to the two crystal structures of B_2O_3 and are then compared with the potentials previously reported for vitreous B_2O_3 by the other authors. Finally, the new potentials are applied to other possible polymorphs and also possible vitreous structural units of B_2O_3. We are able to propose not only new candidates for polymorphs but also a new structural unit for vitreous B_2O_3.

5.2 ATOMISTIC SIMULATION TECHNIQUES

Computer simulation techniques have made great progress in recent years and are increasingly explaining or predicting the structures and properties of solids (Catlow and Price 1990). These techniques may be classified into two groups: the first starts from the Schrödinger's equation and calculates the electronic structure of the system; the latter models interatomic potentials and applies the resulting potentials to the system under study.

The first approach is often referred to by the terms 'ab initio' or 'first-principles', because it is based on the quantum-mechanical calculations with the least empirical assumptions. In Chapter 3 and 4, these techniques were applied to borate crystals and they led to a detailed description of the structures and bonding in borate crystals. The results agreed well with the existing empirical concepts.

The second approach is often referred to by the term 'simulation'. Interactions between atoms are replaced by the interatomic forces calculated from 'effective potentials', which are applied to a variety of simulation techniques, based on both static and dynamic methods.

On comparing the two approaches, we note that the first is more fundamental. However it requires large computational resources and it is still not possible to model large and complex systems. On the other hand, the latter approach can deal straightforwardly with such systems. However, the construction of 'effective interatomic potentials' has associated uncertainties. Therefore, it is crucial to test the interatomic potentials thoroughly and make sure that they are valid for the system studied.

The simulation studies reported in this thesis are of two main categories. The first is Lattice Simulation. The formulae used in this

method are given in detail by Catlow and Norgett (1976). They comprize two parts. Static simulations which determine the structure with the minimum energy, allowing both the unit cell dimensions and the internal coordinates to be relaxed until its energy is minimized. These techniques predict not only the stable structure but also several properties (e.g. bulk modulus, elastic constants and dielectric constants) at zero Kelvin. Lattice dynamics simulations calculate vibrational properties of the energy-minimized structure, based on the quasi-harmonic approximation. This approximation assumes that the vibrational motions in the solid are comprised of independent quantized harmonic oscillators whose frequencies vary with cell volume. This simulation gives the phonon frequencies and several thermodynamical properties (e.g. vibrational energy, entropy, free energy and heat capacity). Furthermore, it is possible to minimize the free energy and predict the structure and the thermal expansion coefficient at the finite temperatures, as long as anharmonic effects are negligible and the quasi-harmonic approximation is valid (Parker and Price 1989). We note that these techniques are inherently limited in that time-dependent phenomena (for example, transport coefficients) cannot be simulated directly.

The other approach is the Molecular Dynamics (MD) method. In MD simulations, the dynamical trajectories of the interacting atoms are followed at finite temperatures. The total force acting on each atom is evaluated at a given time and used to determine its new position at time $t+\Delta t$. This method is particularly appropriate for modelling the liquid and vitreous states. The details of this approach are discussed in Chapter 6.

5.3 INTERATOMIC POTENTIAL MODEL

Many studies have been reported concerning interatomic potentials for oxide materials (see Catlow and Mackrodt *eds.* 1982; Catlow et al 1988). We now discuss the functional forms and the methods used to derive appropriate parameters.

5.3.1 POTENTIAL FUNCTION

Oxides have been mostly described by the ionic model with formal or partial ionic charges assigned to point entities which also interact with short-range terms. The interactions between point charges come from long-range electrostatic Coulombic forces between ions, while the short-range interactions come from the overlap of the electron charge clouds of the interacting ions.

The simplest and most widely used short-range form is the central-force pair-potential:

$$V(r_1,r_2,\ldots,r_n) = \sum V_{ij} (|r_i-r_j|) \qquad (5.1)$$

The total potential energy V is summed over all the pair interaction terms, each of which is dependent only on the distance between the ions.

The most widely used function form of this pair-potential for ionic solids is the Born-Mayer or Buckingham potential:

$$V(r_{ij}) = A\exp(-r_{ij}/\rho_{ij}) - Cr_{ij}^{-6} \qquad (5.2)$$

The second term is often added to express dispersion and attractive terms.

The other functional form, which is said to be suitable for modelling the effect of the covalent bonding is the Morse potential:

$$V(r_{ij}) = D_{ij} \{\exp[-2\beta_{ij}(r_{ij}-r_0)] - 2\exp[-\beta_{ij}(r_{ij}-r_0)]\} \qquad (5.3)$$

Although these pair-potentials have reasonably reproduced not only structures but also properties of oxide materials, more sophisticated

models are used to include polarization or covalent bonding effect more precisely.

Polarizability is described effectively using the shell model (Dick and Overhauser 1958). An ion is described as a massless shell of charge Y, a core in which mass is concentrated and a harmonic spring which connect the shell with the core. This model has improved the calculation of dielectric, lattice-dynamical and defect properties of ionic solids.

On the other hand, in order to express covalent effects, a three-body term is added. The most common form is the simple-harmonic, bond-bending form;

$$V(\theta) = 1/2\ K_B\ (\theta - \theta_0)^2 \qquad (5.4)$$

where K_B is the bond-bending force constant and θ_0 is the equilibrium bond angle.

For crystalline silicates, pair-potential models (Tsuneyuki et al 1988; Beest et al 1990), and shell models with three-body potential (Sanders et al 1984; Price et Parker 1984) have successfully been employed to model structures and properties.

5.3.2 DERIVATION OF INTERATOMIC POTENTIAL

Interatomic potentials have been derived by two main procedures.

The first is the so-called empirical method. The parameters in the potential model are fitted so that they can reproduce the experimental structures and/or properties (e.g. elastic constants, dielectric constants or vibrational properties) as well as possible. This method may be applied even when the only data available are the crystallographic parameters. But care must be taken when such potentials are applied to related structures which are different from the fitted structure. And in general it

is crucial to use as many data as possible for fitting and testing potential models.

The other approach is to use non-empirical or semi-empirical methods, employing quantum-mechanically calculated data for the potential energy surface. In the electron gas method (Gordon and Kim 1972), electron densities are calculated for the isolated interacting atoms, and then the Coulomb interactions, the kinetic energy, exchange and correlation contributions to the interacting energy are calculated. On the other hand, ab-initio methods may be employed on clusters or periodic arrays of atoms. For example, using ab-initio, periodic Hartree-Fock techniques, Gale et al (1992) reproduced the structure and elastic constants of α-Al_2O_3 from using the calculated potential energy surface obtained using the CRYSTAL code. In the case of cluster calculations, the importance of crystal field effects must be stressed. For example, Mackrodt and Stewart (1979) introduced the Madelung potential appropriate to the crystal when the wavefunctions were solved, and Tsuneyuki et al (1988) and Beest et al (1990) were obliged to use experimental data on elastic constants to determine the partial charge values.

One of the most important aspects concerning a potential model is its transferability. Some potentials (for example, Price and Parker 1984; Tsuneyuki and al 1988) successfully reproduced the structures of several polymorphs using the same potentials. However, several potentials are not transferable between polymorphs. However, potentials fitted to the crystal structure and properties of SiO_2 were applied to vitreous states and they reproduced successfully the experimental RDFs (Vessal et al 1989). However, it is still not clear to what extent such potentials can

reproduce highly distorted structures using the potentials which are fitted to a particular crystal structure and its properties.

5.4 APPLICATION OF PREVIOUSLY REPORTED POTENTIALS TO CRYSTALLINE B_2O_3

As noted earlier several potential models have been reported specifically for vitreous B_2O_3. The details of these potentials are given in Appendix B. Among them, seven potentials (Verhoef and Hartog 1992), which have more general functional forms, are now applied to B_2O_3 crystals.

Lattice energy minimizations are performed with these potentials, starting from the experimental structure of B_2O_3-I or B_2O_3-II, using the GULP code (Gale 1993). As the original potentials were not applied for four-fold coordinated boron atoms, the equilibrium angle θ_0 in the O-B-O three-body interactions is set to be 109.47° in B_2O_3-II. The calculated results are shown in Table 5.1 and Table 5.2 (see also Appendix B). They are summarized as follows:

i. For the structure of B_2O_3-I, potentials v4,v5,v6, and v7 reproduce the experimental lattice parameters, B-O bond lengths and O-B-O bond angles reasonably. However, none of them can reproduce the B-O-B bond angles. Even for the potential v4, which includes the B-O-B three-body term, the B1-O1-B2 angle is still 8° larger than the experimental value. This behaviour suggests why the B-O-B bond angles were always large when these potentials were applied to MD calculations. The reproduction of the B-O-B bond angles is crucial for reproducing the manner of connection of the BO_3 triangles. It is interesting to note that potentials which cannot reproduce the B-O-B bond angles cannot reproduce the experimental density of B_2O_3-I, even if they can reproduce the experimental bond lengths.

ii. None of the potentials can reproduce the structure of B_2O_3-II, indicating that the bonding for the four-fold coordinated boron atom is

different from that for the three-fold coordinated. Even potential v5, which used the crystal structure of the alkaline borate KB_5O_8 which is comprised of BO_4 tetrahedra, cannot reproduce the structure reasonably. The explanation is possibly in the difference in the bonding, because it is shown in Chapter 3 that a considerable difference exists in the ionicity and the nature of the bonding between B_2O_3-II and the alkaline borates. It is interesting to note that these potentials may prevent the generation of a BO_4-type environment in molten B_2O_3. Such a mechanism for the structural transformation in the same stoichiometry may be different from the trigonal to tetrahedral conversion of a boron atom with the addition of alkaline oxide. This point will be discussed further in Chapter 6.

B_2O_3-I		potential sets						
	exp.	v1	v2	v3	v4	v5	v6	v7
i. lattice energy (eV/B_2O_3)								
before relaxation		-179.34	-80.40	-80.20	-80.19	-202.26	-24.78	-24.48
after relaxation		-182.25	-81.70	-81.70	-80.80	-203.91	-24.98	-24.96
ii. structure (after relaxation)								
volume (%)	±0	+79.49	+73.99	+74.12	+6.10	+8.66	+8.64	+6.84
a (%)	±0	+9.96	+8.84	+8.92	+2.62	+6.12	+6.11	+5.07
b (%)	±0	+9.96	+9.96	+8.92	+2.62	+6.12	+6.11	+5.07
c (%)	±0	+48.44	+46.89	+46.78	+0.76	-3.52	-3.52	-3.22
bond length (Å)								
B1-O1	1.404	1.378	1.364	1.364	1.394	1.348	1.348	1.376
-O2	1.366	1.378	1.364	1.364	1.370	1.406	1.406	1.375
-O3	1.337	1.372	1.358	1.358	1.383	1.408	1.408	1.408
B2-O1	1.336	1.378	1.364	1.364	1.370	1.406	1.406	1.375
-O2	1.400	1.378	1.364	1.364	1.394	1.348	1.348	1.376
-O3	1.384	1.372	1.358	1.358	1.383	1.408	1.408	1.408
bond angle (deg)								
O1-B1-O2	119.0	119.8	119.8	119.9	119.7	120.2	124.1	120.0
O1-B1-O3	114.7	120.1	120.1	120.0	121.4	124.1	124.1	120.4
O2-B1-O3	126.1	120.1	120.1	120.0	118.6	115.4	115.4	119.3
O1-B2-O2	121.5	119.8	119.8	119.9	119.7	120.2	120.2	120.0
B1-O1-B2	130.5	179.1	179.1	179.1	136.6	150.3	150.3	146.0
B1-O2-B2	128.3	179.1	179.1	179.1	136.6	150.3	150.3	146.0

Table 5.1. Static simulation in B_2O_3-I using reported potentials

B_2O_3-I		potential set						
	exp.	v1	v2	v3	v4	v5	v6	v7
iii. property (after relaxation)								
elastic constant (GPa)								
E(1,1)	---	167.8	77.99	107.4	162.5	183.6	22.5	30.3
E(1,2)	---	71.8	33.0	37.3	45.0	31.7	3.9	-1.1
bulk modulus (GPa)								
	---	103.8	47.9	60.7	84.2	82.3	10.1	9.4
static dielectric constant (experiment : 3.0 ~ 3.5)								
$\varepsilon_0(1,1)$	---	2.14	2.17	1.90	2.64	2.78	2.78	1.83
$\varepsilon_0(2,2)$	---	2.14	2.17	1.90	2.64	2.78	2.78	1.83
$\varepsilon_0(3,3)$	---	2.12	2.18	1.58	6.40	3.49	3.49	2.53

Table 5.1.(continued) Static simulation in B_2O_3-I using reported potentials

B_2O_3-II		potential sets						
	exp.	v1	v2	v3	v4	v5	v6	v7
i. lattice energy (eV/B_2O_3)								
before relaxation		-179.39	-80.39	-80.07	-79.38	-201.36	-24.67	-24.18
after relaxation		-182.20	-81.67	-80.98	-80.04	-204.71	-25.08	-24.84
ii. structure (after relax)								
volme (%)	±0	+119.13	+116.72	+17.82	+15.15	+30.50	+38.48	+15.65
a (%)	±0	+29.02	+28.98	+2.28	+2.26	+10.13	+10.13	+3.03
b (%)	±0	+29.02	+28.98	+2.28	+2.26	+10.13	+10.13	+3.03
c (%)	±0	+15.34	+14.16	+8.27	+6.73	+8.74	+8.74	+5.81
bond length (Å)								
B1-O1	1.373	1.374	1.360	1.360	1.371	1.363	1.363	1.412
-O2	1.506	1.378	1.363	1.559	1.538	1.399	1.399	1.546
-O2	1.508	1.378	1.363	1.577	1.542	1.399	1.399	1.547
-O2	1.512	---	---	1.603	1.656	---	---	1.558
bond angle (deg)								
O1-B1-O2	110.2	120.2	120.2	111.4	108.1	120.9	120.9	110.1
O1-B1-O2	115.8	120.2	120.2	110.3	112.4	120.9	120.9	110.0
O1-B1-O2	113.1	---	---	110.0	111.0	---	---	109.9
O2-B1-O2	107.4	---	---	109.7	110.5	---	---	109.2
B1-O1-B1	138.6	180.0	180.0	164.8	146.1	180.0	180.0	161.2
B1-O2-B1	118.7	180.0	180.0	121.4	118.6	180.0	144.7	121.4

Table 5.2. Static simulation in B_2O_3-II using reported potentials

B_2O_3-II		potential sets						
	exp.	v1	v2	v3	v4	v5	v6	v7
iii. property (after relaxation)								
elastic constant (GPa)								
E(1,1)	---	480.6	217.6	418.7	406.2	2043.	250.3	326.8
E(1,2)	---	2.6	1.0	57.0	6.3	-42.1	-5.2	46.6
bulk modulus (GPa)								
	---	161.9	73.2	177.5	139.6	652.9	80.0	140.0
static dielectric constant (experiment : 3.0 ~ 3.5)								
$\varepsilon_0(1,1)$	---	2.13	2.17	2.26	2.02	2.00	2.00	1.44
$\varepsilon_0(2,2)$	---	2.11	2.05	2.29	1.83	3.33	3.33	1.29
$\varepsilon_0(3,3)$	---	2.16	2.20	2.34	1.82	2.71	2.71	1.29

Table 5.2.(continued) Static simulation in B_2O_3-II using reported potentials

5.5 NEW POTENTIAL DERIVATION METHOD

(LP FITTING METHOD)

5.5.1 PROBLEMS OF EXISTING FITTING METHOD

We first review the common method for fitting interatomic potentials, as in the widely used codes (THBREL and GULP) which have been successfully applied to many systems. The general algorithm in such fitting procedures is as follows:

i. Give the experimental structures, properties and initial potential parameters

ii. Calculate cell strains ($\varepsilon(i)$; i=1~6), internal strains ($\varepsilon_{ij}(i,j)$; i=1~N,j=1~3) and properties (C(i); i=1~m)

iii. Calculate the weighted square sum of the errors S

$$S = \sum_i w_{1i} \cdot \varepsilon(i)^2 + \sum_{ij} w_{2ij} \cdot \varepsilon_{ij}(i,j)^2 + \sum_i w_{3i} \cdot (C(i)-C(i))^2 \quad (5.5)$$

where w_{1i},w_{2ij} and w_{3i} are weighting factors to control the fitness of each value.

iv. Change the potential parameters toward the direction which reduces the residual S

v. Iterate from i. to iv. until S converges

This algorithm can be used for a wide range of fitting problems; and especially, when the reasonable initial potential parameters exist, the procedure is easily applied or refined.

However, when this method was applied for B_2O_3 crystals starting from either reported potential parameters or from modified ones, reasonable potentials were not obtained. In most cases, the 'best fit' potential distorts the experimental structure excessively.

The reason for this problem is thought to be as follows:

i. If an initial parameter set is poor, the least squares fitting procedure will go to the nearest local minimum which is not always the desired solution. One alternative way is to try as many initial sets as possible, but such a procedure may require a lot of trial and error. Obviously if possible one borrows good initial parameters from other studies, but this is not practical when no study has been done before.

ii. The weighting factors affect S very much and they easily change the shape of S, and may lead to an undesirable local minimum. In the case of a layered system, even if quite small residuals of strain are obtained, they are enough to distort its structure very much. The other problem is that completely different types of measurements (e.g. structure and properties) are expressed in the unique formula of S, and it is not always easy to set up the proper weighting factors to unify such different data.

iii. If the initial potential functions are suitable for describing the potential surface, a good solution will be obtained finally, despite problems such as (i) and (ii) above. However, when good solution is not obtained because of the poor potential function, it is not easy to analyze the reason.

5.5.2 NEW FITTING METHOD ('LP FITTING METHOD')

The LP fitting method is designed to fit to ab-initio surfaces with the added constraint of requiring observed experimental structures to reproduced. Some ideas are proposed in order to overcome the problems described in Section 5.5.1.

First, regarding the problem of finding the global minimum, if the problem can be linearized, the global minimum can be found within a finite number of iterations. The second point is that separating the

criterion of crystal stability from the evaluation of properties can make the fitting problem much easier. It is also desirable that the experimental data (such as the structural stability conditions) should be separated from the ab-initio potential energy data as components of the cost function. On the other hand, when common potentials that can reproduce several different structures at the same time are desired, the introduction of independent sets of structural stability conditions is more reasonable than the use of a unique formula of S. The third point is that it is very helpful to know whether a solution of the problem is feasible or not, and also which condition obstructs the solution. In particular, it is not clear how well the B_2O_3 system with covalent bonding can be described with the existing potential functions.

These ideas lead to new potential fitting method based on the Linear Programming (LP) method. The LP method is a well-known technique in the field of economics and mathematics (see Duntzig 1963).

Several special considerations are given in order to adapt the potential fitting problem to the general LP problem as follows:

i. All the conditions are separated into two categories: one is several sets of inequality equations; the other component is a cost function which should be minimized. The fitting problem is replaced with the problem which finds the optimum solution that minimizes the cost function within the solution space that satisfies all the inequality equations.

ii. The conditions of structural stability are defined in the form of inequality equations. Here, the term 'structural stability' means that the relaxed structure does not distort much from the experimental structure. The lattice energy in the experimental structure is thought to be the minimum point in the configurational space (3N-dimension) of energy.

The lattice energy E is defined:

$$E = E(x_1, x_2, \ldots, x_n), \tag{5.6}$$

where the x_i show the position vectors of the i-th atom.

$$\partial E / \partial x_i = 0 \quad ; \quad \partial^2 E / \partial x_i^2 > 0 \tag{5.7}$$

at the experimental structure ($x_1=x_{1e}, \ldots, x_n=x_{ne}$).

then $\forall \Delta x_i$:

$$E(x_{1e}, x_{2e}, \ldots, x_{ie}+\Delta x_i, \ldots, x_{ne}) > E(x_{1e}, x_{2e}, \ldots, x_{ie}, \ldots, x_{ne}) \tag{5.8}$$

and

$$E(x_{1e}, x_{2e}, \ldots, x_{ie}-\Delta x_i, \ldots, x_{ne}) > E(x_{1e}, x_{2e}, \ldots, x_{ie}, \ldots, x_{ne}) \tag{5.9}$$

must be satisfied. When lattice parameter a,b,c,α,β and γ (6 variables) and n atomic positions (n x 3 variables) are taken into account, total (6n + 12) inequality conditions are generated.

iii. The weighted sum of the residuals between the ab-initio data on the potential energy surface and the estimated values using the unknown variables of potential parameters is defined as the cost function. Therefore, the LP method tries to find the solution which realizes the global minimum residual within the solution space that satisfies the structural stability conditions. However, there are two limitations for applying the LP method. One is that it is not easy to implement the evaluation of various physical properties as the cost functions, because within the LP scheme the complex form of such properties must be linearized using the potential parameters. The other is that the cost function must be the linear weighted sum of potential parameters instead of the square weighted sum of them. But there is little difference between two ways of summation.

The most important point of the LP method is that the structural stability conditions are not included in the cost function, but in the inequality equations. Therefore, the merit of this method is that, even if

the potential functions are poor in describing the structure, it finds a solution which maintains the structure in equilibrium, otherwise it returns the message saying that there is no feasible solution.

iv. Once the problem is described within the frame of LP, the solution is quickly solved even by a personal computer. The most significant problem with this method is that the fitting problem must be linearized regarding the potential parameters. Inevitably some parts (e.g. ρ parameter in Buckingham form in (5.2), or β_{ij} and r_0 parameters in Morse form in (5.3)) cannot be linearized simply and must remain fixed as constants during one solution cycle. However, each solution cycle is very quick, allowing a thorough search of a variety of combinations of ρ, D_{ij} or β_{ij} to be easily performed, in order to find the global minimum.

The algorithm used by the LP fitting method is shown as below:

i. Linearization of each of the terms of which the total lattice energy E is comprised:

$$E = Ec + E_2 + E_3 + E_4 \tag{5.10}$$

where Ec, E_2, E_3 and E_4 are the contribution of Coulombic energy, pair-potentials, three-body terms and four-body terms.

For Coulombic terms, they are calculated only from the crystal structure when the charge values are fixed, and they are dealt as constants in inequality equations.

In case of Buckingham form,

$$\begin{aligned} E_2 &= \Sigma_{i>j} \{A\exp(-r_{ij}/\rho) - C/r_{ij}^6\} \\ &= A \cdot \{\Sigma_{i>j} \exp(-r_{ij}/\rho)\} - C \cdot \{\Sigma_{i>j} 1/r_{ij}^6\} \end{aligned} \tag{5.11}$$

The values in the parentheses { } are calculated only from the crystal structures, and are independent of the unknown variables A and C, when ρ is fixed.

In case of Morse form,

$$E_2 = D_{ij} \cdot \Sigma_{i>j} [\exp\{2\beta_{ij}(r_{ij}-r_0)\} - 2\exp\{\beta_{ij}(r_{ij}-r_0)\}] \quad (5.12)$$

Once more the value in the parenthesis [ ] is calculated only from the crystal structures, and is independent of the unknown parameters D_{ij} when β_{ij} and r_0 are fixed.

For the simple harmonic-type three-body terms,

$$E_3 = K_B \cdot \Sigma_{i>j>k}\{1/2\ (\theta_{ijk} - \theta_0)^2\} \quad (5.13)$$

The value in the parenthesis { } is again calculated only from the crystal structures, and is independent of the unknown parameters K_B when θ_0 is fixed. Four-body terms are dealt in the same way as the three-body terms.

ii. To set up the inequality conditions for the structural stability:

$$E\ (x_{1e}, \ldots, x_{ie}\pm\Delta x_i, \ldots, x_{ne}) > E\ (x_{1e}, \ldots, x_{ie}, \ldots, x_{ne}) \quad (5.14)$$

The coefficients of the unknown variables (A, C, D_{ij} and K_B etc.) are calculated for each structural configuration, and (6n+12) sets of inequality equations are generated. For example,

$$c_{1,1} \cdot D_{B\text{-}O} + c_{1,2} \cdot A_{O\text{-}O} - c_{1,3} \cdot C_{O\text{-}O} + C_{1,4} \cdot K_{O\text{-}B\text{-}O} > 0$$

$$c_{2,1} \cdot D_{B\text{-}O} + c_{2,2} \cdot A_{O\text{-}O} - c_{2,3} \cdot C_{O\text{-}O} + C_{2,4} \cdot K_{O\text{-}B\text{-}O} > 0$$

$$\begin{array}{ccc} \bullet & \bullet & \bullet \\ \bullet & \bullet & \bullet \end{array}$$

$$c_{6n+12,1} \cdot D_{B\text{-}O} + c_{6n+12,2} \cdot A_{O\text{-}O} - c_{6n+12,3} \cdot C_{O\text{-}O} + C_{6n+12,4} \cdot K_{O\text{-}B\text{-}O} > 0$$

In the case of the B_2O_3 system, the Morse form for the B-O interaction, the Buckingham form for the O-O interactions, and the three-body term for the O-B-O interactions are used, and there are four variables ($D_{B\text{-}O}$,$A_{O\text{-}O}$,$C_{O\text{-}O}$ and $K_{O\text{-}B\text{-}O}$). Among the inequality equations, twelve come from the variations of the cell parameters ($a\pm\Delta a$, $b\pm\Delta b$, $c\pm\Delta c$, $\alpha\pm\Delta\alpha$, $\beta\pm\Delta\beta$, $\gamma\pm\Delta\gamma$), and 6n come from tha variations of internal coordinates ($x_i\pm\Delta x_i$, $y_i\pm\Delta y_i$, $z_i\pm\Delta z_i$).

iii. To define the cost function S:

The deviation between the ab-initio data on the potential energy surface and the corresponding value estimated from the linearized sum of the parameters are summed up as the cost function S.

$$S = \sum_i w_i \cdot | E_i^{ab} - E_i^{es} | \qquad (5.15)$$

where w_i is the weighting factor, and E_i^{ab} and E_i^{es} are the energies derived from the ab-initio calculations and the estimated energies as the linear sum of the potential parameters. Usually all the weighting factors are set to 1, and do not need to be changed.

iv. To add the extra inequality conditions if necessary:

For example, if the total lattice energy is restricted within some specific range (for example, Emin < E and E < Emax are given), two inequality equations are added in the same manner as in (ii). It is also very easy to specify the difference of energies between several different structures (for example, when the energy differences $\Delta E12$ and $\Delta E23$ between three polymorphic structures are given, $E_1 + \Delta E_{12} < E_2$ and $E_2 + \Delta E_{23} < E_3$ are added) .

v. To apply the general LP algorithm:

The coefficients calculated from i. to iv. generate the general matrix elements for LP and the variables are solved so that they minimize the cost function S at the finite calculation steps.

vi. Iterate from (i) to (v), changing the non-linear parts (e.g. ρ, β, or r_0) to yield the solution which realize the global minimum. As many combinations as possible of the unknown parameters are applied systematically.

We may compare this LP fitting method with the other general algorithms as follows:

The strengths of the method are:

i. It is especially suitable for the ill-conditioned problem, where the crystal structure is apt to move toward a catastrophic change (for example, in the case of layered or planar structure). Because the structural stability conditions are absolutely satisfied during the solution, it can always prevent the distortion of its structure. The method is also suitable for the simultaneous fitting among several structures, because all the structural stability conditions are satisfied independently and simultaneously.

ii. When the linearised coefficients are output, the potential energy surface which depends on the variables (A, C, D_{ij} and K_B) can be easily analyzed, because it is simply the linear sum of each term. In particular, when a satisfactory potential cannot be obtained, it is straightforward to find which stability condition obstructs the solution.

iii. The global minimum can be obtained with a very modest computer resources. There is no problem about setting initial conditions or the weighting factors, and no empirical adjustments necessary.

The weak points of this method are;

i. The method cannot be applied generally. The requirement that all the conditions must be linearized is very restrictive. Therefore, features including fitting to crystal properties or use of the shell model cannot be included at the moment. In such cases it is possible to refine the LP-fitted parameters by using more general fitting programs. It is interesting to note that this LP method is based on linearized optimization with constraints, while the other general method is based on non-linear optimization without constraint. In future, when LP method is iteratively solved on one hand and the other general method

adds the constraint conditions on the other hand, both methods will approach one another.

5.6 APPLICATION OF LP FITTING METHOD TO B_2O_3 CRYSTALS

We now apply the new LP fitting method to the derivation of interatomic potentials for B_2O_3 crystals.

5.6.1 FITTING TO B_2O_3-I STRUCTURE

The experimental structural data of B_2O_3-I are used to obtain the structural stability conditions (thirty-four structural configurations), while the ab-initio potential energy data (nine structural configurations) derived from CRYSTAL calculations (see Chapter 3) are used as components of the cost function.

The fitted potentials and the resulting static simulations are shown in Tables 5.3 ~ 5.5.

The Morse potential in the B-O interactions can compensate for some part of the lattice energy that is lost on reducing the effective charges, so a 90% ionicity model is used instead of the formal charge in potential a1 to potential a3. Buckingham potentials are used for the O-O and B-B interactions. Potential a1 includes pair, three-body plus four-body terms, potential a2 includes pair and three-body terms and potential a3 includes only pair-potential terms. In potential a4 and potential a5 charges are reduced to 50% and 40% ionicity. For the four-body term, the O-B-O-O type torsion on the BO_3 triangle is taken into account:

$$V = K4 \cdot (1 - \cos(2\phi)), \qquad (5.16)$$

where K4 is a force constant and ϕ is the torsion angle. This term works to keep the BO_3 triangle planar.

The fitted results are summarised as follows:

i. When the Buckingham potential was used for the B-O interactions, no acceptable solution was obtained. Therefore, the Morse potential was subsequently employed.

ii. When the results of potential a1, potential a2 and potential a3 are compared, it is found that the pair-potential model (potential a3) is very poor in describing the B-O-B bond angles and the cell volume (or density), as shown in Section 5.4. It is interesting to note that the fitting O-B-O force constant is zero both for potential a1 and for potential a2. It may mean that the effects of the O-B-O interactions can be mimiced by the O-O interactions, while the B-O-B interactions cannot be easily replaced with the B-B interactions.

iii. It is interesting to note that the potentials which are fitted only using the data of B_2O_3-I can reproduce the structure of B_2O_3-II well.

iv. Even if charges are varied, the experimental structure can be reproduced with the short-range potentials being refitted, but the elastic constants or bulk modulus are dependent upon the charge values. Generally speaking, the more ionic model has the larger bulk modulus. When the bulk modulus (30~50 [GPa] for B_2O_3-I and 100-~130 [GPa] for B_2O_3-II) calculated in Chapter 4 are taken into account, ionicity of 40% or less may be appropriate (see Chapter 4). Ionicities of this magnitude also agree with the Mulliken charge ($qB \approx =+1.2$) calculated in Chapter 3.

iv. For the rigid ion model, the calculated static dielectric constants are smaller than the experimental values (3.0 ~ 3.5) as expected. If the shell model is used, such problems may be overcome.

5.6.2 FITTING TO BOTH B_2O_3-I AND B_2O_3-II STRUCTURES

Next, in order to reproduce better the structures of both B_2O_3-I and B_2O_3-II, simultaneous fitting is performed. For B_2O_3-I, thirteen structural configurations and twelve ab-initio data are used for the structural stability conditions and as components of the cost function; while for B_2O_3-II, seven structural configurations and twelve ab-initio

data are used for the structural stability conditions and as components of the cost function. The fitted potential (potential b1) and the resulting static simulations are shown in Tables 5.6 ~ 5.8.

Potential b1 can reproduce both crystal structures very well. With the simultaneous fitting, both structures can be equally reproduced. However, two problems still remain. The first is that the difference in the B-O bond lengths of B_2O_3-II is not well reproduced. As discussed in Chapter 3, the coordination numbers around O1 and O2 are two and three, and their difference is thought to be one of the reasons for changing the B-O bond lengths. The second problem is that the lattice energy of B_2O_3-II is sometimes lower or almost same as that of B_2O_3-I. This trend which becomes stronger as the ionic charges are reduced clearly causes problems concerning the relative stabilities of the different structures.

In order to overcome these problems, we have developed a new approach. We recall from Chapter 3 that the B-O bond strength changes according to its coordination number. Moreover, in the case of B_2O_3, the coordination number around the oxygen atoms seems especially important. Therefore, different Morse and Buckingham potentials are assigned for two-fold and three-fold coordinated oxygen. In order to keep the energy of B_2O_3-I lower than that of B_2O_3-II, one inequality condition:

$$E_{B2O3\text{-}I} < E_{B2O3\text{-}II} \qquad (5.17)$$

is added during fitting. The fitted potential (potential c1 and potential c2) and the resulting static simulations are shown in Tables 5.6 ~ 5.8. Potential c1 is fitted with charges corresponding to 40% ionicity, while potential c2 is fitted with 30% ionicity. Both potentials reproduce not only the lattice parameters but also the bond lengths and bond angles in

the two crystals, while keeping the energy of B_2O_3-I lower than that of B_2O_3-II. These potentials will be applied to MD calculations in Chapter 6.

parameters	potential sets				
	a1	a2	a3	a4	a5
Charge					
q(B)	+2.7	+2.7	+2.7	+1.5	+1.2
q(O)	-1.8	-1.8	-1.8	-1.0	-0.8
Morse potential for B-O					
D [eV]	2.580	1.549	1.344	0.466	0.326
β[1/Å]	2.5	2.7	2.7	2.7	2.7
ro [Å]	1.55	1.59	1.59	1.59	1.59
Buckingham potential for O-O					
A [eV]	2229.	6317.	5878.	795.	727.
ρ [Å]	0.36	0.35	0.35	0.35	0.35
C [eV·Å^6]	0.0	935.2	662.2	60.9	80.9
Buckingham potential for B-B					
A [eV]	0.	0.	0.	0.	0.
ρ [Å]	0.35	0.35	0.35	0.35	0.35
C [eV·Å^6]	314.9	0.	456.3	9.1	19.4
three-body term for O-B-O (θ_0 = 120 for three-fold; θ_0 = 109.47 for four-fold)					
k [eV/rad^2]	0.	0.	0.	---	---
three-body term for B-O-B (θ_0 = 120)					
k [eV/rad^2]	8.08	4.79	---	6.63	2.53
four-body term for O-B-O-O					
k[EV]	0.85	---	---	---	---

Table 5.3. Fitted potentials using B_2O_3-I structure and ab-initio data

B_2O_3-I		potential sets				
	exp.	a1	a2	a3	a4	a5
i. lattice energy (eV/B_2O_3)						
before relaxation		-182.47	-183.95	-181.11	-52.99	-34.81
after relaxation		-182.76	-184.81	-181.70	-53.05	-34.90
ii. structure (after relaxation)						
volume (%)	±0	+1.89	-3.60	+2.05	-2.92	-5.48
a (%)	±0	+1.49	+0.79	+2.54	+0.19	+0.04
b (%)	±0	+1.49	+0.79	+2.54	+0.19	+0.04
c (%)	±0	-1.09	-5.09	-2.94	-3.29	-5.55
bond length (Å)						
B1-O1	1.404	1.386	1.375	1.372	1.405	1.393
-O2	1.366	1.358	1.384	1.374	1.357	1.371
-O3	1.337	1.366	1.384	1.373	1.374	1.381
B2-O1	1.336	1.358	1.385	1.374	1.356	1.371
-O2	1.400	1.386	1.375	1.372	1.404	1.392
-O3	1.384	1.366	1.384	1.373	1.375	1.382
bond angle (deg)						
O1-B1-O2	119.0	120.3	118.6	119.1	119.3	118.7
O1-B1-O3	114.7	117.7	121.4	120.7	115.4	117.6
O2-B1-O3	126.1	122.0	119.9	120.2	125.2	123.6
O1-B2-O2	121.5	120.3	118.5	119.1	119.3	118.7
B1-O1-B2	130.5	134.7	134.6	140.1	130.4	131.1
B1-O2-B2	128.3	134.7	134.6	140.1	130.4	131.2

Table 5.4. Static simulation in B_2O_3-I using fitted potentials (a1 ~ a5)

B_2O_3-I		potential sets				
	exp.	a1	a2	a3	a4	a5
iii. property (after relaxation)						
elastic constant (GPa)						
E(1,1)	---	473.9	642.7	488.5	176.5	116.7
E(1,2)	---	122.8	157.9	96.4	52.3	32.4
bulk modulus (GPa)						
	---	239.8	319.5	227.1	93.7	60.5
static dielectric constant (experiment : 3.0 ~ 3.5)						
$\varepsilon_0(1,1)$	---	1.64	2.08	2.17	1.80	1.84
$\varepsilon_0(2,2)$	---	1.64	2.08	2.17	1.80	1.84
$\varepsilon_0(3,3)$	---	1.68	4.05	2.77	2.41	2.57

Table 5.4.(continued) Static simulation in B_2O_3-I using fitted potentials (a1 ~ a5)

B_2O_3-II		potential sets				
	exp.	a1	a2	a3	a4	a5
i. lattice energy (eV/B_2O_3)						
before relaxation		-183.74	-183.89	-179.54	-54.08	-35.70
after relaxation		-184.12	-184.20	-180.08	-54.29	-35.77
ii. structure (after relaxation)						
volme (%)	±0	+0.52	+4.12	+5.15	+3.83	+0.56
a (%)	±0	+0.24	+0.94	+2.11	+0.48	-0.38
b (%)	±0	+0.24	+0.94	+2.11	+0.48	-0.38
c (%)	±0	-0.33	+2.03	+1.12	+1.82	+0.96
bond length (Å)						
B1-O1	1.373	1.429	1.398	1.445	1.393	1.406
-O2	1.506	1.450	1.492	1.509	1.439	1.462
-O2	1.508	1.471	1.540	1.510	1.470	1.497
-O2	1.512	1.532	1.555	1.521	1.672	1.553
bond angle (deg)						
O1-B1-O2	110.2	107.1	110.3	111.0	104.1	106.8
O1-B1-O2	115.8	113.6	114.4	110.8	117.0	115.2
O1-B1-O2	113.1	111.3	111.7	111.8	112.5	111.8
O2-B1-O2	107.4	109.3	110.6	108.1	109.3	110.4
B1-O1-B1	138.6	138.6	138.7	142.0	131.5	134.7
B1-O2-B1	118.7	119.3	118.5	117.7	119.3	118.7

Table 5.5. Static simulation in B_2O_3-II using fitted potentials (a1 ~ a5)

B_2O_3-II	potential sets					
	exp.	a1	a2	a3	a4	a5
iii. property (after relaxation)						
elastic constant (GPa)						
E(1,1)	---	1429.6	1339.7	1179.3	257.0	265.7
E(1,2)	---	167.2	217.2	89.9	-26.9	45.3
bulk modulus (GPa)						
	---	588.0	591.4	453.0	67.8	118.7
static dielectric constant (experiment : 3.0 ~ 3.5)						
$\varepsilon_0(1,1)$	---	2.33	2.24	3.09	2.02	2.19
$\varepsilon_0(2,2)$	---	2.45	3.45	4.58	1.83	3.35
$\varepsilon_0(3,3)$	---	2.43	3.16	5.78	1.82	2.40

Table 5.5.(continued) Static simulation in B_2O_3-II using fitted potentials (a1~a5)

parameters	potential sets		
	b1	c1	c2
Charge			
q(B)	+1.2	+1.2	+0.9
q(O)	-0.8	-0.8	-0.6
Morse potential for B-O			
for two-fold oxygen atom O2			
D [eV]	2.322	1.84	1.79
β[1/Å]	2.5	2.7	2.7
ro [Å]	1.35	1.35	1.35
for three-fold oxygen atom O3			
D [eV]	2.322	10.98	0.96
β[1/Å]	2.5	2.7	2.7
ro [Å]	1.35	1.475	1.475
Buckingham potential for O-O			
A [eV] for O2-O2	2231.5	1990.8	485.8
A [eV] for O2-O3	2231.5	1650.9	422.9
A [eV] for O3-O3	2231.5	692.3	193.4
ρ [Å]	0.30	0.30	0.30
C [eV·Å^6]	0.0	0.0	0.0
Buckingham potential for B-B			
A [eV]	0.	323.1	0.0
ρ [Å]	0.30	0.30	0.35
C [eV·Å^6]	0.0	0.0	0.0

Table 5.6. Fitted potentials using both crystal structures and ab-initio data

parameters	potential sets		
	b1	c1	c2
three-body term for O-B-O (θ_0 = 120 for three-fold; θ_0 = 109.47 for four-fold)			
for three-fold boron atom			
k [eV/rad^2]	2.0	0.	3.24
for four-fold boron atom			
k [eV/rad^2]	2.0	1.66	1.94
three-body term for B-O-B (θ_0 = 120)			
for two-fold oxygen atom			
k [eV/rad^2]	5.58	6.38	4.60
for three-fold oxygen atom			
k [eV/rad^2]	5.58	4.22	4.53
four-body term for O-B-O-O			
k [eV/rad2]	0.02	---	---

Table 5.6.(continued) Fitted potentials using both crystal structures and ab-initio data

B_2O_3-I		potential sets		
	exp.	b1	c1	c2
i. lattice energy (eV/B_2O_3)				
before relaxation		-44.74	-42.05	-27.16
after relaxation		-44.83	-42.11	-27.24
ii. structure (after relaxation)				
volume (%)	±0	+0.30	+1.87	+1.32
a (%)	±0	+0.89	+0.87	+0.83
b (%)	±0	+0.89	+0.87	+0.83
c (%)	±0	-1.47	+0.12	-0.34
bond length (Å)				
B1-O1	1.404	1.396	1.409	1.398
-O2	1.366	1.358	1.346	1.367
-O3	1.337	1.365	1.362	1.364
B2-O1	1.336	1.358	1.346	1.367
-O2	1.400	1.396	1.409	1.398
-O3	1.384	1.365	1.362	1.364
bond angle (deg)				
O1-B1-O2	119.0	120.3	120.1	120.4
O1-B1-O3	114.7	116.6	115.3	116.1
O2-B1-O3	126.1	122.7	124.0	121.7
O1-B2-O2	121.5	120.3	120.1	120.4
B1-O1-B2	130.5	131.9	131.4	130.7
B1-O2-B2	128.3	131.9	131.4	130.7

Table 5.7. Static simulation in B_2O_3-I using fitted potentials (b1, c1 and c2)

B_2O_3-I		potential sets		
	exp.	b1	c1	c2
iii. property (after relaxation)				
elastic constant (GPa)				
E(1,1)	---	223.4	191.6	138.6
E(1,2)	---	58.9	52.4	38.5
bulk modulus (GPa)				
	---	113.8	98.8	71.9
static dielectric constant (experiment : 3.0 ~ 3.5)				
$\varepsilon_0(1,1)$	---	1.44	1.60	1.40
$\varepsilon_0(2,2)$	---	1.44	1.60	1.40
$\varepsilon_0(3,3)$	---	2.13	2.38	2.59

Table 5.7.(continued) Static simulation in B_2O_3-I using fitted potentials (b1, c1 and c2)

B_2O_3-II		potential sets		
	exp.	b1	c1	c2
i. lattice energy (eV/B_2O_3)				
before relaxation		-44.50	-40.70	-25.77
after relaxation		-44.73	-40.84	-25.84
ii. structure (after relaxation)				
volme (%)	±0	+1.52	-2.53	-1.96
a (%)	±0	+0.09	-0.27	-0.79
b (%)	±0	+0.09	-0.27	-0.79
c (%)	±0	+0.75	-0.49	+0.42
bond length (Å)				
B1-O1	1.373	1.419	1.346	1.367
-O2	1.506	1.449	1.476	1.489
-O2	1.508	1.469	1.502	1.501
-O2	1.512	1.597	1.564	1.543
bond angle (deg)				
O1-B1-O2	110.2	105.8	110.6	109.5
O1-B1-O2	115.8	113.5	117.9	116.1
O1-B1-O2	113.1	112.3	115.2	114.3
O2-B1-O2	107.4	109.3	107.5	108.3
B1-O1-B1	138.6	133.5	134.1	133.2
B1-O2-B1	118.7	118.8	120.0	119.7

Table 5.8. Static simulation in B_2O_3-II using fitted potentials (b1, c1 and c2)

B_2O_3-II		potential sets		
	exp.	b1	c1	c2
iii. property (after relaxation)				
elastic constant (GPa)				
E(1,1)	---	531.4	577.4	403.2
E(1,2)	---	-3.0	83.2	65.7
bulk modulus (GPa)				
	---	175.1	248.0	178.2
static dielectric constant (experiment : 3.0 ~ 3.5)				
$\varepsilon_0(1,1)$	---	1.67	1.59	1.32
$\varepsilon_0(2,2)$	---	1.56	1.65	1.34
$\varepsilon_0(3,3)$	---	1.57	1.68	1.40

Table 5.8.(continued) Static simulation in B_2O_3-II using fitted potentials (b1, c1 and c2)

5.7 COMPARISON OF CRYSTALLINE POTENTIALS WITH MOLECULAR POTENTIALS

5.7.1 POTENTIALS DERIVED FROM MOLECULAR CLUSTERS

For the SiO_2 system, several sets of interatomic potentials derived from ab-initio calculations on the related molecular clusters have been applied to crystalline and vitreous states. In the B_2O_3 system, Gupta and Tossell (1981,1983), Gibbs et al. (1981) and Zhang et al. (1985) showed that molecular clusters mimic the geometry of polyanions in borate minerals. In order to obtain several potential energy surfaces of molecular clusters, ab-initio calculations were performed on the monomer HBO_3, the dimer $H_4B_2O_5$ and the trimer $H_3B_3O_6$ using a 6-31G* basis set in the GAUSSIAN-90 program. The schematic diagrams of the three structures are shown in figure 5.1. For HBO_3, its structure is optimized with C_1 symmetry. After optimisation, the B-O bond lengths (the optimised value of which is 1.374 Å) are varied from 1.0 [Å] to 2.0 [Å] and the O-B-O bond angles are varied from 105° to 135°. For $H_4B_2O_5$, the structure is optimized with C_2 symmetry. After the optimization, the B-O-B bond angle (the optimized value of which is 134.5°) is varied from 120° to 150°. For $H_3B_3O_6$, its structure is optimised with C_{3h} and the O-B-O and the B-O-B angles remain fixed at 120°. The optimized B-O bond length is 1.384 [Å] for in-ring bonds and 1.358 [Å] for out-of-ring bonds.

There are several assumptions made in deriving the resulting potentials. In order to keep charge neutrality, the charge of the hydrogen atom (qH) is varied, with the charges of boron atom (qB) and oxygen (qO) being changed so as to keep the relations:

$$qB = 3 \cdot qH \quad \text{and} \quad qO = -2 \cdot qH$$

Hydrogen atoms are derived solely in terms of the point charge (qH) and the interactions between oxygen atom and hydrogen atom bonded to it

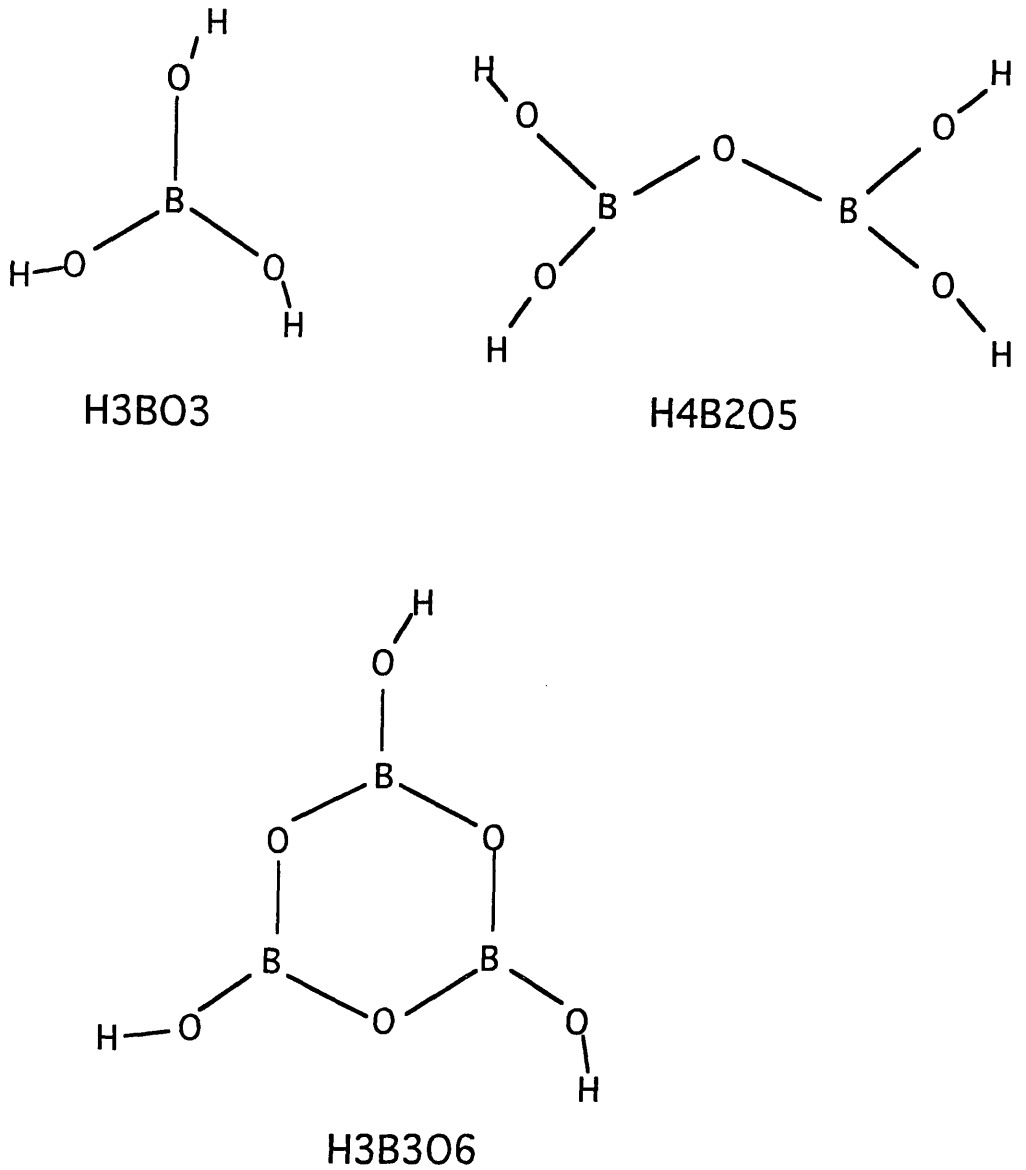

Figure 5.1. Molecular clusters used for deriving potentials

are assumed to be unchanged, because the H-O bond lengths remain fixed.

The general least-square fitting procedure is employed, varying the charge qH. We used partial charge model with Buckingham potentials for the B-O and O-O interactions and three-body terms for the O-B-O and B-O-B interactions. The fitted potentials are shown in Table 5.9. Potential d1 or potential d2 is fitted using the long-range B-O data (1.0Å < R(B-O) < 2.0Å) or the short-range B-O data (1.15Å < R(B-O) < 1.55Å).

When used in modelling the B_2O_3-I crystal, both potentials d1 or d2 results in an expansion of the cell volume by 35% or 17%. Several other fittings were performed (for example, using a Morse potential or with different charges), but none of them could reproduce the B_2O_3 structure well. This difficulty means that the effects of the crystalline environments are not simply expressed by the addition of the electrostatic Madelung potential; and it may suggest that the short-range terms must be varied according the change in the slope of charge distribution. More detailed discussion is given in the following chapter.

parameter	potential d1			potential d2		
Charge	q(B)	q(O)		q(B)	q(O)	
	+1.11	-0.74		+1.11	-0.74	
Buckingham potential for B-O						
	A[eV]	ρ[Å]	C[eVÅ^6]	A[eV]	ρ[Å]	C[eVÅ^6]
	1843.0	0.169	0.	592.4	0.192	0.
Buckingham potential for O-O						
	A[eV]	ρ[Å]	C[eVÅ^6]	A[eV]	ρ[Å]	C[eVÅ^6]
	1919.8	0.284	0.	8207.0	0.235	0.
Three body terms for O-B-O (θ_0=120) and B-O-B (θ_0=120)						
	k(O-B-O)		k(B-O-B)	k(O-B-O)		k(B-O-B)
	0.0004		1.625	1.675		1.251

Table 5.9. Fitted potentials using ab-intio data on molecular clusters

5.7.2 POTENTIALS DERIVED BOTH FROM CRYSTALS AND MOLECULAR CLUSTERS

In the previous chapter, the simple application of the potentials derived from the ab-initio data on the molecular clusters failed to reproduce the B_2O_3-I structure. Is there any common potential transferable for both crystal structures and molecular clusters?

Here, several simultaneous LP fitting calculations were performed using both the crystal structural and the molecular cluster data. LP fitting is very suitable for this sort of study, because the conditions for molecular clusters and crystals are dealt with independently and equally. The input conditions used for the LP fitting are shown in Table 5.10. A total of seven fits were performed which differ in the data that were used; the fitted potentials and the resulting static simulations are shown in Tables 5.11~5.13.

The calculated results are discussed as follows;

i. Before investigating the models based on 40% and 20% ionicity (potentials e1~e7), several other charge values were tested. In general, the models with higher ionicity (>30%) are good for reproducing the crystal structures, while the lower ionicity model (<20%) is good for reproducing the molecular structures. 40% ionicity (qB=+1.2, qO=-0.8) is close to the Mulliken charge (qB=+1.1) in B_2O_3-I calculated by the CRYSTAL codes (STO3-21G basis set), and 20% ionicity (qB=+0.6, qO=-0.4) is close to that (qB=+0.65) in HBO_3 calculated by the GAUSSIAN-90 code (MP2/6-311G**). The aim of the present fitting is to explore the possibility of a common potential for both crystals and molecules, so a common charge value is used in the LP fitting, although the crystal is clearly more ionic than the molecules.

ii. When all the conditions are used at the same time in the LP fitting, no feasible solution existed. Therefore, several combinations of conditions are used in the LP fitting.

iii. Potential e3 and potential e6 show the case where only ab-initio data and the stability conditions of the molecules are used without data on the crystals. It is interesting to note that the D parameter in the B-O Morse potential is larger than those of the other cases, and this seems to lead to the smaller cell volume in B_2O_3-I. We also find that the experimental B-O bond lengths in the crystalline states are almost the same as those calculated from the ab-initio simulations in the molecular states (see Table 3.1 and Table 5.13). Thus in the molecular state there are no crystal effects (due to long-range electrostatic forces), and the effects of B-O covalent bonding on the Morse term are stronger than in the crystalline states.

iv. Potential e1 and potential e4 refer to the case where the ab-initio data on the molecules are used as components of the cost function, while the stabilisation conditions of the crystals are used. The fitted results give a smaller D value in the B-O Morse potential and a larger force constant (K) of the B-O-B interactions, compared with the results of potential e3 and potential e6. The smaller D value suggests that in the crystalline states the crystal field can substitute some part of the B-O attractive terms. Regarding the larger K value, a possible reason may be that in the crystalline state the bond interactions between the B and O atoms may be reduced because of the reduction of the charge overlaps, while the B-B Coulombic repulsive interactions in this ionic model are too large to express the former interactions, and finally only the B-O-B term can compensate for such difference, as long as the same charge

values are used. Therefore, the role of the B-O-B three-body term seems to be very important in the ionic model of the crystalline system.

v. Potential e2 and potential e5 show the case where only ab-initio data and the structural stability conditions of crystals are used. As for potential e2, both crystal structures are reproduced very well, while it does not reproduce molecular structures. In contrast to the case of potential e3 and potential e6, the D parameter in the B-O Morse potential has a small value corresponding to the crystalline state. However, the potential behaves poorly for the molecular states and results in long B-O bond lengths. Moreover, potential e5 fails to reproduce the structure of B_2O_3-I; the relaxed structure, using potential e5, has four-fold coordination around boron atoms. In general, the smaller charge value is used, the more difficult becomes the simultaneous fitting of B_2O_3-I and B_2O_3-II, and small charge models cannot reproduce both structures at the same time. One of the reasons may be that the latter model has nothing to compensate the difference in the Madelung potential caused from the structural differences between polymorphs.

vi. Potential e7 shows the case where both the molecular and the crystal data are used, except the data of B_2O_3-II. There is no feasible solution for 40% or higher charge model, or in the case when the data for B_2O_3-II is added. However, potential e7 reproduces the B-O bond lengths for the three molecules and the cell volumes in both crystals reasonably at the same time, except the B-O-B bond angles in B_2O_3-I. It suggests that it is difficult to reproduce both molecular and crystalline structures precisely with the common potential, but that the 20% charge model can reproduce them both to some extent.

vii. There are two problems remaining in applying these potentials to MD simulations. One is the large C value in the O-O interactions fitted

in the 20% ionicity model. It generates too large an attractive force when the O-O distance becomes short. The other is the energy difference between B_2O_3-I and B_2O_3-II. In the cases of potentials e1, e2, e3, e6 and e7, the energy of B_2O_3-II is lower than that of B_2O_3-I. During the LP fitting, one inequality condition shown in (5.17) can be added, but it is very difficult to find an acceptable solution for the smaller charge models (20% or less) with reproducing both structures. The MD simulations will be discussed in Chapter 6.

To summarize, it is difficult to find such transferable potential models that reproduce the two crystal structures and the three molecular structures at the same time. Even the best model often fails to reproduce the order of the lattice energies. When compared with the 'molecular' potentials, the 'crystalline' potentials prefer to the higher charge models, then if the same charges as for the 'molecular' potentials, the B-O attractive terms are weaker and the force constant of the B-O-B interactions is larger.

Finally, it is interesting to note that although the bond lengths and bond angles are very similar for the molecular states and the crystalline states, the potentials parameters are different fitted so that the bonding and the crystal field effects compensate each other.

	ab-initio data	structural stability data
Monomer HBO_3	10 configurations	2 configurations
$E(R_{(B-O)}, \theta_{(O-B-O)})$ optimized value $R_{(B-O)}=1.374$ $\theta_{(O-B-O)}=120.$	E(1.374, 120.), E(1.3, 120.), E(1.35, 120.), E(1.40, 120.), E(1.45, 120.), E(1.50, 120.), E(1.374, 110.), E(1.374, 115.), E(1.374, 125.), E(1.374, 130.)	E(1.384, 120.) > E(1.374, 120.) E(1.364, 120.) > E(1.374, 120.)
Dimer $H_4B_2O_5$	7 configurations	2 configurations
$E(\theta_{(B-Obr-B)})$ optimized value $R_{(B-Obr)}=1.365$ $R_{(B-Onbr)}=1.355$ $\theta_{(O-B-O)}=134.5$	E(134.5), E(120.), E(125.), E(130.), E(140.), E(145.), E(150.)	E(139.5) > E(134.5) E(129.5) > E(134.5)
Trimer H3B3O6	no data used	4 configurations
$E(R_{(B-Obr)},R_{(B-Onbr)})$ optimized value $R_{(B-Obr)}=1.384$ $R_{(B-Onbr)}=1.358$		E(1.374, 1.358) > E(1.384, 1.358) E(1.364, 1.358) > E(1.384, 1.358) E(1.384, 1.368) > E(1.384, 1.358) E(1.384, 1.348) > E(1.384, 1.358)
B_2O_3-I crystal	9 configurations	12 configurations
exp = experimental structure	E(exp), E(a,b,c:+4%), E(a,b,c:+2%), E(a,b,c:-4%), E(a,b,c:-2%), E(c:+3%), E(c:-2%), E(a:+2%), E(a:-1%)	E(a:+1%or-1%) > E(exp) E(b:+1%or-1%) > E(exp) E(c:+1%or-1%) > E(exp) E(α:+2.5°or-2.5°) > E(exp) E(β:+2.5°or-2.5°) > E(exp) E(γ:+2.5°or-2.5°) > E(exp)
B_2O_3-II crystal	no data used	12 configurations
exp = experimental structure		E(a:+1%or-1%) > E(exp) E(b:+1%or-1%) > E(exp) E(c:+1%or-1%) > E(exp) E(α:+2.5°or-2.5°) > E(exp) E(β:+2.5°or-2.5°) > E(exp) E(γ:+2.5°or-2.5°) > E(exp)

Table 5.10. Input conditions used for LP fitting

	potential sets						
parameters	e1	e2	e3	e4	e5	e6	e7
Charge							
q(B)	+1.2	+1.2	+1.2	+0.6	+0.6	+0.6	+0.6
q(O)	-0.8	-0.8	-0.8	-0.4	-0.4	-0.4	-0.4
Momomer							
ab-initio data	@		@	@		@	@
stability data			@			@	@
Dimer							
ab-initio data	@		@	@		@	@
stability data			@			@	@
Trimer							
stability data			@			@	@
B_2O_3-I							
ab-initio data		@			@		@
stability data	@	@		@	@		@
B_2O_3-II							
stability data	@	@		@	@		

Table 5.11. Input table for LP fitting

(@ means its data is used during LP fitting.)

	potential sets						
parameter	e1	e2	e3	e4	e5	e6	e7
Charge							
q(B)	+1.2	+1.2	+1.2	+0.6	+0.6	+0.6	+0.6
q(O)	-0.8	-0.8	-0.8	-0.4	-0.4	-0.4	-0.4
Morse potential for B-O							
D [eV]	2.48	2.53	4.05	2.65	3.90	4.28	4.09
β [1/Å]	2.7	2.7	2.7	2.9	2.7	2.7	2.8
ro [Å]	1.35	1.35	1.30	1.28	1.28	1.28	1.28
Buckingham potential for O-O							
A [eV]	2250.	2286.	1679.	1632.	2245.	2371.	2447.
ρ [Å]	0.30	0.30	0.30	0.30	0.30	0.30	0.30
C[eV·Å^6]	0.	0.	0.	0.	0.1	37.1	42.0
Buckingham potential for B-B							
A [eV]	0.	0.	440.8	0.	0.	1348.	1290.
ρ [Å]	0.30	0.30	0.30	0.30	0.30	0.30	0.30
C[eV·Å^6]	0.	0.	0.	0.	0.	0.	0.
three-body term for O-B-O (k3,θ_0=120 for three-fold; k4,θ_0=109.47 for four-fold)							
k3 [eV/rad^2]	0.	0.	0.93	1.09	0.	0.08	0.01
k4 [eV/rad^2]	5.00	1.78	---	7.47	17.79	---	1.04
three-body term for B-O-B (θ_0=120)							
k [eV/rad^2]	1.37	4.47	0.50	0.14	0.02	0.88	1.04

Table 5.12. LP fitted potentials using molecular data and crystal data (e1~e7)

		potential sets						
parameter	exp.	e1	e2	e3	e4	e5	e6	e7
Monomer R[Å]								
R(B-O)	1.374	1.374	1.464 #	1.374	1.384	1.394	1.374	1.374
Dimer R[Å], θ[deg]								
R(B-Obr)	1.365	1.455#	1.455#	1.365	1.395	1.385	1.365	1.365
θ(B-Obr-B)	134.5	131.5	127.5	132.5	132.5	144.5#	132.5	133.5
Trimer								
R(B-Obr)	1.384	1.459#	1.455#	1.374	1.384	1.384	1.394	1.394
R(B-Onbr)	1.358	1.458#	1.458#	1.368	1.388	1.398	1.368	1.368
B_2O_3-I cell volume [%], lattice energy [eV/B_2O_3]								
energy	---	-46.21	-46.11	-57.69	-20.38	-26.60	-29.76	-28.39
cell volume	±0	+9.8#	+0.9	-25.8#	+11.0#	-5.29	-4.46	+0.93
θ(B-O-B)av	130.	140.1#	132.4	126.7	138.5#	##	136.5#	138.5#
B_2O_3-II								
energy	---	-46.31	-46.16	-59.87	-20.14	-26.48	-30.44	-28.64
cell volume	±0	+2.1	+0.4	-15.1#	-1.55	+0.50	-2.33	-1.27

Table 5.13. Static simulation using fitted potentials (e1~e7)

(# means its result is away from the experiment.)

5.8 'COMPUTER SYNTHESIS' OF NEW POSSIBLE POLYMORPHS AND POSSIBLE STRUCTURAL UNIT OF VITREOUS B_2O_3

We now investigate whether it is possible to construct polymorphs based on boroxol-rings type. We will report several computer experiments which were performed in order to explore new structures for B_2O_3. The starting point is to look for the starting structures which seem to be closest to the new polymorphs or the vitreous structures, among the borate crystals. It was shown in Chapter 2 and 3 that the structure of B_2O_3 is far from the borate structures which have a high content of modifier oxides; and as the content of modifier oxides increases, a three-dimensional type of infinite network changes into a assembly of isolated structural units with non-bridging oxygen atoms. Therefore, it is desirable to start from the structure with the least content of modifier oxides found in the borate minerals. Cesium enneaborate $Cs_2O \cdot 9B_2O_3$ (Krogh-Moe and Ihara 1967) is the first starting structure. This structure has two three-dimensional interlocking, twin networks base on B-O bonds (see Figure 5.2). The topology is such that it is not possible to pass from the one network to the other. The network consists of two kinds of basic unit, a triborate group (containing a six-membered ring, but with one of the boron atoms coordinated tetrahedrally by oxygen atoms) and a boroxol group in the ratio one to two. We recall that the vitreous structure of B_2O_3 is claimed to have a high fraction of boroxol rings, and such a structure as metaboric acid HBO_2-III (Peters and Milberg 1964), which comprises only boroxol rings, with only a small effect due to H_2O, is another good starting structure. The structure is hydrogen bonded with sheets of trimeric HBO_2 molecules (six-membered rings) loosely stacked to form a mica-like, platey crystal in the orthorhombic system (Peters and Milberg 1964) as shown in Figure 5.3.

5.8.1 CONSTRUCTION OF NEW POLYMORPHS FROM HBO_2-III

It is necessary to dehydrate HBO_2-III, for which there are several possible routes. One is that some of the hydrogen bonding between layers may be easily rearranged. Two of the three hydroxyl groups, -O(3)H(3) and -O(6)H(6), are almost directly above and below the BO_3 groups of the boron atoms B(1) and B(2), while the remaining -O(1)H(1) group interacts to a lesser degree with its centre related counterpart (Peters an Milberg 1964; see figure 5.3). At first, all the O(1) atoms are extracted with all the H(1) hydrogen atoms. Next, half of the O(3) and O(6) atoms, and all the H(3) and H(6) atoms are extracted. The O(3) or O(6) atoms must be extracted alternately in the vertical direction so that the bonding of B(1)-O(6) or B(2)-O(3) can be generated.

After the extraction of the hydrogen and oxygen atoms, the remaining O(3) and O(6) atoms are moved to the middle point between the two neighbouring boron atoms which are expected to bond to the O(3) and O(6) atoms. Next, the static simulations are performed using the potential c2 potential. Before the expected bondings are generated, the B-O Morse D parameter is set to be five times its normal value and is restored to the original value after the generation of the bonding.

The resulting completely relaxed structure (B_2O_3-a) is as follows: its unit cell includes six molecules; its lattice parameters are a= 13.63 [Å], b= 5.73 [Å], c= 7.79 [Å], α= 86.0 [deg], β= 98.7 [deg], γ= 99.8 [deg]; and its density is 1.17 [g/cm^3]. It comprises 100% boroxol rings with no independent BO_3 triangle. It is interesting to note three points. The first point is that this structure is similar to the vitreous structure, because the average B-O bond length is 1.36 [Å] and the average B-O-B bond angle outside boroxol rings is 128 [deg]. The other point is that its density is much higher than that of the glass (1.84 [g/cm^3]), in line with previous claims that the 100%

boroxol model cannot reproduce the glass density (see, for example, Cooper 1978; Elliot 1978). The third point is that although its original structure is layered, its final structure turns out to be close to the two three-dimensional interlocking type of networks, found in the crystal structure of $Cs_2O \cdot 9B_2O_3$.

Next, in order to get such higher density as the experimental vitreous density, a final change was made to this structure: half of the B_3O_6 unit are replaced with a BO_3 unit. After this change, static simulations were performed using the potential c2 potential in the same manner as for B_2O_3-a.

The completely relaxed structure of (B_2O_3-b) is as follows: its unit cell includes four molecules; its lattice parameters are a= 10.22 [Å], b= 5.71 [Å], c= 6.13 [Å], α= 78.2 [deg], β= 87.3 [deg], γ= 94.6 [deg]; and its density is 1.33 [g/cm^3]. It comprises of 100% boroxol rings with no independent BO_3 triangle. All the B-O bond lengths and bond angles are almost same as B_2O_3-a, while the density increases by 14% compared with that for B_2O_3-a. The results show that the final density is strongly affected by the intermediate-range structure However, they may suggest that it would be difficult to construct such crystal structure that comprises 100% boroxol rings, keeping the experimental glass density.

5.8.2 CONSTRUCTION OF NEW POLYMORPHS FROM $Cs_2O \cdot 9B_2O_3$

The first problem here is again how to extract Cs_2O from the original crystal structure. We must check whether reasonable new B-O bonded structures can be generated or not, after the oxygen atoms have been extracted. One of the obvious routes is to extract half of the O(3) atoms so that the O(3)-O(5') bonding is disconnected and new B(2)-O(3)

bonding is generated in the manner that the network above is connected with the network below (see Figure 5.2). After these manipulations, static simulations are performed using the potential c2 in the same way as with B_2O_3-a.

The completely relaxed structure (B_2O_3-c) is as follows: its unit cell includes eighteen molecules; its lattice parameters are a= 7.99 [Å], b= 10.05 [Å], c= 16.20 [Å], α= 94.4 [deg], β= 90.0 [deg], γ= 90.0 [deg]; and its density is 1.60 [g/cm^3], which is only 15% smaller than that of B_2O_3 glass. The ratio of B_3O_6 units to BO_3 units is 2 : 3, that is a fraction of 66.7% of the boron atoms are in boroxol rings. The basic structure comprises interlocking three-dimensional networks which is the same as the structure of $Cs_2O \cdot 9B_2O_3$, but one BO_3 unit connects two neighbouring networks together. In the same network, three BO_3 units are connected in series. One BO_3 is connected with two B_3O_6 units, while the other two units are connected with one B_3O_6 unit. The manner of connecting the BO_3 units is shown in Figure 5.4. The average B-O bond length is 1.36 [Å] and the average B-O-B bond angle outside the boroxol rings is 128 [deg].

Next, in order to get a density as high as the experimental vitreous density, a final change was made to this structure: two BO_3 units, (B(2), O(3), O(4), O(8')) and (B(2'), O(8), O(4'), O(5')) were replaced with one BO_3 unit simply by topological manipulations. After the manipulation, static simulations were performed with the potential c2 in the same manner as the case of B_2O_3-a. The completely relaxed structure (B_2O_3-d) is as follows: its unit cell includes sixteen molecules; its lattice parameters are a= 7.94 [Å], b= 8.58 [Å], c= 16.55 [Å], α= 96.1 [deg], β= 85.0 [deg], γ= 88.0 [deg]; and its density is 1.72 [g/cm^3], which is only 6.9% smaller than that of B_2O_3 glass.

The ratio of B_3O_6 units to BO_3 units is 1 : 1, this comprises a fraction 75% of the boron atoms are in boroxol rings. The basic structure comprises two interlocking three-dimensional networks without any connection between them, which is same as $Cs_2O \cdot 9B_2O_3$. Two BO_3 units are connected in series and each BO_3 unit is connected with two B_3O_6 units. The manner of connection of the BO_3 units is shown in Figure 5.5.

5.8.3 DISCUSSION

It is interesting to note that all four new structures have almost the same B-O bond lengths and B-O-B bond angles outside the boroxol rings the same as those of B_2O_3-I and vitreous B_2O_3. Although there is no known crystal structure containing boroxol rings, the calculated lattice energies of these four structures are lower than that of B_2O_3-I, and even if they are metastable at finite temperatures, it seems possible that they are candidates for a new polymorph.

On the other hand, for vitreous B_2O_3, it has been claimed that there is no structure model with the experimental density and a high fraction of boron atoms in boroxol rings without layered rings. Artificially, crystals constructed in the manner of the layer model proposed by Bell and Carnevale (1981) were generated and the static simulations were performed. However, the calculated distances between the layers became longer and longer, and a stable structure could not be obtained. Our potential model show that boric oxide does not favour a layer structure.

Structures B_2O_3-d as well as B_2O_3-c could be structural units in the vitreous B_2O_3. Thus they have as much as a 75% fraction of boron atoms in boroxol rings: this figure agrees with that estimated for the vitreous material by Jellison et al (1977) and Johnson et al (1982). In addition they

not only have reasonable B-O bond lengths and B-O-B bond angles, but they also have a reasonable density, although it is still smaller than that observed for vitreous B_2O_3. Thirdly we note that the structure has a three-dimensional network without layered rings.

The most realistic structure for vitreous B_2O_3 is thought to be that in which B_2O_3-d and B_2O_3-e are randomly connected and also some B_3O_6 units are replaced with BO_3 units in order to reproduce the experimental density. The most characteristic feature of such structures is that the three-dimensional networks are interlocking, and two or three BO_3 units are the main connecting parts between B_3O_6 units, so that the density of the vitreous B_2O_3 can be reproduced. The new structures constructed in this chapter will be compared with the vitreous structures obtained employing the MD method in chapter 6.

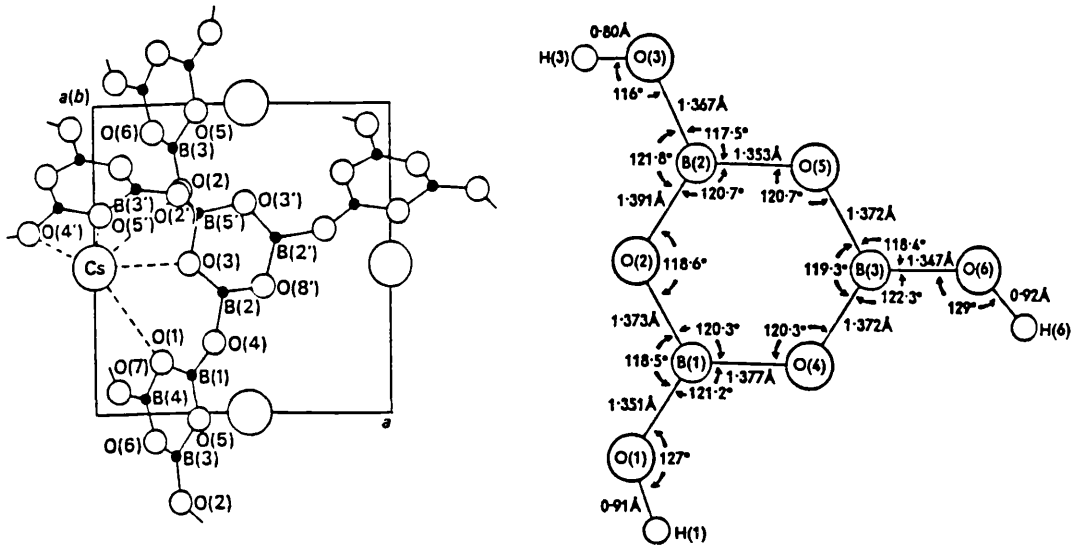

(a)

Figure 5.2 Crystal structure of $Cs_2O \cdot 9B_2O_3$

(Krogh-Moe and Ihara 1967)

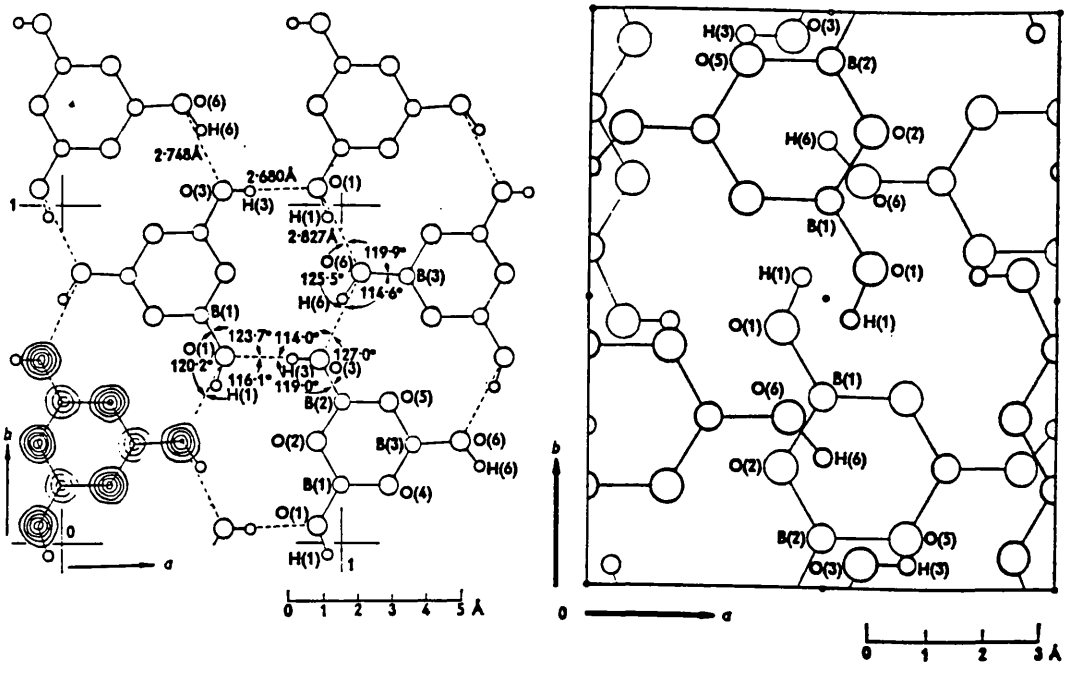

(b)

(c)

Figure 5.3.(a),(b),(c) Crystal structure of HBO_2-III (Peters and Milberg 1964)

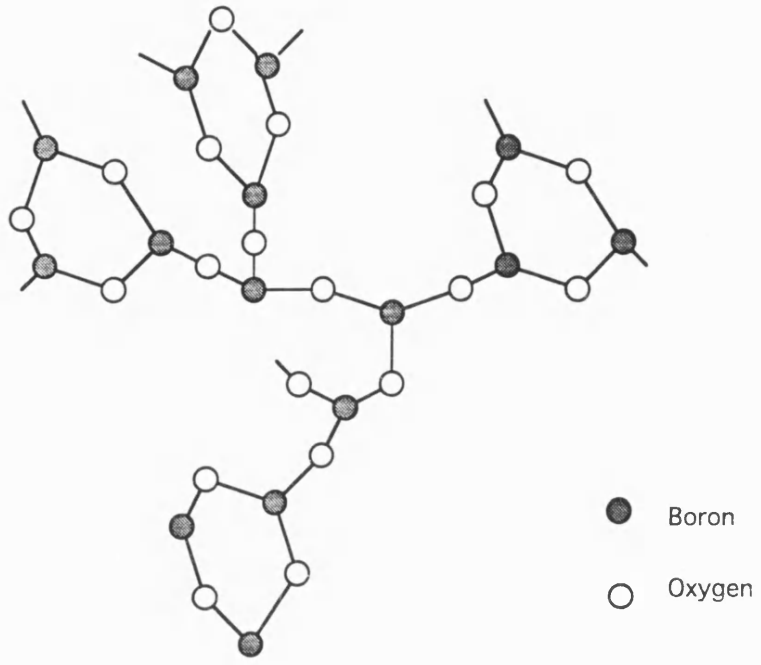

Figure 5.4 Connecting of B_3O_6 units with BO_3 units in B_2O_3-c

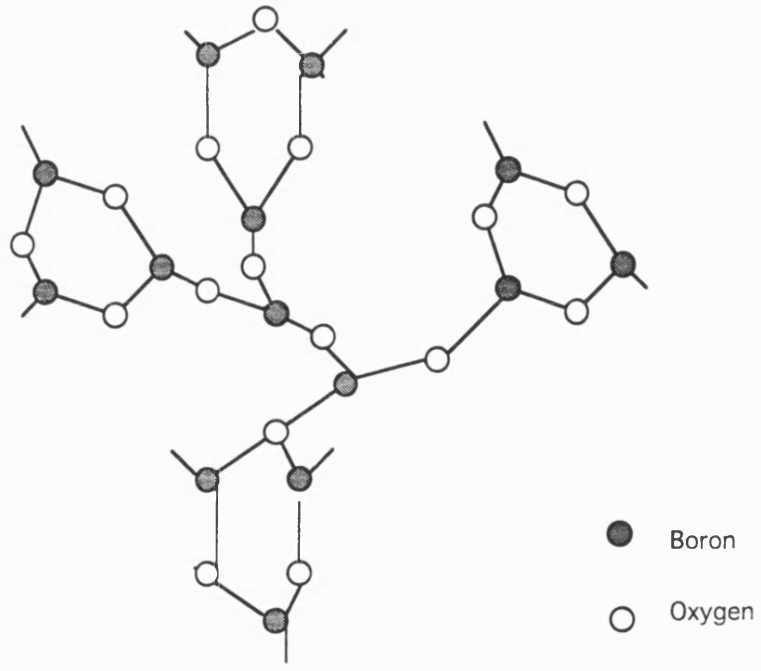

Figure 5.5 Connection of B_3O_6 units with BO_3 units in B_2O_3-d

5.9 LATTICE DYNAMICS SIMULATION

The strong peak of the Raman spectrum of B_2O_3 glass at 806 cm^{-1} is one of the strongest pieces of evidence for the existence of boroxol rings.

Verhoef and Hartog (1991,1992) performed MD simulations of B_2O_3 glass. Although their structures comprised of only BO_3 triangles without boroxol groups, they concluded that the vibrational modes of adjacent BO_3 triangles are decoupled sufficiently and a local breathing mode can occur; indeed the peak at 806 cm^{-1} in the experimental Raman spectra was assigned to such a breathing mode of three oxygen atoms within each of the BO_3 triangles.

On the other hand, Bronswijk and Strijks (1977) compared the experimental Raman spectrum of vitreous B_2O_3 with that of crystalline B_2O_3. They concluded that the spectrum of crystalline B_2O_3 does not show a strong, sharp and polarized band around 806 cm^{-1} (see Figure 5.6).

Since the structures discussed in the previous chapter contain a high percentage of boroxol rings, lattice dynamics simulations were performed for the B_2O_3-I crystal, and for B_2O_3-a and B_2O_3-d pseudo super crystals using potential c2 employing the GULP program (Gale 1993). The calculated vibrational densities of states at 300K are shown in Figure 5.7. As it is not easy to calculate their Raman spectra, only experimental peaks both in B_2O_3-I crystal and that of B_3O_6 (v2; see Figure 2.9) are compared with the calculated spectra.

In the spectrum of B_2O_3-I, there is a sharp peak at around 750 cm^{-1} (see the position A in Figure 5.7 (a)). It can be assigned to a bending mode in the chain structure (Kamitsos and Chryssikos 1991), and is close to the experimental wavenumber of 720 cm^{-1}. There is no peak at 806 cm^{-1}; however, in the spectrum of B_2O_3-a, the peak at ~ 750 cm^{-1} disappears and is replaced by a new peak at ~ 820 cm^{-1} (see position B in

Figure 5.7 (B)). It can be assigned to the breathing mode of B_3O_6 (v2), and is close to the experimental wavenumber 806 cm^{-1}. In the spectrum of B_2O_3-d, which may be closest to the vitreous B_2O_3, there is no peak at around 750 cm^{-1}, although the structure includes BO_3 units. It shows the peak at ~ 820 cm^{-1}, although it is a little weaker than in the case of B_2O_3-a.

Therefore, these results support the hypothesis that the peak at 806 cm^{-1} in the experimental Raman spectrum in vitreous B_2O_3 can be assigned to the breathing mode of B_3O_6 units, although there are two problems remaining. The first is that the potential used (c2) was not adjusted in order to reproduce the vibrational frequencies and there is therefore a small off-set in the calculated wavenumber. Secondly the structure of the pseudo super crystal (B_2O_3-d) must of course differ from the vitreous structure of B_2O_3. However, even if this structure were more distorted, its vibrational character is assumed not to be too different, as long as the same fraction of boroxol rings exist in the structure.

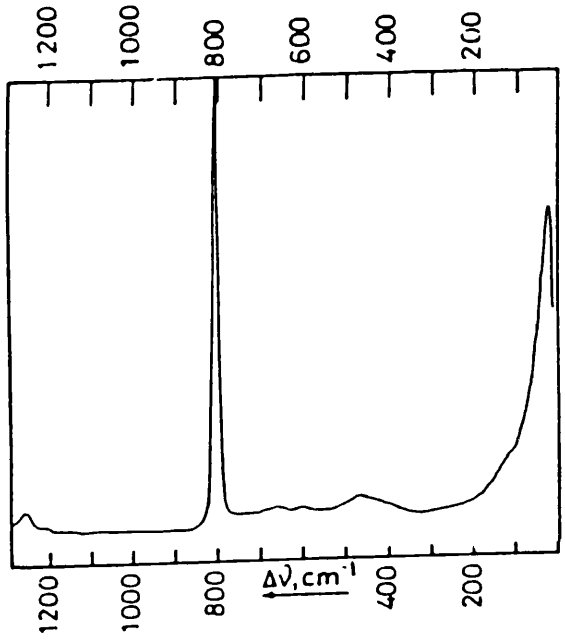

(a)

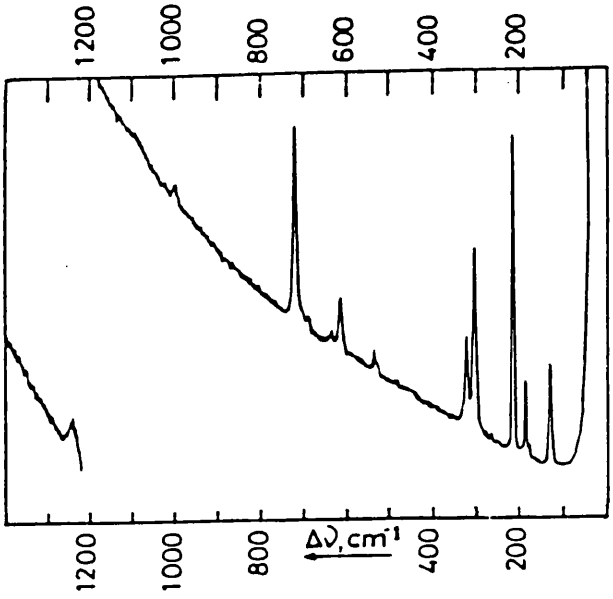

(b)

Figure 5.6. Experimental Raman spectra

(a) vitreous B_2O_3

(b) crystalline B_2O_3-I

(Bronswijk and Strijks 1977)

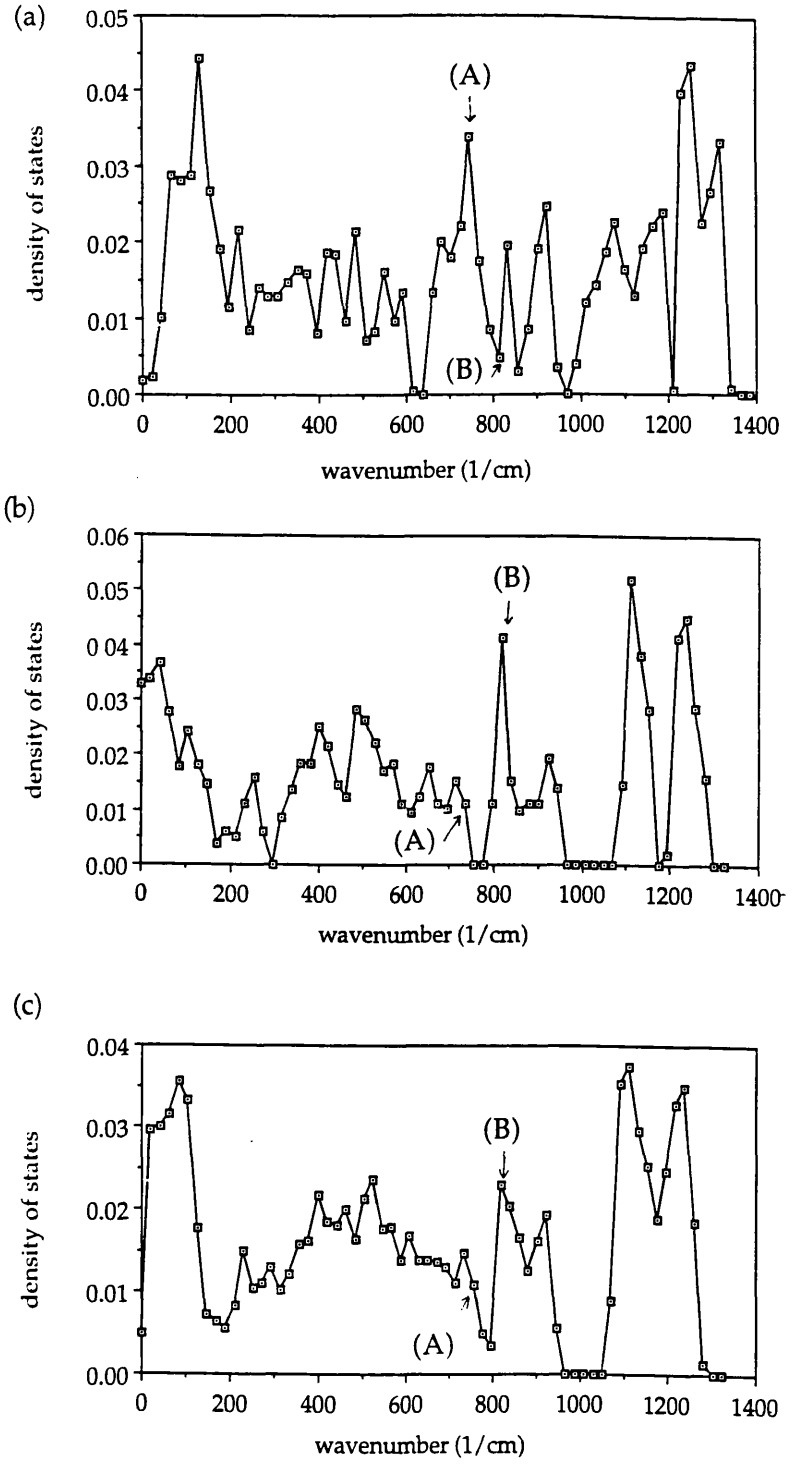

Figure 5.7. Calculated densities of states

(a) crystalline B_2O_3-I

(b) pseudo super crystal B_2O_3-a

(c) pseudo super crystal B_2O_3-d

5.10 CONCLUSIONS

In order to overcome the difficulty of deriving the interatomic potentials for B_2O_3 crystals, a new LP fitting method has been developed. This method has been successfully applied to crystals and molecular clusters of B_2O_3; and several sets of potentials which can reproduce both crystal structures have been derived.

This LP method shows that the partial charge model with a B-O Morse potential and a B-O-B bond-bending, three-body term can reproduce both crystal structures very well. It is also found that the B-O Morse potential and the force constant for B-O-B is differently fitted for the crystal states and for the molecular states in a manner which compensates crystal field effects. The comparison of the lattice energies between two structures suggests that different short-range potentials must be defined to reproduce the order of their energies, and new potential sets (potential c1 and potential c2) which depend on the coordination number around the oxygen atoms have been developed. These potentials can reproduce not only the structures but also the order of the lattice energies.

Finally, several new possible polymorphs of B_2O_3 are obtained by performing static simulations using the potential c2 potential. In particular, B_2O_3-d is the first structural model for the basic unit of vitreous B_2O_3, which can reproduce not only the B-O bond lengths and the B-O-B bond angles, but also the density, with 75% of boron atoms in boroxol rings. The lattice dynamic simulations using this structure and the potential c2 also shows that the peak of the experimental Raman peak at 806 cm^{-1} can be assigned to the breathing mode of the boroxol rings. The important feature in this structure is thought to be the

interlocking three-dimensional networks with two or three BO_3 units connecting the B_3O_6 units.

Since the transferable potential models obtained employing the LP fitting method have elucidated several features in the structure and bonding on the crystalline B_2O_3 in this chapter, these will be applied to vitreous structures employing the MD method in Chapter 6.

6. COMPUTER MODELLING OF VITREOUS B_2O_3

6.1 INTRODUCTION

In Chapter 5 several sets of potentials which can reproduce both crystal structures of B_2O_3 were developed. In this chapter we use the MD method with these potentials to investigate the vitreous states of B_2O_3.

First, we discuss the particular features of the MD method, when used to study glassy materials. Our MD calculations were performed employing the modified version of the code FUNGUS (Walker 1982; Vessal 1991; Hernandez 1993). The potential model (e1), which reproduces both crystal structures of B_2O_3 was applied to the simulated melting and quenching of the B_2O_3-I crystal. Next, new potential models (modification of potentials c1 and c2), which can overcome some problems apparent in the calculations employing the previous potentials, were developed. These new models vary parameters automatically depending on the coordination number. The results of the MD calculations using these potentials are compared with the X-ray diffraction data and the neutron scattering data. These results not only confirm the existence of the boroxol rings, but also give some information about the intermediate-range order and the structural transformations in the vitreous structures. Finally, the ratio of the boron atoms contained in the boroxol rings are estimated.

6.2 THE MOLECULAR DYNAMICS (MD) METHOD

In modelling crystal structures, conventional lattice statics and dynamics are powerful tools. However, when vitreous structures are modelled, the Molecular Dynamics technique, which treats dynamic effects explicitly and includes anharmonic effects, is the appropriate method.

As noted in Chapter 2, since vitreous structures do not have long-range order, it is difficult for experimental techniques to determine their detailed structures. Moreover, the final vitreous structures are considerably affected by their thermal history including the quench rate, which it is difficult to investigate experimentally. MD simulations can therefore provide valuable complementary information concerning these complex phenomena. Theoretical and technical aspects of the MD method are given in detail in many books (for example, Ciccotti and Hoover 1986; Ciccotti et al 1987; Allen and Tildesley 1987; Soules 1990). Here, we summarize the special features of the MD method when applied to the structures and properties of vitreous materials.

6.2.1 THEORETICAL OUTLINE

The basis of the method is the calculation of the classical trajectories of the interacting ions. The total force acting on each ion is evaluated from the interatomic potentials at a given time and used to determine new positions at time $t + \Delta t$. An initial set of ionic positions, $x(0)$ may be chosen randomly or taken from the crystallographic coordinates. An initial set of velocities is usually taken from a Boltzmann distribution of velocities.

First, the forces acting on each ion is calculated by evaluating the gradient of the interatomic potentials:

$$F_i(t) = -q_i \cdot \Sigma_{j \neq i} q_j/(r_{ij})^2$$
$$- \Sigma_{j \neq i}[\nabla_i \cdot V2_{ij}(|r_i - r_j|)] - \Sigma_{k \neq i}\Sigma_{j \neq i}[\nabla_i \cdot V3_{ijk}(\theta_{ijk})] \qquad (6.1)$$

where $f_i(t)$ is the force acting on atom i at time t. The first term is the long-range Coulombic interaction corresponding to the interaction between the effective charges q_i and q_j. The second and the third are the pair and the three-body potentials.

In order to deal with an infinite lattice, periodic boundary conditions are usually implemented; the simulation box is replicated throughout space. In the course of the simulation, as an ion moves in the original box, its periodic image in each of the neighbouring boxes moves in exactly the same way. The typical number of ions in the simulation box is 100 ~ 1000. It is important to consider whether the properties of such a small, infinite, periodic system and the macroscopic system which it represents, are the same.

To calculate the long-range Coulombic interactions, the Ewald sum has been used (Ewald 1921). This technique efficiently sums the interactions between an ion and all its periodic images. It transforms the slowly convergent summation into two rapidly convergent series: one in real and the other in reciprocal space.

For the short-range interactions, the 'minimum image convention' is usually implemented: ion i interacts with all the ions whose centres lie within such region that is with the closest periodic images of the other N-1 atoms. The details of the potentials is discussed in the following section.

After the force ($f_i(t)$) acting on each ion is computed, the positions of all ions are updated using a finite-difference discretization of Newton's equations:

$$\ddot{x}_i(t) = m_i^{-1} \cdot f_i(t) \qquad (6.2)$$

where m_i is the mass of atom i. The most widely used method of integrating the equations of motion is the scheme initially adopted by Verlet (1967). The equation for advancing the positions are as follows:

$$x_i(t+\Delta t) = 2 \cdot x_i(t) - x_i(t-\Delta t) + (\Delta t^2/m_i) \cdot f_i(t), \quad (6.3)$$

$$v_i(t+\Delta t) = (x_i(t+\Delta t) - x_i(t)) / \Delta t \quad (6.4)$$

where v_i is the velocity of the ion i. A small time step is required for stability of the integration scheme (usually 1fs = 10^{-15}s). This time step must be considerably shorter than the smallest period of oscillation of any ions moves around. It is important to note that the computer resources strongly restrict the period of real time sampled in MD simulations (at most 1ns).

Finally, properties as lattice energy (U), kinetic energy (KE), temperature (T) and pressure (P) in the system are evaluated at each time step.

$$U = -\Sigma_{j\neq i} q_i q_j / r_{ij} + \Sigma_{j\neq i}[V2_{ij}(|r_i - r_j|)] + \Sigma_{k\neq i}\Sigma_{j\neq i}[V3_{ijk}(\theta_{ijk})] \quad (6.5)$$

$$KE = 1/2 \cdot \Sigma_i m_i v_i \cdot v_i \quad (6.6)$$

$$T = 2/3 \cdot (KE) / (kN) \quad (6.7)$$

$$P = 1/ (3V) \cdot (\Sigma_i m_i v_i \cdot v_i - x_i \cdot f_i) \quad (6.8)$$

where k is the Boltzmann constant and V is the volume of simulation box.

MD simulations always have two stages: an equilibration phase in which the simulated system attains a full thermal distribution of kinetic energy and equipartition between potential and kinetic energy; secondly a production phase in which the time evolution of the system is monitored. The first stage takes typically 5~20 ps; while production stage can extend by up to ~1 ns in modern calculations. In simulating glasses, we first meet a crystalline phase. These MD simulations are usually

carried out at temperatures which are much higher than the melting temperature so that all ions can diffuse sufficiently enough to generate the equilibrium state. Then the system is cooled by removing kinetic energy, following the desired cooling schedule. After the equilibrium state is obtained, such properties as discussed in Section 6.2.4 are calculated.

6.2.2 POTENTIAL MODELS FOR GLASSES

The most widely used potential function is the pair-potential, fully ionic model, as explained in Section 5.3.1. Such potentials can be efficiently implemented in simulation codes and are easily applied to multi-component systems. Partial charge models may be superior in reproducing the structures and properties of individual systems, but some care must be taken when they are applied to multi-component systems especially in preserving charge neutrality.

Compared with static or lattice dynamics simulations, several approximations are usually made in MD simulations because of the restrictions of computer resources. The first is that the rigid ion model is normally used, although it is possible to implement the shell model (Lindan and Gillan 1993). Regarding covalent effects, three-body terms are often used provided that the coordination numbers do not change much. Vessal et al (1989) demonstrated that the three-body terms can reproduce the detailed structure of vitreous SiO_2 as well that of the crystalline α-quartz structure.

The second approximation is to construct a look-up table for calculations of potentials and forces. Spline functions are used for interpolation between these values. When the size of the simulation box is not changed, the construction of the table is only set up once, while

when the size of simulation box is varied, it must be reconstructed frequently and its efficiency is therefore reduced.

6.2.3 SELECTION OF STATISTICAL ENSEMBLE

Since MD method simulates systems of finite temperature. It is important to define the ensemble of the system. Two schemes are often used separately or together: first, the constant-temperature and second is constant-pressure (see, for example, Allen and Tildesley 1987 for more details).

The constant temperature method is used to control the temperature of an MD ensemble. Several techniques have been proposed. The most widely used technique is to scale the velocities of all ions at each time step by the factor $\sqrt{(T_0/T)}$, which ensures that the total kinetic energy of the system corresponds to the desired temperature T_0 (Woodcock 1971). The constant-temperature method is essential in simulating the glass formation process. The system is kept in the molten state for some interval after which it is slowly quenched.

Several techniques have been proposed for constant pressure simulations. In the method proposed by Andersen (1980), the surroundings behave like a linear elastic volumeric piston which oscillates in time and exerts an external pressure, P_{ext}, on the system. The system finally approaches a steady state at which $P = P_{ext}$. In the FUNGUS code, the method proposed by Berendsen (1984) is adopted, because it does not drastically alter the dynamic trajectories, although the appropriate ensemble has not been identified. The system is made to obey the equation

$$dP/dt = (P_0-P)/t_p \qquad (6.9)$$

where P_0 is the desired pressure and t_p is a time constant. At each step, the volume of the simulation box is scaled by a factor χ, and the molecular centre-of-mass coordinates by a factor $\chi^{1/3}$

$$r' = \chi^{1/3} r \tag{6.10}$$

where

$$\chi = 1 - \beta_T \cdot \Delta t/t_p \cdot (P_0 - P). \tag{6.11}$$

Here, β_T is the isothermal compressibility and Δt the simulation time step. The constant-pressure method is necessary in modelling structural transformations. In particular, the extended constant-pressure algorithm, which allows the simulation box shape to change, has been successfully used to model phase transformations in solids (Parrinello and Raman 1982). However, the method often results in large distortions of the simulation box in the molten state and high-pressure must be applied to the simulation box in such cases.

6.2.4 ANALYSES OF CALCULATED RESULTS

MD simulations yield a large amount of data (for example, see Appendix C). As vitreous structures do not have long-range order, the Radial Distribution Functions (RDFs) contain the most important information about their structures. The calculated RDFs are compared with those from the X-ray or neutron studies. The positions of the peaks in the RDFs and coordination numbers are also used. Bond Angle Distributions (BADs) are helpful in examining the bonding topology.

Diffusion coefficients can also be calculated directly from the results of MD simulations. This is achieved very simply, from plots of the mean displacement (MSD) of the appropriate particles which increases linearly with time if diffusion is occurring.

6.2.5 LIMITATIONS OF MD METHOD

There are three main limitations with present MD methods. The first is provided by finite-size effects, although compared with quantum-mechanical simulations, classical MD methods can simulate much larger systems. When the simulated system is a perfect crystal or its structure has only short-range order, this limitation may not be too serious. However, when the system is disordered, the simulation box must be large enough so that the artificial periodicity does not significantly affect the results. For the Lennard-Jones type potentials the calculations with as many as one million particles may be possible. However, for the case of oxide materials the more sophisticated potentials needed for accurate simulations do not allow such large calculations. The main reason is that for ionic materials the calculation of the long-range Coulombic terms is computationally expensive, although the efficient method of the Ewald sum is now generally used. The other reason is that in order to express covalent effects the potentials have to include three-body and in some cases four-body terms; and these terms require much larger numbers of interactions.

The second limitation is the finite real time sampled in the simulations, which is at most ~1ns and typically 20 ~ 100ps in modern simulations. Most physical properties are calculated by averaging over the simulation. But the period of real time sampled may be insufficient to model the processes occurring in the real system. Thus, in glass formation, the quench rate is crucial in controlling the final vitreous structures. MD quench rates are several orders of magnitude greater than the real rates, nevertheless it still appears possible to simulate the structures of vitreous materials by these techniques.

The third limitation is the accuracy and transferability of the potential model. In MD simulations of vitreous states there are two procedures: in the first, potentials are estimated so as to reproduce the experimental RDF in a trial-and-error manner and in the other the potentials are fitted so as to reproduce the crystal structure or to reproduce the ab-initio potential energy surfaces of molecular clusters; the latter procedure is used in this thesis. The experimental RDF gives only "one-dimensional" information and several different sets of potential models may reproduce it reasonably. The latter method is clearly to be preferred, provided sufficient data are available. Generally, the more data for different structural configurations are used, the more transferable are the potentials so derived. The ab-initio MD method (Car and Parrinello 1985) is clearly promising, because it does not require interatomic potentials. However, it requires a very large amount of CPU time and it cannot easily overcome the first and second limitations. Ab-initio MD simulations may replace classical MD in studying relatively small systems, while the classical MD will continue to be the only viable technique for large complex systems.

6.3 APPLICATION OF TRANSFERABLE POTENTIAL B1 TO MD

Here we apply potential b1 derived in Chapter 5, which reproduces both crystal structures of B_2O_3 to simulating the melting and quenching process of B_2O_3.

The calculated conditions are as follows. The total number of atoms was 480 (192 boron atoms and 288 oxygen atoms). The time step in the calculation was 1 fs. When we started MD simulations, two problems occurred. The first is that when the system was heated to a temperature higher than 1500K in the constant pressure calculations using ambient pressures, the simulation box expanded to become several times larger than the original size and reasonable dimension could not be restored. The second is that when the constant volume method was used, a large fraction of four-fold coordinated boron atoms was generated, which remained even at the 300K. Therefore, we adopted the constant pressure method using ambient pressures and a maximum temperature of 1500K.

The detailed procedure was as follows. The crystal of B_2O_3-I was kept at 1500 K for 10,000 steps. The system was then quenched down to 300 K in 100 K intervals each of 3000 steps and kept at 300 K for 10,000 steps. This melting and quenching process was repeated once more. To check the rate of atomic diffusion during the melting, the rate of disruption of the B-O bonds was counted. In this case, 17% of the initial bonds were broken and rebonded with another partner. Although the atomic diffusion is small, it is encouraging that the simulation reproduced the change in density. Further studies of diffusion processes are reported in Section 6.5.

The calculated coordination numbers, ring sizes, and densities are given in Tables 6.1 ~ 6.3. The results show that 17 six-membered rings, were generated (that is, 27% of boron atoms are present in six-membered

rings), although the proportion is smaller than that estimated experimentally (see Chapter 2). It is interesting to note that even the ambient pressure simulation gave a reasonable density, in contrast to most of the published constant pressure calculations which require extremely high pressures in order to reproduce the experimental density.

The Pair Distribution Functions (PDFs) and the Bond angle Distributions (BADs) are shown in Figures 6.1 ~ 6.4. The assignments of the peaks are shown in Figure 6.5 (Mozzi and Warren 1970). Although the volume of the simulation box expanded about 10% in the ambient pressure simulation, the positions of the peaks of B-O, O-O and B-B seems to be reasonable. It is interesting to note that there are several peaks (for example, G and H) which suggest the existence of boroxol rings and which are not present in the calculated results based on pair-potentials. There is also a major difference in the BADs. All the pair-potential models exhibited a broad distribution of the B-O-B bond angles around ≈ 160°, while the present calculation shows a sharp distribution around 120~130°. As explained in Chapter 5 the B-O-B bond angles were important for reproducing the crystal structure of B_2O_3-I, and they also seem important in the case of the vitreous structures. The average B-O-B bond angle in the borate crystals is approximately 130° and the quantum-chemical calculations on the molecular clusters suggested around 135°. Therefore, it is unlikely that the B-O-B angles are around 160° in the vitreous structures. However, if the potential favours wide B-O-B bond angles, it may prevent the generation of the boroxol rings. The pair-potential model with the full ionic charge results in excessive repulsion between the B-O bonds, as explained in Chapter 5. This is almost certainly one of the reasons why previous MD studies could not generate the boroxol rings. Inclusion of the three-body terms, combined with the

partial charge and the Morse potential, seems to be very effective in modelling partial covalency in compounds such as B_2O_3. In order to check the calculated structures and discuss the more detailed structural features, the comparisons with X-ray diffraction data and the neutron scattering data are useful, and they will be given in Section 6.5.

The next step was to relax this calculated structure to equilibrium at zero Kelvin using the THBREL program. No significant changes in the dimensions of the simulation box occurred during the constant pressure runs. The calculated bulk modulus was 11.4 GPa, compared with the experimental value of ≈ 15 GPa, and the calculated Young's modulus was 15.4 GPa, compared with the experimental value of ≈ 17 GPa.

Although all these results seems to be very satisfactory, there is one problem: 9 four-fold coordinated boron atoms and 9 three-fold coordinated oxygen atoms were observed. Many experiments suggest that almost all the boron atoms are three-fold coordinated (see Chapter 2). Furthermore, half of the six-membered rings contain more than one four-fold coordinated boron atoms, that is, they are not true boroxol rings which are defined to have only three-fold coordinated boron atoms. The observations may be associated with the fact that the lattice energy of B_2O_3-II is calculated to be lower than that of B_2O_3-I, thus this potential would favour four-fold coordination rather than the three-fold coordination in some environments. We attempt to overcome this problem in the next section.

Finally, we attempted to include the aromatic stabilization effects of boroxol rings in our MD simulations. As explained in Section 2.5, the quantum-mechanical calculations suggested that such stabilization effects would not be so large as to control the geometries and networks. We roughly estimated the energy differences in the B-O bond in the

monomer, dimer and trimer(boroxol ring), from the quantum-mechanically calculated energies, and expressed it with the additional attractive Buckingham terms between the B-O interactions. These terms were only added to the B-O interactions present in boroxol rings. Even with these extra terms, there was no significant difference in the structures. The aromatic stabilization effects do not therefore appear to have a significant effect on the simulated structure.

	2-fold	3-fold	4-fold
boron	0%	96%	4%
oxygen	97%	3%	0%

Table 6.1. Distribution of coordination numbers in calculated glass
(constant pressure calculations using potential b1)

ring size	4	6	8	10	12
number	1	17	5	9	14

Table 6.2. Distribution of ring sizes in calculated glass
(total number of atom = 480; constant pressure calculations using potential b1)

	300K crystal	1500K melt	300K glass	[g/cm^3]
experiment	2.56	1.51	1.80	
calculation	---	1.52	1.63	

Table 6.3. Experimental and calculated densities
(constant pressure calculations using potential b1; experimental data from : Macedo et al 1966)

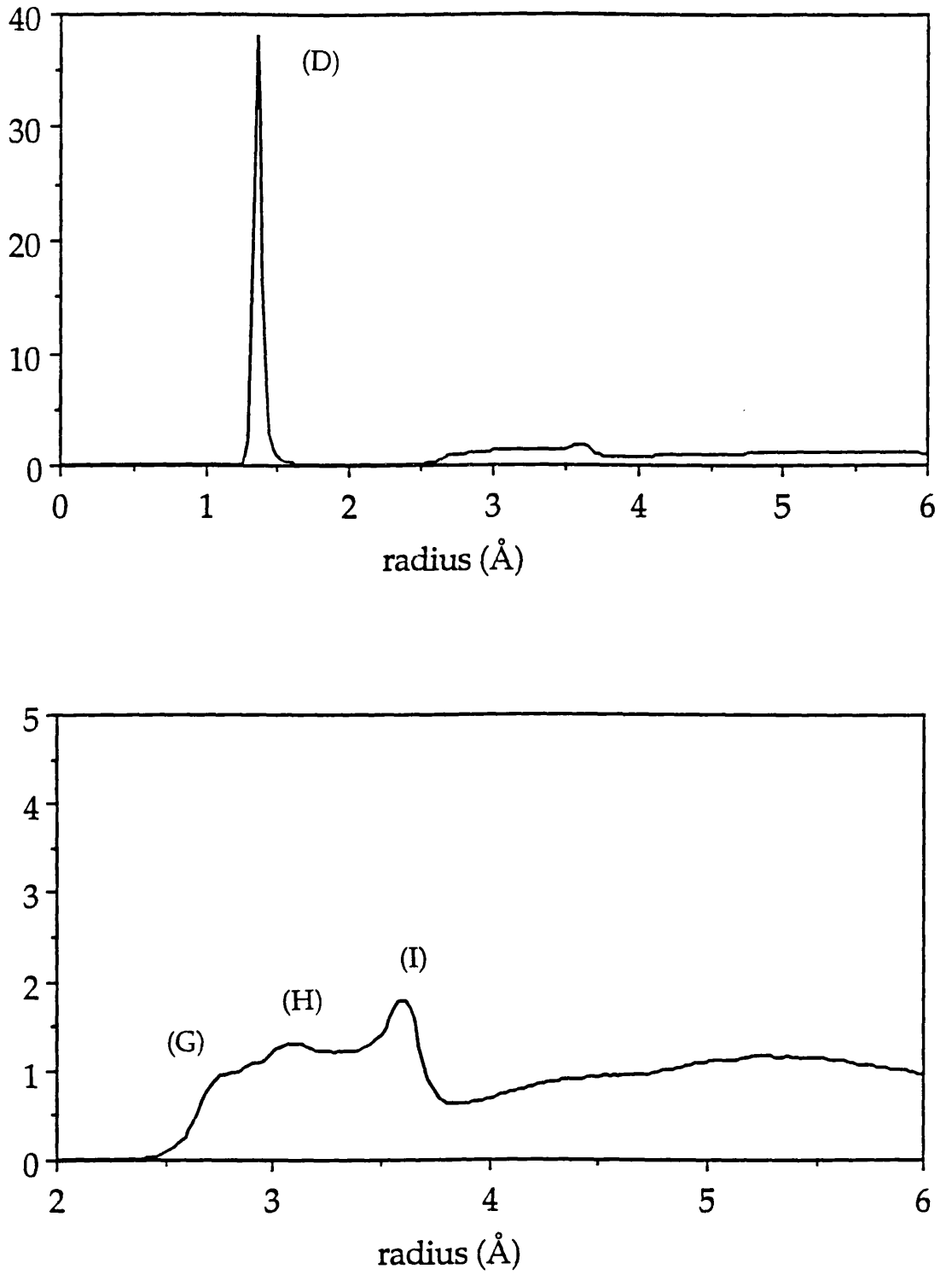

Figure 6.1. Calculated B-O PDF for B_2O_3 glass at 300K
(Potential b1 is used.)

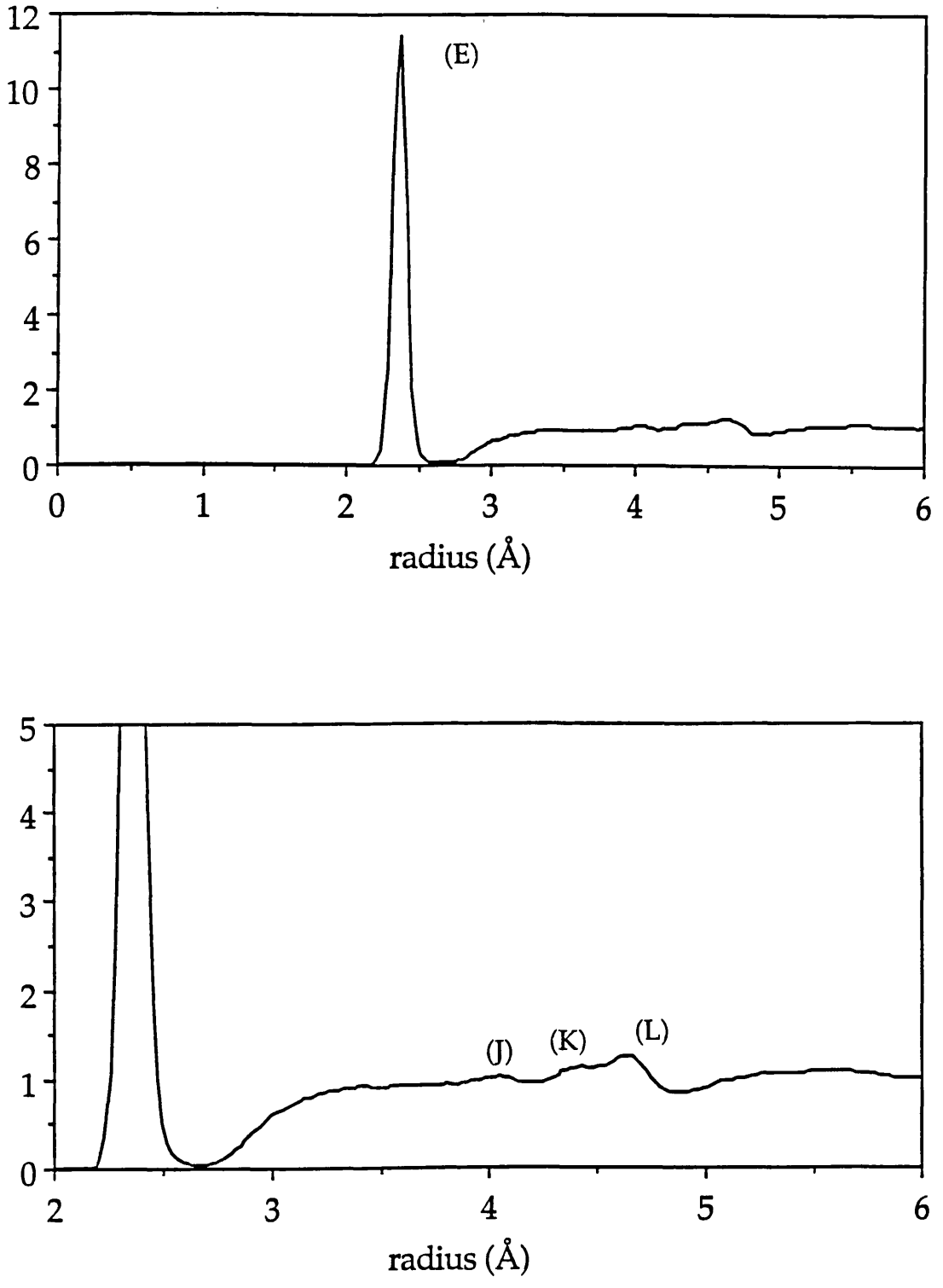

Figure 6.2. Calculated O-O PDF for B_2O_3 glass at 300K
(Potential b1 is used.)

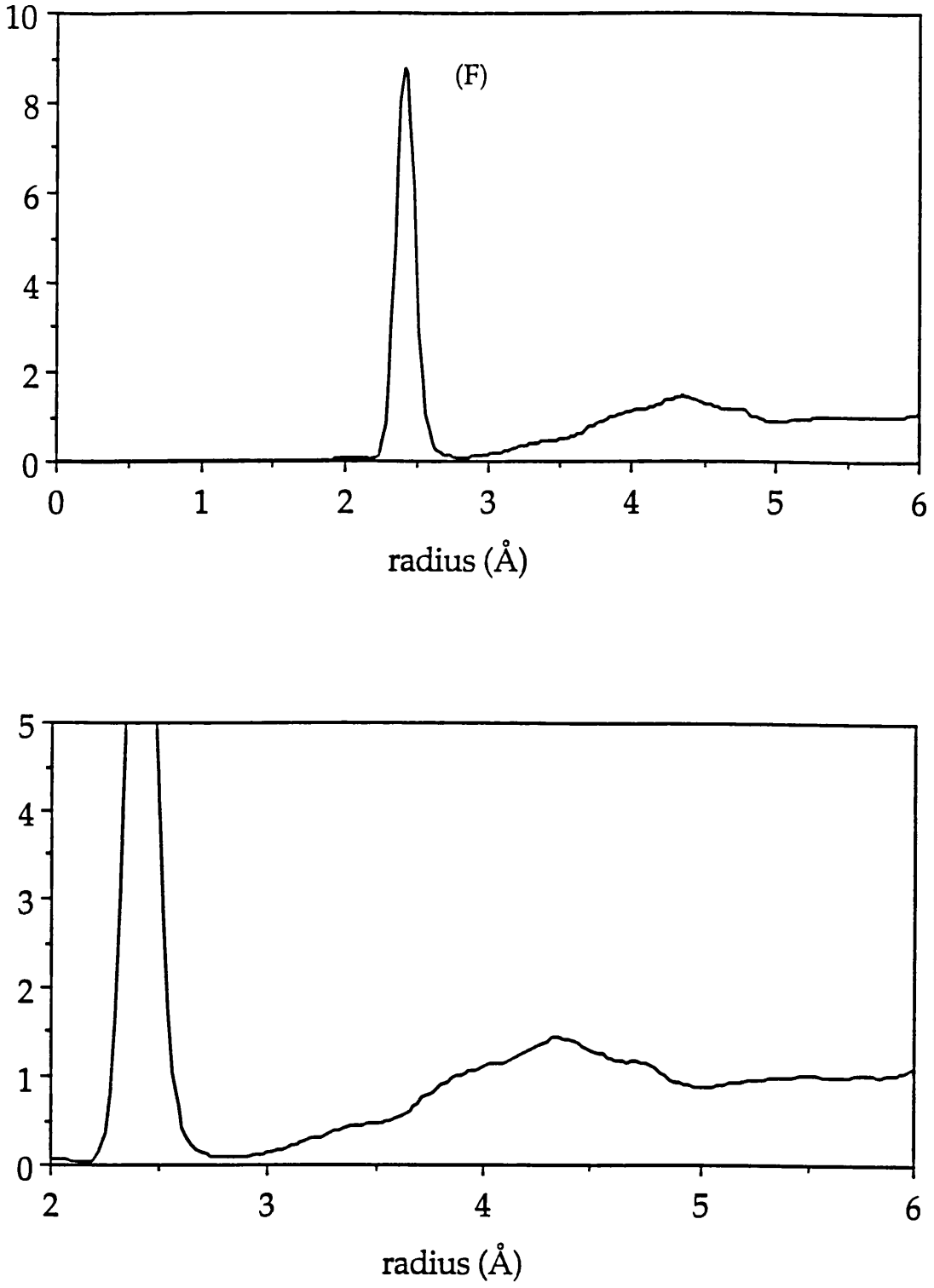

Figure 6.3. Calculated B-B PDF for B_2O_3 glass at 300K
(Potential b1 is used.)

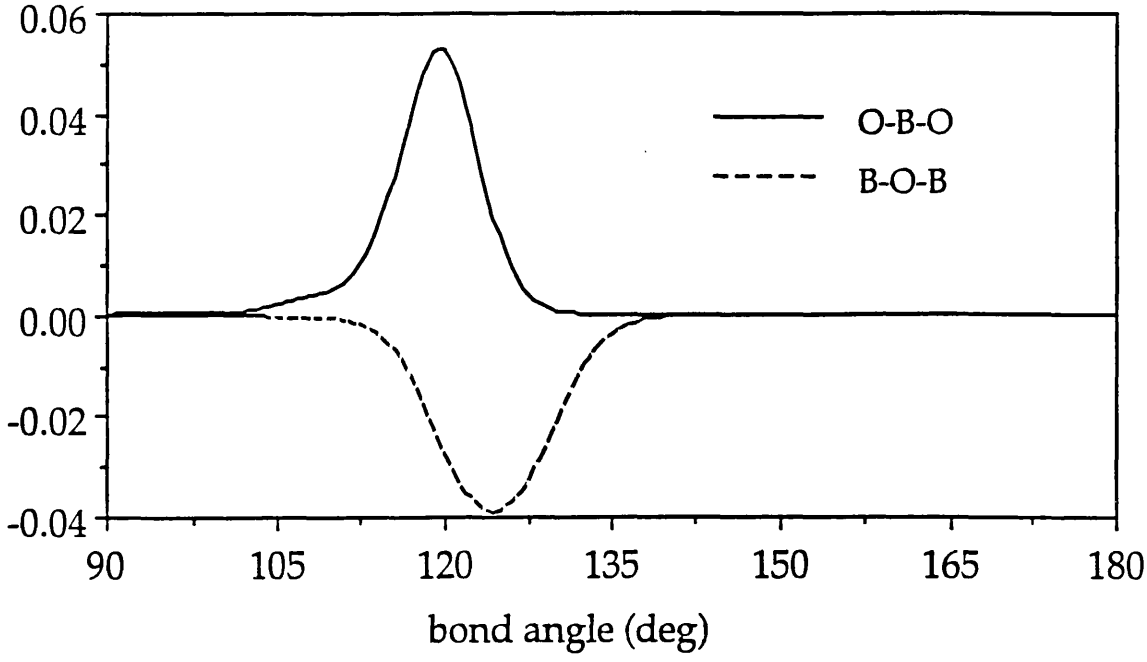

Figure 6.4. Calculated O-B-O and B-O-B bond angle distribution for B_2O_3 glass at 300K
(Potential b1 is used.)

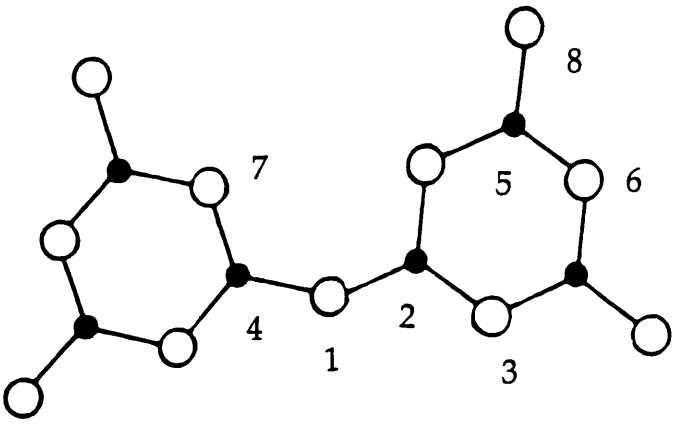

Peak	Kind of atoms	Designation on figure	Interatomic distance
D	B-O	1-2	1.37 Å
E	O-O	1-3	2.37
F	B-B	2-4, 2-5	2.43
G	B-O	2-6	2.74
H	B-O	2-7	Variable
I	B-O	2-7	3.63
J	O-O	3-8	4.10
K	O-O	3-7	Variable
L	O-O	1-8	4.75
M	B-O	4-6	5.25
N	B-O	5-7	Variable
O	B-O	4-8	Variable

Figure 6.5. Assignment of peaks in X-ray RDF for B_2O_3 glass (Mozzi and Warren 1970)

6.4 NEW POTENTIAL MODEL ('TCP POTENTIAL') FOR POLYMORPHIC AND VITREOUS STRUCTURES

We recall that the transferable potentials which could reproduce the two different crystal structures for B_2O_3 often failed to reproduce the difference in the lattice energy. In considering this difficult problem, the following points discussed in Chapter 5 should be considered.

i. The LP simultaneous fittings were applied to two B_2O_3 polymorphs after imposing the inequality conditions of their energies. But there was no feasible solution obtained as long as a transferable potential form was used.

ii. Experimental data show that bond lengths strongly depend on coordination number. But not all the 'transferable' potentials can reproduce such differences well. In the case of B_2O_3 crystals, the variation in the B-O bond lengths with the coordination number around the boron atoms is reproduced well by the transferable potential, while the dependence of the bond lengths on the oxygen coordination are not expressed well by the transferable potential. We note that potentials may be explicitly formulated so as to depend on the coordination number in a way similar to the bond strength concept defined by Pauling (1960).

iii. When the B-O potential alone was allowed to depend on the coordination number, there was no better solution than with the original transferable potential. However, when both the B-O and the O-O potentials were modified, better solutions (potential c1 and c2) were found.

In view of these difficulties and observations we have developed new potential which depends on the coordination number. The concepts of this "TCP potential" (developed by Takada, Catlow and Price) are as follows;

i. The TCP potential as noted depends on the coordination. At first, in order to express the wide range of coordination states including the transient state around a bond breaking or rebonding state, the 'bonding state function' F_b is defined for each interaction.

$$\begin{aligned} F_b &= 1 && r < (R-D) \\ &= \{1-\sin(\pi(r-R)/2D\} && (R-D) \le r \le (R+D) \\ &= 0 && (R+D) < r \end{aligned} \qquad (6.12)$$

where r is the distance between an oxygen atom and a boron atom. The range R-D to R+D represents the distances over which bond formation and breaking occur. At distances r<(R-D) full B-O bonding is generated. For (R-D)≤r≤(R+D) the extent of B-O bonding varies. When (R+D)<r, the B-O bonding is broken. The first derivative of this function is continuous when r=R-D and r=R+D.

ii. Next, the 'coordination function' F_c is defined for each atom;

$$F_c = \Sigma_i F_{bi} \qquad (6.13)$$

where i is the sequential number of the B-O interactions around the atom concerned. When there is no transient bonding state, F_c is the same as the coordination number. In this sense F_c can be said to be an "extended" coordination number.

iii. When the structure concerned has no transient bonding, we use the potential set corresponding to the appropriate coordination state. However, when the structure has some transient bonding, we interpolate between the two coordination states. The 'interpolation factor' α is introduced. α is defined so that it becomes zero for one coordination state, while it becomes one for the other state. The simplest procedure is to make α proportion to F_c. For example, when the potential V in the transient state is interpolated from the potential V2 in

the two-fold coordinated state and the potential V3 in the three-fold coordinated state, V become;

$$\alpha = F_C - 2 \tag{6.14}$$

and

$$V(r) = (1-\alpha)V2(r) + \alpha V3(r) \tag{6.15}$$

iv. These procedures are generally applied to the coordination environments of cations and/or anions. In the case of the B_2O_3 system, it is found that the change in the cation coordination can be expressed via the O-O interaction, while the change in the anion coordination cannot be well expressed with the B-B interaction. Therefore, only the changes in oxygen coordinations are expressed via the TCP potential form. For the three-body interactions, the respective three-body terms are applied to each coordination state.

v. For the pair-potential term for the B-O interactions, the potential V(r) (the Morse form) and its force $\partial V(r)/\partial r$ are calculated as follows:

$$V(r) = (1-\alpha)V2(r) + \alpha V3(r) \tag{6.16}$$

$$\partial V(r) / \partial r = \{(1-\alpha) \cdot \partial V2(r)/\partial r + \alpha \cdot \partial V3(r)/\partial r\} + \partial\alpha/\partial r \cdot (-V2(r) + V3(r)) \tag{6.17}$$

where V2(r) and V3(r) are the pair-potential term for the two-fold coordinated oxygen and for the three-fold coordinated oxygen,

and

$$\partial\alpha/\partial r = -\pi/(4D) \cdot \cos\{\pi(r-R)/2D\} \tag{6.18}$$

when $r < R-D$ or $r > R+D$

$$\partial\alpha/\partial r = 0 \tag{6.19}$$

when $R-D < r < R+D$

vi. For the pair-potential term for the O-O interactions, the potential V(r) (Buckingham form) and its force $\partial V(r)/\partial r$ are calculated as follows.

First, the general Buckingham form for the two oxygen atoms with the same coordination function F_C is :

$$V(r) = A(F_C) \cdot \exp\{-r/\rho(F_C)\} \quad (6.20)$$

$$\partial V(r)/\partial r = \partial A(F_C)/\partial r \cdot \exp\{-r/\rho(F_C)\} + A(F_C) \cdot \partial[\exp\{-r/\rho(F_C)\}]/\partial r \quad (6.21)$$

$$A(F_C) = (1-\alpha)A2 + \alpha A3 \quad (6.22)$$

$$\rho(F_C) = (1-\alpha)\rho 2 + \alpha\rho 3 \quad (6.23)$$

where A2, A3, ρ2 and ρ3 are the A parameters and ρ parameters for two-fold or three-fold coordinated oxygen atoms. In the case of the B_2O_3 system, there are three interactions in the material: two-fold coordinated oxygen interacts with a second two-fold coordinated oxygen; two-fold coordinated oxygen with a three-fold coordinated oxygen; and three-fold coordinated oxygen with a second three-fold coordinated oxygen. These three sets of potential parameters can be derived from the two polymorphic structures of B_2O_3. After several tests of the LP fitting, it was found only A(Fc) should be varied, ρ(r) being fixed in this system.

$$V(r) = A(F_C) \cdot \exp(-r/\rho) \quad (6.24)$$

$$\partial V(r)/\partial r = \partial A(F_C)/\partial r \cdot \exp(-r/\rho) - A(F_C) \cdot \exp(-r/\rho)/\rho \quad (6.25)$$

$$A(F_C) = (1-\alpha)A2 + \alpha A3 \quad (6.26)$$

In the next step, the Buckingham form for the two oxygen atoms which have intermediate coordination is derived. As the simple geometric average did not work well as reported by Pertsin ad Kitaigorodsky (1987), a new interpolating function was introduced. When one atom has the coordination function F_{C-1} and the A parameter A_{-1}, and the other atom has the coordination function F_{C-2} and A parameter A_{-2}, the potential for the interaction between these two atoms is defined as follows;

$$A_{-1\&2} = \sqrt{(A_{-1} \cdot A_{-2})}\,[\{(\max(A_{-1},A_{-2})/\min(A_{-1},A_{-2})-1)-1\}\,k + 1] \quad (6.27)$$

$$V(r) = A_{-1\&2} \cdot \exp(-r/\rho) \quad (6.28)$$

where k is the interpolating factor; k can be derived from the three sets of O-O parameters as explained above. When both oxygens have the same F_{C-3} and A_{-3}, V(r) has a simple form of $A_{-3} \cdot \exp(-r/\rho)$.

In this case the force $\partial V(r)/\partial r$ is approximated as follows:

$$\partial V(r) / \partial r = - A_{-1\&2} \cdot \exp(-r/\rho)/\rho \quad (6.29)$$

To summarize the TCP potential, has two main features. The first is that the change in the coordination environment affects the bond strength between atoms. It seems quite reasonable that as the number of the bonds increases, the bond strengths are reduced, as the Tersoff's potential expresses (Tersoff 1986; see Appendix D). The second is that the pair-potential terms change continuously between the two coordination states and the shape of the potential energy surface in the transient region can be adjusted smoothly by varying the R and D parameters, independent of the energy difference between the two polymorphs.

6.5 APPLICATION OF TCP POTENTIALS TO MD

6.5.1 SELECTION OF POTENTIAL MODEL

Two TCP potential models which were modified from potentials c1 and c2 were used in MD simulations of the structures of vitreous B_2O_3. In order to apply the crystal potentials, c1 and c2 (see Chapter 5), to the vitreous states, some parameters which were defined in the previous section were fixed as follows; R=1.8 Å, D=2.0 Å, k=0.320 and 0.295 for potentials c1 and c2 respectively, as discussed Section 6.4.

The total number of atoms was 270 (108 boron atoms and 162 oxygen atoms). Although several runs with 480 atoms were undertaken, there was not any significant difference in the structures found. The time step in the calculations was 1fs. To ensure more diffusion than the case described in Section 6.3, the melting temperature was set at 5000 K.

For the melting and quenching process, the initial crystal structure was kept at 5000 K for 10,000 steps. The system was quenched down to 1500 K in 500 K intervals, each of 1800 steps, after which it was quenched to 300K in 100 K intervals, each of 900 steps. Finally, the system was kept at 300 K for 10,000 steps. 98% of the initial bonds were broken and rebonded with the other partners.

At first, constant pressure simulations (using ambient pressures) were undertaken. The calculated coordination numbers, ring sizes and densities are shown in Tables 6.4 ~ 6.6. Both potential models give simulated structures with a higher proportion of boroxol rings: 53% (potential c1) or 36% (potential c2) of boron atoms are present in boroxol rings, which values are around the lower limit (40%) suggested by Johnson (1982). As the new potential models favours three-fold rather than four-fold coordination (i.e. energy of B_2O_3-I is lower than that of B_2O_3-II), the four-fold coordinated boron atoms are no longer present.

However, one new problem appears: the final calculated density is too low compared with the experimental one. Thus, although these potential models successfully generate boroxol rings, it would still appear to be difficult for the present MD method to reproduce the whole structural transformation during the melting process at high temperatures so as correctly to reproduce the density.

Next, therefore, the constant volume method was applied using the same potential sets, in order to study the structural transformations keeping the experimental density. The calculated coordination numbers and ring sizes are shown in Tables 6.7 and 6.8.

The percentage of the boron atoms consisting of the six-membered rings (25% for potential c1; 42% for potential c2) was lower than that observed with the constant pressure calculations, and four-fold coordinated boron atoms were observed in the simulations using potential c2.

To summarize, using the constant pressure method these new potentials generated almost the same percentage of boroxol rings as that estimated from the experiment, but they resulted in a lower density (i.e. they may have different intermediate ordering) While under the constant volume method the results could not reject the generation of four-fold boron atoms, although they necessarily kept the experimental density. Therefore, it is not easy to realize both the high proportion of the boroxol rings and the experimental density at the same time in the MD simulations.

	1-fold	2-fold	3-fold	4-fold
potential	**c1**			
boron	0%	1%	99%	0%
oxygen	1%	99%	0%	0%
potential	**c2**			
boron	0%	1%	99%	0%
oxygen	2%	96%	2%	0%

Table 6.4. Distribution of coordination numbers in calculated glass
(constant pressure calculations using potentials c1 and c2)

ring size	4	6	8	10	12
potential	**c1**				
number	0	13	3	0	2
potential	**c2**				
number	2	19	4	2	2

Table 6.5. Distribution of ring sizes in calculated glass
(total number of atom = 270; constant pressure calculations using potentials c1 and c2)

	experiment	calculation		[g/cm^3]
		potential c1	**potential c2**	
	2.56	1.43	1.15	

Table 6.6. Experimental and calculated densities at 300K
(constant pressure calculations using potentials c1 and c2; experimental data from : Macedo et al 1966)

	1-fold	2-fold	3-fold	4-fold
potential	**c1**			
boron	0%	1%	99%	0%
oxygen	1%	98%	1%	0%
potential	**c2**			
boron	0%	0%	94%	6%
oxygen	4%	89%	7%	0%

Table 6.7. Distribution of coordination numbers in calculated glass
(constant volume calculations using potentials c1 and c2)

ring size	4	6	8	10	12
potential	**c1**				
number	0	9	8	2	9
potential	**c2**				
number	0	15	7	5	10

Table 6.8. Distribution of ring sizes in calculated glass
(total number of atom = 270; constant pressure calculations using potentials c1 and c2)

6.5.2 COMPARISON WITH X-RAY DIFFRACTION AND NEUTRON SCATTERING DATA

In order to examine the calculated vitreous structures, we made the comparison with the X-ray diffraction data of Mozzi and Warren (1970) and the neutron scattering data of Johnson et al (1982). From the calculated structures using potentials c1 and c2, the RDFs and interference functions were simulated and compared with those obtained from the experimental data. In order to compare with the latter, the same filtering and conversion procedures were used.

For the X-ray diffraction data, two points must be carefully noted. The first is that the peak at 2.8Å in the X-ray RDF data in the original paper of Mozzi and Warren (1970) appeared to be absent after a retransformation of the interference function using a window, as Johnson et al (1982) pointed out. Therefore, the comparison with the interference function may be better than that with the RDF. The other is that the atomic form factors are dependent on the X-ray wave length and the atomic charge state, and it is not easy to use precise values. Verhoef and Hartog (1992) demonstrated that the difference in the approximation of the atomic form factors considerably affected the height of the first and second peaks within 6Å in the interference functions. Here, the interpolating function appropriate for neutral atoms was used from the International Tables for X-ray Crystallography (1974).

For the neutron scattering data, the atomic scattering factors are independent of q (wavevector), and the experimental intensity was measured up to 40 $Å^{-1}$. The neutron data may be more suitable for comparison with the calculated results, and therefore more emphasis is placed on neutron data in this chapter.

The calculated RDFs and the interference functions for the X-ray diffraction data are shown in Figures 6.6 and 6.7; those for the neutron scattering data are shown in Figures 6.8 and 6.9.

The calculated RDFs and the interference functions for both potentials agree reasonably with both X-ray and neutron experimental data. For the calculated RDF appropriate to the neutron scattering data, the peaks at 1.37Å, 2.37Å agree with experiment, although their heights are still a little too large. However, two small and broad peaks around 3Å in distance cannot be distinguished. This is possibly due to the small proportion of boroxol rings, as it is certain that boroxol rings result in these two peaks (G and H), as the PDF of B-O demonstrated in Figure 6.1.

For the interference function of the neutron scattering data, the shapes of branches in the peaks around $10Å^{-1}$ and $15Å^{-1}$ agree very well with the experimental data. All these features seem to be related to the structures of boroxol rings and to originate from the intermediate-range rather than the short-range order. This point is discussed further in the following section.

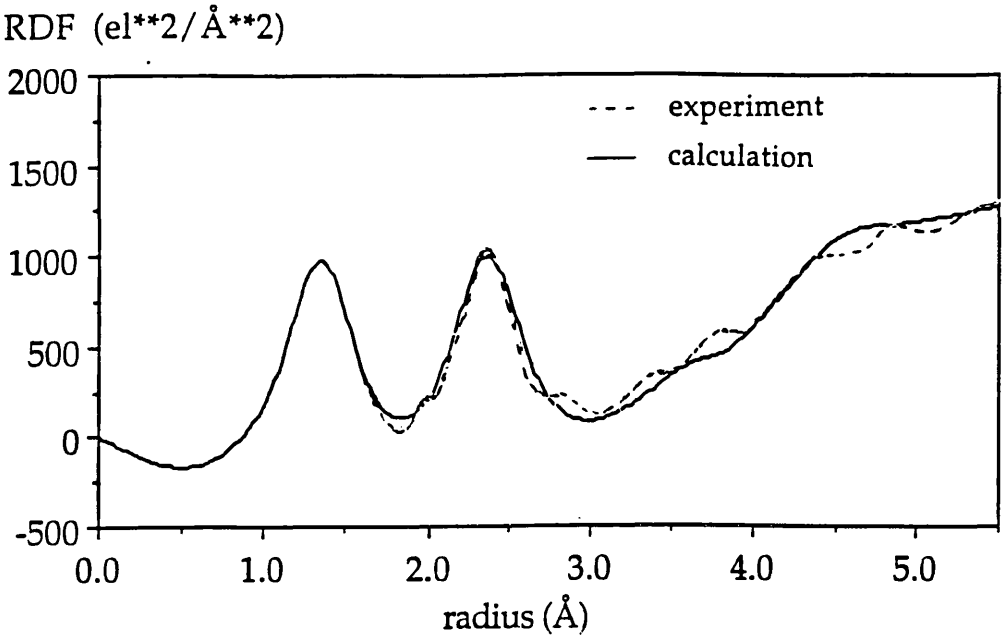

(a)

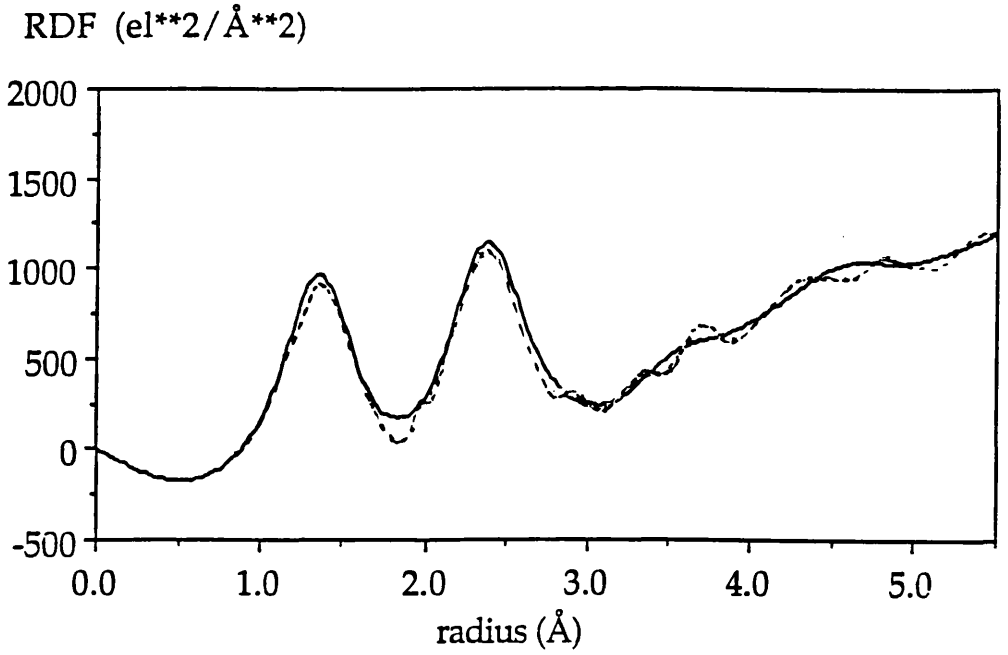

(b)

Figure 6.6. X-ray RDF for B_2O_3 glass at 300K
(a) potential c1; (b) potential c2

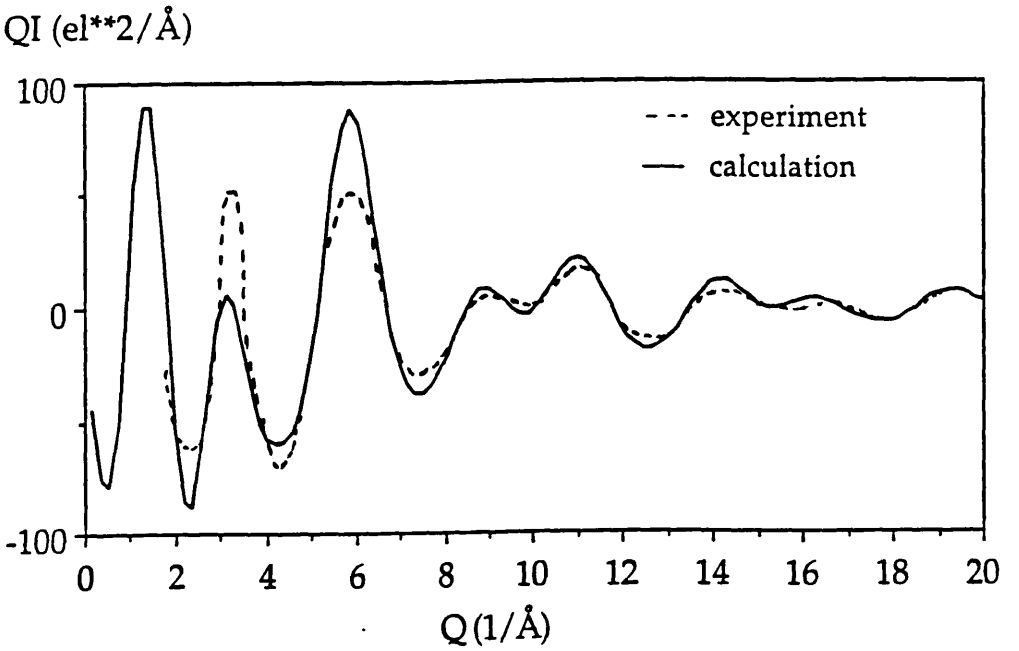

(a)

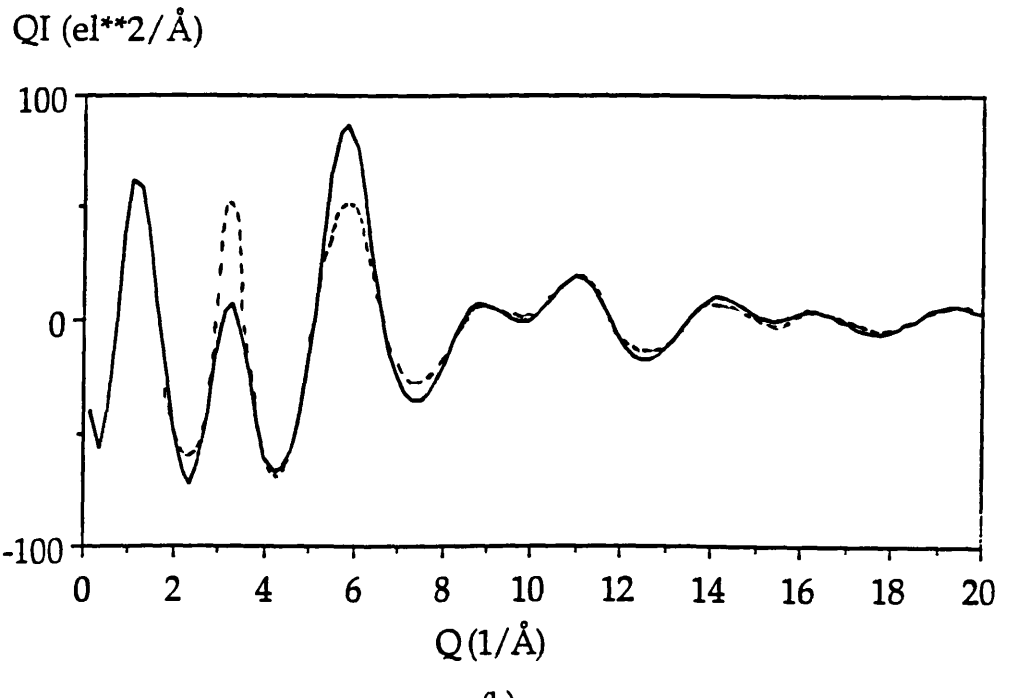

(b)

Figure 6.7. X-ray interference function for B_2O_3 glass at 300K
(a) potential c1; (b) potential c2

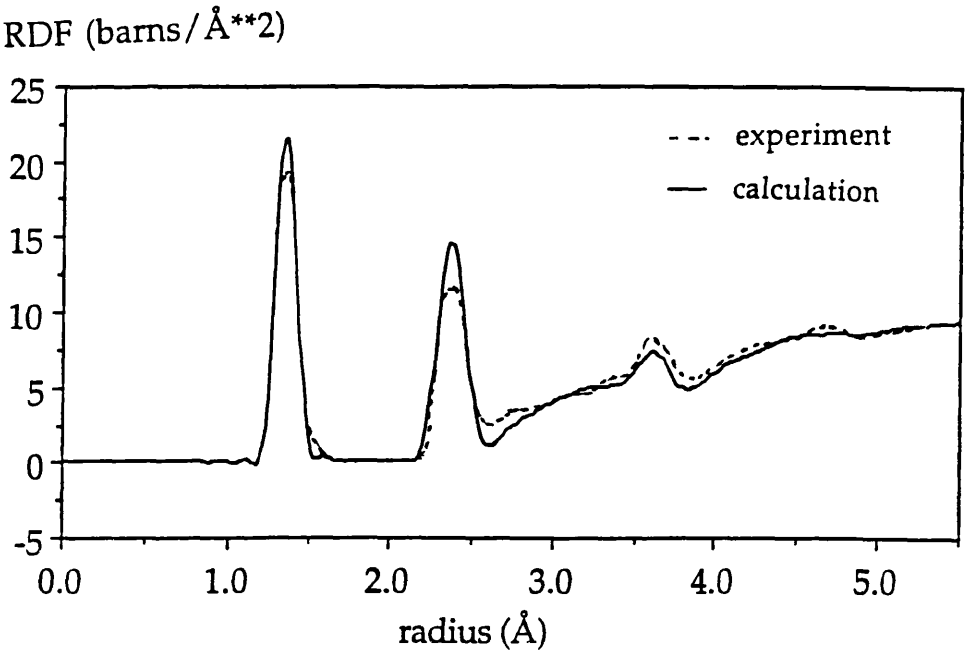

(a)

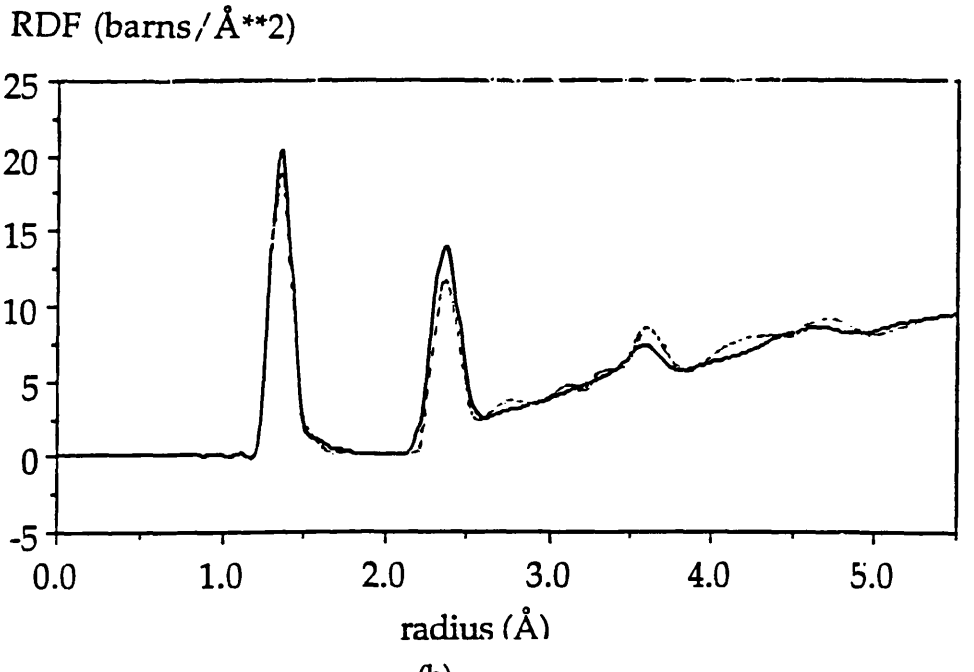

(b)

Figure 6.8. Neutron RDF for B_2O_3 glass at 300K
(a) potential c1; (b) potential c2

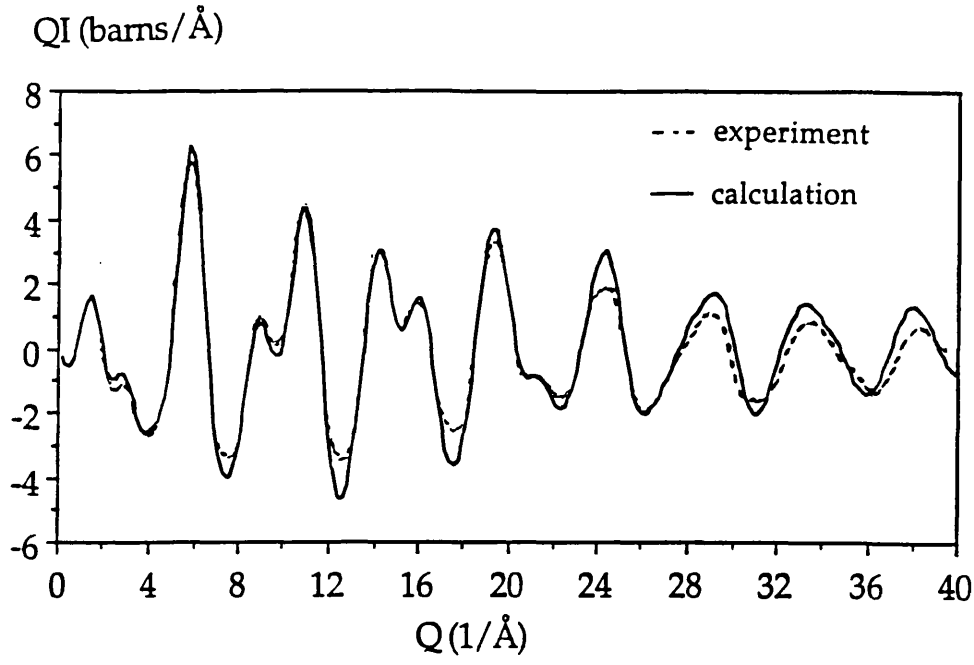

(a)

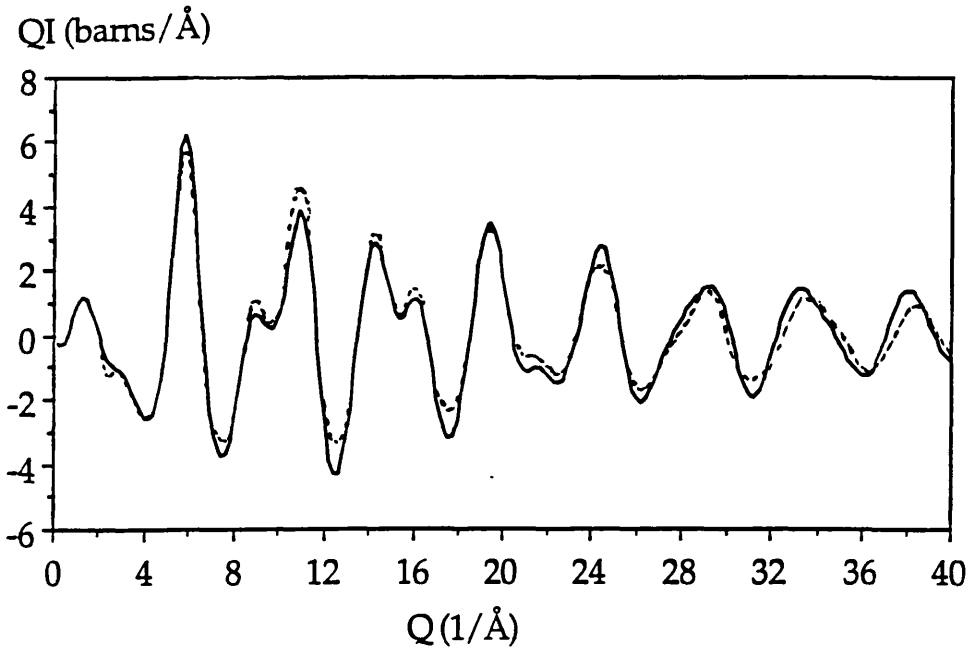

(b)

Figure 6.9. Neutron interference function for B_2O_3 glass at 300K
(a) potential c1; (b) potential c2

6.5.3 SHORT-RANGE AND INTERMEDIATE-RANGE ORDER

Our calculated results showed that the existence of the six-membered rings can reproduce the X-ray and neutron scattering data well, as many experimentalists have previously suggested. However, it is very difficult to discuss the intermediate-range order present in vitreous structures using only experimental data. In contrast, not only the short-range but also the intermediate-range order is available from analyzing the calculated structures.

First, the O-B-O and the B-O-B Bond Angle Distributions (BADs) at 300 K in the cases of potentials c1 and c2 are shown in Figure 6.10. As their peaks are more easily distinguished and compared at zero Kelvin, all the BAD data are calculated at zero Kelvin (i.e. after energy minimization) and are shown in Figures 6.11 ~ 6.13. For the sake of comparison the experimental structures (B_2O_3-I and $Cs_2O \cdot 9B_2O_3$) and the calculated structures (pseudo super crystals and the MD results) are shown. They exhibit several peaks around 120° for the O-B-O bond angles, and two groups of peaks around 120° and 128° for the B-O-B bond angles. For the latter it is interesting to note that the peak around 120° corresponds to the angles within the boroxol rings, while that around 128° corresponds to the angles outside the rings. The latter value agrees with that estimated from the NMR experiment by Jellison (1977); the B-O-B angles for the oxygen atoms not included in the boroxol rings have a narrow distribution (rms deviation ~1.7°) centred around either 134.6° or 128.1° (which cannot be distinguished by experiment). This value, which contrasts with the much larger angles calculated from the pair-potential models, almost certainly implies the presence of the boroxol rings, as explained in Section 6.3.

The existence of boroxol rings and the B-O-B angles of 128° outside the boroxol rings is clearly demonstrated. However, if these are randomly connected, the structural model cannot reproduce the experimental density (see Section 2.3). In order to analyze the topology of the connections, we need the Torsion Angle Distribution (TADs) between the BO_3 triangles, and between the BO_3 triangle and the B_3O_6 ring, or between the BO_3 triangle and the B_3O_6 ring. (To define the torsion angles between two planes, we consider each plane as defined by the three oxygen atoms present in the BO_3 triangles whether within or outside the B_3O_6 rings.) The BO_3 triangles with more than one four-fold coordinated boron atoms were excluded from the analysis. The calculated results are shown in Figure 6.14 ~ 6.20. It must be noted that all the peaks are sharp, because they are calculated at zero Kelvin and confined to several equilibrium values.

The TAD in the crystal of B_2O_3-I has two peaks of 7° and 74° (Figure 6.14). It is interesting to note that two triangles even on the same chain are twisted by 7°, while those on the different chains, by 74°, which is close to the perpendicular, these contrast with the quantum-chemically calculated value of 29.4° for the $(HO)_2B\text{-}O\text{-}B(OH)_2$ molecule (Uchida et al 1985). For the TAD in the crystal of $Cs_2O \cdot 9B_2O_3$, two of the peaks are almost the same as those in B_2O_3-I and the other has a peak around 44° (Figure 6.14). The latter value is close to the quantum-chemically calculated value of 32.2° obtained for $(HO)_2B_3O_3\text{-}O\text{-}B_3O_3(OH)_2$ by Uchida et al (1985). These two results may mean that the B_2O_3 systems do not favour a layer structure and they prefer the large torsion angle which does not appear in the molecular state and is probably caused by crystal effects.

The calculated structures of pseudo super crystals also have large torsion angles (Figures 6.15 ~ 17); and the structures calculated by the MD method similarly exhibit large torsion angles, although they also have other peaks at the lower region (Figures 6.18 and 6.19). It is interesting to note that in the calculated structures the torsion angles within the B_3O_6 rings exhibit the twisted angles from 10° to 30 ° (Figure 6.20); this means that the three oxygen atoms outside the B_3O_3 rings do not lie on the same plane as the B_3O_3 rings and that they are easily distorted.

The hypothesis that a considerable proportion of the torsion angles would be as large as 74° and that the oxygen atoms outside the rings do not lie in the same plane as those within the rings may explain the experimental density, in contrast to the lower density obtained from the models base on the randomly connected boroxol rings. Appreciation of this point, which was also explained using the term 'interlocking structure' for $Cs_2O \cdot 9B_2O_3$ in Section 5.5, may lead to accurate models for the intermediate-range order in vitreous B_2O_3 structures.

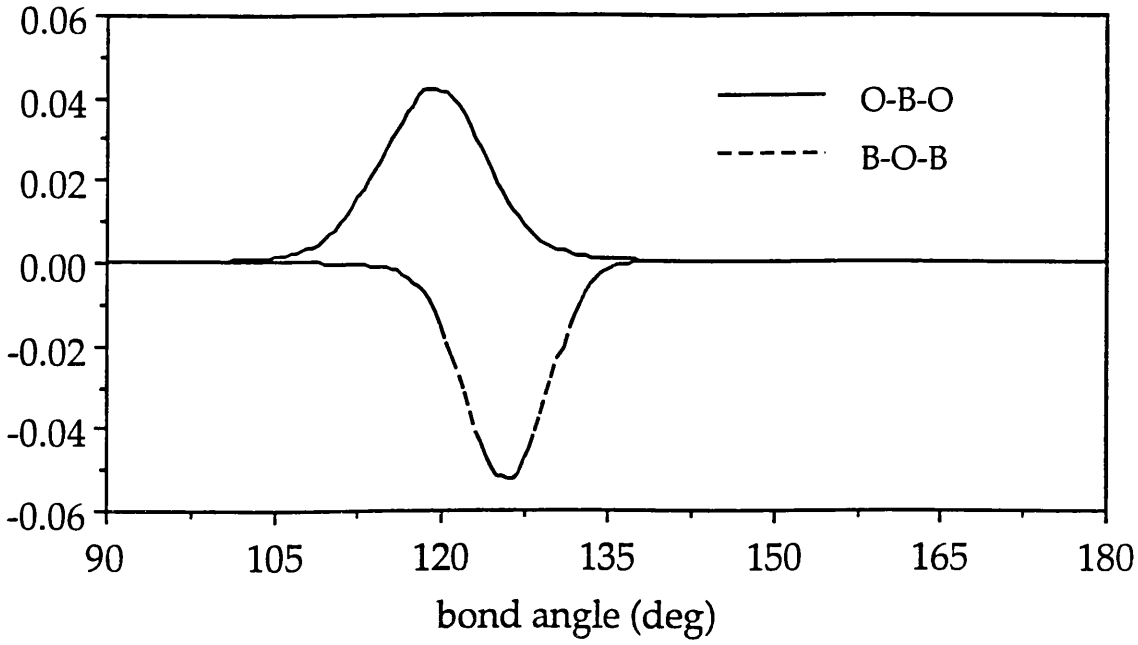

(a)

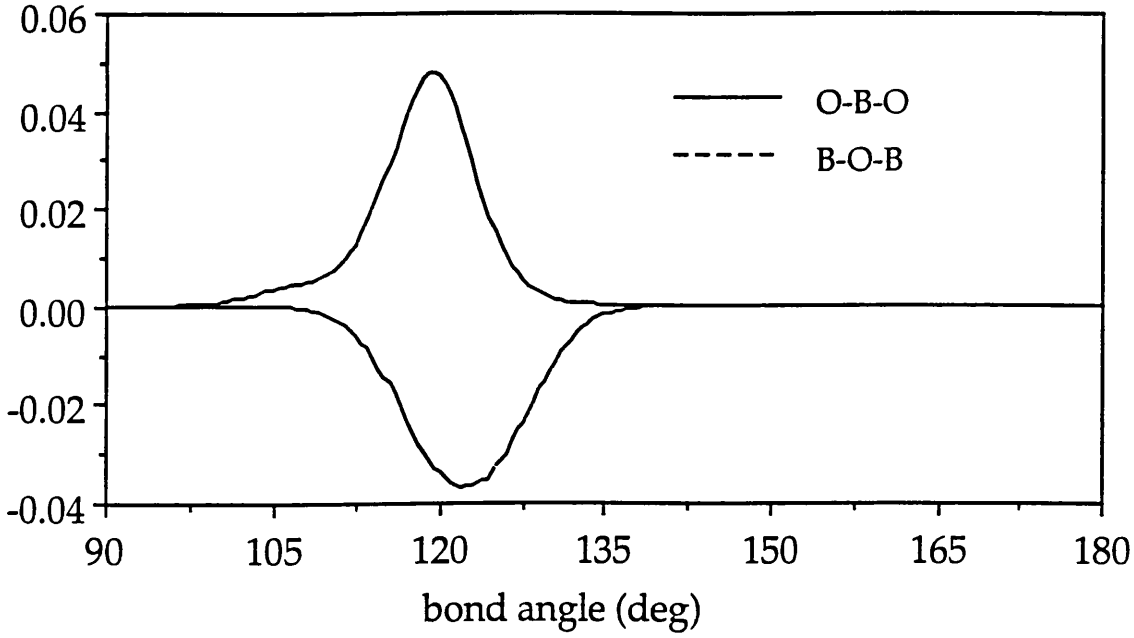

(b)

Figure 6.10. Bond angle distribution in calculated vitreous structures at 300 K
(a) potential c1 (b) potential c2

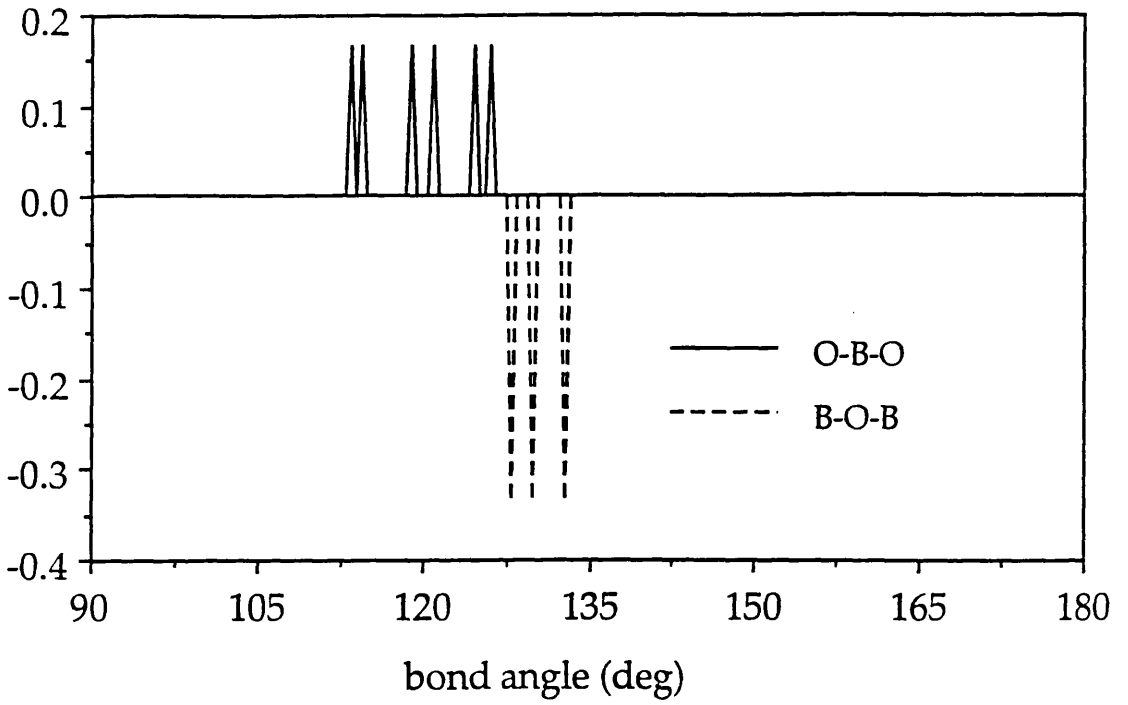

(a)

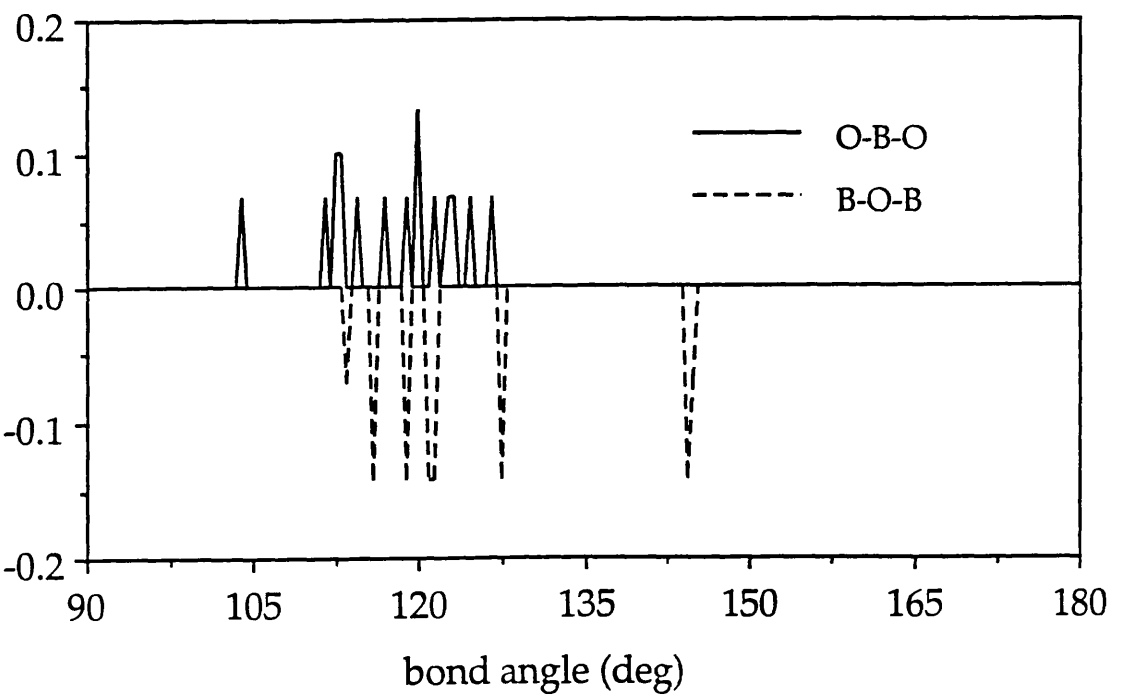

(b)

Figure 6.11. Bond angle distribution in B_2O_3-I and $Cs_2O \cdot 9B_2O_3$ crystals at 0 K

(a) B_2O_3-I (b) $Cs_2O \cdot 9B_2O_3$

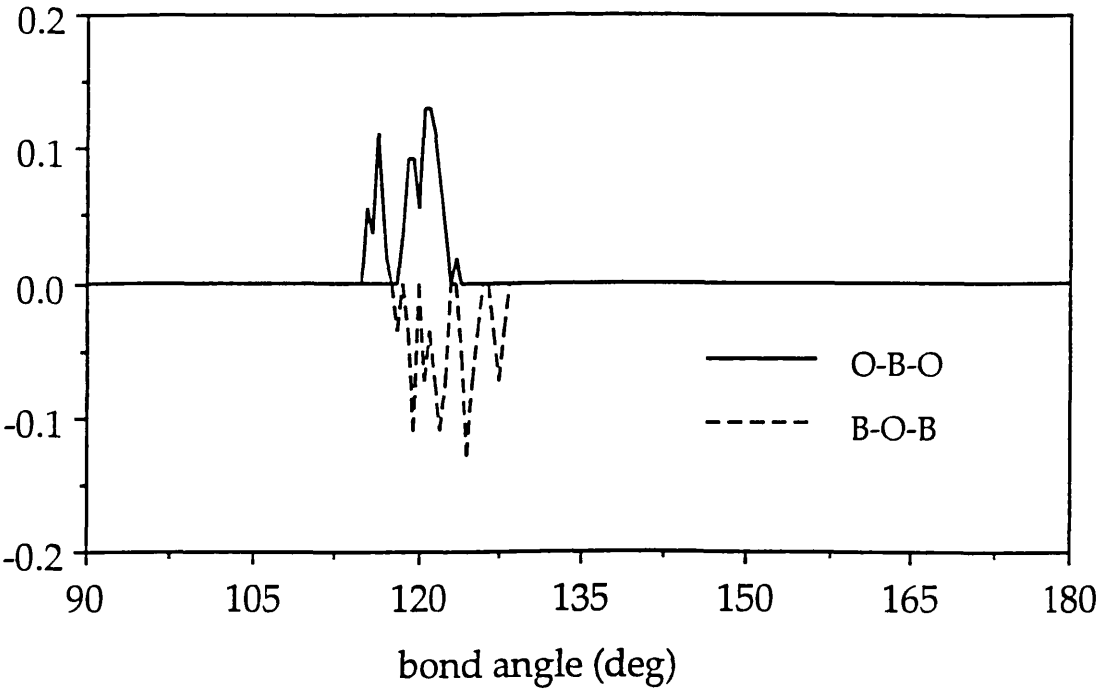

(a)

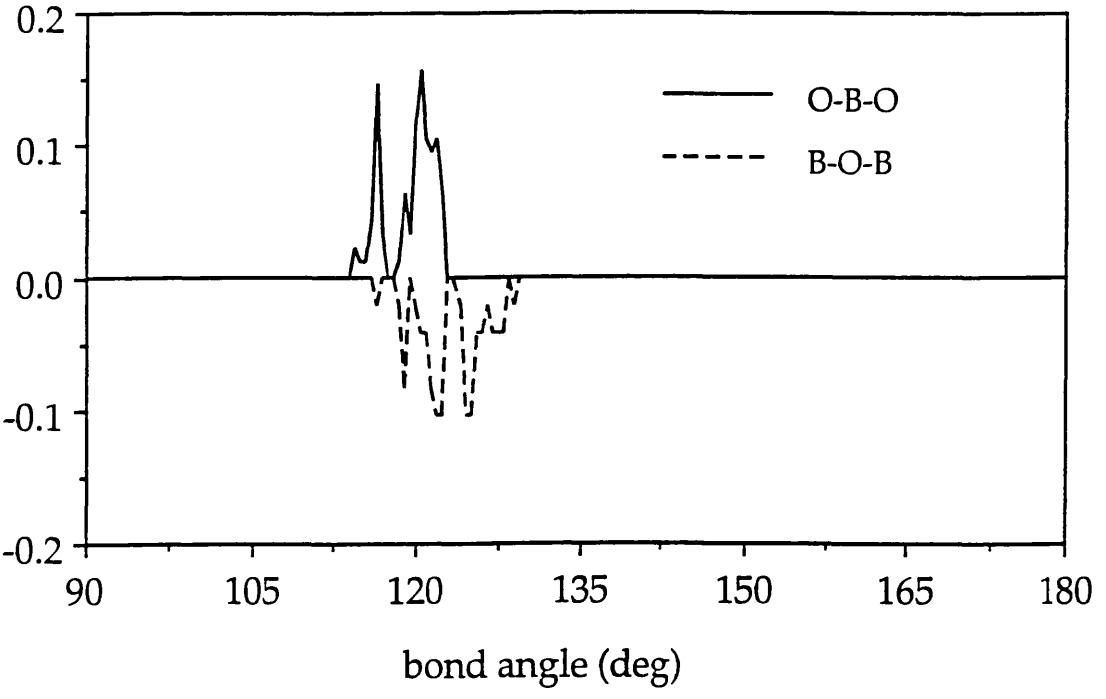

(b)

Figure 6.12. Bond angle distribution in pseudo super crystal at 0 K
(a) B_2O_3-c (b) B_2O_3-d

(Potential c2 is used.)

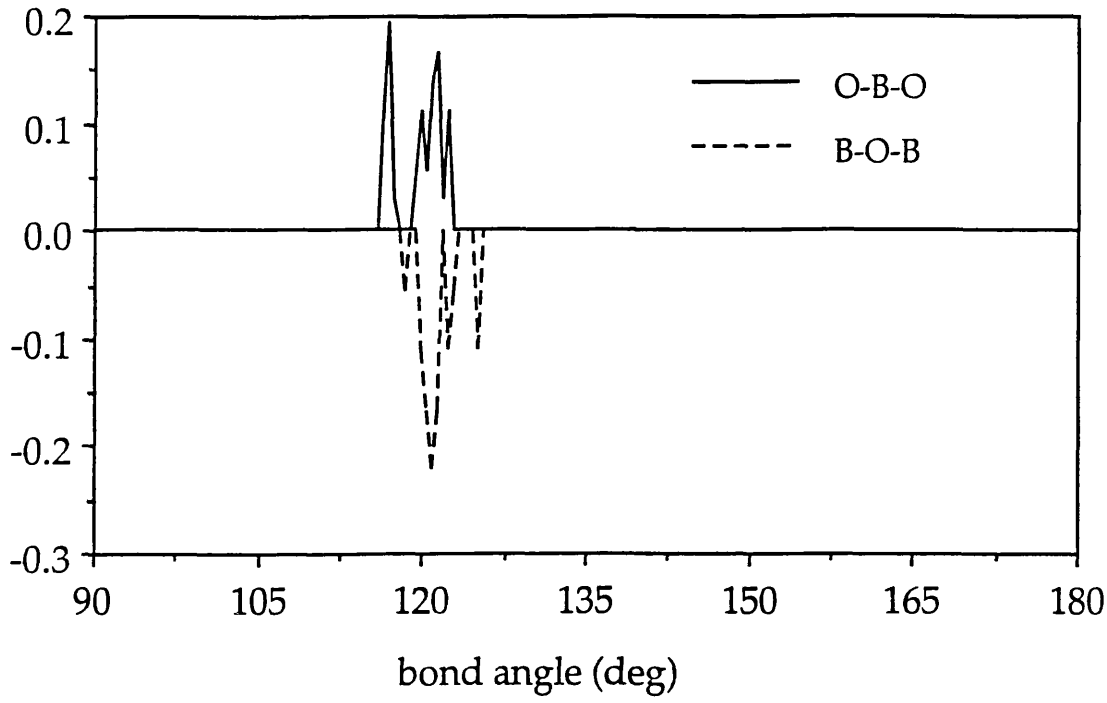

(c)

Figure 6.12. (continued) Bond angle distribution in pseudo super crystals
at 0 K

(c) B_2O_3-a (100% boroxol ring model)

(Potential c2 is used.)

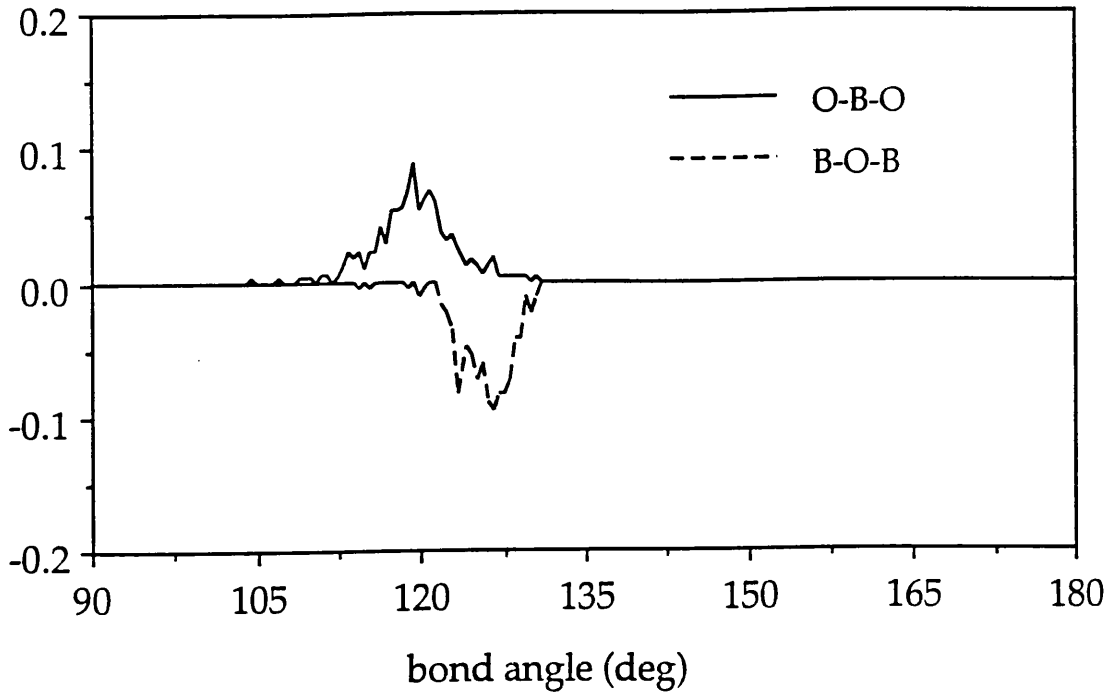

(a)

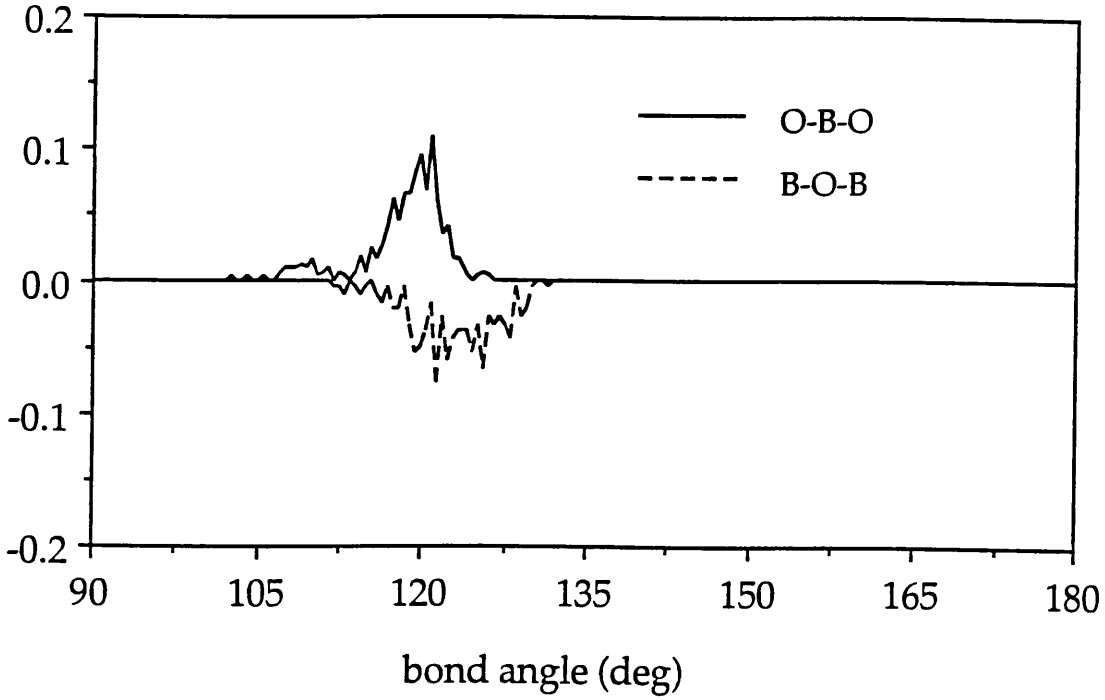

(b)

Figure 6.13. Bond angle distribution in calculated vitreous structures at 0 K

(a) potential c1 (b) potential c2

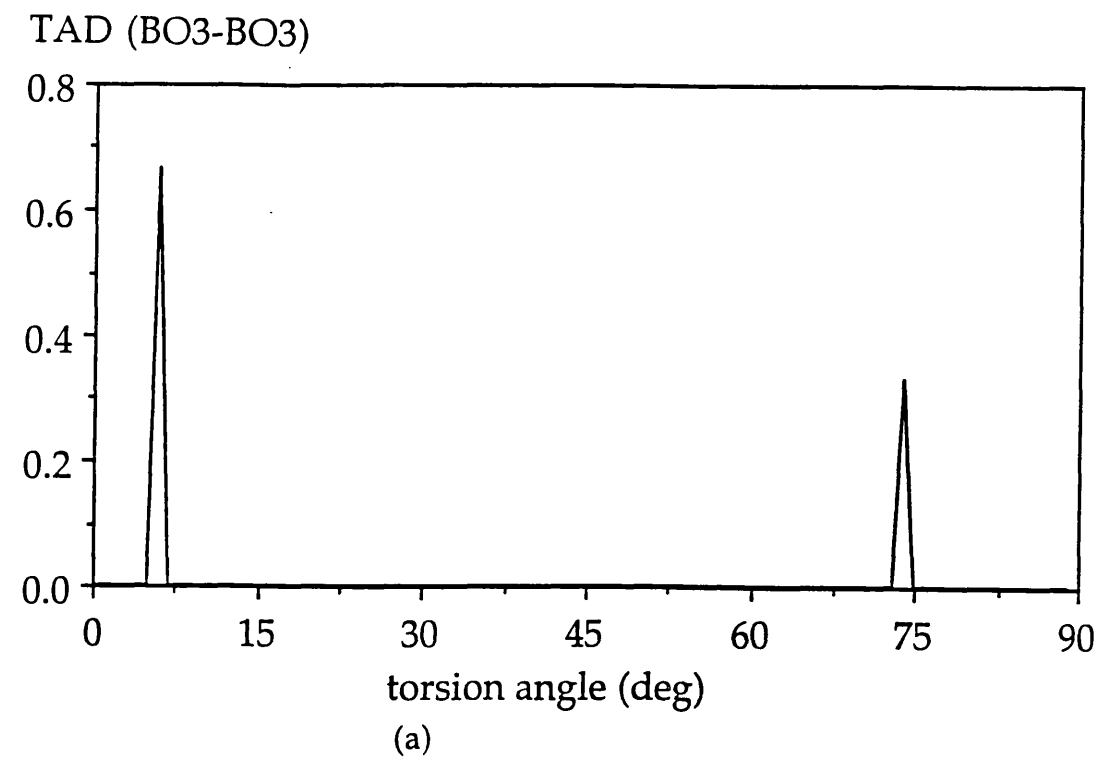

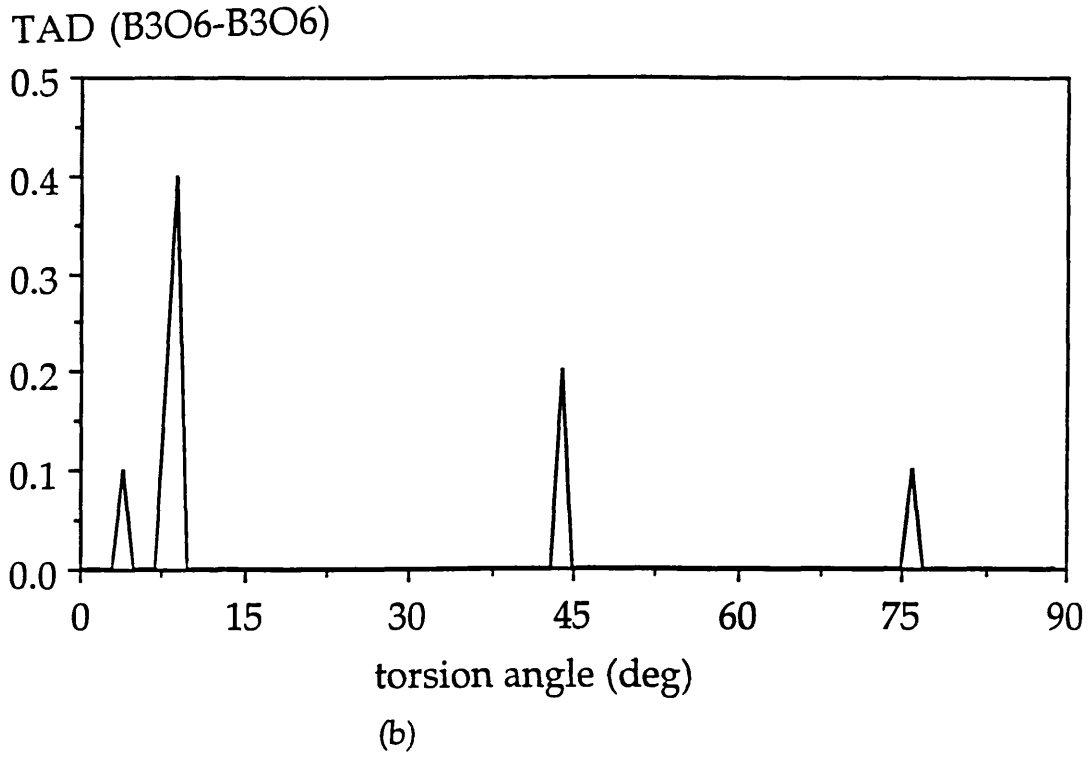

Figure 6.14. Torsion angle distribution in B_2O_3-I and $Cs_2O \cdot 9B_2O_3$ crystals at 0 K

(a) B_2O_3-I (b) $Cs_2O \cdot 9B_2O_3$

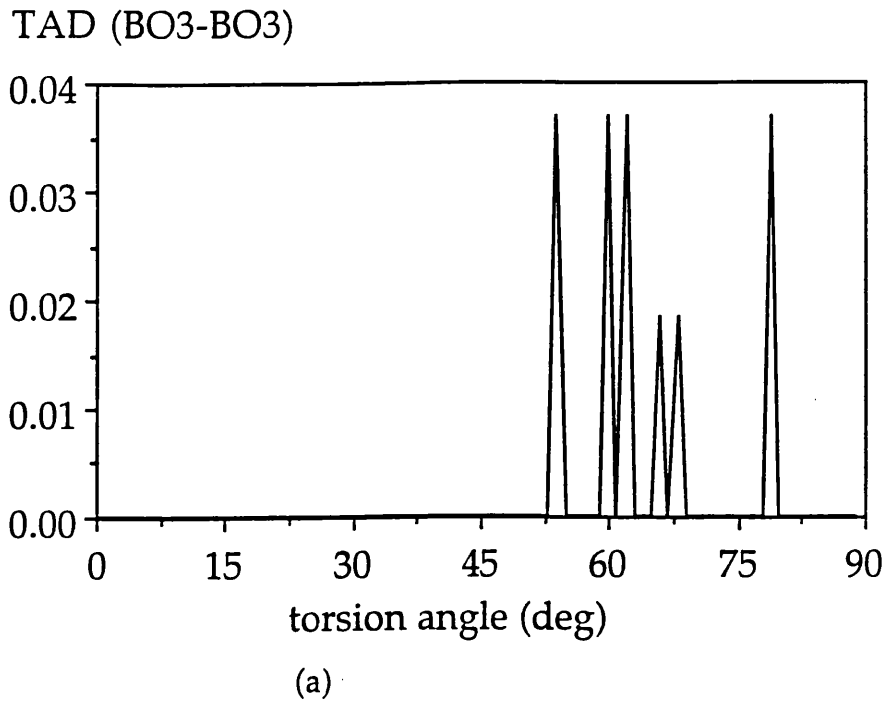

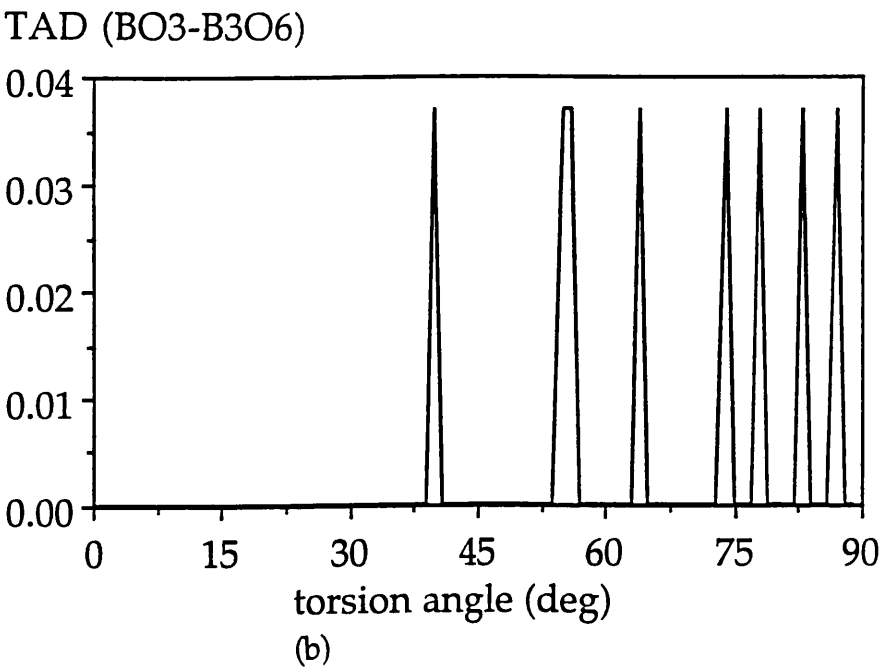

Figure 6.15. Torsion angle distribution in pseudo super crystal B_2O_3-c at 0 K

(a) between BO_3 triangles

(b) between BO_3 triangle and B_3O_6 ring

(Potential c2 is used.)

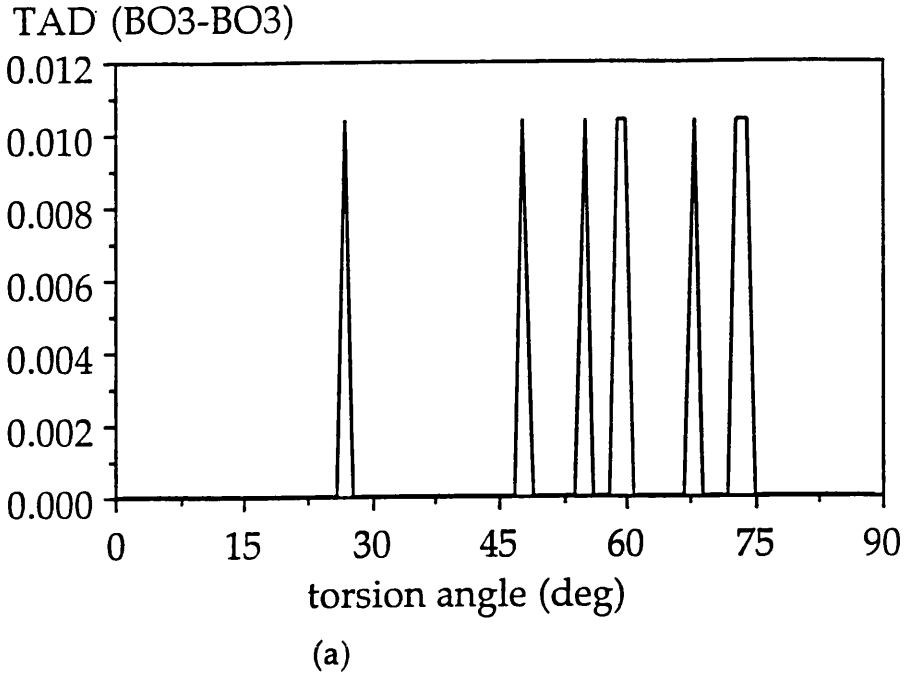

(a)

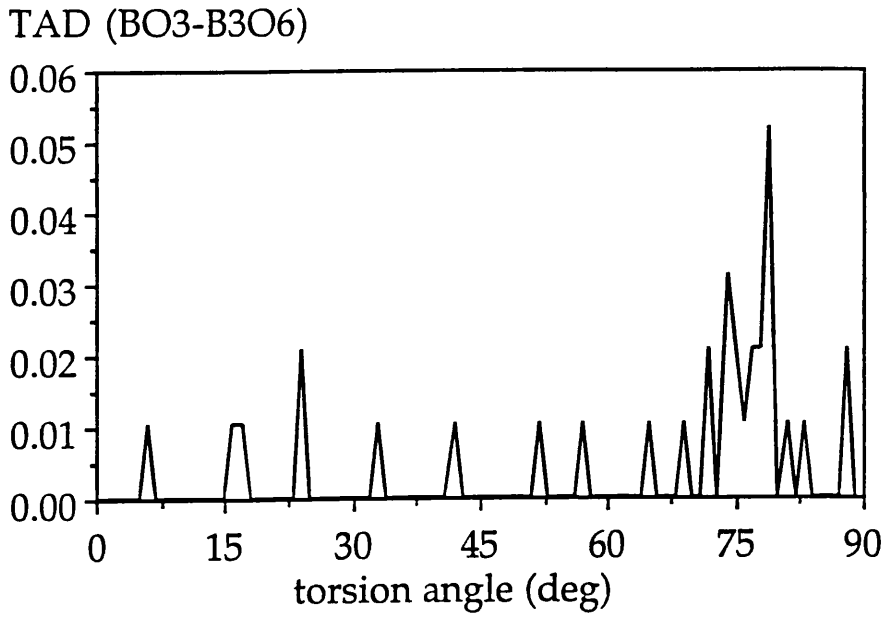

(b)

Figure 6.16. Torsion angle distribution in pseudo super crystal B_2O_3-d at 0 K

(a) between BO_3 triangles

(b) between BO_3 triangle and B_3O_6 ring

(Potential c2 is used.)

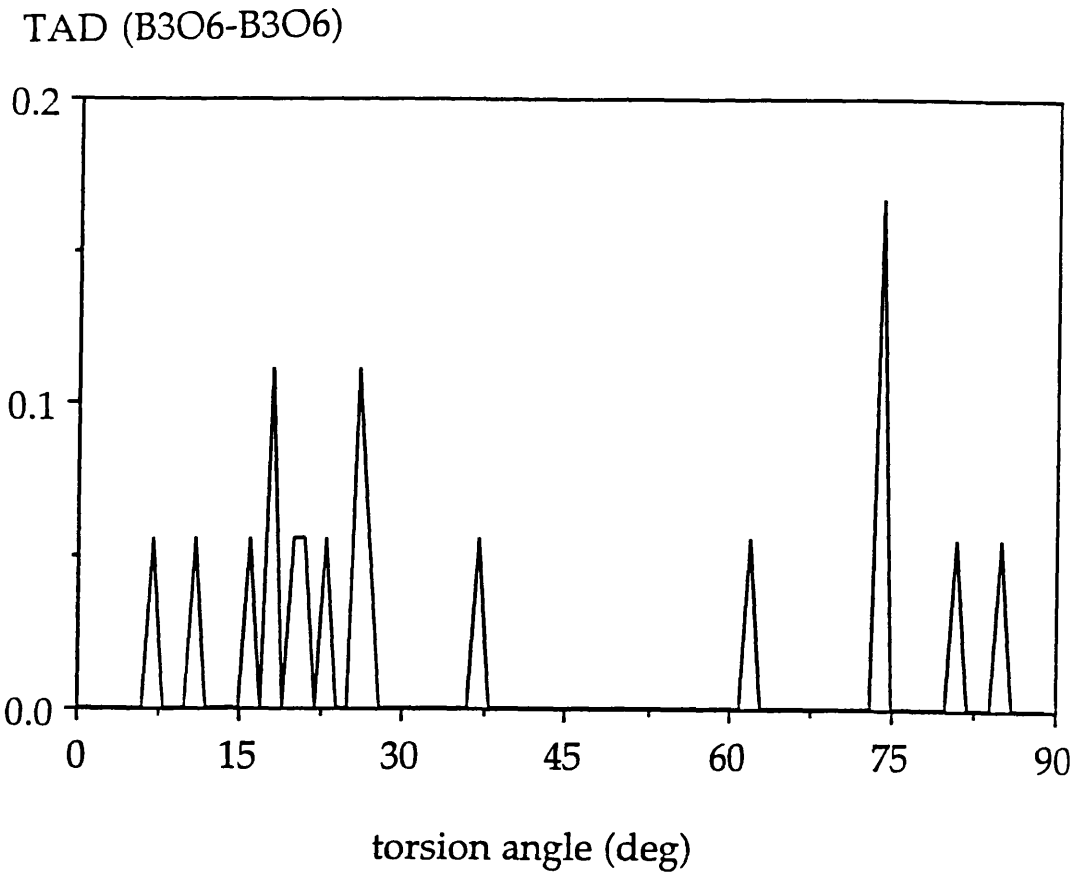

Figure 6.17. Torsion angle distribution in pseudo super crystal B_2O_3-a at 0 K

Angles smaller than 45° are all between the same B_3O_6 rings.

Angles larger than 45° are all between the different B_3O_6 rings.

(Potential c2 is used.)

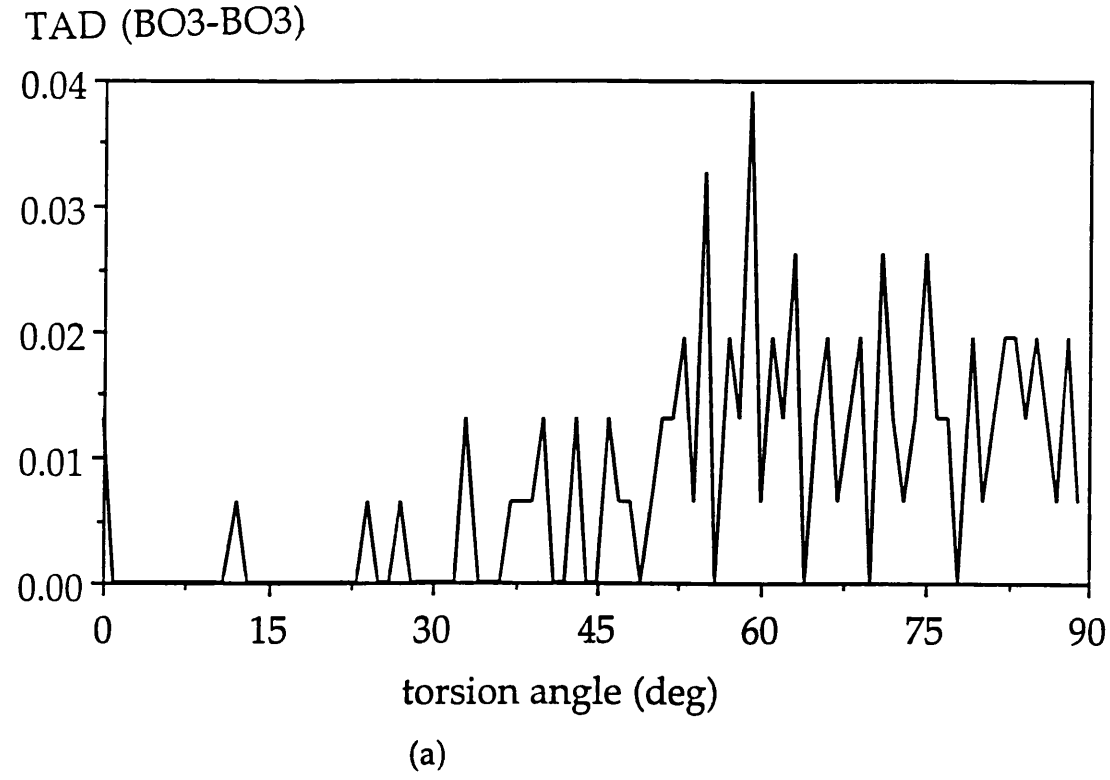

(a)

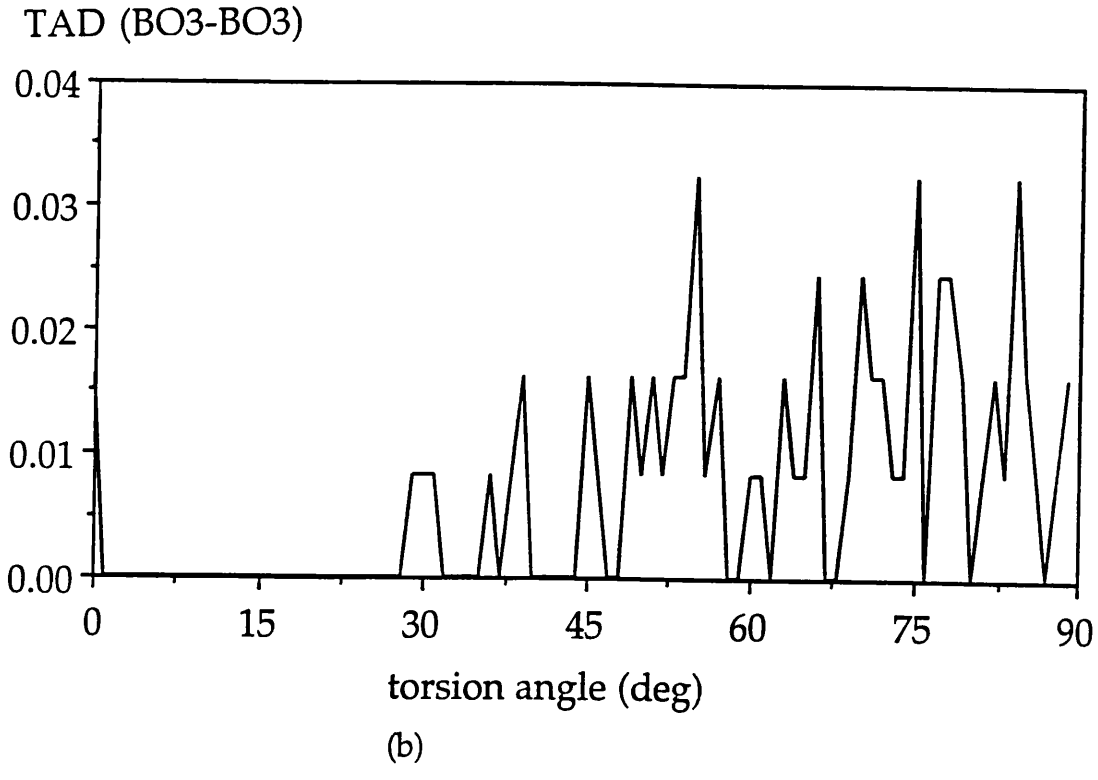

(b)

Figure 6.18. Torsion angle distribution in calculated vitreous structure using potentials c1 and c2 at 0 K
All angles are between BO_3 triangles.

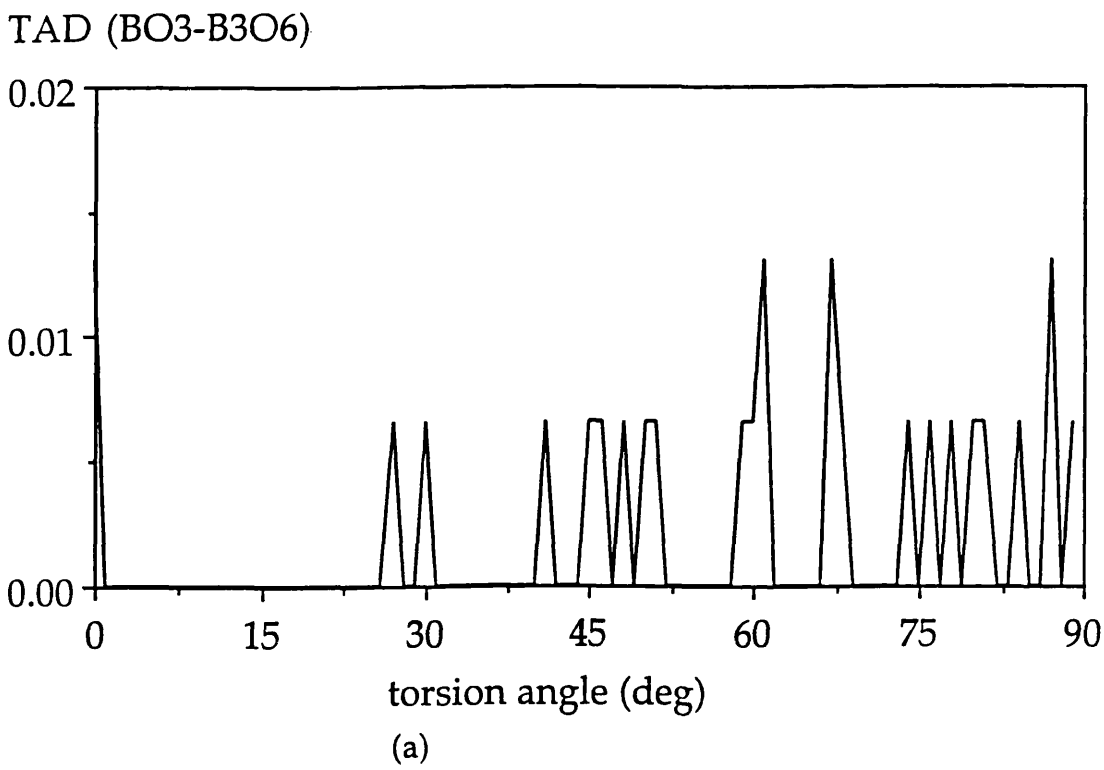

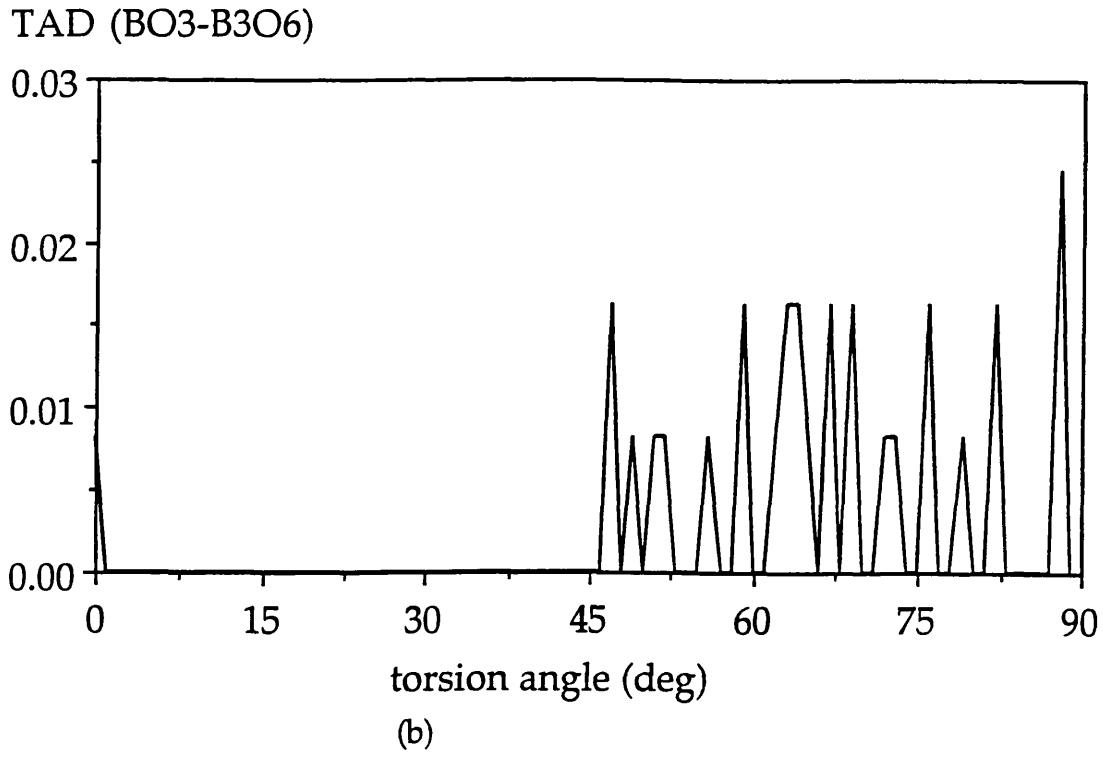

Figure 6.19. Torsion angle distribution in calculated vitreous structure using potentials c1 and c2 at 0 K
All angles are between BO_3 triangle and B_3O_6 ring.
(a) potential c1 (b) potential c2

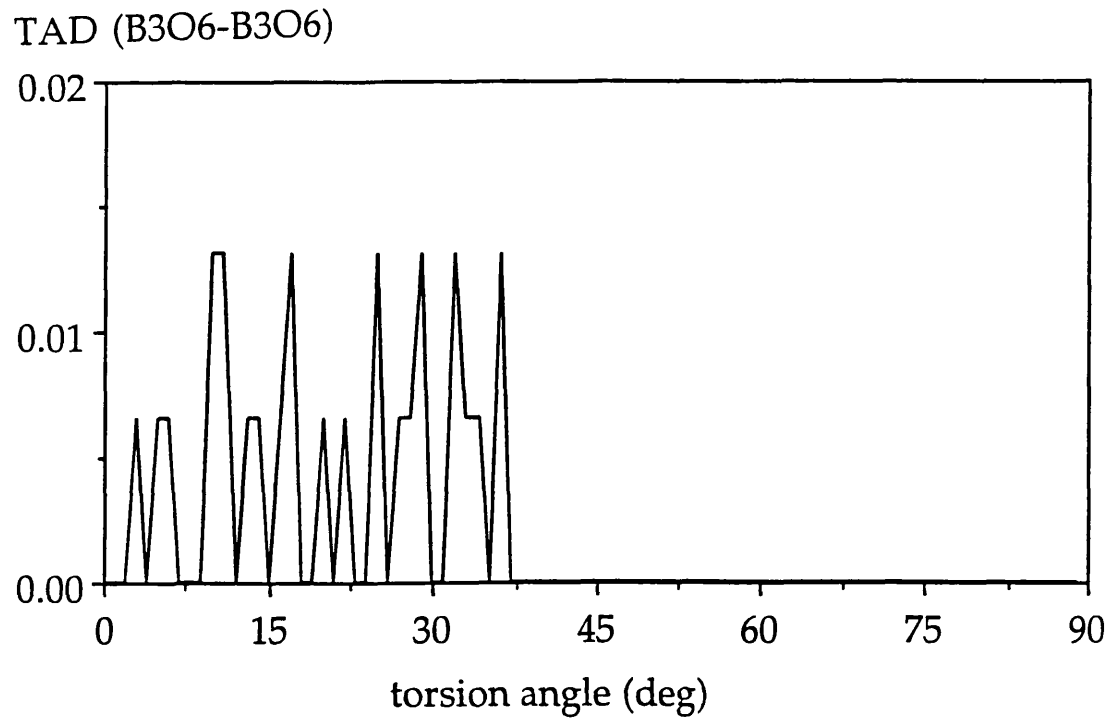

(a)

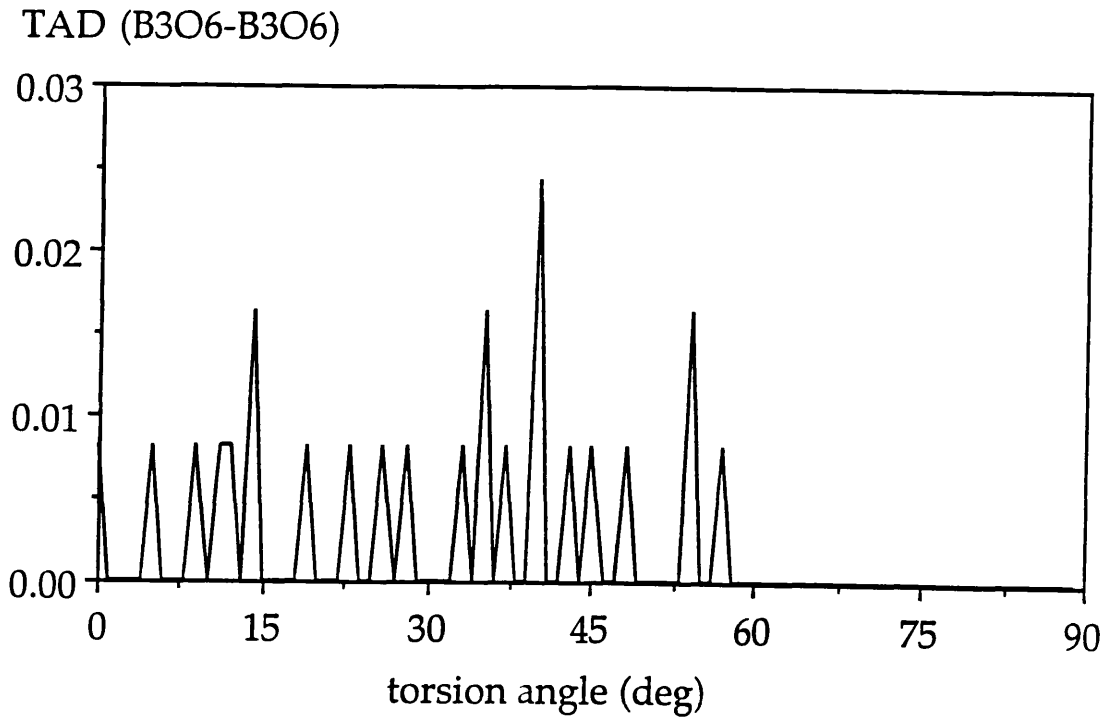

(b)

Figure 6.20. Torsion angle distribution in calculated vitreous structure using potentials c1 and c2 at 0 K
All angles are within B_3O_6 rings.
(a) potential c1 (b) potential c2

6.5.4 LATTICE DYNAMICS SIMULATION

The vitreous structure calculated using potential c2 was energy-minimized and its lattice dynamical properties were calculated employing the GULP program discussed in Chapter 5 (Gale 1993). The calculated vibrational densities of states at 300K are shown in Figure 6.20 (see also Section 5.9). They have two peaks at 740 cm^{-1} and 805 cm^{-1} which correspond to peak (A) in B_2O_3-I and peak (B) in B_2O_3-a, and the structure appears to have intermediate features between these of B_2O_3-I and the B_2O_3-a. Furthermore, they have the other higher peak (C) of 775 cm^{-1}, which does not exist either in the B_2O_3-I or B_2O_3-a. This calculated structure still contains several BO_4 tetrahedra, and peak (C) is assigned to a vibration of the six-membered rings with one or two BO_4 tetrahedra, as noted by Konijnendijk and Stevels (1978) in their study of the spectra of the alkali-borate crystals.

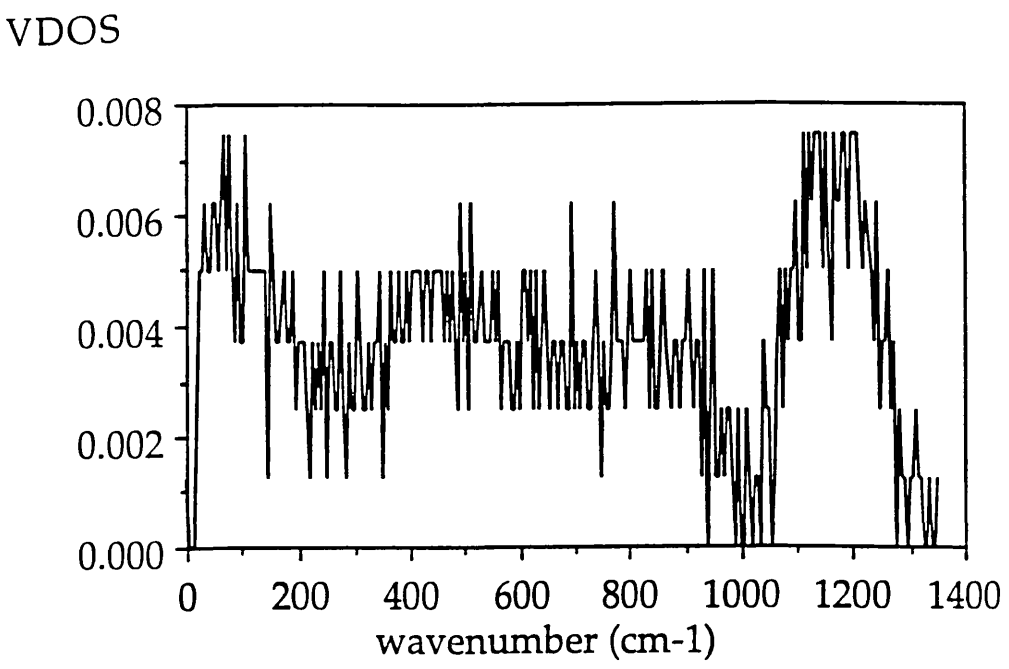

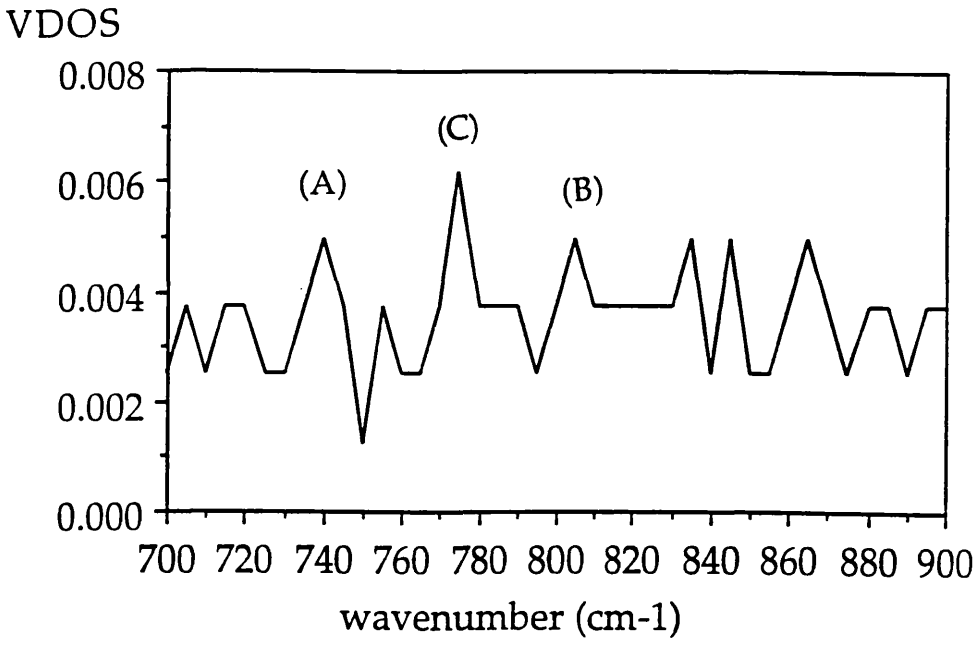

Figure 6.21. Vibrational density of states in calculated vitreous structure using potential c2 at 0K

(See text for (A), (B) and (C).)

6.5.5 STRUCTURAL TRANSFORMATION IN THE GLASS FORMATION

In Chapter 4 the structural transformation from the BO_3 triangular structural unit to the BO_4 tetrahedral unit was observed to occur smoothly without breaking any B-O bonds. However, such a smooth transformation without bond breaking seems to be topologically impossible between the independent BO_3 triangular structural unit and the B_3O_6 boroxol ring unit.

Here, we investigated the nature of the structural transformations in the melting and quenching simulations. Two types of transformations were observed. In the first at 1500K, two-thirds of the boron atoms have the two-fold coordination, and as the system is quenched, the two-fold coordinated boron atoms bond with the non-bridging or the two-fold coordinated oxygen atoms (see Figure 6.22 (a) and (b)). In the latter case, after the generation of a six-membered ring, one original B-O bond is broken. In the second below 1000K the three-fold coordinated boron atoms bond with the fourth oxygen atom. The transient state has four-fold coordinated boron and three-fold coordinated oxygen atoms (see Figure 6.22 (c)). Then after the generation of a six-membered ring, two new B-O bonds are created.

It is interesting to note that Mackenzie (1959) proposed non-bridging –B=O groups were present as higher energy species in molten B_2O_3, while Krogh-Moe (1960) proposed four-fold coordinated boron and three-fold coordinated oxygen atoms. Both hypotheses were proposed independently. However, they correspond to our results and we can now distinguish between them; the first is the 'high temperature structural transformation', while the second is the 'low-temperature structural transformation'. It is also interesting to note that the latter hypothesis

may explain one of the reasons why a proportion of the four-fold coordinated boron was always observed in our MD simulations even when the TCP potential model was used; the transient structures would be frozen before finding the appropriate bonding partners because of the rapid quench rates.

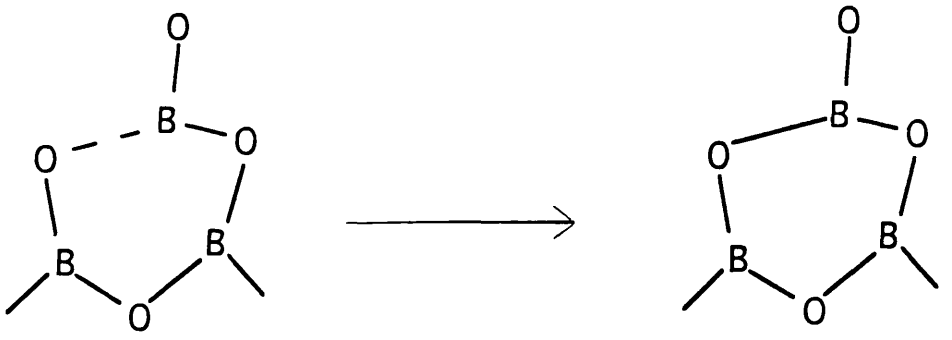

(a) 2 fold coordinated boron + non-bridging oxygen

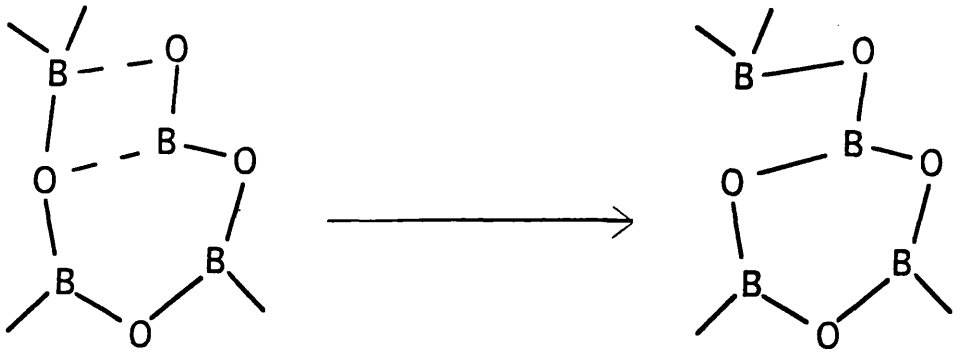

(b) 2-fold coordinated boron + 2 fold coordinated oxygen

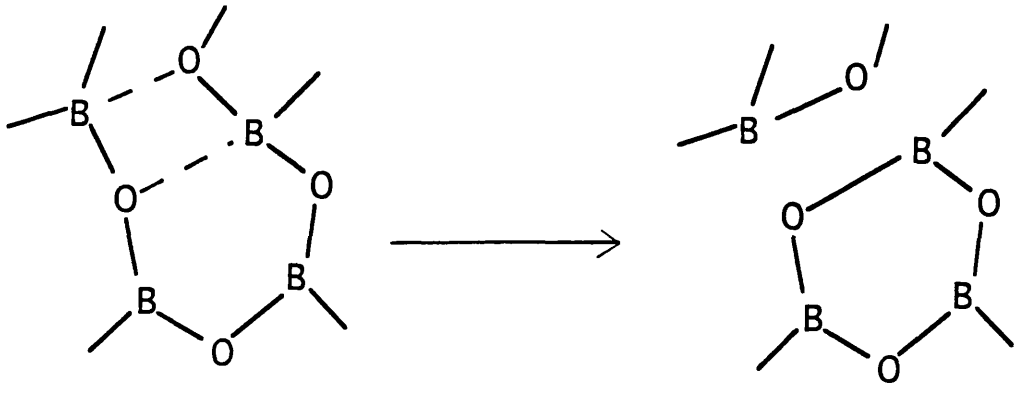

(c) 3 fold coordinated boron + 2 fold coordinated oxygen

Figure 6.22. Schematic diagram for structural transformation observed in MD simulations

6.6 ESTIMATION OF THE RATIO OF BOROXOL RINGS TO INDEPENDENT BO_3 UNITS

One of the major concerns in our MD simulations is the ratio of the boroxol rings to the independent BO_3 units. As explained in Chapter 2, the NMR study (Jellison et al 1977) and the neutron diffraction study (Johnson et al 1982) estimated the fraction of the boron atoms included in the boroxol rings as 82±8 % and 60±20% respectively The MD simulated structures contained 30~50 % fraction of the boroxol rings. However, we must note that there are still several limitations in the latter techniques as explained in Section 6.2.

One of the most useful clues in unravelling these complexities may be the glass density which strongly depends on the structure. After the construction of the possible polymorphs shown in Section 5.8, we now have one experimental density for B_2O_3-I and four simulated densities for B_2O_3-a, B_2O_3-b, B_2O_3-c and B_2O_3-d. The relation between the fractions of the boron atoms contained in the boroxol rings and the densities are plotted in Figure 6.23. We note that the bond lengths and angles in these structures are all very similar. So the changes in density are due to changes in the intermediate-range order. There is a clear correlation between the density and the boroxol ring content, although there is appreciable variance in the correlation. However, the fraction which corresponds to the glass density can be estimated as 50~64%. When the calculated structures explained in Chapter 5 and 6 are taken into account, one of the possible crystalline analogues for vitreous B_2O_3 may be the disordered structure based on B_2O_3-c and B_2O_3-d, with some B_3O_6 rings replaced with BO_3 triangular units.

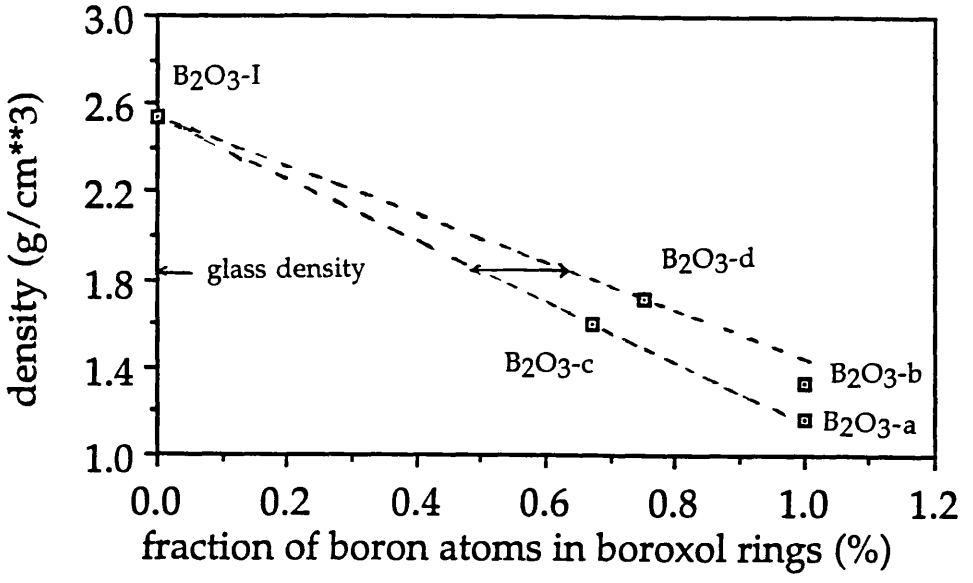

Figure 6.23. Relation between fractions of boron atoms contained in boroxol rings and densities

6.7 CONCLUSIONS

In applying the transferable potential model which can reproduce both crystal structures of B_2O_3 to the melting and quenching MD simulations, we obtained a vitreous structure containing six-membered rings (with 27% of the boron atoms), but is also containing several four-fold coordinated boron atoms which is inconsistent with much experimental data. The problem may be related to the fact that the difference between the lattice energies of two polymorphs cannot be reproduced by this potential.

Next, in order to overcome this problem, the new potential model (the TCP potential) was developed and used in the MD simulations. In the constant pressure calculations this new potential model successfully reduced the proportion of the four-fold boron atoms and increased the proportion of the six-membered rings closer to the lower limit (40%) of that estimated by the neutron study, although the calculated densities became too large. In the constant volume calculations, the proportion of the six-membered rings was reduced and the four-fold boron atoms appeared. However, the calculated structures agree with the RDFs and interference functions derived from the X-ray diffraction data and with the neutron scattering data. It is interesting to note that all these structural models have one important feature concerning the intermediate-range order, namely, that a considerable proportion of the torsion angles between the BO_3 triangles, between the BO_3 triangle and the B_3O_6 ring, and between the B_3O_6 rings are around 74°, although the MD simulated structures contain smaller torsion angles. This feature seems to be important in reproducing the experimental density without the presence of four-fold coordinated boron atom.

Regarding the vibrational properties, as the calculated structure contained four-fold coordinated boron atoms, the lattice dynamics simulation of the structure exhibited two characteristic peaks seen in the Raman spectra; the first is at 805 cm^{-1} and is due only to the boroxol ring with BO_3 triangles; and the other is at 775 cm^{-1} and corresponds to the six-membered ring with one or two BO_4 units.

These MD studies using the new potential model demonstrate structural transformation in the glass formation and confirm the existence of the boroxol rings, in contrast with the other MD studies employing the pair-potentials. However, there are several four-fold coordinated boron atoms remaining and the proportion of the boroxol rings is still smaller than that estimated by experiments. There are three possible explanations: the first concerns the effect of the finite simulation time explained in Section 6.2.4. Although our new potential model favours the three-fold coordinated environment rather than the three-fold one, the simulation must have sufficient time for the structure to rearrange during the quench process, and the present time scale would not be sufficient. The second is the finite size effect explained in Section 6.2.4. As the B_2O_3 system has much more pronounced intermediate-range order than in the other oxide materials, the simulation box may need to be much larger. The third concerns the accuracy of the potential models. The new potentials could reproduced two crystal structures well, but it may require still further improvement using spectroscopic data and properties of the molten state.

Several MD simulations which started from the structure of pseudo super crystal B_2O_3-d (good candidate for vitreous B_2O_3) were also performed. The system was melted and then quenched in the same way as explained in Section 6.5. The final vitreous structure turned out to be

almost same as those calculated in Section 6.5. An improvement was not observed, because the system probably lost most of its initial structure. However, further work based on the pseudo super crystal structures may lead to the possibility of simulating more realistic vitreous structures.

Finally, we estimated the fraction of boron atoms present in boroxol rings as 50~64%, from the relation between the calculated structures and densities for polymorphs.

7. SUMMARY, CONCLUSIONS AND SUGGESTIONS FOR FUTURE STUDY

As we have proceeded through the simulations reported in this thesis, we have realized the complexities in structure and bonding in borate materials. We now attempt to summarize the results and insights obtained in this thesis.

The starting point for our work was the experimental and computational studies previously reported in the field of the B_2O_3 materials which were reviewed in Chapter 2. We saw that none of these provided single comprehensive methods to elucidate the structure and bonding in these materials and that it is essential to employ them in a complementary manner.

In our first theoretical approach, we employed quantum-chemical calculations based on periodic ab-initio Hartree-Fock methods on borate crystals in the crystalline state. Our calculated results highlighted both ionic and covalent features in the bonding, and they showed that such features accord well with empirical concepts regarding the structure and bonding of borates. Future applications of these techniques to the other borate minerals should explain common and different features among borates more systematically.

Our second approach was the first-principles total energy calculations on the two B_2O_3 crystals employing the LDA, pseudopotential techniques. The calculated results obtained by the full optimization of the structures reproduced not only lattice parameters but also internal coordinates. Using the optimized structures, the bulk moduli for B_2O_3-I and B_2O_3-II were estimated for subsequent use in the development of interatomic potentials for B_2O_3 crystals. Furthermore,

when the simulation cell volume was reduced, the structural transformation from the BO_3 triangular structural unit into the BO_4 tetrahedral unit was observed and the manner of its transformation was also elucidated.

Using the information gained from these fundamental study of structure and bonding, we proceeded to the computer modelling of crystalline B_2O_3. In contrast to the previous two quantum-mechanical approaches, we employed atomistic simulation techniques. First, in order to overcome the difficulties in deriving interatomic potentials, the new procedure known as the LP fitting method was developed. By using this method several sets of potentials which can reproduce both crystal structures were derived. The fitted potentials showed that the partial charge model with a B-O Morse potential and a B-O-B bond-bending, three-body term can reproduce both structures well. It is interesting to note that the crystalline and molecular potentials yielded different parameters. The best potentials, which reproduce the order of the lattice energies between the polymorphs, were found to have pair-potential terms which varied depending on the coordination numbers.

Next, these potentials were applied to other possible polymorphs containing boroxol rings and also possible structural units for vitreous B_2O_3. The pseudo super crystal structure (B_2O_3-d) which was obtained by performing static simulations is the first structural model for the basic unit of vitreous B_2O_3, which can reproduce not only the B-O bond lengths and the B-O-B bond angles, but also the density, with 75% of boron atoms in boroxol rings. The lattice dynamic simulations using this structure also showed that the peak of the experimental Raman peak at 806 cm^{-1} can be assigned to the breathing mode of the boroxol rings. It is interesting to note that the important feature in this structure is thought

to be the interlocking three-dimensional networks with two or three BO_3 units connecting the B_3O_6 units. More extensive 'computer synthesis' will enable us to obtain further possible candidates for polymorphs and vitreous structures.

Using the potentials which had been successfully derived for the crystal structures, we applied the MD method to vitreous B_2O_3. To overcome the problem that the transferable potentials are often favour four-fold coordinated boron atoms, we developed a new model (the TCP potential model) which varies parameters automatically depending on the coordination number. In the constant pressure calculations this new model reduced the proportion of the four fold coordinated boron atoms and increased the proportion of the six-membered rings close to the lower limit (40%) of that estimated by the neutron study, although the calculated density became too large. In the constant volume calculations the proportion of the six-membered rings was reduced and the four-fold boron atoms reappeared. However, the calculated structures agree with the RDFs and the interference functions derived from the X-ray and neutron diffraction data.

In order to analyze the intermediate-range order, the torsional angle distributions (TADs) were calculated for the experimental and calculated structures. These calculated results suggested that a considerable proportion of the torsion angles between the BO_3 triangles, between the BO_3 triangle and the B_3O_6 ring, and between the B_3O_6 rings must be ~74° in order to produce the experimental density. The structure obtained from the MD simulations showed that it has reasonable frequencies in the vibrational density of states. The manner of the structural transformations in the glass formation at finite temperatures was proposed. It is interesting to note that from the structures and the

densities simulated in Chapter 5 we estimated the fraction of the boron atoms contained in the boroxol rings (50~64%). Further studies will investigate the alkali borates, alkaline-earth borates and borosilicate glasses.

The structural properties of crystalline and vitreous borates are clearly highly complex. This thesis shows, however, that computational methods, when used in conjunction with experiment, can make an important contribution to their study.

APPENDIX A

CHRIST'S POSTULATION ON THE STRUCTURES OF BORATE MINERALS

Christ postulated several rules regarding to formation of hydrated borate polyanions (Christ 1960; Christ and Clark 1977).

His rules are as followings:

i. Boron will link either three oxygens to form a triangle or four oxygens to form a tetrahedron.

ii. Polynuclear anions are formed by corner sharing only of boron-oxygen triangles and tetrahedra in such a manner that a compact insular group results.

iii. In the hydrated borates, protonatable oxygen atoms will be protonated in the following sequence: protons are first assigned to free O^{2-} ions to convert these to free OH^- ions; additional protons are assigned to tetrahedral oxygens in the borate ion; protons are next assigned to triangular oxygens in the borate ion; and finally any remaining protons are assigned to free OH^- ions to form H_2O molecules.

iv. The hydrated insular groups may polymerize in various ways by splitting out water; this process may be accompanied by the breaking of boron-oxygen bonds within the polyanion framework.

v. Complex borate polyanions may be modified by attachment of an individual side group, such as (but not limited to) an extra borate tetrahedron, an extra borate triangle, 2 linked triangles, an arsenate tetrahedron, and so on.

vi. Isolated $B(OH)_3$ groups, or polymers of these, may exist in the presence of other anions.

APPENDIX B

THE REPORTED POTENTIALS FOR B_2O_3

There are several potential models reported specifically for vitreous B_2O_3. The details of these potentials are explained as follows.

i. Soules's potential (1980,1981)

The effective pair-potentials V were assumed to be purely ionic (formal charge model) and their parameters were determined empirically.

$$V_{ij}(r) = A_{ij} \exp(-r/0.29) + (q_i q_j e^2/r)\ \mathrm{erfc}(r/0.35L) \qquad (A2.1)$$

$$A_{ij} = 0.338*10^{-12}\ [\mathrm{erg}] \cdot (1+z_i/n_i + z_j/n_j) \cdot \exp(r_i + r_j/0.29) \qquad (A2.2)$$

where r is interatomic distance, L is size of simulation box; for boron atom r_i is 0.74 [Å], q_i is +3 and n_i is 2; for oxygen atom r_i is 1.42 [Å], q_i is -2 and n_i is 8.

This potential was applied to B_2O_3 glass and sodium borosilicate glasses. It successfully reproduced the trigonal to tetrahedral conversion of boron with the addition of sodium in agreement with the NMR results. But the glass studied showed no tendency to form boroxol groups. In B_2O_3 glass, the broad distribution of B-O-B bond angles peaking near 155° was observed, similar to that found in vitreous silica. Soules stressed the absence of directional covalent bonding as the limitation. This potential was also used for B_2O_3 glass by Soppe et al (1988) and for silver borate glass by Abramo and Pizzimenti (1986).

ii. Amini's potential (1981)

A power-type force law was used in the study. The charge values, +1.125 and -0.75 for boron and oxygen atoms, were determined so that

the MD simulation can reproduce reasonably the glass transition temperature of ~ 600K (physical value of 540K, Ubbelohde 1978). The force law is

$$F(r_{ij}) = q_i q_j / r_{ij}^2 \, [\, 1 + \mathrm{sgn}(q_i q_j) \, \{(s_i+s_j)/r_{ij}\}^n \,] \qquad \text{(A2.3)}$$

where F is force, r_{ij} is interatomic distance, n is 8; for boron atom, s is 0.153 [Å], q is +1.125; for oxygen atom, s is 1.07 [Å], q is -0.75.

This potential was applied to B_2O_3 glass and gave pair correlation functions which agree with X-ray and neutron diffraction results. However, no boroxol groups were observed. The distribution of B-O-B angles was very broad with an average of 154° suggesting that higher-fold rings were predominant in the system.

iii. Hirao's potential (1985)

A new potential $V_{B\text{-}B}$ of the form $-A \exp[-C(r-0.239)^2]$ was added to the regular modified Born-Mayer-Huggins-type potentials, $V_{B\text{-}B}$, to account for the directional tendency of the borate network structure. For B-B, B-O and O-O interactions we have;

$$V_{ij}(r) = q_i q_j e^2/r + (1 + q_i/n_i + q_j/n_j) \, b \exp\{(\sigma_i+\sigma_j-r)/\rho\} \qquad \text{(A2.4)}$$

while only for B-B interactions, we add the following term,

$$V_{B\text{-}B}(r) = V_{ij}(r) - A \exp[-C(r-0.239)^2] \qquad \text{(A2.5)}$$

where r is the interatomic distance, $b = 0.338 \times 10^{-19}$ [J], $\rho = 0.029$ [nm], $A = 6.94 \times 10^{-19}$ [J], C = 7.62, for boron atom, $\sigma = 0.074$ [Å], q = +3 and n = 2; for the oxygen atom, $\sigma = 0.142$ [Å], q = -2 and n = 8. The parameters A and C were chosen so that the B-B distance and the population of B-O-B angles in B_2O_3 glass became similar to those obtained from X-ray measurements.

This potential was applied to sodium borate glasses containing a small amount of Eu_2O_3 to investigate the local structures of cations in

the glass. It reproduced both the radial distribution of the sodium borate glasses observed by small-angle X-ray diffraction and the change in coordination number of boron with sodium content obtained by NMR. They observed a high proportion of B-O-B bond angles at ≈ 120° and a smaller number at 145°. They suggested that the population at 120° might come from the connection of boroxol groups.

iv. Inoue's potential (1987)

This pseudo three-body model is explained in Chapter 2.5.2.

Three types of potentials were used.

1) Born-Mayer-type pair-potential for B-O (> 0.2 nm), O-O and B-B pairs. The potential parameters are described in Table B.1.

$$V_{ij}(r) = B \exp(-r/\rho) + (q_i q_j e^2/r) \qquad \text{(A2.6)}$$

2) Pair-potentials calculated by the intermediate neglect of differential overlap (INDO) method, for the B-O bond (< 0.2nm).

3) As with the three-body effects, the interaction between the ghost atoms and the other atoms are supposed to be of the Born-Mayer type, and the parameters were determined so that the sum of these potentials was a minimum when the bond lengths and bond angles of the triangles took the value in Table B.2.

This potentials were applied to B_2O_3 glass and $Na_2O{\cdot}2B_2O_3$ glass, and reproduced boroxol rings and diborate groups. In B_2O_3 glass, O-B-O and B-O-B bond angles have sharp distributions around 120°. However, the ratio of boron atoms present in boroxol rings in the simulated B_2O_3 glass is 22.5% and smaller that reported (see Chapter 2).

	B ($x10^{-16}$ J)	ρ(nm)
Na-Na	1.49	0.03
Na-B	0.62	0.03
B-B	3.08	0.03
Na-B	6.33	0.03
B-O (>0.2 nm)	2.13	0.03
O-O		
For O-B-O in BO_3		
G-O	19.64	0.015
G-B	1.39	0.015
For O-B-O in BO_4		
G-O	22.56	0.015
G-B	1.92	0.015
For B-O-B		
G-O	1.46	0.015
G-B	24.53	0.015

Table B.1 Parameter in the Inoue's potential (Inoue et al 1987)

	Angle (deg)	B-O distance (nm)
O-B-O in BO_3	120	0.137
O-B-O in BO_4	109	0.148
B-O-B	120	0.144

Table B.2 Shapes of BO_2 and B_2O triangles at the minimum potential energy (Inoue et al 1987)

v. Xu's potential (1988)

This potential was determined so that the MD calculations of B_2O_3 and KB_5O_8 crystals could reproduce well the experimentally derived

crystal structures. The pair-potential used is the Busing approximation of Born-Mayer-Huggins' form without the dispersion terms and is purely ionic.

$$V(r_{ij}) = q_i q_j e^2 / r_{ij} + f_0 \cdot (b_i + b_j) \cdot \exp[\,(a_i + a_j - r_{ij}) / (b_i + b_j)\,] \qquad \text{(A2.7)}$$

where r_{ij} is the interatomic distance, f_0 is 6.9472 $*10^{-11}$ N; for the boron atom, q = +3, a = 0.720 and b = 0.080; for oxygen, q = -2, a = 1.629 and b = 0.085.

This potential was applied to B_2O_3 glass and sodium borate glasses, and it was shown that the calculated compositional dependence of the fraction of the boron ions having tetrahedral coordination is in good agreement with the results measured by NMR. However, in B_2O_3 glass the B-O-B bond angle distribution has a broad peak around 160° and no boroxol ring was observed.

vi. Verhoef's potentials (1992)

Soules's potential (V1) and Xu's potential (V5) were modified. All the seven potentials have the same Born-Mayer-Huggins form

$$V_{ij}(r) = A_{ij} \exp(-r/\rho_{ij}) + q_i q_j e^2 / r \qquad \text{(A2.8)}$$

The V2 potential was modified so that correct vibrational frequencies were obtained. The V3 potential has the same pair-potential component as the V2 potential and supplemented with the O-B-O three-body bond-bending term of the form

$$V_{ijk}(\theta) = 1/2\, K_{ijk} (\theta - \theta_0)^2 \qquad \text{(A2.9)}$$

where θ_0 is 120° for O-B-O and 130° for B-O-B. The force constant K_{ijk} was determined so that the correct energy for the high frequency mode in the simulated infrared spectra was obtained. The B-O-B three-body term was also added in the V4 potential. In the same manner, the pair-

potential parts of the V6 and V7 potentials were modified from the V5 potential to obtain correct frequencies, and the B-O-B three-body term was added to the V7 potential. The potential parameters are given in Table B.3.

These potentials were applied to B_2O_3 glass, and the structural and dynamical properties of the simulated systems ware compared with experimental neutron diffraction, X-ray, Raman and infrared data. They concluded that in all cases no boroxol ring was present, but the potentials with the three-body terms reproduced the experimental vibrational modes.

case	ABB	ABO	AOO	ρBB	ρBO	ρOO	qB	qO	KO-B-O	KB-O-B
	[10^{*3} KJ/mol]			[Å]					[KJ / (mol rad^2)]	
V1	13.4	78.63	182.3	0.29	0.29	0.29	3.0	-2.0	0	0
V2	9.614	33.72	79.63	0.29	0.29	0.29	2.0	-1.333	0	0
V3	9.614	33.72	79.63	0.29	0.29	0.29	2.0	-1.333	1000	0
V4	6.614	33.72	79.63	0.29	0.29	0.29	2.0	-1.333	1000	500
V5	5.424	1052	149700	0.16	0.165	0.17	3.0	-2.0	0	0
V6	0.6645	128.8	18330	0.16	0.165	0.17	1.050	-0.7	0	0
V7	0.6645	128.8	18330	0.16	0.165	0.17	1.050	-0.7	1500	0

Table B.3 Pair-potential and three-body parameters in Verhoef's potentials (Verhoef and Hartog 1992)

APPENDIX C

PHYSICAL PROPERTIES OBSERVED IN MD SIMULATION

(Kimura and Yonezawa 1983)

[I] Structural properties

1) g(r) : Pair distribution function
2) S(q) : Structure factor

[II] Thermodynamic properties

1) PvT Equation-of-state data (isobars in vT plane)
2) α_p : Isobaric thermal expansion coefficient
3) H : Enthalpy
4) C_p : Specific heat at constant pressure
5) C_v : Specific heat at constant volume
6) κ_T : Isothermal compressibility

[III] Dynamical properties

1) $\psi(t)$: Velocity autocorrelation function (VAF)
2) $f(\omega)$: Power spectrum

[IV] Transport properties

1) D : Diffusion constant (from VAF and from mean square displacement)
2) η : Shear viscosity (from stress autocorrelation function)

[V] Microscopic information of the atomic distributions

1) g(r) : Pair distribution function of time-averaged atomic positions
2) Distribution of volumes of Voronoi polyhedra
3) Distribution of shape parameters of Voronoi polyhedra
4) Distribution of selected types of Voronoi polyhedra

APPENDIX D

TERSOFF'S POTENTIAL

An empirical interatomic potential for covalent systems such as Si was proposed by Tersoff (1986).

A pair potential is used:

$$E = \sum E_i = 1/2 \cdot \sum_{i,j \neq i} V_{ij} \qquad (D.1)$$

$$V_{ij} = f_C(r_{ij}) [A_{ij} \exp(-\lambda_1 r_{ij}) - B_{ij} \exp(-\lambda_2 r_{ij})] \qquad (D.2)$$

where E is the total energy of the system, E_i is the site energy for site i (introduced to make the asymmetry of V_{ij} more intuitively), V_{ij} is the interaction energy between atoms i and j, r_{ij} is the distance between them, and A, B, $\lambda_1$and λ_2 are all positive, with $\lambda_1 > \lambda_2$. (The Morse potential is defined by $\lambda_1 = \lambda_2$.) F_C is an optional cutoff function to restrict the range of the potential. The first term in (D.2) is repulsive. The second term is interpreted as representing bonding. B_{ij} therefore implicitly includes the bond order and must depend on the local environment. All deviations from a simple pair potential are ascribed to the dependence of B_{ij} on the local environment. Specifically, the bonding strength B_{ij} for the pair ij should be a monotonically decreasing function of the number of competing bonds, the strength of the competing bonds, and the cosines of the angles with the competing bonds. These three factors have been incorporated in the following simple trial potential:

$$B_{ij} = B_0 \exp(-z_{ij}/b) \qquad (D.3)$$

$$z_{ij} = \sum_{k \neq i,j} [w(r_{ik})/w(r_{ij})]^n \cdot [c + \exp(-d \cos\theta_{ijk})]^{-1} \qquad (D.4)$$

where w(r) is the "bare" bonding potential, $w(r) = fc(r)\exp(-\lambda_2 r)$. Here z_{ij} is a weighted measure of the number of bonds competing with the bond ij, and b determines how rapidly the bond strength falls off with increasing effective coordination. The first term in (D.3) is just the ratio

of the unscaled bond strengths of the bonds ik and ij, raised to the power n. The parameter n thus determines how much the closer neighbours are favoured over the more distance ones in the competition to form bonds. The final term gives the dependence on bond angle, which is taken as a function of $\cos(\theta_{ijk})$ to insure the proper analytic behaviour. θ_{ijk} is the angle between bonds ij and ik. Note that this formulation is not symmetric, i.e., $V_{ij} \neq V_{ji}$.

This model accurately described bonding and geometry for many structures of Si, including highly rebonded surfaces.

REFERENCES

Abe T. J., 1952, Am. Ceram. Soc., **35**, 284.

Abramo M.C. and Pizzimenti G., 1986, J. Non-Cryst. Solids, **85**, 233.

Allan D.A. and Teter M.P., 1987, Phys. Rev. lett., **59**, 1136.

Allan M.P. and Tildesley D.J., 1987, *Computer Simulation of Liquids*, Clarendon Press.

Amini M., Mitra S.K. and Hockney R.W., 1981, J. Phys. C, **14**, 3689.

Andersen H.C., 1980, J. Chem. Phys., **72**, 2384.

Barone V., Bucci P., Lelj F. and Russo N., 1981, J. Molec. Struct., **76**, 29.

Beest B.W.H., Kramer G.J. and Santen R.A., 1990, Phys. Rev. lett., **64**, 1955.

Bell R.J. and Carnevale A., 1981, Phil. Mag. **B43**, 389.

Berendsen H.J.C., Pastma J.P.M., Van Gunsteren W.F., Di Nola A. and Haak J.R., 1984, J. Chem. Phys., **81**, 3684.

Berger S.V., 1952, Acta Cryst., **5**, 389.

Berger S.V., 1953, Acta. Scand., **7**, 611.

Bokii G.B. and Kravchenko V.B, 1966, J. Struct. chem. (USSR), **7**, 860.

Borelli N.F. and Su G.J., 1963, Phys. Chem. Glasses, **4**, 206.

Bouteiller Y., Mijoule C., Nizam M., Barthelat J.C., Daudey J.P., Pelissier M. and Silvi B., 1988, Mol. Phys., **65**, 295.

Bray P.J. and O'Keefe J.G., 1963, Phys. Chem. Glasses, **4**, 37.

Bril T.W., 1975, Thesis, Technological University of Eindhoven, The Netherlands. Also Bril T.W., 1976, Philips Res. Repts. suppl. **2**.

Bronswijk J.P. and Strijks E., 1977, J. Non-Cryst. Solids, **24**, 145.

Car R. and parrinello M., 1985, Phys. Rev. lett., **55**, 2471.

Catlow C.R.A. and Norgett M.J., 1976, AERE Harwell Report M2936.

Catlow C.R.A. and Mackrodt W.C. (eds.), 1982, *Computer Simulation of Solids* (Lecture Notes in Physics 166), Springer-Verlag.

Catlow C.R.A. and Stoneham A.M., 1983, J. Phys. C., **16**, 4321.

Catlow C.R.A., Freeman C.M., Islam M.S., Jackson R.A., Leslie M. and Tomlinson S.M., 1988, Phil. Mag., **A58**, 123.

Catlow C.R.A. and Price G.D., 1990, Nature, **347**, 243.

Chadi D.J. and Cohen M.L., 1973, Phys. Rev., **B8**, 5747.

Christ C.L., 1960, Amer. Mineral., **45**, 334.

Christ C.L. and Clark J.R., 1977, Phys. Chem. Minerals, **2**, 59.

Ciccotti G. and Hoover W.G. (eds.), 1986, *Molecular-Dynamics Simulation of Statistical-Mechanical Systems* , North-Holland.

Ciccotti G., Frenkel D. and McDonald L.R., 1987, *Simulation of Liquids and Solids,* North-Holland.

Clark T., *A Handbook of Computational Chemistry : A Practical Guide to Chemical Structure and Energy Calculations,* John Wiley & Sons, Chapter.5.

Coulson C.A., 1964, Acta Cryst., **17**, 1086.

Coulson C.A., 1968, Acta Cryst, **B24**, 153.

Coulson C.A. and Dingle T.W., 1968, Acta Cryst., **B24**, 153.

Dick B.G. and Overhauser A.W., 1958, Phys. Rev., **112**, 90.

Dovesi R., Pisani C., Roetti C. and Silvi B., 1987, J. Chem. Phys., **86**, 6967.

Duntzig G.B., 1963, *Linear Programming and Extensions,* Princeton University Press.

Durand P.H. and Barthelat J.C., 1975, Theor. Chim. Acta, **38**, 283.

Effenberger H. and Pertlik F., 1984, Z. Kristallogr., **166**, 129.

Elliot S.R., 1978, Phil. Mag., **B37**, 435.

Eversteijn F.E., Stevels J.M. and Waterman H.I., 1960, Phys. Chem. Glasses, **1**, 123.

Ewald P.P., 1921, Ann. Phys. (Paris), **21**, 1087.

Fajans K. and Barber S.W., 1952, J. Am. Chem. Soc., **74**, 2761.

Fang J.H. and Newnham B.E., 1965, Min. Mag., **35**, 196.

Fang S.M., 1938, Z. Kristallogr., **99**, 1.

Gale J.D., Catlow C.R.A. and Mackrodt W.C., 1992, Modelling Simul. Mater. Sci. Eng., **1**, 73.

Gale J.D., 1993, Private Communication.

Galeener F.L., Lucovsky G. and Mikkelsen J.C. Jr., 1980, Phys. Rev., **B22**, 3983.

Gibbs G.V., Meagher E.P., Newton M.D., Swanson D.K., 1981, in *Structure and Bonding in Crystals* (O'Keeffe M. and Navrotsky A., eds.), Academic Press.

Gillan M.J., 1989, J. Phys. C, **1**, 689.

Gordon R.G. and Kim Y.S., 1972, J. Chem. Phys., **56**, 3122.

Goubeau J. and Keller H., 1953, Z. Anorg. Chem., **272**, 303.

Griscom D.L., 1978, in *Borate Glasses : Structure, Properties, Applications* (Pye L.D., Frechett V.D. and Kreidl N.J., eds.), Plenum.

Gurr G.E., Mongomery D.W., Knutson C.D. and Gorres B.T., 1970, Acta Cryst., **B26**, 906.

Gupta A. and Tossel A., 1981, Phys. chem. miner., **7**, 159.

Gupta A. and Tossel A., 1983, Amer. Mineral., **68**, 989.

Hahre W.J., Radom L., Schleyer P.v.R. and Pople J.A., 1986, *Ab Initio Molecular Orbital Theory*, John Wiley & Sons.

Hannon A.C., Sinclair R.N., Blackman J.A., Wright A.C. and Galeener F.L., 1988, J. Non-Cryst. Solids, **106**, 116.

Hay P.J. and Wadt W.R., 1985a, J. Chem. Phys., **82**, 270.

Hay P.J. and Wadt W.R., 1985b, J. Chem. Phys., **82**, 299.

Hayward C.L., 1993, PhD. Thesis, University College London, london.

Heine V. and Cohen M.L., 1970, Solid State physics, **24**.

Hernandez E., 1993, Private Communication.

Hirao K. and Soga N., 1985, J. Am. Ceram. Soc., **68**, 515.

Hohenberg P. and Kohn W., 1964, Phys. Rev., **136**, B864.

Holloway J.R. and Wood B.J., 1988, *Simulating the Earth*, Unwin Hyman.

Huggins M.L. and Abe T., 1957, J.Amer. Ceram. Soc., **40**, 287.

Inoue H., Aoki N. and Yasui I., 1987, J. Am. Ceram. Soc., **70**, 622.

Jellison G.E. Jr., Panek L.W., Bray D.J. and Rouse G.B. Jr., 1977, J. Chem. Phys., **66**, 802.

Johnson P.A.V. and Wright A.C., 1982, J. Non-Cryst. Solids, **50**, 281.

Kamitsos E.I. and chryssikos G.D., 1991, J. Molec. Struct., **247**, 1.

Kawazoe H., Hosono H. and Kanazawa T., 1978a, J. Non-Cryst. Solids, **29**, 159.

Kawazoe H., Hosono H. and Kanazawa T., 1978b, J. Non-Cryst. Solids, **29**, 173.

Kimura M. and Yonezawa F., 1983, in *Topological Disorder in Condensed Matter* (Solid State Sciences 46) (Yonezawa F. and Ninomiya T., eds.), Springer-Verlag, p.80.

Kohn W. and Sham L.J., 1965, Phy. Rev., **140**. A1133.

Konijnendijk W.L., 1975, Philips Res. Repts. Suppl. **1**.

Konijnendijk W.L. and Stevels J.M., 1978, in *Borate Glasses : Structure, Properties, Applications* (Pye L.D., Frechett V.D. and Kreidl N.J., eds.), Plenum.

Kracek F.C, Morey G.W. and Merwin H.E., 1938, Am. J. Sci., **35A**, 143.

Krogh-Moe J, 1960, Phys. Chem. Glasses, **1**, 26.

Krogh-Moe J. and Ihara M., 1967, Acta Cryst., **23**, 427.

Krogh-Moe J., 1969, J. Non-Cryst. Solid., **1**, 269.

Lasaga A.C. and Gibbs G.V., 1988, Phys. Chem. Miner., **16**, 29.

Lasaga A.C. and Gibbs G.V., 1991, Phys. Chem, Miner., **17**, 485.

Lee M.H., 1992, Private Communication.

Lin J.S., Qteish A., Payne M.C. and Heine V., 1993, Phys. Rev. , **B47**, 4174.

Lindan P.J.D. and Gillan M.J., 1993, J. Phys. C, **5**, 1019.

Macedo P.B., Capps W. and Litovitz T.A., 1966, J. Chem. Phys., **44**, 3357.

Mackenzie J.D., 1959, J. Phys. Chem., **63**, 1875.

Mackenzie J.D. and Claussen W.F., 1961, J. Amer. Ceram. Soc., **44**, 79.

Marezio M, Plettinger H.A. and Zachariasen W.H., 1963a, Acta Cryst., **16**, 390.

Marezio M, Plettinger H.A. and Zachariasen W.H., 1963b, Acta Cryst., **16**, 594.

Mazurin O.V., Streltsina M.V., Shvaiko-Shvaikovskaya T.P., 1983, *Handbook of Glass Data* (Physical Sciences Data 15), Elsevier.

Monkhorst H.J. and pack J.D., 1976, Phys. Rev., **B13**, 5188.

Mozzi R.L. and Warren B.E., 1970, J. Appl. Crystallogr., **3**, 251.

Mulliken R.S., 1955, J. Chem. Phys., **23**, 1833, 1841, 2338, 2343.

Murnaghan F.D., 1944, Proc. Nat. Acad. Sci. U.S.A., **30**, 244.

Nada R., Catlow C.R.A., Dovesi R. and Pisani C., 1990, Phys. Chem. Miner., **17**, 353.

O'Keeffe M. and Navrotsky A., 1981, *Structure and Bonding in Crystals*, Academic Press.

Parker S.C. and Price G.D., 1989, Advances in Solid-State Chemistry (Catlow C.R.A., ed.), **1**, 295.

Parrinello M. and Rahman A., 1982, J. Chem. Phys., **76**, 2662.

Paul A., 1982, *Chemisty of Glasses*, Chapman and Hall.

Pauling L., 1945, *The Nature of the Chemical Bond* 1st Ed., Cornell University Press.

Pauling L., 1960, *The Nature of the Chemical Bond* 3rd Ed., Cornell University Press.

Payne M.C. and Joannopoulos J.D., Allan D.C., Teter M.P., and Vanderbilt D.H., 1986, Phy. Rev. Lett., **56**, 2656.

Payne M.C., Weng X., Hammer B., Francis G., Stich I., Bertram U., A. de Vita, Lin J.S., Qteish A. and Milman V., 1992, CCP9 Summer School unpublished materials, Cavendish Laboratory, Cambridge.

Pertsin A.J. and Kitaigorosky A.I., 1987, *The Atom-Atom Potential Method : Application to Organic Molecular Solids*, Springer-Verlag.

Peters M.C. and Milberg M.E., 1964, Acta Cryst., **17**, 229.

Philips J.C., 1958, Phys. Rev., **112**, 685.

Pisani C., Dovesi R. and roetti C., 1988, *Hartree-Fock Ab Initio Treatment of Crystalline Systems* (Lecture Notes in Chemistry 48), Springer-Verlag.

Poirier J.P., 1991, *Introduction to the Physics of the Earth's Interior*, Cambridge University Press.

Pople J.A. and Binkley J.S., 1975, Mol. Phys., **29**, 599.

Prewitt C.T. and Shannon R.D., 1968, Acta Cryst., **B24**, 869.

Price G.D. and Parker S.C., 1984, Phys. Chem. Miner., **10**, 209.

Price G.D. and Parker S.C., 1988, in *Physical Properties and Thermodynamic behaviour of Minerals* (Salje E.K.H., ed.), p.591.

Pye L.D., Frechett V.D. and Kreidl N. J. (eds.), 1978, *Borate Glasses : Structure, Properties, Applications* , Plenum.

Riebling E.F., 1966, J. Am. Ceram. Soc., **49**, 19.

Roso V.F. and Edwards, 1967, in *The Chemistry of Boron and its Compounds* (Muetterties E.L., ed.),John Wiley & Sons, Chapter.3.

Saunders M.J., Leslie M. and Catlow C.R.A., 1984, J. Chem. Soc. Chem. Commun., 1271.

Schneider W. and Carpenter G.B., 1970, Acta Cryst. **B26**, 1189.

Sellers H., Boggs J.E., Nemukhin A. and Almlof J., 1981, J. Molec. Struct., **85**, 195.

Shmidt N.E., 1966, Russ. J. Inorg. Chem., **11**, 241.

Silvi B., D'arco Ph., Saunders V.R. and Dovesi R., 1991, **17**, 674.

Snyder L.C., Peterson G.E. and Kurkjian C.R., 1976, J. Chem. Phys., **64**, 1569.

Snyder L.C., 1978, in *Borate Glasses : Structure, Properties, Applications* (Pye L.D., Frechett V.D. and Kreidl N.J., eds.), Plenum.

Snyder L.C. and Wasserman Z., 1980, J. Chem. Phys., **73**, 998.

Soppe W., C. van der Marel, W.F. van Gunsteren and H.W. den Hartog, 1988, J. Non-Cryst. Solids., **103**, 201.

Soppe W. and H.W. den Hartog, 1988, J. Phys. C, **21**, L689.

Soppe W. and H.W. den Hartog, 1989, J. Non-Cryst. Solids, **108**, 260.

Soules T.F., 1979, J. Chem. Phys., **71**, 4570.

Soules T.F., 1980, J. Chem. Phys., **73**, 4032.

Soules T.F. and Varshneya A.K., 1981, J. Am. Ceram. Soc., **64**, 145.

Soules T.F., 1990, in *Glass Science and Technology* Vol.4A (Uhlmann D.L. and Kreidl N.J., eds.), Academic Press, Chapter.6.

Sperry L.L. and Mackenzie J.D., 1968, Phys. Chem. Glasses, **9**, 91.

Strong S.L. and Kaplow R., 1968, Acta Cryst., **B24**, 1032.

Strong S.L., Wells A.F. and Kaplow R., 1971, Acta Cryst., **B27**, 1662.

Szabo A. and Ostlund N.S., 1982, *Modern Quantum Chemistry : Introduction to Advanced Electronic Theory*, Macmillan Publishing.

Takada A., Adachi K., Keitora M., Mitsuhashi F. and Kawaguchi T, 1991, in *Computer Aided Innovation of New materials* (Doyama M., Suzuki T., Kihara J. and Yamamoto R., eds.), North-Holland.

Takeuchi Y., 1952, Acta Cryst., **5**, 574.

Tazaki H., J. Sci. Hiroshima Univ. **A**, **10**, 55.

Tersoff J., 1986, Phys. Rev. lett., **56**, 632.

Teter M.P., Payne M.C. and Allan D.C., 1989, Phys. Rev., **B40**, 12255.

Tossell J.A. and Vaughan D.J., 1992, *Theoretical Geochemistry : Application of Quantum Mechanics in the Earth and Mineral Sciences*, Oxford University Press.

Tsuneyuki S., Tsukada M. and Aoki H., 1988, Phys. Rev. Lett., **61**, 869.

Ubbelohde A.R., 1978, *The Molten State of Matter*, John Wiley & Sons.

Uchida N., Maekawa T. and Yokokawa T., 1985, J. Non-Cryst. Solids, **74**, 25.

Uchida N., Maekawa T. and Yokokawa T., 1986, J. Non-Cryst. Solids, **85**, 290.

Uhlmann D.R., Hays J.F. and Turnbull D., 1967, Phys. Chem. Glasses. **8**, 1.

Verhoef A.H. and H.W. den Hartog, 1991, Rad. Effects Defects Solids, **119-121**, 493.

Verhoef A.H. and H.W. den Hartog, 1992, J. Non-Cryst., **146**, 267.

Vessal B., Leslie M and Catlow C.R.A., 1989, Molec. Simulation, **3**, 123.

Vessal B., 1991, Private Communication.

Volf M.B., 1984, *Chemical Approach to Glass*, Elsevier.

Walker J.R., 1982, in *Computer Simulation of Solids* (Lecture Notes in Physics 166), (Catlow C.R.A. and Mackrodt W.C. eds.), Springer-Verlag, Chapter.5.

Walrafen G.E., samanta S.R. and Krishnan P.N., 1980, J. Chem. Phys., **72**, 113.

Wimmer E., 1991, in *Density Functional Methods in chemistry* (Labanowski J.K. and Andzelm W., eds.), Springer-Verlag.

Woodcock L.V., 1971, Chem. Phys. Lett., **10**, 1087.

Woodcock L.V., Angell C.A. and Cheeseman P., 1976, J. Chem. Phys., **65**, 1565.

Xu Q., Kawamura K. and Yokokawa T., 1988, j. Non-Cryst. Solids, **104**, 261.

Yin M.T. and Cohen M.L., 1982, Phys. Rev., **B26**, 5668.

Zachariasen W.H., 1932, J. Am. chem. Soc., **54**, 3841.

Zachariasen W.H., 1934, Z. Kristallogr., **88**, 305.

Zachariasen W.H., 1937, J. Chem. Phys., **5**, 919.

Zachariasen W.H., 1954, Acta Cryst., **7**, 305.

Zachariasen W.H., 1963, Acta Cryst., **16**, 385.

Zarzycki J., 1978, in *Borate Glasses : Structure, Properties, Applications* (Pye L.D., Frechett V.D. and Kreidl N.J., eds.), Plenum.

Zhang Z.G., Boisen M.B. Jr., Finger L.W. and Gibbs G.V., 1985, Amer. Mineral., **70**, 1238.